General relativistic dynamics of spinning particles

"Don't part with your illusions. When they are gone, you may still exist, but you have ceased to live."

Mark Twain

Daniela Knickmann geb. Kunst

Universität Bremen 2015

General relativistic dynamics of spinning particles

Vom Fachbereich Physik und Elektrotechnik
der Universität Bremen

zur Erlangung des akademischen Grades eines

Doktor der Naturwissenschaften (Dr. rer. nat.)

genehmigte Dissertation

von

M.Sc. (DIC) Daniela Knickmann geb. Kunst

wohnhaft in Twistringen

1. Gutachter: Prof. Dr. Claus Lämmerzahl
2. Gutachter: Prof. Dr. Domenico Giulini
Eingereicht am: 31.07.2015
Tag des Promotionskolloquiums: 26.10.2015

Abstract

Coalescing binary systems are supposed to be good sources for gravitational radiation. The data analysis of gravitational wave signals is very much involved with matched filtering procedures. Thus, a detailed theoretical understanding of the dynamical characteristic of binary systems is an essential pillar of gravitational wave astronomy.

This thesis is devoted to improve the theoretical description of binary systems consisting of spinning objects. An essential ingredient for many approaches to model their evolution is provided by the general relativistic motion of spinning test particles in Lagrangian as well as Hamiltonian formulation. As the present thesis covers many aspects of this subject restricted to the pole-dipole approximation, it is divided into two main parts.

The first part concentrates on the study of the dynamical properties of spinning test particles as described by the Mathisson-Papapetrou equations. Provided that the frequencies offer a straight link to observations the pairs of geometrically different timelike geodesics with the same radial and azimuthal frequencies is examined for spinning test particles moving in Schwarzschild-de Sitter spacetime. Both the cosmological constant and the particle's spin have distinct impacts on the description of bound motion in the frequency domain.

One major backbone of the theory of spinning particles is the requirement of a spin supplementary condition (SSC) in order to solve the equations of motion. A promising condition in the context of a Hamiltonian formalism of general relativistic spinning particles is the Newton-Wigner SSC. As it is little known about the properties of the NW SSC the evolution of a worldline defined by the Mathisson-Papapetrou equations supplemented with the NW SSC is compared to one that is obtained by the Tulczyjew SSC, which is well understood and frequently used in the literature and therefore provides a robust reference.

The second part of this thesis deals with the Hamiltonian formulation of spinning particles in general relativity. Due to the spin condition the derivation of a Hamiltonian involves the implementation of constraints. A Hamiltonian function linearised in the particle's spin that includes the constraints by means of Dirac brackets is analysed. Since the Hamiltonian offers a wide range of applications to dynamical systems, the significance of the approximation in the spin is investigated. A comparison of the orbital evolution of a spinning particle of mass $\mathcal{M}$ in the gravitational field of a Kerr black hole of mass M described by the Mathisson-Papapetrou equations, which are exact in the particle's spin, to the one given by Hamilton's equations of motion is performed. The range of validity is stated to be between $S = 10^{-6} - 10^{-4}\mathcal{M}M$.

In order to improve the Hamiltonian formulation and expand it to higher orders in the particle's spin an action approach is employed in this thesis to impose the constraints at the level of the action. In contrast to the use of Dirac brackets the computations are

greatly simplified. The canonical structure of the variables is retained up to second order in spin. By giving up on the canonical formulation a Hamiltonian valid to all orders in the particle's spin is derived.

At the end of this thesis applications to future work and implications on observations are discussed.

List of Publications

The list of publications has been updated in March 2016, as two publications have been processed since July 2015, the date of the submission of this thesis.

- G. Lukes-Gerakopoulos, J. Seyrich and D. Kunst, "Investigating spinning test particles: Spin supplementary conditions and the Hamiltonian formalism", *Phys. Rev. D* **90**, 104019 (2014).

- D. Kunst, V. Perlick and C. Lämmerzahl, "Isofrequency Pairing of spinning particles in Schwarzschild-de Sitter spacetime", *Phys. Rev. D* **92**, 024029 (2015)

- D. Kunst, T. Ledvinka, G. Lukes-Gerakopoulos and J. Seyrich, "Comparing Hamiltonians of a spinning test particle for different tetrad fields", arXiv:1506.01473 (2015); *Phys. Rev. D* **9**3, 044004 (2016)

- J. Vines, D. Kunst, J. Steinhoff and T. Hinderer, "Canonical Hamiltonian for an extended test body in curved spacetime: To quadratic order in spin", in preparation; arXiv:1601.07529 (2016)

Statement of Contributions

- G. Lukes-Gerakopoulos, J. Seyrich and D. Kunst, "Investigating spinning test particles: Spin supplementary conditions and the Hamiltonian formalism", *Phys. Rev. D* **90**, 104019 (2014) [1]

This study was published under lead-authorship of Georgios Lukes-Gerakopoulos. The contents of the paper spread over chapters 3 and 6 as well as section 5.2. The physical studies, during which the plots in the paper were generated, were carried out by Georgios Lukes-Gerakopoulos with the codes of of Jontathan Seyrich. The studies and discussions are based on theoretical input by D. K. . The plots in this thesis in the chapters 3 and 6 were generated by D. K. in order to be consistent with the notation and provide supplementary figures in the appendices C and D. The appendices A and B were elaborated by Jonathan Seyrich.

- D. Kunst, V. Perlick and C. Lämmerzahl, "Isofrequency Pairing of spinning particles in Schwarzschild-de Sitter spacetime", *Phys. Rev. D* **92**, 024029 (2015) [2]

This study was published under lead-authorship of D. K. . The contents of the paper are discussed in chapter 2. The physical studies were carried out by D. K. in collaboration with Volker Perlick and Claus Lämmerzahl. The calculations, the plots and the codes were generated by D. K. .

- D. Kunst, T. Ledvinka, G. Lukes-Gerakopoulos and J. Seyrich, "Comparing Hamiltonians of a spinning test particle for different tetrad fields", *Phys. Rev. D* **93**, 044004 (2016) [3]

This study was published under lead-authorship of D. K. . The contents of the paper are discussed in chapter 7. The theoretical work was done by D. K. and Tom'a š Ledvinka. The simulations, which triggered the theoretical considerations and which corroborated the theoretical results, were carried out by Georgios Lukes-Gerakopoulos and Jonathan Seyrich. The plots in the publication and in this thesis were produced by D. K. and Georgios Lukes-Gerakopoulos.

- J. Vines, D. Kunst, J. Steinhoff and T. Hinderer, "Canonical Hamiltonian for an extended test body in curved spacetime: To quadratic order in spin", in preparation; arXiv:1601.07529 (2016) [4]

This study has been finished in March 2016 and was in preparation while writing and submitting this thesis. The contents of the paper are discussed in chapter 8. The theoretical work was done by D. K., Jan Steinhoff and Justin Vines. Computations of the periastron shift and the curvature terms are performed by Tanja Hinderer.

Acknowledgements

I would like to express my gratitude to my supervisor Prof. Dr. Claus Lämmerzahl for the opportunity to conduct my research at ZARM, for his continuous support of my PhD study and related research. Without his patience and motivation this dissertation would not have been possible.

A very special thanks goes to PD Dr. Volker Perlick who always encouraged me in pursuing my research. His wholehearted support and guidance helped me in all the time of research and writing this thesis. I deeply appreciate his immense knowledge, his never ending interest in my studies and the fruitful discussions which led the way to complete this thesis.

Furthermore I would like to thank my referee Prof. Dr. Domenico Giulini for his insightful comments and encouragements. I admire his broad knowledge in physics and always loved the ease in his talks and the discussions in our group meetings.

My sincere thanks also goes to Prof. Dr. Oldrich Semerak, who provided me an opportunity to join his group in Prague for a few months. It was a wonderful experience and the starting point for my collaboration with Dr. Georgios Lukes-Gerakopoulos, Jonathan Seyrich and Dr. Tomáš Ledvinka. I enjoyed working in a team and learned a lot from them.

I would particularly like to thank Dr. Jan Steinhoff for his invitation to a collaboration and a research stay at the Albert-Einstein-Institut in Golm, which would not have been possible without the support from Prof. Dr. Alessandra Buonanno. Working in her group was a great pleasure. During my collaboration with Dr. Jan Steinhoff and Dr. Tanja Hinderer I entered a different area of research so that I learned a lot about gravitational waves, Hamiltonian mechanics and the EOB formalism. I gratefully acknowledge their patience in answering my never ending questions and the ease we had in working together.

During my time as a PhD student I profited from the nice people around at the ZARM and within the research training group Models of Gravity. In particular I would like to thank Arne Grenzebach, Dr. Saskia Grunau, Melanie Vogelsang and Dr. Samae Bagheri for the great times we had in our colloquia, winter school and at conferences. The broad range of subjects extended my interest and curiosity in diverse areas of physics. Moreover, I am grateful to Dr. Eva Höne for her support in mathematical questions and the stimulating discussions, to Dr. Dirk Pützfeld for his assistance in my understanding of the theory of spinning particles.

The financial support from the Deutsche Forschungsgemeinschaft within the Research Training Group 1620 “Models of Gravity”, within the SFB 1128 “Relativistic Geodesy and Gravimetry with Quantum Sensors” and from the “Centre for Quantum Engineering and Space-Time Research (QUEST)” is gratefully acknowledged.

Finally, I would like to thank my family: my parents and my sister for supporting me spiritually throughout writing this thesis and for alwys being there for me my whole life. Special thanks goes to my husband Daniel who always stands by, encourages and motivates me to never give up and pursue my goals to the very end.

Contents

Notation and Conventions

- $\eta_{\mu\nu}$ Minkowski metric in Lorentzian signature $diag(-1,1,1,1)$
- geometric units: $G = c = 1$
- affine worldline parameter: σ
- proper time: τ
- coordinate basis: μ, ν, ...
- spatial part in coordinate basis: i, j, ...
- temporal part in coordinate basis: t
- local Lorentz basis: a, b, ...
- spatial part in local Lorentz basis: (i), (j), ...
- temporal part in local Lorentz basis: (t)
- body-fixed Lorentz basis: A, B, ...
- spatial part in body-fixed Lorentz basis I, J, ...
- temporal part in body-fixed Lorentz basis T
- Lorentz matrix: $\Lambda_A{}^b$ the first index is in the body-fixed frame and the second one in the local frame
- tetrad field: $e_A{}^\mu$, $e_a{}^\mu$ the first index is in the body-fixed or local frame and the second in the coordinate frame
- mass of the gravitating object: M
- dynamical rest mass of a spinning test particle: $\mathcal{M}$
- (constant) rest mass of a (spinning) test particle (pole-dipole approximation): m
- kinematical rest mass of a spinning test particle: μ
- partial derivative: ∂, or denoted by a , in index notation
- covariant derivative: ∇ or denoted by a ; in index notation
- covariant differential: D

- covariant variation: Δ
- symmetric tensor: $T^{(\mu\nu)} = \frac{1}{2}\left(T^{\mu\nu} + T^{\nu\mu}\right)$
- antisymmetric tensor: $T^{[\mu\nu]} = \frac{1}{2}\left(T^{\mu\nu} - T^{\nu\mu}\right)$

Introduction

Chapter 1

Introduction

1.1 Overview

When describing phenomena happening in our Universe, in particular systems containing massive and strong gravitating bodies, such as black holes, we can no longer neglect the influence of the spacetime's curvature. Therefore we have to use Einstein's field equations [5, 6, 7]

$$G_{\mu\nu} = 8\pi T_{\mu\nu} \ ,$$

when investigating such dynamical systems. The beauty of general relativity is, that these equations contain all information on the description of the interaction between the geometry of spacetime and energy and momentum manifesting themselves in matter.
Experimental support for Einstein's ideas was delivered shortly after their publications when Eddington observed the predicted effect of light deflection during a solar eclipse in 1919 [8]. Further experimental verifications are provided by measurements of the perihelion shift of Mercury and the gravitational redshift [7, 9]. One major prediction of general relativity has not yet been observed, though: gravitational waves. So, where do they hide? Gravitational waves can be described by oscillations in the gravitational field propagating at the speed of light. They are generated by a wide range of phenomena in our Universe. Good candidates are coalescing binary systems consisting of two compact objects, such as neutron stars or black holes [10, 11, 12].
Although there exist many gravitational wave detectors all over the world which are continuously being upgraded none of them has been successful yet. Earthbound detectors are for example LIGO (US), Virgo (Italy), GEO (Hanover, Germany), TAMA (Japan) and ACIGA (Australia). The reasons why no direct observation has been reported yet are especially the technological challenges [7, 11, 12]. Only indirect evidence is given by the observations of the Hulse-Taylor pulsar, a double neutron star system. Measurements of the

orbital period show that it is continuously decreasing and the two neutron stars approach one another. The system therefore loses energy. In fact, the corresponding energy loss is in very good agreement with Einstein's theory predicting gravitational waves to carry this amount of energy away from the system [13, 14]. This is why scientists are still very confident that in the near future one of the gravitational wave detectors will be successful in measuring such a signal.
The current problems with the detectors on earth are the noises produced by seismic motion, gravity gradients or by thermal energy. Thus, it is planned to launch a space based gravitational wave detector called LISA in 2034 [11]. Since gravitational waves are not absorbed by dust or stellar envelopes they probably will offer an unprecedented insight into some of the mysteries in our universe.
In order to be able to discern a gravitational wave signal a special kind of data analysis is necessary. Compared to the data obtained from telescopes in the electromagnetic spectrum theoretical input is of great importance. In particular the matched filtering method requires a detailed understanding of the sources so that templates of corresponding waveforms can be constructed. This is why the promise of gravitational wave astronomy relies upon our ability to accurately model the gravitational wave signals [15, 16].
A detailed theoretical understanding of the dynamical characteristics and evolution of coalescing binary systems serves as the basis for modelling gravitational waves. We distinguish the binary systems into equal-mass and extreme-mass ratio systems, because the computation of the corresponding gravitational waves is treated slightly differently.

Extreme-mass ratio inspirals (EMRIs) consist for example of stellar-mass compact objects (SCO) that spiral into massive black holes in the centre of galaxies. Based on black-hole perturbation theory and the self-force formalism we are provided with a well developed and robust approach to calculate the gravitational waveforms and the orbital evolution under radiation reaction [16]. Assuming the adiabatic approximation which neglects the energy loss over one orbit, the evolution of an EMRI is modeled by transitions through the orbits of the dynamical system [17, 18, 19, 20]. Hence, modelling EMRIs involves the solution of the general relativistic two-body problem in the extreme mass ratio regime, which can be performed to a great deal analytically.
Analytic solutions to the geodesic equation in a great variety of spacetimes, such as Schwarzschild, Schwarzschild-(anti)-de Sitter, Kerr or Reissner-Nordström, have been studied in [21, 22, 23]. The classification and parametrisation of geodesic orbits has also been extensively discussed in the literature, see e.g. [23, 24, 25]. In the context of gravitational wave physics bound and plunging orbits are of particular interest because they represent two different stages that are significant for the evolution of an EMRI, the inspiral and the plunge.

Bound orbits are characterised by a set of fundamental frequencies which were thought to uniquely parametrise these orbits until Barack et al. showed the existence of isofrequency pairs in the strong field regime in Schwarzschild spacetime in 2011 [26]. Indeed, the gravitational wave signal of an EMRI is composed of a number of harmonics of the independent fundamental frequencies of the system [16, 27]. The discovery of the feature of isofrequency pairs amounted to an additional degeneracy one has to consider in gravitational wave data analysis but revealed at the same time a new invariant characteristic, which is useful for the calibration of different approaches to the general relativistic two-body problem. Thus, analysing the dynamics in the frequency picture allows a straight link to the frequency spectra of gravitational waveforms and provides a fundamental insight into the dynamics of the system.
The phase where the SCO passes over from inspiral to plunge is characterised by a special type of orbits, the homoclinic orbits. Since they separate bound motion from unbound motion, this borderline is frequently called *separatrix*. As it happens, this event has a distinct imprint on gravitational wave signals and is related to the zoom-whirl feature close to the separatrix that is located in the strong field regime [20, 28, 29].

One goal of this thesis is to improve the understanding of the orbital properties of the general relativistic two-body problem in the test particle limit including the test particle's spin. Gravitational waves produced by binaries containing spinning particles are computed using the black-hole perturbation approach, numerical relativity etc. However, spinning particles make the procedure more complicated, since not only a large number of parameters is necessary to characterise the system but also spin induced effects are modulating the gravitational wave signal. For instance, the spin precession, spin-orbit, or spin-spin coupling change the amount of emitted gravitational radiation and affect the gravitational wave signal [19, 30, 31, 32, 33, 34]. In addition, the spin is supposed to introduce chaotic behaviour to the dynamics which makes the system sensitive to the choice of initial conditions influencing the gravitational waveforms [35, 36, 37, 38]. We will approach the problem from a different angle, though. Instead of investigating the general properties of spinning particles or looking at the gravitational waveforms we will focus on the properties of the extreme-mass ratio binary system in the frequency domain. This allows us to directly search for features that may be relevant to gravitational wave astronomy.
As already mentioned it was discovered only recently that the fundamental frequencies of a test particle moving in Schwarzschild spacetime do not provide a unique parametrisation of the orbits. These findings have been generalised to Kerr spacetime and charged particles moving in Schwarzschild spacetime in the presence of a magnetic field [39, 40]. We extend this analysis to spinning particles and include a positive cosmological constant,

which introduces a second equilibrium point far away from the centre in the weak field region where the attractive gravity and the repulsive dark energy are compensated. The region of bound motion is analysed and special classes of orbits, such as homoclinic and heteroclinic orbits, are characterised in terms of the fundamental frequencies.

In the case of equal-mass ratio binary systems, the modelling of the system involves a more complicated scheme, see e.g. [15] for an overview. The different stages of the evolution put distinct demands on the theoretical description so that a variety of analytic approximation schemes and numerical techniques are employed to investigate the orbital dynamics and the gravitational radiation emission. The three most prominent approaches to compute and model gravitational waves encompass numerical relativity (NR) primarily used for the merging phase [41], post-Newtonian approximation (PN) in the far field and slow motion [27, 42, 43], and the effective-one-body theory (EOB) for the late inspiral close to the plunge [44, 45, 46]. To obtain the gravitational wave emission during the entire evolution of a binary system these different approaches have to be combined. On that account they contain free parameters that have to be calibrated using coordinate invariant quantities and relationships, such as the frequency of the innermost stable circular orbit (ISCO), the periastron shift or the binding energy, just to name the most frequent ones [46, 47, 48].

The second topic of this thesis deals with the properties of Hamiltonian formulations of spinning particles which provide the basis for the PN approximation and EOB theory. Generally, the Hamiltonian formalism of general relativistic systems implies some obstacles, such as the necessity of a spacetime split, since the time variable is treated differently from the spatial ones. A sophisticated procedure was developed by Arnowitt, Deser, and Misner giving the canonical ADM Hamiltonian [49, 50, 51, 52] which is used for the PN approximation and a key ingredient for EOB theory.
EOB theory maps the real dynamics of binary systems onto some non-geodesic effective dynamics of a reduced mass moving in an effective metric, e.g. a deformed Schwarzschild or Kerr metric. Starting from the real PN-expanded ADM Hamiltonian the effective Hamiltonian is computed using the EOB mapping prescription, introduced by Buonanno and Damour in [44]. The conservative dynamics, i.e. the motion of a reduced mass in an effective metric, is generated by a Hamiltonian based on test particle dynamics which is then augmented by a deformation parameter adjusted to the PN-expanded Hamiltonian based on the real dynamics. Thus, the starting point is a Hamiltonian function of a spinning test particle moving in curved spacetime.
One approach is proposed by Barausse, Racine and Buonanno in [53] ensuing from a

general unspecified Lagrangian function, which is Legendre transformed and yields a canonical Hamiltonian formulation. However, this formulation is only valid at linear order in the particle's spin. As a Hamiltonian formalism offers a wide range of applications besides the EOB and PN theory, particularly chaos and perturbation theory, it is useful to check the reliability of the approximated Hamiltonian. More precisely, we compare the results obtained by the Hamiltonian to the dynamical properties of and the solution to the Mathisson-Papapetrou equations (MP) describing the motion of a spinning particle within the pole-dipole approximation to all orders in the particle's spin. This set of equations has to be supplemented by a spin condition defining the centre of mass within the extended body in order to be closed. There exist many such supplementary conditions each of which defines a different observer who sees a particular selected worldline to be the centre of mass. For instance the so-called Pirani condition chooses the observer to be in the rest frame of the particle.

Although it is sometimes said, that the quadratic spin terms are attributed to the quadrupole, see e.g. [54], justifying the linearisation of the Hamiltonian in contradiction to the MP equations, which include higher order spin terms, they do matter when choosing a supplementary condition [55]. Thus, the linearisation should be considered as an approximation for small spins and the differences in the results should be thoroughly investigated.

In the context of a canonical Hamiltonian formalism the so called Newton-Wigner condition is the preferred spin condition [53, 56, 57, 58], since it allows to choose the phase space variables in such a way that they possess a canonical structure. However, it is little known about the dynamical behaviour of this condition so far.

Since we would like to apply the canonical Hamiltonian function in different fields than EOB or PN theory, this thesis is concerned with a thorough analysis of the linearised Hamiltonian and the corresponding supplementary condition. First, we compare the evolution of a worldline prescribed by the MP equations supplemented by the Newton-Wigner condition to one that is obtained by the Tulczyjew supplementary condition, which has been widely used and is well understood in the context of the MP equations due to its analytical properties. After characterising the behaviour of the Newton-Wigner condition in the MP equations, we investigate the differences in the solutions of the MP equations and Hamilton's equations in order to evaluate the range of validity of the approximated Hamiltonian in terms of the spin parameter. Thereby, we notice that the numerical behaviour of some important constants of motion is unphysical along the evolution prescribed by the Hamiltonian. Subsequently, we rewrite the Hamiltonian in such a way that the numerical results match physically realistic situations so that the resulting form is applicable to numerical investigations within chaos or perturbation theory.

As the constraints, such as the supplementary condition, are imposed on the Hamilto-

nian by replacing Poisson brackets by Dirac brackets, the derivation involves lengthy and hideous computations [53]. An alternative way to compute the Hamiltonian of spinning particles is based on an action approach where the constraints are implemented on the level of the action [58, 59]. The problem, though, is that the results rely on explicit Lagrangian functions which are related to the choice of a spin supplementary condition and have to be given beforehand. Only recently Steinhoff presented a spin gauge invariant action that is based on a Lagrangian function whose form is invariant under the choice of the spin supplementary condition, i.e. the explicit expression does not depend on the spin condition [59]. Thus the constraints are implemented as gauge constraints in the action offering a straightforward procedure to obtain a Hamiltonian formalism. Here, we focus on a canonical formulation up to quadratic order in the particle's spin and the exact Hamiltonian formulation within the pole-dipole approximation in terms of non-canonical coordinates. This is the first time that a Hamiltonian for a spinning particle to all orders in spin in the pole-dipole approximation is achieved. The results can be used to improve the EOB Hamiltonian to higher orders in the particle's spin as well as for chaos theory, such as Poincaré sections or recurrence plots.

The present thesis is structured as follows. It begins with an introduction to the geometry of spacetime where the relevant solutions to Einstein's field equations are described. Then, basic information on the theory of spinning particles in general relativity within the pole-dipole approximation are presented.
After the introductory section the thesis is divided into two main parts. The first part concentrates on the investigation of the dynamics of spinning particles as described by the MP equations. The dynamics of spinning particles in Schwarzschild-de Sitter spacetime is characterised in the frequency picture. After that the properties of the supplementary conditions are analysed by numerically comparing two selected spin conditions, the Tulczyjew and Newton-Wigner condition.
In the second part we deal with the description of general relativistic spinning particles in Lagrangian and Hamiltonian mechanics. After giving a short overview of the Lagrangian formalism and the relation to Hamiltonian mechanics we first focus on the Hamiltonian derived by Barausse et al. [53]. This is followed by a detailed analytical as well as numerical analysis of the properties of this Hamiltonian. We compare the solutions of the Hamiltonian formulation to the ones given by the MP equations and state conditions for the numerical results to be physical. After that, we use an alternative approach to compute the canonical Hamiltonian function to higher orders in the particle's spin as well as a Hamiltonian that is exact to all orders in the particle's spin in non-canonical coordinates. At the end we summarise our results and give an outlook for future work.

1.2 Spacetime Geometry

Flat Spacetime

Mathematically, we describe the spacetime by a four dimensional manifold where the dimensions correspond to time and the three spatial directions. In order to equip the manifold with a measure of volume and length, etc., we define a symmetric bilinear form on each tangent space of the manifold known as the Minkowski metric [7]

$$\eta_{\mu\nu} = \begin{pmatrix} -1 & 0 & 0 & 0 \\ 0 & 1 & 0 & 0 \\ 0 & 0 & 1 & 0 \\ 0 & 0 & 0 & 1 \end{pmatrix} , \tag{1.1}$$

where we use the Lorentzian signature $(-,+,+,+)$. The parameters (μ,ν) run from $0-3$ where 0 denotes the time coordinate and $1-3$ the three spatial dimensions. Therewith the spacetime interval is expressed by

$$ds^2 = \eta_{\mu\nu} dx^\mu dx^\nu \ ,$$

corresponding to proper distance and

$$d\tau^2 = -\eta_{\mu\nu} dx^\mu dx^\nu \ ,$$

for proper time for a chosen coordinate system x^μ. Using either of the notions from above the relation between two events are classified to be spacelike, timelike or lightlike [6, 7]. In other words, a causal structure between events can be worked out assuming that nothing is able to travel faster than the speed of light. Subsequently, physical bodies have to move on timelike curves $\left(ds^2 < 0,\, d\tau^2 > 0\right)$, since their trajectories have to connect timelike separated events that are in causal contact.

The Minkowski metric is often called the flat metric, since it describes the structure of "empty space", i.e. the corresponding spacetime is not affected by any matter or energy, which is why the geometry of the manifold is flat.

Curved spacetime

In order to include gravity into the geometric concept of spacetime Einstein connected gravitational physics to the mathematics of differential geometry yielding the famous Einstein field equations [7]. Amazingly they contain all information on how the curvature of spacetime influences matter and how energy and momentum shape the geometry of

spacetime [6, 7, 60]

$$G_{\mu\nu} := R_{\mu\nu} - \frac{1}{2} R g_{\mu\nu} = 8\pi T_{\mu\nu} \ , \tag{1.2}$$

where $R_{\mu\nu}$ is the Ricci tensor, R the Ricci scalar, $g_{\mu\nu}$ the metric tensor and $T_{\mu\nu}$ the energy momentum tensor. Compared to flat spacetime the metric $g_{\mu\nu}$ is no longer Minkowskian (1.1) but it may contain off-diagonal terms and its components depend on the chosen coordinates. The Riemann tensor $R_{\mu\nu\alpha\beta}$ is the curvature tensor which yields the Ricci tensor after contraction of two indices. It is defined by

$$R^{\mu}{}_{\nu\alpha\beta} := \Gamma^{\mu}{}_{\nu\beta,\alpha} - \Gamma^{\mu}{}_{\nu\alpha,\beta} + \Gamma^{\rho}{}_{\nu\beta}\Gamma^{\mu}{}_{\rho\alpha} - \Gamma^{\rho}{}_{\nu\alpha}\Gamma^{\mu}{}_{\rho\beta} \ , \tag{1.3}$$

with the connection given by the Christoffel symbols

$$\Gamma^{\mu}{}_{\nu\alpha} := \frac{1}{2} g^{\mu\lambda} \left(g_{\nu\lambda,\alpha} + g_{\alpha\lambda,\nu} - g_{\nu\alpha,\lambda} \right) \ . \tag{1.4}$$

Curvature can mathematically be understood as a characterisation of the change of a vector parallel transported along a closed loop. Physically, curvature manifests itself in gravity. More precisely, the energy-momentum tensor $T_{\mu\nu}$ on the right-hand-side of (1.2) includes all the sources of gravity, i.e. all kinds of matter. It therewith prescribes the way how spacetime is curved in the presence of matter. Einstein's field equations provide the corresponding set of complicated and non-linear second-order differential equations for the metric $g_{\mu\nu}$. Given a mass-energy distribution these equations can in principle be solved for the gravitational field represented by $g_{\mu\nu}$. However, the complicated structure of the differential equations makes it hard to find solutions [7]. This is the reason why it is common to start with some simplifying assumptions on the metric and draw conclusions on the underlying gravitational source from backwards. One of the simplest solution is the gravitational field produced by a maximally spherically symmetric mass distribution in otherwise empty space and is known as the Schwarzschild solution [61].

1.2.1 Schwarzschild Solution

As already mentioned one of the simplest solution is the maximally spherically symmetric mass distribution producing a gravitational field which is also spherically symmetric. To a good approximation the gravitational fields of the earth or the sun can be modeled using the assumptions from above providing a wide range of applications, such as navigation systems. Moreover, the motion of particles, such as planets, in the exterior region of the gravitating mass, such as the sun, are of great interest and easier accessible than the behaviour in the interior of the central object, so that we confine the topic to the exterior solutions [7].

Given the symmetries the metric is required to satisfy makes it easier to solve Einstein's

field equations for $g_{\mu\nu}$. Spherical symmetry demands the metric to be invariant under spatial rotations, time independent and invariant under time reversal. This means the metric has to be stationary, which requires a timelike Killing vector at infinity, and may not contain any cross terms between time and space which is denoted by static. Lastly, we want it to look like flat spacetime at spatial infinity. The general solution to such a spacetime can be obtained by solving the Einstein's field equations yielding the metric in spherical coordinates (r, θ, ϕ) [6, 7, 62]

$$ds^2 = -f(r)dt^2 + \frac{1}{f(r)}dr^2 + r^2 d\Omega^2 \ , \tag{1.5}$$

with the two dimensional angular line element

$$d\Omega^2 := d\theta^2 + \sin(\theta)^2 d\phi^2 \ ,$$

and M as the mass of the gravitating body. The function $f(r)$ has to be chosen according to the environmental condition, i.e. whether the surroundings of the gravitating mass are empty vacuum or influenced by some kind of vacuum energy denoted by the cosmological constant Λ . The first one is referred to as the Schwarzschild solution and the latter as the Schwarzschild-de-Sitter solution [63].

Interestingly, the properties of the exterior gravitational field are not affected by the characteristics of the source except for its mass. In particular, the source can be a point particle or even a collapsing star as long as it preserves the symmetries during the collapse [7]. This feature is similar in electromagnetism where the electromagnetic fields produced by spherically symmetric charge distributions are independent of the radial distribution of the charges.

Let's have a closer look at the Schwarzschild metric where

$$f(r) \ = \ 1 - \frac{2M}{r} \ . \tag{1.6}$$

It is obvious from (1.5) and (1.6) that the metric components have two singularities:

$$r \to 0 \quad \text{and} \quad r \to 2M \ .$$

While $r \to 0$ is a true curvature singularity, $r \to 2M$ is merely a coordinate singularity and can be removed by an appropriate coordinate transformation [6, 7, 62].

The coordinate singularity $r = 2M$ hides some striking characteristics visible in the coefficients of the metric $g_{\mu\nu}$ opening up the window for black holes. Notice that g_{tt} changes its sign at this radius which means that the time coordinate becomes spacelike for smaller radii. Simultaneously, g^{rr} vanishes as well, transforming the radial coordinate

from a spacelike to a timelike one. When changing the coordinates to Eddington-Finkelstein coordinates which remove the coordinate singularity, we are able to see that if a particle has crossed the surface of $r = 2M$, it keeps falling to decreasing values of r. More precisely, after a particle went past this surface it can never escape to infinity again. Instead it will eventually fall into the centre at $r = 0$ colliding with the true singularity. Because the corresponding surface marks a boundary which can be entered but never escaped from it is called the event horizon. Therefore, we will never obtain any signals emitted beyond the event horizon which is the reason why we call those objects black holes. The gravitating object must be smaller than $r = 2M$, though. Otherwise the event horizon lies inside the object which does not prevent us from receiving information from the object's surface and it no longer behaves like a black hole [6, 7]. But this is a different story which we are not interested in here. Observations imply that black holes do exist in our universe so we think it is more fascinating to deal with these strange objects which we still have much to learn about.

1.2.2 Schwarzschild-de Sitter solution

If we allow for dark energy which we think to be responsible for the accelerated expansion of our Universe we have to consider the Schwarzschild-de-Sitter metric, see e.g. [63], with

$$f(r) \quad = \quad 1 - \frac{2M}{r} - \frac{\Lambda}{3} r^2 \ , \tag{1.7}$$

where Λ corresponds to the cosmological constant. We restrict ourselves to a positive Λ here, since observations indicate that the expansion is accelerating.

In principle we repeat the investigation from the Schwarzschild case. First, we have a look at the metric components, in particular, at $f(r)$. Just like before, we have a singularity at $r \to 0$ which proves to be a true curvature singularity. For further investigation we now consider the Schwarzschild-de Sitter metric to be a combination of the Schwarzschild spacetime in a de Sitter universe. We have seen that the Schwarzschild metric contains a coordinate singularity at $r = 2M$ being the event horizon of the black hole. On the other hand the de Sitter universe possesses a cosmological horizon which is of different kind than an event horizon of a black hole in the sense that particles can come out of the horizon but nothing goes in. It corresponds to the size of our observable universe, i.e. the farthest distance we can see.

When combining these two solutions of Einstein's field equations we consequently obtain a spacetime with two horizons for $0 < \Lambda < (3M)^{-2}$: an event horizon and a cosmological horizon. From $f(r)$ we can see that the event horizon located at small radii is approximately

$$r_{H_1} \approx 2M \ ,$$

and the cosmological horizon at large radii

$$r_{H_2} \approx \sqrt{\frac{3}{\Lambda}} > 3M \ .$$

These two horizons divide the spacetime into three different regions: $r < 2M$ is already known from the Schwarzschild black hole and forces an observer to continuously approach the centre. Then there is a static region $2M < r < \sqrt{\frac{3}{\Lambda}}$ with $f(r) > 0$ where an observer has not fallen into the black hole but can still receive signals from objects moving at radii close to $r = 2M$. The third region, however, $r > \sqrt{\frac{3}{\Lambda}}$ is behind the cosmological horizon which prevents an observer from seeing the black hole. For $\Lambda < (3M)^{-2}$ there is no horizon and no static region.

Moreover, from Noether's theorem we know that each dynamical system exhibiting symmetries possesses conserved quantities connected to these symmetries. In Riemannian geometry these conserved quantities along geodesics are linked by a Killing vector field to the symmetries. Both for geodesic motion in Schwarzschild and Schwarzschild-de Sitter spacetime we have four Killing vectors ξ^μ resulting in the conservation of energy, total angular momentum and the direction of the angular momentum vector making the dynamical system completely integrable [7, 21].

These are the most prominent vacuum spacetimes for spherically symmetric black holes. When giving up on spherical symmetry by removing one of the symmetries we end up with axial symmetry. A gravitational field satisfying such a prescription corresponds to a rotating black hole, which is discussed in the next section.

1.2.3 Kerr solution

The axial symmetric gravitational field generated by a rotating mass is called Kerr spacetime and was discovered by Roy Kerr in 1963 [64]. In contrast to Schwarzschild spacetime, which describes the gravitational field produced by any spherically symmetric isolated object, the Kerr metric describes merely the exterior of a black hole [7].

We can already deduce some properties of the spacetime simply by only taking into account the presumed rotation of the central object. As mentioned before the metric has to be axisymmetric about the axis of rotation. Furthermore, it has to be stationary because the black hole rotates in the same manner for all times. However, reversing time changes the direction of the spin and leads to the conclusion that the metric cannot be static. The explicit solution of the Einstein's field equations fulfilling these assumptions looks like [62]

$$ds^2 \quad = \quad g_{tt}\ dt^2 + 2\ g_{t\phi}\ dt\ d\phi + g_{\phi\phi}\ d\phi^2 + g_{rr}\ dr^2 + g_{\theta\theta}\ d\theta^2 \quad , \tag{1.8}$$

with the coefficients

$$\begin{aligned} g_{tt} &= -1 + \frac{2Mr}{\Sigma} \quad , & g_{t\phi} &= -\frac{2aMr\sin^2\theta}{\Sigma} \quad , \\ g_{\phi\phi} &= \frac{\Lambda \sin^2\theta}{\Sigma} \quad , & g_{rr} &= \frac{\Sigma}{\Delta} \quad , \\ g_{\theta\theta} &= \Sigma \quad , \end{aligned} \tag{1.9}$$

and the abbreviations

$$\begin{aligned} \Sigma &= r^2 + a^2\cos^2\theta \quad , & \Delta &= \varpi^2 - 2Mr \quad , \\ \varpi^2 &= r^2 + a^2 \quad , & \Lambda &= \varpi^4 - a^2\Delta\sin^2\theta \quad , \end{aligned} \tag{1.10}$$

in Boyer-Lindquist coordinates (t, r, θ, ϕ), with a as the spin of the black hole J/M. Having the metric at hand, we see that it is asymptotically flat for large radii and reduces to Schwarzschild metric for vanishing spin a. The singularities are also obvious:

$$\Delta = 0 \quad \text{and} \quad \Sigma = 0 \ .$$

Again, by computing the curvature scalars we find that $\Sigma = 0$ is a curvature singularity whereas $\Delta = 0$ is merely a coordinate singularity which can be removed by going to the so called Kerr-Schild coordinates [62]. We have seen before in the spherically symmetric case that the coordinate singularity gives rise to the event horizon, $g^{rr} = 0$. Notice that indeed $g^{rr} = \Delta/\Sigma = 0$ for $\Delta = 0$, so that the radial coordinate again changes from being spacelike to being timelike and gives the event horizons in Kerr spacetime:

$$r_\pm = M \pm \sqrt{M^2 - a^2} \ . \tag{1.11}$$

There exist two solutions for $M > a$, one solution for $M = a$ and no solution for $M < a$. In the latter case there is no event horizon covering the true curvature singularity at $\Sigma = 0$. This is known as a naked singularity which is thought to be less realistic. Thus, we assume $M \geq a$ yielding at least one solution for the event horizon.

Interestingly, both solutions $r_\pm$ in (1.11) are positive which means we can divide the spacetime in three domains: a region $r > r_+$ where the radial coordinate is spacelike, then a region $r_- < r < r_+$ where the radial coordinate becomes timelike so that an observer located in this region has to move towards the inner horizon r_-, and a third region $r < r_-$ where the radial coordinate becomes spacelike again. However, since we are not able to obtain any information from beyond the outer horizon we are only interested in the domain that lies outside.

Interestingly, the stationary limit $g_{tt} = 0$ does no longer coincide with the event horizon,

so that an additional structure in spacetime emerges. The corresponding radii can be calculated as

$$r_{E\pm} = M \pm \sqrt{M^2 - a^2 \cos(\theta)^2} \ . \tag{1.12}$$

Only the positive solution is located outside the outer horizon $r_{E+} > r_+$ which allows an observer to cross r_{E+} and move inside the region between the outer horizon r_+ and r_{E+} where $g_{tt} > 0$, i.e. where the time coordinate becomes spacelike, see Fig. 1.1 . This

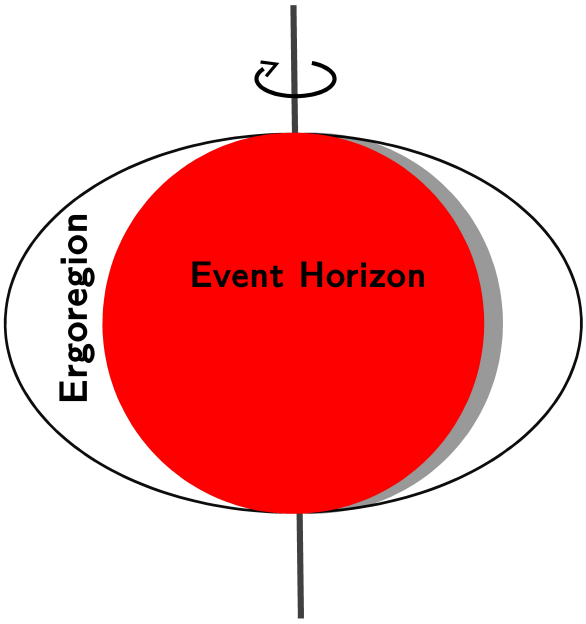

Figure 1.1: The figure shows the horizon structure around a rotating (Kerr) black hole. The outer horizon (r_{E+}) corresponds to the black ellipsoid representing the static limit. The event horizon is visualised by the red sphere (r_+). The region between those radii is called ergoregion within which an observer is forced to corotate with the rotation of the black hole.

domain is called ergoregion and the boundary is known as the ergosphere [7, 62]. Within the ergoregion an observer cannot stay still but is forced to corotate with the black hole while outside the ergosphere an observer is allowed to be static. It is worth to stress at this point, that an observer entering the ergoregion can still escape to infinity; he is not trapped to a confined domain in spacetime.

As previously said symmetries admit for conserved quantities. Since Kerr spacetime is axisymmetric and stationary, two Killing vector fields are admitted for geodesic motion. They correspond to the conservation of energy and the component of the angular momentum aligned with the rotation axis. Moreover, an additional Killing tensor has been

found by Carter in [65] leading to a third conserved quantity. It is called the Carter constant but has no direct physical interpretation. Hence, there are in total three conserved quantities making the geodesic motion in Kerr spacetime completely integrable, too [23].

After extensively discussing how spacetime shapes under the influence of matter we will focus on how matter behaves under the influence of gravitational fields. In particular we will deal with the dynamics of spinning particles and investigate their characteristics and peculiarities.

1.3 Spinning Particles in General Relativity

Before we can start with the investigation of the properties of the motion of spinning particles we first have to know how such a particle behaves in a gravitational field and how it can be described by some set of equations of motion. As a matter of fact, the Einstein field equations (1.2) contain all information necessary to find the equations of motion of a spinning particle without assuming them separately. However, since the field equations are non-linear due to the gravitational backreaction, we obviously have to simplify the problem. First of all, the spinning particle is taken to be small compared to the object that is producing the gravitational field and can be treated as a test body. In addition, this means that the particle's gravitational radiation and its contribution to the gravitational field can be assumed to be negligible so that the description of its dynamics merely has to deal with the motion of a particle in a given gravitational field.

Even though these strict constraints simplify the problem compared to the integration of the full set of field equations, we encounter further difficulties when searching for solutions. This is because the spin allows for further degrees of freedom and therewith for internal structure the equations of motion depend on. Nevertheless, if the particle is supposed to be small compared to the curvature length scale, i.e. the gravitational field occupied by the particle is sufficiently homogeneous so that the particle does not experience any gravitational tidal forces, the internal structure can be expressed by a multipole expansion of the matter distribution. The coefficients of such an expansion are the moments of the stress-energy-momentum tensor describing the properties of matter, i.e. of the spinning testparticle. The evolution equations are then obtained by the integration of the covariant conservation law for the stress-energy-momentum tensor, so that they result in a series of multipole contributions, introduced by M. Mathisson in his pioneering work from 1937 [66]. Now, it is possible to simplify the equations of motion by cutting off the series at a certain number of multipoles which become more complicated the higher the orders are, since they depend on multiples and derivatives of the Riemann curvature tensor. One of the simplest approaches cuts off the expansion at second order called the pole-dipole approximation and traces back to the works of Mathisson and Papapetrou [66, 67].

1.3.1 Pole-Dipole-Approximation

The pole-dipole approximation deals with the equations of motion of a spinning particle only including the mass monopole and spin dipole. Multipoles of higher orders and non-gravitational effects are ignored. The spinning particle is modeled to be some narrow tube evolving in spacetime inside of which $T^{\mu\nu}$ does not vanish [66, 68, 69, 70]. In order to define the multipoles we have to choose a representative worldline $x^{\mu}(\tau)$ inside this tube about which the multipoles, such as the spin, are computed. We already know from classical mechanics that the moments of inertia are calculated with respect to some reference point so that this approach is transferred to relativistic motion. Therewith, we obtain for the multipole moments of $T^{\mu\nu}$ [71, 72, 73]

$$\int_{\Sigma(x,V)} T^{\mu\nu}\delta x^{\alpha_1}...\delta x^{\alpha_n}\sqrt{-g}d\Sigma_{\nu} \ , \tag{1.13}$$

where the integration runs over a three dimensional volume within a spacelike hypersurface $\Sigma(x,V)$ generated by all the geodesics through $x^{\mu}(\tau)$ orthogonal to observer's four-velocity V^{μ} at constant proper time τ, $\delta x^{\alpha} = (z^{\alpha} - x^{\alpha})$ is the tangent vector to the geodesic connecting x^{α} and z^{α} running through the body's volume, $d\Sigma_{\nu} = n_{\nu}d\Sigma$ with n_{ν} as the unit normal vector to $\Sigma(x,V)$, $d\Sigma$ is the three dimensional volume element on the hypersurface and $g = g_{\mu\nu}g^{\mu\nu}$ is the determinant of the metric. The prefactor $\sqrt{-g}$ arises when the volume undergoes coordinate transformations. In order to ensure that the form of the integral remains covariant, i.e. that it is independent of the choice of coordinates, we require the volume element to be invariant by introducing the factor $\sqrt{-g}$ in the integral.

The infinite set of multipole moments has been called the *gravitational skeleton* by Mathisson [66], since it fully describes the gravitational properties of the extended body. There is some ambiguity, though, in the definition of these multipoles in the sense, that the integration procedure in(1.13) is not uniquely fixed. While in flat spacetime the approach is indeed straightforward, problems occur in curved spacetime: During the integration process tensors at different spacetime points are summed over. Different generalisations from flat to curved spacetime have been developed in the course of time [74]. However, a precise definition of the momenta becomes important not until quadrupole and higher orders are considered, i.e. at pole-dipole order these various approaches are indistinguishable and lead to the same form of equations of motion [72, 74].

When the analysis is restricted to particles whose dynamics is only affected by the monopole moments the motion is simply geodesic. If the next higher order multipole moment, the dipole moment, is included, the motion corresponds to a test particle with inclusion of spin and is no longer geodesic. Then the monopole and dipole moments give rise to the definition of the kinematic momentum p^{μ} and the spin tensor $S^{\mu\nu}$ of the body

as measured by an observer moving along the reference worldline with velocity V^μ [74, 75]

$$\begin{aligned} p^\mu &= \int_{\Sigma(x,V)} T^{\mu\nu}\sqrt{-g}d\Sigma_\nu \ , \\ S^{\mu\nu} &= 2\int_{\Sigma(x,V)} \delta x^{[\mu}T^{\nu]\gamma}\sqrt{-g}d\Sigma_\gamma \ . \end{aligned}$$

The corresponding equations of motion can be obtained using the conservation law

$$T^{\mu\nu}{}_{;\nu} = 0 \ ,$$

and derived in their covariant form as [72, 73, 76, 77]

$$\frac{Dp^\mu}{d\tau} = -\frac{1}{2}R^\mu{}_{\nu\rho\sigma}u^\nu S^{\rho\sigma} \ , \tag{1.14}$$

$$\frac{DS^{\mu\nu}}{d\tau} = p^\mu u^\nu - p^\nu u^\mu \ , \tag{1.15}$$

with $u^\mu = dx^\mu/d\tau$ being the tangent to the worldline parametrised by proper time τ and $\frac{D}{d\tau}$ denotes the covariant directional derivative. While Papapetrou used a non-covariant method to obtain the set of equations (1.14), (1.15), Tulczyjew and Dixon succeeded in the derivation of these equations within a manifestly covariant approach [54, 73, 76, 77]. Since the pioneering works trace back to Mathisson and Papapetrou, we will refer to these equations as the MP equations, though [66, 67].

Still, there are less equations than unknown variables so that the system is underdetermined and a spin supplementary condition (SSC) has to be imposed in order to close the set of equations. This implies some arbitrariness in the choice of the supplementary condition and is reflected in the choice of the representative worldline [78]. One might think of getting rid of this ambiguity by switching to the concept of point particles. If the size of the test body goes to zero it should not make any difference which worldline is chosen to represent the particle. However, the concept of a point particle is no longer valid for spinning bodies, as Möller has shown. In the framework of special relativity he deduced that a classical body with spin $S_{\mu\nu}S^{\mu\nu} = 2S^2$ and rest mass $m^2 = -p_\mu p^\mu$ must have a size of $r_0 \geq \frac{S}{m}$ in order not to rotate at superluminal speed [79]. This argument can be transferred to general relativity so that we have to treat spinning particles as extended bodies of finite size in order to be physically relevant. Thus, the problem of the unclosed set of equations in (1.14) and (1.15) can be physically understood by the requirement that the particle must have a finite size which does not make the choice of the reference worldline redundant.

In principle the supplementary condition can consequently be related to the choice of a centre of mass whose evolution is described by the reference worldline seen by an

appropriate observer, see e.g. [58, 80, 81, 82, 83]. Despite being independent of a chosen reference frame in classical mechanics, the centre of mass is no longer covariant in special and general relativity. J. Steinhoff uses a nice visualisation [58] which we adapt here in Fig. 1.2: The centre of mass corresponds to the centre where the mass dipole vanishes. However, if the spinning particle moves with a constant velocity v the part which moves faster appears to be heavier and the one that moves more slowly appears to be lighter. Therefore, the

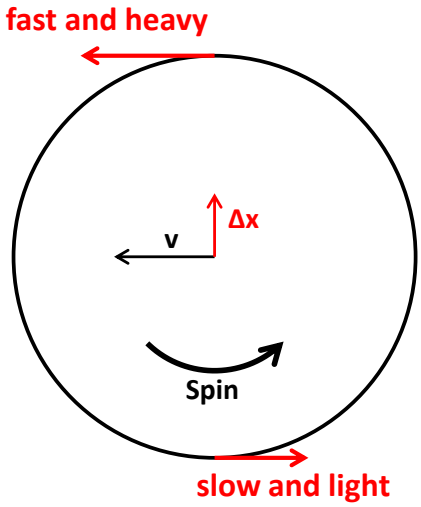

Figure 1.2: The figure shows a spinning particle moving with velocity v. The upper part of the particle appears to move faster than the lower part due to the direction of the particle's spin. Thus the centre of mass is shifted upwards Δx with respect to the centre of mass seen by an observer with zero-3-momentum frame.

particle acquires a mass dipole inducing a shift of the centre of mass Δx compared to an observer with zero-3-momentum. By prescribing a reference worldline within the particle describing its evolution it is always possible to find an observer for whom the reference worldline coincides with the centre of mass. To conclude, the supplementary condition defines not only a reference worldline but also a reference frame in which an observer sees the evolution of the centre of mass.

During the past 70 years, several spin supplementary conditions have been established and are widely used today, see e.g. [9, 74, 75, 80, 81, 83, 1]. Basically, the criteria by which such a supplementary condition is selected are subject to the question one intends to investigate, e.g. certain SSCs are better suited for a canonical formalism than others. Therefore, it is often useful to invest time in the conceptual framework in order to make the best decision for the supplementary condition. We will give a detailed description on the four most popular ones below in section 1.3.2.

Moreover, the necessity of a supplementary condition is also reflected by the fact that

generally the four-momentum p^μ is no longer a rescaling of the velocity u^μ so that by fixing a SSC the relation between those quantities is also defined. Such a relation is not always explicit, though, making analytical computations more complicated. Thus, a possible argument for a choice of a specific SSC might be that it leads to an explicit relation between p^μ and u^μ, see e.g. [32, 84].

Further simplifications of the analysis of a dynamical system are achieved by symmetries, or physically speaking, by constants of motion. The symmetries of the background spacetime can be described by Killing vectors, which we have briefly mentioned in section 1.2.2. If the spacetime in which the particle moves admits a Killing vector ξ, the corresponding constant of motion is given by [70]

$$K = p^\mu \xi_\mu - \frac{1}{2} S^{\mu\nu} \xi_{\mu;\nu} \ . \tag{1.16}$$

In addition, there may exist further non-linear constants of motion that are related to Killing-Yano tensors of the spacetime [85, 86].

As mentioned previously the dynamical system needs a spin supplementary condition in order to be fully determined which is the topic of the following section.

1.3.2 Spin Supplementary Conditions (SSC)

The supplementary condition serves as the choice of a reference point within the spinning extended body whose evolution is described by the equations of motion. From classical mechanics we usually intend to choose the centre of mass as the point of reference. However, in general relativity the centre of mass is no longer the same in every reference frame, i.e. it is not covariant and therefore observer dependent. Nevertheless, it is always possible to find an observer who sees a given representative worldline as being the centre of mass of the spinning particle. More precisely, such a frame is defined by a vanishing mass dipole S^{i0} [58, 83]. This can be expressed in covariant form by

$$S^{\mu\nu} V_\nu = 0 \ , \tag{1.17}$$

with V_μ being a timelike vector corresponding to the four-velocity of the observer who sees the respective reference worldline as being the evolution of the centre of mass. In order to ensure that the reference worldline lies within the body the vector V_μ is required to be timelike [58, 75, 83, 84].

The choice of an SSC is closely related to the ability to find an expression between u^μ and p^μ, which are, in general, no longer parallel to each other, i.e. $p^\mu \neq m u^\mu$ as we know it from geodesic motion. This is the first hint that the motion of a spinning particle does not follow geodesics. Generally, the rest mass m can no longer be considered as a constant

of motion so that we redefine the kinematical mass by [87]

$$p_\mu u^\mu = -m \ , \tag{1.18}$$

corresponding to the mass with respect to the kinematical four-velocity u^μ. Then, we denote the dynamical mass with respect to the four-momentum p_μ by $\mathcal{M}$, satisfying the mass shell constraint

$$p_\mu p^\mu = -\mathcal{M}^2 \ .$$

It contains information on the inner structure of the particle characterised by the spin $S^{\mu\nu}$ and therefore depends on the contributions of the terms obtained by the multipole expansion. In this context a dynamical velocity is defined by [72, 87]

$$v^\mu = \frac{p^\mu}{\mathcal{M}} \ . \tag{1.19}$$

Indeed, $m = \mathcal{M}$ holds only if the tangent vector u^ν coincides with the dynamical four-velocity given in eq. (1.19).

The MP equations do not explicitly state how we can evaluate the tangent vector u^μ throughout the evolution. To find u^μ information from the SSCs is needed. Taking eq. (1.14) and the covariant derivative of eq. (1.17), we obtain an implicit relation between the kinematic momentum and the particle's velocity [53, 88]

$$p^\mu = \frac{1}{V_\nu u^\nu}\left((V_\nu p^\nu)\, u^\mu - S^{\mu\nu}\frac{DV_\nu}{d\tau} \right) \ , \tag{1.20}$$

or, alternatively

$$p^\mu = m\ u^\mu - u_\nu\ \frac{D\ S^{\mu\nu}}{d\tau} \quad , \tag{1.21}$$

by multiplying eq. (1.15) with u_ν.

Moreover, neither of the masses have to be a constant of motion in general. It depends on the relation between p^μ and u^μ which is determined by the SSC. Namely, for the time evolution of m we obtain

$$\frac{dm}{d\tau} = \frac{D\ m}{d\tau} = -\frac{D\ u_\nu}{d\tau}\ p^\nu \quad ,$$

since from eq. (1.14) we see that $\dfrac{D\ p^\nu}{d\tau} u_\nu = 0$, and by using eq. (1.21) for replacing p^ν, we arrive at

$$\frac{dm}{d\tau} = \frac{D\ u_\nu}{d\tau}\ u_\mu\ \frac{D\ S^{\nu\mu}}{d\tau} \quad . \tag{1.22}$$

For the time evolution of the dynamical mass $\mathcal{M}$ we have

$$\frac{d\mathcal{M}}{d\tau} = \frac{D\ \mathcal{M}}{d\tau} = -\frac{p_\nu}{\mathcal{M}}\ \frac{D\ p^\nu}{d\tau} \quad ,$$

and again by using eq. (1.21) for replacing p^ν, it yields

$$\frac{d\mathcal{M}}{d\tau} = \frac{D\ p_\nu}{d\tau}\ \frac{p_\mu}{\mathcal{M}\ \mu}\ \frac{D\ S^{\nu\mu}}{d\tau} \quad . \tag{1.23}$$

In addition to the masses, the spin measure is another scalar quantity given by

$$S^2 = \frac{1}{2}\ S_{\mu\nu}\ S^{\mu\nu} \quad . \tag{1.24}$$

Just as we have seen for the masses the spin measure is also generally not a constant of motion. Its time evolution yields

$$\frac{d\ S^2}{d\tau} = \frac{D\ S^2}{d\tau} = S_{\mu\nu}\ \frac{D\ S^{\mu\nu}}{d\tau} \quad , \tag{1.25}$$

and by eq. (1.14) we obtain

$$\begin{aligned} \frac{d\ S^2}{d\tau} &= S_{\mu\nu}\ (p^\mu\ u^\nu - u^\mu\ p^\nu) \\ &= 2S_{\mu\nu}\ p^{[\mu}\ u^{\nu]} \quad , \end{aligned} \tag{1.26}$$

It is often more useful to work with a spin four-vector S^μ instead of the spin tensor, since this is more physically intuitive and also computationally more convenient than the tensor $S^{\mu\nu}$. The antisymmetry of the spin tensor only allows for six independent spin values which mathematically can be reduced to a usual four-vector [89]. This four-vector resembles the angular momentum vector we know from Newtonian mechanics and therefore is easier physically understood than the tensor. Generally, S^μ depends of course on the SSC, since the spin is always computed with respect to the chosen reference worldline. This dependency is considered for by the four-velocity of the corresponding observer V^μ entering the SSC. Therewith, the spin four-vector is generally defined by [83]

$$S^\mu \quad \propto \quad \eta_{\mu\nu\rho\sigma} V^\nu S^{\rho\sigma} \quad , \tag{1.27}$$

which allows us to formulate the spin measure as

$$S^2 \propto S_\mu S^\mu \ , \tag{1.28}$$

yielding a more intuitive expression than eq. (1.24). The measure of the spin divided by the dynamical rest mass, i.e. $S/\mathcal{M}$ defines the minimal radius of a volume which a spinning body has to have in order not to rotate with a superluminal speed. The same radius defines the upper bound of the separation between worldlines defined by various SSC , i.e. a disc of centres of mass inside of which the worldlines have to lie [83]. This radius was introduced

by Möller in [79], and therefore is often called the Möller radius.

It now depends on the choice of V_μ how the dynamics behave, i.e. whether the masses and/or the spin measure are conserved or the relation between the velocity and the momentum is given explicitly. One of them is the SSC introduced by *Tulczyjew (T SSC)* [54] where V_μ is chosen to be p_μ:

$$S^{\mu\nu} p_\nu = 0 \ . \tag{1.29}$$

It is covariant and has been proven to guarantee the existence and uniqueness of the respective worldline [90, 91, 92]. Also, the relation between u^μ and p^μ has been shown to be manifestly covariant, explicit and unique [88, 93, 94]. The appropriate observer has zero 3-momentum.

In the case of T SSC, u^μ is found via the relations given in eq. (1.20) or eq. (1.21) and results in

$$v^\mu = N\,(u^\mu + w^\mu) \quad , \tag{1.30}$$

where

$$w^\mu = \frac{S^{\mu\nu} R_{\nu\gamma\sigma\lambda}\ u^\gamma\ S^{\sigma\lambda}}{2\ \left(\mathcal{M}^2 + \frac{1}{4} R_{\alpha\beta\gamma\delta}\ S^{\alpha\beta}\ S^{\gamma\delta}\right)} \quad , \tag{1.31}$$

and $N = m/\mathcal{M}$ being a normalisation factor [32, 87, 88]. It depends on the choice of the normalisation of the tangent vector u^μ and therewith on the choice of the worldline parameter. If proper time τ is chosen to be the affine worldline parameter and the velocity is normalised by $u^\mu u_\mu = -1$ we obtain

$$N = \frac{1}{\sqrt{1 - w_\mu\ w^\mu}} \tag{1.32}$$

Therewith it is also guaranteed that the particle follows a timelike path. For more details on how to derive the above expression see, e.g. [87].

Moreover, the T SSC implies some further advantages: Both the particle's dynamical mass $\mathcal{M}$ and the measure of the spin vector in eq. (1.28) are conserved quantities which can easily be seen by the eq. (1.23) and (1.26) using the T SSC from eq. (1.29). Conserved quantities simplify the dynamical problem in particular for analytical investigations and the determination of initial conditions in numerical studies.

As already mentioned, the definition of the spin vector in eq. (1.27) is usually adapted to the chosen SSC and yields for the T SSC

$$S_\mu = -\frac{1}{2} \eta_{\mu\nu\rho\sigma} v^\nu S^{\rho\sigma} \quad , \tag{1.33}$$

where $\eta_{\mu\nu\rho\sigma}$ is the Levi-Civita tensor density $\eta_{\mu\nu\rho\sigma} = \sqrt{-g}\epsilon_{\mu\nu\rho\sigma}$ with $\epsilon_{\mu\nu\rho\sigma}$ as the Levi-Civita Symbol and $\epsilon_{0123} = -1$. The factor $\sqrt{-g}$ ensures the density to be invariant

under coordinate transformations, as we have seen for the volume element in the multipole expansion in eq. (1.13). Moreover, we deduce that

$$S_\mu p^\mu = 0 \quad , \tag{1.34}$$

so that the spin four-vector is perpendicular to the four-momentum. The corresponding inverse relation between the two spin forms is

$$S^{\rho\sigma} = -\eta^{\rho\sigma\gamma\delta} S_\gamma v_\delta \quad , . \tag{1.35}$$

Therewith the spin measure results in

$$S^2 = S_\mu S^\mu \ , \tag{1.36}$$

which becomes a useful relation when performing numerical calculations and comparing the results obtained by two different SSCs or formalisms used to formulate the equations of motion in chapter 3.

Although not being covariant another supplementary condition introduced by *Corinaldesi and Papapetrou (CP SSC)* [80] is

$$S^{i0} = 0 \ , \tag{1.37}$$

closely related to the non-covariant derivation in [67]. It basically states that the mass dipole must vanish in a non-covariant form. It is clearly coordinate dependent and has no meaning until a reference frame is chosen. The reason why it was thought to be a good choice is that it defines the centre of mass of the particle in the rest frame of the central gravitating body [80, 83].

Another one is defined by

$$S^{\mu\nu} u_\nu = 0 \ , \tag{1.38}$$

which appeared in Mathisson's covariant derivation of the equations of motion for a spinning particle subject to this specific supplementary condition [66]. The appropriate observer is comoving with the particle and sits in the rest frame of the particle. Although it provides not a unique choice of representative worldline, as it is dependent on the observer's velocity and therewith on the initial conditions [79], it seems to be the most natural choice of SSC which is the reason why it is often referred to as the *proper centre of mass* [75].

Nevertheless, it was long thought to be unphysical, since it exhibits helical motions in contrast to a straight line in flat spacetime. However, Costa *et al.* [75] showed that it is completely consistent with physics and interpreted the helical motion as some kind of hidden momentum. Actually, these helical motions appear within Möller's work when he

related different centre's of mass by Lorentz transformations in order to define the minimum size of a body with structure in order to prevent a rotation at superluminal speed [79]. It became famous, though, through the work of Pirani in which he showed that the spin tensor undergoes Fermi-Walker transport [95]. That is why it is known under the *Pirani SSC (P SSC)*.

Lastly, the *Newton-Wigner* spin supplementary condition *(NW SSC)* [56, 57] has gained increasing attention during the last decades. In principle, it is a combination of the T SSC eq. (1.29) and P SSC eq. (1.38)

$$S^{\mu\nu}\zeta_\nu = 0 \ , \tag{1.39}$$

with $\zeta_\nu := p_\nu + \mathcal{M} n_\nu$ and n_ν being some timelike vector. Neither the masses, eq. (1.22), (1.23), nor the spin, eq. (1.26), are preserved. Thus, from this point of view it is a strange selection of a SSC. However, we should keep in mind that our framework is a pole-dipole approximation neglecting quadrupole and higher order effects. Attributing the terms that are quadratic in the particle's spin to the quadrupole and higher orders, it is somehow adequate for the just mentioned quantities to be conserved only up to linear order in the spin. For the spin, this can be seen from eq. (1.25) but for the mass $\mathcal{M}$ the proof is quite more complicated and was provided in [53].

In the case of NW SSC, according to our knowledge, there is no explicit expression which gives u^μ as a function of p^μ and $S^{\mu\nu}$. However, we can reformulate the relation in eq. (1.20) to

$$u^\mu = \frac{1}{\zeta_\nu p^\nu}\left((\zeta_\nu u^\nu)p^\mu + S^{\mu\nu}\frac{D\ \zeta_\nu}{d\tau}\right) \ , \tag{1.40}$$

which only provides us with an implicit relation between the four-momentum and the worldline's tangent vector.

Again, the definition of the spin four-vector depends on the observer, i.e. the SSC. Thus, for the NW SSC in eq. (1.39) we define the four-vector as [1]

$$S_\mu = -\frac{1}{2\ \mathcal{M}}\eta_{\mu\nu\rho\sigma}\zeta^\nu S^{\rho\sigma} \ , \tag{1.41}$$

which is combined with the NW SSC and leads to

$$S_\mu \zeta^\mu = 0 \ . \tag{1.42}$$

Thus, the spin four-vector is perpendicular to the timelike vector ζ_μ. In the NW case the inverse relation of eq. (1.41) between the two spin forms is

$$S^{\rho\sigma} = \eta^{\rho\sigma\gamma\delta}\ S_\gamma\ \frac{\mathcal{M}\ \zeta_\delta}{\zeta_\nu\zeta^\nu} \ . \tag{1.43}$$

Then, the spin measure (1.24) reads

$$S^2 = -\frac{\mathcal{M}^2}{\zeta_\nu \zeta^\nu}\, S_\sigma\, S^\sigma \quad . \tag{1.44}$$

In the context of a Hamiltonian formalism one major advantage is that the NW SSC has been proven to lead to canonical spatial coordinates in special relativity [57, 58]. Using the generators of the Poincaré group, which are related to rotations and translations in physics and satisfying the Poincaré algebra, it is possible to show for the reference point x^i and the spin tensor S^{ij} computed around x^i fixed by the NW SSC in eq. (1.39) that the following Poisson bracket relations hold

$$\begin{aligned} \left\{x^i, p_j\right\} &= \delta^i_j \\ \left\{S^{ij}, S^{kl}\right\} &= \delta^{ik} S^{jl} - \delta^{jk} S^{il} - \delta^{il} S^{jk} + \delta^{jl} S^{ik} \end{aligned}$$

where (i, j, k, l) run over the spatial components $(1, 2, 3)$. All other Poisson brackets vanish. Newton and Wigner indeed found that this is the only choice of reference worldline yielding a canonical structure of the variables. Despite the fact that this has not yet been proven to lead to a canonical structure in general relativity, Barausse *et al.* [53] implemented it into their Hamiltonian formalism for a spinning test particle and linearised it in spin which indeed resulted in canonical variables up to linear order in spin. Thus, the NW SSC offers a handy condition when working in the Hamiltonian formulation, which is easiest dealt with in canonical variables.

Part I

The Dynamics of Spinning particles

Spinning particles briefly reviewed

The first part of this thesis deals with the dynamical properties of spinning particles investigated by both numerical and analytical methods. The characteristics of the motion is discussed in terms of the orbital evolution of the particles.

Spinning particles have already been extensively studied in the literature. In particular, the effects and behaviour that are different from geodesic motion. The influence of spin-curvature coupling, especially of spin-orbit and spin-spin coupling, on the spin motion has been discussed in [9, 96, 97, 98, 99, 100, 101] and the resulting orbits are compared to geodesic motion in [30, 81, 99, 100, 102, 103, 104]. Analogies to electromagnetism were found in [55, 78, 105]. Their influence on orbital properties such as the periastron shift, the radius of the innermost stable circular orbit or general classification of orbits are studied in [34, 106, 107] for Schwarzschild and Kerr spacetimes by numerical as well as analytical techniques. Experimental tests were already proposed in the 1960s and 70s in [9, 81, 96] based on the precession frequency of the spin and the orbit which can be interpreted by curvature and gravitomagnetic effects in terms of geodetic precession and frame-dragging. In 2004 the satellite-based mission Gravity Probe B was launched and confirmed the expectations from general relativity, see e.g. [108].

As geodesic motion is integrable in many spacetimes [21, 22, 23], the spin can be treated as a perturbation which leads to the assumptions that the system becomes chaotic. Several studies using numerical techniques such as the Lyapunov exponent, Poincaré sections or effective potential analysis [35, 36, 37, 38] have found good indications for chaotic behaviour in the vicinity of special types of orbits or a certain range of parameter values. Chaos may have a severe impact on gravitational wave signals and the corresponding data analysis.

As EMRIs are supposed to be good candidates for sources of gravitational waves, several studies comitted to the calculation of gravitational radiation emitted by non-spinning as well as spinning particles inspiraling into (non-)rotating black holes using the black-hole perturbation approach [18, 24, 30, 31, 32, 98, 109]. In the adiabatic limit the evolution of the particle can be modeled by a transition through the orbits of the conservative system [17, 19, 110]. In fact, the corresponding waveforms show a distinct feature in the frequency spectrum when the particle passes over from bound orbits, i.e. the inspiral, to plunge

[20, 28, 29]. A theoretical understanding of the relation between the different types of orbits and the gravitational frequencies provides information on possible features in the gravitational wave signal. This is the reason why we are interested in the description of the orbital properties of non-spinning and spinning particles in Schwarzschild-de Sitter spacetime in chapter 2.

The great variety of spin supplementary conditions has been discussed in different contexts. The effects of different SSCs on the coupling terms or the shift of the centre of mass within the body and the corresponding evolution are studied in [9, 58, 81, 83, 99, 111, 112]. While the P SSC and CP SSC were the most favourable ones at first [9, 80, 96, 113] the T SSC became more popular when the opinion was established that the P SSC exhibited unphysical helical motion in flat spacetime [32, 37, 87, 114, 115]. A few years ago, it was shown by Costa *et al.* [75] that the P SSC yields indeed physical solutions as every other SSC. The desire to have a canonical Hamiltonian formalism for spinning particles, though, has increased the attention to the NW SSC [47, 53, 58, 116]. Nevertheless, the properties of the NW SSC and the corresponding evolution of worldlines have not yet been compared to other SSCs in the framework of the MP equations. In order to obtain a better understanding of its characteristics we perform a numerical study to check it against the well understood T SSC in chapter 3.

Chapter 2

Isofrequency Pairing in Schwarzschild-de Sitter Spacetime[1]

The occurrence of *isofrequency pairs* in the strong field regime of the Schwarzschild spacetime was noticed only recently by Barack and Sago [26]. At first, this degeneracy feature may not be much of a surprise. After all, it is known from Newtonian Mechanics that the frequencies of the Kepler ellipses are all degenerate, i.e. the radial and azimuthal frequencies have the same value, see e.g. [117]. This is the reason why the orbits in Newtonian physics are closed.

When general relativistic effects are considered, though, one major difference to Newtonian physics is the periastron shift of bound orbits which are no longer closed. This manifests itself in the non-degeneracy of the frequencies. In the Schwarzschild spacetime we have two independent orbital frequencies, for the radial and for the azimuthal motion. It was long thought that these two frequencies provide another unique parametrisation of the orbits, as an alternative to the ones already known. However, Barack and Sago [26] showed that in the strong field of Schwarzschild spacetime, i.e. in the highly relativistic regime, there exist pairs of timelike geodesics which are described by the same frequencies. In a follow-up study, Warburton, Barack and Sago [39] generalised the isofrequency pairing to the Kerr geometry. In contrast to the Schwarzschild case, timelike geodesics in the Kerr spacetime have three degrees of freedom and even triperiodic partners have been found. As outlined in Refs. [26, 39], the occurrence of isofrequency pairing is of relevance in view of gravitational wave analysis because it implies that, for the case of an EMRI, from the observation of the fundamental frequencies one cannot uniquely determine the shape of the orbit. Shortly after Refs. [26, 39] had appeared, Shaymatov, Atamurotov and Ahmedov [40] investigated the influence of a magnetic field on the orbital frequencies of a charged

[1] This chapter is based on the work published in [2] and parts of it follow closely the lines of [2].

particle moving in Schwarzschild spacetime and found that the region where isofrequency pairing occurs shrinks for high values of the magnetic field.

Apart from the isofrequency pairing, we analyse the properties of bound motion in the frequency picture. Gravitational radiation reaction of an infalling object is, among other approaches, modeled by a transition of the particle through its possible orbits, see e.g. [17]. Therewith, it has been suggested that the homoclinic orbits exhibit a distinct imprint on the gravitational wave spectrum [20, 25, 28, 29]. Thus, the investigation of the boundaries of bound motion, which an infalling particle must cross, in the frequency domain is still of interest for gravitational wave physics.

2.1 A general Characterisation of bound Orbits

First, we focus on the motion of freely-falling test particles. By freely-falling we mean that these particles are not subject to any external forces except for gravity and "test" implies that the particle does not exert any backreaction onto the underlying gravitational field. The curve $x^\mu(\sigma)$, along which such a particle moves, is parametrised by an affine parameter $\sigma = a\tau + b$ and defined by the geodesic equation [6, 7]

$$\frac{d^2x^\mu}{d\sigma^2} + \Gamma^\mu_{\alpha\beta}\frac{dx^\alpha}{d\sigma}\frac{dx^\beta}{d\sigma} \quad = 0 \ . \tag{2.1}$$

Although the corresponding dynamical system suffers from approximations the solutions of the geodesic equation turn out to be very useful for practical applications. One example is the perihelion shift of Mercury which can be calculated using an analytical solution of the geodesic equation and is then compared to observational measurements, see [21, 23]. Therewith we can test Einstein's theory of General Relativity.

As soon as the approximations are given up it becomes harder or even impossible to find an analytic solution so that numerical methods have to be employed. Therewith, numerical errors emerge which may obscure tiny general relativistic effects. Although analytical calculations often use highly simplified situations, they provide a general understanding of general relativistic motion and are able to reveal general relativistic effects which are not necessarily noticed in numerical calculations if they are not expected to show up. Moreover, it is easier to use the analytical approaches to investigate more complex system, which such effects may be transferred to, so that one knows what to look for in numerical results.

The parametrisation of the path by an affine parameter that is merely connected to proper time τ by a linear relation, has been chosen by the requirement that the tangent vector is parallel transported [118]. Nevertheless, we have to be careful when parametrising the path, which can be either spacelike, timelike or null, i.e. $ds^2 > 0$, $ds^2 < 0$ or $ds^2 = 0$, as we have briefly mentioned in the introduction section 1.2. Two events connected by a

spacelike path cannot be in causal contact while a timelike curve links cause and effect to each other. Massive particles will thus follow timelike curves. Null geodesics, on the other hand, describe the motion of light and are also called lightlike geodesics. In order to distinguish these three cases we combine the metric compatibility $g_{\alpha\beta;\mu} = 0$ with the geodesic equation (2.1) and arrive at a conserved quantity

$$\epsilon \;:=\; g_{\mu\nu}\frac{dx^\mu}{d\sigma}\frac{dx^\nu}{d\sigma}\;. \tag{2.2}$$

Choosing the parametrisation of a timelike curve to be proper time τ yields $\epsilon = -1$. Spacelike geodesics are usually parametrised by proper length resulting in $\epsilon = 1$. Notice, that for lightlike geodesics it is not that simple since $ds^2 = -d\tau^2 = 0$ gives $\epsilon = 0$, which is always satisfied and thus does not fix the affine parameter.

2.1.1 Parametrisation

In this work, we are only interested in massive particles so that we will no longer incorporate the other two cases. As an example, we analyse the geodesic equation for massive particles in a Schwarzschild gravitational field, following [7, 23].

First, we fix the path parameter to be proper time by setting $\epsilon = -1$. Secondly, due to the three rotational symmetries and the invariance under time translations we have four conserved quantities corresponding to the three components of angular momentum and the energy. The direction of the angular momentum is consequently fixed and the motion takes place in a plane. Without loosing generality we fix this plane to be the equatorial plane $\theta = \pi/2$. Thus, we have a constant angle θ and can ignore its equation of motion. Using eq. (2.1), the remaining equations of motion yield

$$\begin{aligned} &\tfrac{d^2t}{d\tau^2} + \tfrac{2M}{r^2\left(1-\frac{2M}{r}\right)}\tfrac{dr}{d\tau}\tfrac{dt}{d\tau} &&= 0 \\ \Leftrightarrow \quad &\tfrac{d}{d\tau}\left(\left(1-\tfrac{2M}{r}\right)\tfrac{dt}{d\tau}\right) &&= 0\;, \end{aligned} \tag{2.3}$$

for the time coordinate and

$$\begin{aligned} &\tfrac{d^2\phi}{d\tau^2} + \tfrac{2}{r}\tfrac{d\phi}{d\tau}\tfrac{dr}{d\tau} &&= 0 \\ \Leftrightarrow \quad &\tfrac{d}{d\tau}\left(r^2\tfrac{d\phi}{d\tau}\right) &&= 0\;, \end{aligned} \tag{2.4}$$

for the azimuthal angle. They provide an easy access to two of the constants of motion, the energy $H = \left(1-\frac{2M}{r}\right)\frac{dt}{d\tau}$ and the angular momentum component perpendicular to the plane of motion $J_z = r^2\frac{d\phi}{d\tau}$ both measured in units of the particle's mass m, e.g. $\tilde{J}_z = mr^2\frac{d\phi}{d\tau} \Rightarrow \tilde{J}_z \mapsto mJ_z$. Another approach to obtain these quantities is to use the

Killing vectors ∂_t and ∂_ϕ and apply Killing's equation [6, 7]. In order to characterise the motion it is sufficient to write the equation of motion for the radial coordinate using eq. (2.2) and setting $\epsilon = -1$

$$\left(\frac{dr}{d\tau}\right)^2 = \frac{P_3(r)}{r^3} , \tag{2.5}$$

with

$$P_3(r) = -\left(1 - H^2\right) r^3 + 2Mr^2 - J_z^2 r + 2MJ_z^2 .$$

The general relativistic correction to the Newtonian effective potential is given by the last term of $P_3(r)$, i.e. $2MJ_z^2$ and is responsible for Mercury's perihelion shift.

Physically relevant motion requires the right-hand side of eq. (2.5) to be positive. By investigating the polynomial $P_3(r)$ the kinds of orbits in Schwarzschild spacetime are classified. Making use of the rule of signs by Descartes we deduce that the polynomial can have at most three positive zeroes for $1 - H^2 > 0$ and only two for $1 - H^2 < 0$. In fig. 2.1 the function $P_3(r)$ is shown for an appropriate choice of H and J_z to have three zeros.

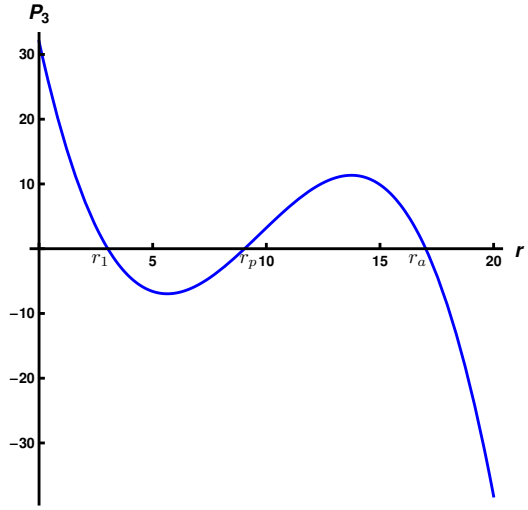

Figure 2.1: The polynomial $P_3(r)$ is plotted for the choice of the following parameters $H = 0.965$, $J_z = 4$ and $M = 1$. It has three positive real zeroes r_1, r_p and r_a. Physical motion is possible for radial coordinates between 0 and r_1 (terminating orbits) as well as between r_p and r_a (bound orbits).

Physical motion is only possible for such radial coordinates where $P_3(r)$ is positive. We see that there exist bound orbits between the two outermost zeros (r_p, r_a) and terminating orbits for radii smaller than the innermost zero r_1. As already mentioned, the shape of the function depends on the values of the coefficients depending on H and J_z, which means

that only for $1 - H^2 > 0$ the motion can be bound. For a more detailed classification of the types of orbits see [23].

It is worth to remark here, that the pair of constants of motion (H, J_z) completely determines the orbit of the particle. Consequently, they serve as a good parameterisation and no further information is needed to characterise the particle's motion. However, they are not accessible by observations so we might consider some other approaches to characterise the orbits. We are solely working with bound orbits, since we will be interested in their radial and azimuthal frequencies. Thus, we ignore any other kinds of orbits in the following discussion. Moreover, we set $r \to rM$ and $J_z \to J_z M$ in further calculations, i.e. we measure the radius and the angular momentum in units of the central mass.

Bound motion requires two turning points in the radial motion with $\left(\frac{dr}{d\tau}\right) = 0$, i.e. they correspond to two zeros of $P_3(r)$. It has already been indicated that bound motion only exists for $1 - H^2 > 0$ allowing for at most three positive real zeroes in the polynomial. Consequently, we rewrite eq. (2.5) as

$$\frac{P_3(r)}{-(1-H^2)} = (r - r_1)(r - r_p)(r - r_a) \equiv V_r \ ,$$

with $0 < r_1 < r_p < r_a$. The radial coordinate of a bound orbit oscillates between the periastron r_p and the apastron r_a so that it is highly suggestive for (r_p, r_a) to be a good parametrisation as well. To check this, we relate the turning points to the constants of motion by expanding V_r and compare its coefficients to the ones in eq. (2.5). The result is

$$\begin{aligned} H^2 &= \frac{(r_a - 2)(r_p - 2)(r_a + r_p)}{(r_a + r_p)\left(r_a r_p - 2\left(r_a + r_p\right)\right) + 2 r_a r_p} \ , \\ J_z^2 &= \frac{2 r_a^2 r_p^2}{(r_a + r_p)\left(r_a r_p - 2\left(r_a + r_p\right)\right) + 2 r_a r_p} \ , \\ r_1 &= \frac{2 r_a r_p}{r_a r_p - 2\left(r_a + r_p\right)} \ , \end{aligned} \tag{2.6}$$

It can be verified that the map from (H, J_z) to (r_p, r_a) is indeed one-to-one confirming the latter to be a permitted parameterisation for bound orbits.

Extreme cases of bound orbits occur when two zeroes merge, i.e. $r_1 = r_p$ corresponding to unstable circular or homoclinic orbits or $r_p = r_a$ corresponding to stable circular orbits. They both mark the boundaries of the region of bound motion in parameter space.

A nice choice for visualisation is given by the parameter pair (p, e) with p being the semi-latus rectum and e the eccentricity. We are familiar with this kind of parameters from the mathematical description of ellipses. Since Johannes Kepler observed that the planets move on ellipses around the sun in Newtonian physics, it is quite common to characterise the orbits in celestial mechanics by (p, e). They can be related to the apastron

and periastron by

$$r_a = \frac{p}{1-e}\,, \qquad r_p = \frac{p}{1+e}\,. \tag{2.7}$$

It is important to stress and to keep in mind that the semi-latus rectum and the eccentricity merely provide a description for bound orbits. By defining the boundaries of bound motion we can only obtain the parameter region allowed to describe bound orbits and cannot make any statement concerning other possible kinds of motion, though.

The merging of the zeroes gives us the equations for the boundaries: First, $r_p = r_a$ corresponds to stable circular orbits, which immediately results in $e = 0$ and an arbitrary p. Secondly, $r_1 = r_p$ results in $p = 6 + 2e$, which is often called the *separatrix,* because it separates the region of bound orbits from the region of unbound orbits. It represents the unstable circular orbits or, and this is important, the homoclinic orbits [24].

In fig. 2.2 the region of bound motion is shown in a (p, e)-diagram for the Schwarzschild spacetime. Here, the domain of bound orbits, corresponding to the region enclosed by the solid blue lines, is infinitely large. The red dashed line on the boundary represents the separatrix. On the separatrix, each point corresponds to a homoclinic orbit from a radius $r_1 = r_p$ to a radius $r_a > r_p$ and back to $r_1 = r_p$. Such a homoclinic orbit has the same constants of motion H and J_z as the unstable circular orbit at $r_1 = r_p$, which it asymptotically approaches; these unstable circular orbits are situated on the horizontal axis ($e = 0$) to the left of the dashed line. The relation between those two kinds of orbits is visualised by the thick red line on the horizontal axis ($e = 0$, unstable circular orbits) and the red dashed line along the separatrix ($e \neq 0$, homoclinic orbits). The upper boundary curve of the region of bound orbits corresponds to parabolic (unbound) orbits with $e = 1$, while the lower boundary is associated to stable circular orbits with $e = 0$. The lower left-hand corner of the region of bound orbits marks the innermost stable circular orbit (ISCO) at $r = 6$ [7]. These features of the domain of bound orbits in the Schwarzschild spacetime have been discussed by other authors before, see [24, 39].

Physically, the relation between the homoclinic and unstable circular orbits can be understood by thinking of the zoom-whirl feature apparent close to the boundary: A particle performs a certain number of revolutions around the unstable circular orbit before it zooms out following an elliptic trajectory described by the non-vanishing eccentricity. Then it comes back to the unstable circular orbit where it whirls around again for some time before zooming out again. The times spent at the equilibrium point depend on how close to the boundary the orbital parameters are. The zoom-whirl feature usually occurs in the vicinity of a separatrix, which is located, in the Schwarzschild spacetime, in the strong field region where the easiest accessible sources of gravitational waves are thought to exist [25, 28]. Thus, having such features in the strong field regime of a black hole might be useful to obtain information on the underlying source by observing the frequencies of

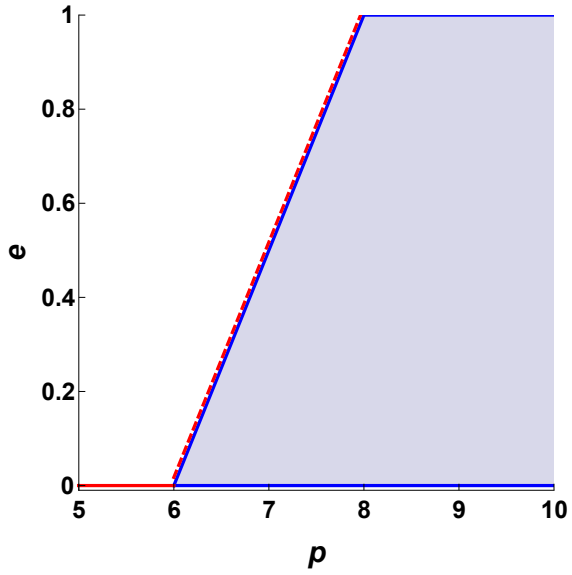

Figure 2.2: The figure presents the region of bound motion in the (p, e) - plane for Schwarzschild spacetime (blue shaded region). The solid blue lines represent the the stable circular orbits $e = 0$, the homoclinic orbits $p = 6 + 2e$ and the parabolic orbits $e = 1$. The unstable circular orbits $e = 0$ are marked by the solid red line. Their relation to the homoclinic orbits is visualised by the dashed red line.

gravitational waves.

2.1.2 Definition of the frequencies

Gravitational wave detectors, although not being successful yet, aim to measure the frequencies of gravitational waveforms [11, 12]. In order to make theoretical predictions for such experiments it is necessary to relate observational features with the quantities we have in our theoretical description. Luckily, we do not have to search very hard. The gravitational frequencies are composed of a number of harmonics of the fundamental frequencies of our dynamical system consisting of the particle's motion around a black hole [16, 110, 119]. Consequently, it is helpful to pass over into the domain of the frequencies to characterise the motion.

The gravitational wave detectors are situated on earth or, if they are in space, close to the earth on astronomical scales. This is far away from the centre of our galaxy, whose black hole serves as a source for the gravitational waves scientists aim to measure. Thus, we define the frequencies in such a way, as they are seen by a static observer at infinity [39]. The corresponding time coordinate is not proper time but simply coordinate time t. In Schwarzschild geometry a general bound orbit exhibits two frequencies: the motion is periodic both in radial and azimuthal direction. Thus, we define the time a massive

particle needs to perform a complete radial revolution by [24]

$$T_r = 2\int_{t(r_p)}^{t(r_a)} dt = 2\int_{r_p}^{r_a} \frac{dt}{dr} dr = 2\int_{r_p}^{r_a} \frac{dt}{d\tau}\left(\frac{dr}{d\tau}\right)^{-1} dr \ , \tag{2.8}$$

where we use the symmetry property of an ellipse. Employing the results from the geodesic equation for $dt/d\tau$ and $dr/d\tau$ from eq. (2.3) and (2.5) we are able to solve the integral. Then the radial frequency is defined by

$$\Omega_r = \frac{2\pi}{T_r} \ . \tag{2.9}$$

In order to determine the azimuthal frequency we take the time the particle needs for a radial revolution as the reference time. Therefore, we calculate the angle the particle covers during a revolution by

$$\Delta\Phi = 2\int_{\phi(r_p)}^{\phi(r_a)} d\phi = 2\int_{r_p}^{r_a} \frac{d\phi}{dr} dr = 2\int_{r_p}^{r_a} \frac{d\phi}{d\tau}\left(\frac{dr}{d\tau}\right)^{-1} dr \ , \tag{2.10}$$

and the corresponding frequency to

$$\Omega_\phi = \frac{\Delta\Phi}{T_r} \ . \tag{2.11}$$

Since $\Delta\Phi$ is not a rational fraction of 2π in general, the orbit is not necessarily closed. This means the angular period does not coincide with the radial one as it does in Newtonian theory and gives rise to the general relativistic periastron shift, which is observable in our solar system, e.g. in the perihelion shift of Mercury.

Observations imply that our universe's expansion is accelerating leading to a positive cosmological constant. The influence of a positive cosmological constant on the dynamics in the frequency picture can be analysed by investigating the motion in Schwarzschild-de Sitter spacetime.

2.2 Motion in Schwarzschild-de Sitter spacetime

Already in the 1920s it has been established that the theory of general relativity leads to a dynamical universe instead of a static one. Hubble, Lemaître and de Sitter were able to describe the dynamics of the Universe as the expansion of spacetime itself [120, 122, 121]. On the other hand, Einstein included the so-called cosmological constant Λ into his field equations to make the universe static, because he did not believe in a dynamical universe at that time keeping with the thinking of contemporary physicists [123]. Later, he is said to have called Λ the "biggest blunder of his life" [124] - although, by adding the

term containing the cosmological constant, he actually made the universe dynamical, just what we observe today. Indeed, in the late 1990s observations of supernovae provided measurements indicating an accelerated expansion corresponding to a positive cosmological constant [125, 126]. Since the source of the acceleration was absolutely mysterious - and still is - scientists invented the theory of dark energy. In order to improve the understanding of the impact of dark energy on general relativistic systems, it is reasonable to include it into our investigation of particle's motion in gravitational fields.

Again, assuming a spherically symmetric mass distribution and the presence of dark energy leads to a gravitational field that is described by the Schwarzschild-de Sitter metric given in eq. (1.5) with eq. (1.7)

$$ds^2 = -\left(1 - \frac{2M}{r} - \frac{\Lambda}{3}r^2\right)dt^2 + \frac{1}{1 - \frac{2M}{r} - \frac{\Lambda}{3}r^2}dr^2 + r^2\left(d\theta^2 + \sin(\theta)^2 d\phi^2\right) \ , \qquad (2.12)$$

in spherical coordinates. Here, we are interested only in the case $\Lambda > 0$.

Thanks to Noether's theorem we immediately deduce that geodesic motion in such a spacetime has four constants of motion or four Killing vectors: they are associated with the energy and the angular momentum vector, two components corresponding to its direction and one to its magnitude. Using the two directional components of the angular momentum we notice that the motion takes place in a plane, which we choose to be the equatorial plane of our coordinate system and set $\theta = \pi/2$. The two constants of motion left are the energy H and the magnitude of the angular momentum which points into the z- direction in our setup, so that we call it J_z.

If the particle's spin is taken into account, further degrees of freedom are added to the system, so that the motion is no longer restricted to the equatorial plane for general spin. However, in the special case of the spin vector being perpendicular to the equatorial plane, the particle does indeed move and stay in this plane.

2.2.1 Non-spinning particles

First, we start with the investigation of the motion of non-spinning particles in order to consider the effects a positive cosmological constant has on the dynamical behaviour of a test particle. The properties of Schwarzschild-de Sitter spacetime, such as the horizon structure and the equations of motion, have been investigated in [21, 127, 128].

Equations of motion

The dynamics of massive non-spinning test particles is determined by the geodesic equation for timelike curves given in eq. (2.1). The spacetime geometry is given by the metric in eq. (2.12). Then the equations of motion, parametrised by proper time τ, for a test particle of

mass m read

$$m^2\left(\frac{dt}{d\tau}\right)^2 = \frac{H^2}{\left(\frac{\Lambda r^2}{3}+\frac{2M}{r}-1\right)^2}\ , \tag{2.13}$$

$$m^2\left(\frac{dr}{d\tau}\right)^2 = H^2+\left(\frac{\Lambda r^2}{3}+\frac{2M}{r}-1\right)\left(\frac{J_z^2}{r^2}+m^2\right)\ , \tag{2.14}$$

$$m^2\left(\frac{d\phi}{d\tau}\right)^2 = \frac{J_z^2}{r^4}\ , \tag{2.15}$$

with H and J_z being two constants of motion to be interpreted as the energy and the angular momentum, respectively. The particle's four-momentum is $p^\mu = m\,dx^\mu/d\tau$ and satisfies the mass shell condition $m^2 = -p_\mu p^\mu$. From hereon we rescale $H \mapsto Hm$ and $J_z \mapsto J_z m$ which is tantamount to setting $m = 1$ in eq. (2.13), (2.14) and (2.15). Then H is dimensionless while J_z has the dimension of a length.

Parametrisation of bound orbits

In order to analyse the different types of orbits it is sufficient to look at eq. (2.14) and require the right-hand side to be positive for physically relevant motion. This is most easily seen when we rewrite the equation in such a way that

$$\left(\frac{dr}{d\tau}\right)^2 = \frac{\Lambda}{3r^3}\,P_5\left(r\right)\ , \tag{2.16}$$

where

$$P_5\left(r\right) = r^5-\left(\left(1-H^2\right)\frac{3}{\Lambda}-J_z^2\right)r^3+\frac{6M}{\Lambda}r^2-\frac{3}{\Lambda}J_z^2 r+\frac{6M}{\Lambda}J_z^2\ . \tag{2.17}$$

As we assume $\Lambda > 0$, the region where $P_5(r) < 0$ is forbidden by eq. (2.16). The number of zeros of $P_5(r)$ determines the types of motion possible for the corresponding values of H and J_z. For positive Λ, there can be at most four positive real zeros as can be derived with the rule of signs by Descartes. In fig. 2.3 the polynomial $P_5\left(r\right)$ is plotted for a particular choice of parameters such that it possesses four positive real zeroes, (r_1, r_p, r_a, r_2) with $r_1 < r_p < r_a < r_2$. Physical motion is possible as long as the polynomial is positive. Thus, in this specific case, we have escaping orbits for radii $r > r_2$, bound orbits oscillating between $r_p < r < r_a$ and terminating orbits for radii $r < r_1$. Changing the parameter values may lead to only two positive real zeros (r_1, r_2) allowing no bound motion but only escaping and terminating orbits. Hence, bound orbits are allowed only when the polynomial has precisely four positive zeros. For other values of H and J_z there will be

escape or terminating orbits or no motion at all. For a more detailed discussion on the classification of orbits see [21].

Since we aim to gain information on the motion within the frequency domain, we concentrate on bound orbits. From eq. (2.14) it is obvious that turning points can exist only at radial coordinates where $f(r) > 0$, with $f(r)$ is given by eq. (1.7). This implies that bound orbits are confined to the region between the two horizons. In particular they do not exist if $\Lambda > (3M)^{-2}$.

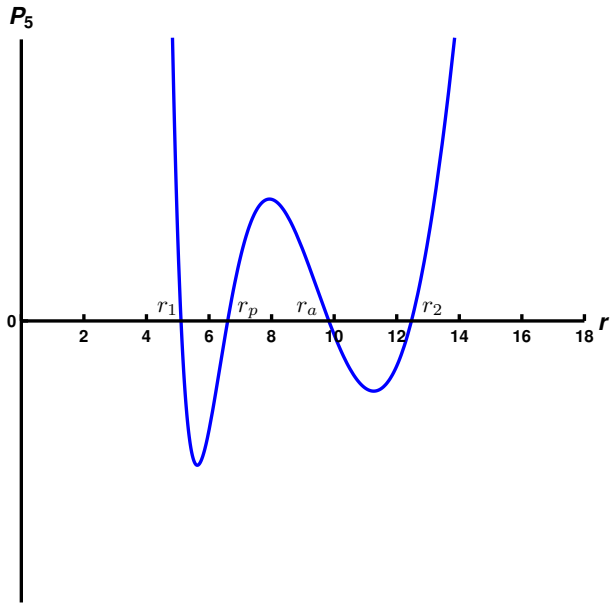

Figure 2.3: The polynomial $P_5(r)$ is plotted for the choice of the following parameters $H = 0.935$, $J_z = 3.420$, $\Lambda = 0.0005$ and $M = 1$. It has four positive real zeroes r_1, r_p, r_a and r_2. Physical motion is possible for radial coordinates between 0 and r_1 (terminating orbits), between r_p and r_a (bound orbits) and between r_2 and ∞ (escaping orbits).

From now on we rescale $r \mapsto rM$, $J_z \mapsto J_z M$ and $\Lambda \mapsto \Lambda M^{-2}$ so that these quantities are dimensionless. (Recall that H already was dimensionless.) This is tantamount to setting $M = 1$ in (2.17). Since we must have four positive real zeros in order to consider bound motion, we can rewrite equation (2.17) as

$$P_5(r) = (r - r_0)(r - r_1)(r - r_p)(r - r_a)(r - r_2) \ , \tag{2.18}$$

with $r_0 < 0$, $0 < r_1 < r_p < r_a < r_2$. Bound motion exists only between r_p and r_a being the two turning points of the radial motion at which $\left(\frac{dr}{d\tau}\right)$ vanishes. Consequently, we are provided with a system of two equations $P_5(r_p) \equiv 0$ and $P_5(r_a) \equiv 0$ which we can solve for H^2 and J_z^2 to obtain

$$H^2 = \frac{\left(\frac{\Lambda}{3}r_a^3 - r_a + 3\right)\left(\frac{\Lambda}{3}r_p^3 - r_p + 3\right)(r_a + r_p)}{r_a^2(r_p - 2) + r_p^2(r_a - 2) - 2r_a r_p} , \tag{2.19}$$

$$J_z^2 = \frac{r_a^2 r_p^2(3 - \frac{\Lambda}{3}r_a r_p(r_a + r_p))}{r_a^2(r_p - 2) + r_p^2(r_a - 2) - 2r_a r_p} . \tag{2.20}$$

By calculating the Jacobian determinant of the transformation from the constants of motion to the radial turning points, it is possible to show that the corresponding map is indeed one-to-one within the region of bound motion. Thus, also (r_p, r_a) provide a unique characterisation of each bound orbit. For further calculations, especially for the integrals appearing in the frequencies, it would be handy, though, to express all zeroes as functions depending on (r_p, r_a). A comparison of the coefficients of the two equations (2.17) and (2.18) yields expressions for r_0 and r_2 dependent on (r_1, r_a, r_p)

$$r_0 = -\frac{1}{2}\left((r_a + r_p + r_1) + \sqrt{R(r_1, r_a, r_p)}\right) ,$$
$$r_2 = -\frac{1}{2}\left((r_a + r_p + r_1) - \sqrt{R(r_1, r_a, r_p)}\right) ,$$

with

$$R(r_1, r_a, r_p) = \frac{12L^2 + \Lambda(r_a + r_p + r_1)\left((r_a + r_p)\left(r_1^2 + r_a r_p\right) + r_1\left(r_a^2 - r_a r_p + r_p^2\right)\right)}{\Lambda\left(r_1(r_a + r_p) + r_a r_p\right)} ,$$

and the equation

$$P_3(r_1) := \Lambda r_a^2 r_p^2 r_1^3 + \Lambda r_a^2 r_p^2(r_a + r_p)r_1^2 + J_z^2(6r_p - 3r_a(r_p - 2))r_1 + 6J_z^2 r_a r_p \equiv 0 ,$$

so that we only have to solve a cubic equation for $r_1(r_p, r_a)$. Now, that we have all zeros as functions of the two radial turning points we will define the parameter space of bound motion which we have to deal with. When two or more zeros of the polynomial in eq. (2.17) merge, the number of zeroes is changed and therewith the kinds of possible orbits. In particular, this means that the number of zeroes of eq. (2.17) is decreased from four to two. While with four zeroes we have three types of orbits only two are allowed with two real positive zeroes. Thus, we can find the relevant region of bound motion by considering the merging of the zeroes or by the condition that the orbit becomes unbound, respectively. As in Schwarzschild spacetime, a merging $r_p = r_a$ physically corresponds to a stable circular orbit. A merging $r_1 = r_p \neq r_a \neq r_2$ corresponds to an unstable circular orbit at r_p and a homoclinic orbit from r_p to r_a and back to r_p, while a merging $r_1 \neq r_p \neq r_a = r_2$ corresponds to an unstable circular orbit at r_a and a homoclinic orbit from r_a to r_p and back to r_a. In the case that $r_1 = r_p \neq r_a = r_2$ we have unstable circular orbits at r_p and

at r_a and heteroclinic orbits from r_a to r_p and from r_p to r_a.

However, before plotting the domain of bound motion we change the parametrisation to the orbital parameters (p, e) because on the one hand they provide an intuitive approach to the orbital structure and therewith a more illustrative analysis of the properties of the test particle's motion and on the other hand they simplify the integrals for the frequencies. Thus, using the relations between the apastron r_a and periastron r_p to the semi-latus rectum p and the eccentricity e from eq. (2.7) we express the constants of motion H and J_z as well as the zeroes of $P_5(r)$ in this parametrisation.

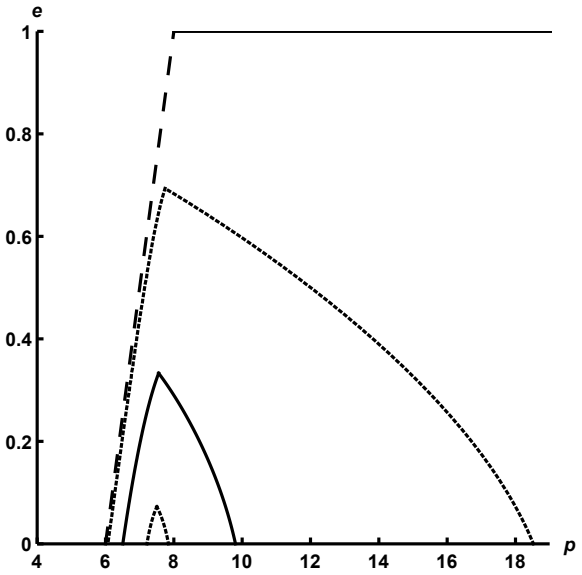

Figure 2.4: The figure presents the boundaries of bound motion in the (p, e) - plane for different values of Λ. The dashed line corresponds to the Schwarzschild case $\Lambda = 0$ with $p = 6 + 2e$. The remaining lines are the separatrices for a cosmological constant of $\Lambda = 0.0001$ (upper dotted line), $\Lambda = 0.0005$ (solid line), and $\Lambda = 0.0006$ (lower dotted line).

In fig. 2.4 the region of bound motion is shown in a (p, e)-diagram for both Schwarzschild and Schwarzschild-de Sitter spacetimes with different values for the cosmological constant. As has been worked out in section 2.1 the domain of bound orbits in Schwarzschild geometry, corresponding to the region that lies right to the dashed line, is infinitely large.

By contrast, in the Schwarzschild-de Sitter spacetime the region of bound orbits in the $(p, e)-$plane is finite. The shape is triangle-like with its tip at an eccentricity $e_{\max} < 1$. This demonstrates that, in this picture, the transition from bound orbits to unbound orbits $(e > 1)$ is not continuous. In particular, it shows that bound orbits with eccentricities higher than a maximal value are not allowed but it does not exclude any other kinds of motion which is not bound. In analogy to the Schwarzschild case, the two sides of the

triangle are called the *separatrices*. They correspond to homoclinic orbits with $r_1 = r_p$ and $r_a = r_2$, respectively. Each homoclinic orbit has the same values for energy and angular momentum as the unstable circular orbit that it approaches asymptotically; these unstable circular orbits can be found on the horizontal axis outside the triangle, cf. fig. 2.2 in the Schwarzschild case. We have already mentioned that in the Schwarzschild spacetime bound orbits near the separatrix show a zoom-whirl behavior, with the "whirling" taking place in the strong-field regime. In the Schwarzschild-de Sitter spacetime with a small positive cosmological constant, the second separatrix gives rise to zoom-whirl orbits that "whirl" near an apastron far away from the centre and periodically "zoom in" to a periastron.

The two separatrices intersect at the tip of the triangle where we have simultaneously $r_1 = r_p$ and $r_a = r_2$. This gives rise to a heteroclinic orbit, i.e. to an orbit that connects two different unstable circular orbits. Such an orbit can be described by a unique pair of values for (p, e). The lower boundary curve of the region of bound orbits corresponds to stable circular orbits ($e = 0$). The two intersection points of the separatrices with the horizontal axis correspond to the innermost stable circular orbit (ISCO) and an outermost stable circular orbit (OSCO). While the ISCO is also present in the Schwarzschild spacetime and merely gets shifted away from the centre with increasing Λ, the OSCO is only existent in the Schwarzschild-de Sitter spacetime where the repulsive force of dark energy is compensated by the attractive gravitational force. For $\Lambda \to 0$ the OSCO approaches infinity. For $\Lambda \to \Lambda_{\text{crit}} = 4/5625$ the ISCO and the OSCO merge into one circular orbit, cf. [127]. Put into mathematical language, this happens if all four positive zeros of (2.17) coincide. For $\Lambda > \Lambda_{\text{crit}}$ bound orbits do not exist.

Let us remark here that Λ_{crit} is much larger than the physically expected one. Observations show evidence for a $\Lambda \approx 10^{-52}\text{m}^{-2}$ [129]. Even for a supermassive black hole with $M \approx 10^{10}$km this corresponds, in our geometrised units, to $\Lambda \approx 10^{-25}$, i.e. to a value that is much smaller than Λ_{crit}. After discussing the effects of a positive cosmological constant we turn our attention to the influences of a non-vanishing spin of the test particle.

2.2.2 Spinning particles

Now, we turn on the spin and investigate the motion of a spinning test particle which is no longer geodesic. The motion of spinning particles in Schwarzschild-de Sitter spacetime has been studied in [88, 130, 131].

Equations of motion

Previously, in section 1.3, the equations of motion of a spinning particle in general relativity have been discussed. They are given by eq. (1.14) and (1.15) and trace mainly back to the works of Mathisson, Papapetrou and Dixon [66, 67, 73, 76, 77]. Different spin

supplementary conditions to close the set of equations have also been presented. Since we are aiming at analytical calculations, we prefer the T SSC, given in eq. (1.29). It yields a unique solution for the evolution of the worldline and provides us with an explicit relation between the kinematical four-velocity u^μ and the four-momentum p^μ. In addition the dynamical mass $\mathcal{M}$ is conserved in the frame fixed by the T SSC in the pole-dipole approximation, see e.g. [1]. Provided the mass shell condition $p_\mu p^\mu + \mathcal{M}^2 = 0$ is satisfied we introduce the dynamical four-velocity $v^\mu = p^\mu/\mathcal{M}$ given in eq. (1.19), [72, 87]. The worldline gauge, i.e. the worldline parameter τ, is fixed by the normalisation condition $v^\mu u_\mu = -1$. Then, $d\tau$ is the time interval along the worldline $x^\mu(\tau)$ as measured in the instantaneous zero-3-momentum frame [72], which matches the choice of the SSC or the observer, respectively. Furthermore, this normalisation implies that the kinematical mass m given in (1.18) is identical to the dynamical mass $\mathcal{M}$, $m = \mathcal{M}$, so that we denote the particle's rest mass in accordance with geodesic motion by m in the following. Subsequently, the relation between u^μ and v^μ is given for the T SSC by eq. (1.30) and the normalisation factor $N = m/\mathcal{M}$ is thus fixed by $v^\mu u_\mu = -1$ to $N = 1$ so that we arrive at [32]

$$u^\mu - v^\mu = \frac{S^{\mu\nu} R_{\nu\gamma\sigma\lambda} v^\gamma S^{\sigma\lambda}}{2\left(m^2 + \frac{1}{4} R_{\alpha\beta\gamma\delta} S^{\alpha\beta} S^{\gamma\delta}\right)} \,. \tag{2.21}$$

Therewith, the equations of motion for a spinning test particle in Schwarzschild-de Sitter spacetime can be derived. Recall that we will restrict ourselves to the special case of a particle moving in the equatorial plane $\theta = \pi/2$, with the spin vector S^μ from eq. (1.33) perpendicular to this plane. Then, we can characterise the spin by the scalar constant of motion S, defined in eq. (1.36) and the property that S is positive if the spin is parallel $(+)$ to the orbital angular momentum and negative if it is anti-parallel $(-)$; for more information on the direction of the spin vector see the appendix in [132]. As in the spinless case, we have a conserved energy H and a conserved angular momentum J_z which we rescale according to $H \mapsto Hm$ and $J_z \mapsto J_z m$. In addition, we now also rescale the spin, $S \mapsto sm$. The resulting equations are calculated from eq. (2.12) and (2.21) as well as the condition for timelike curves $u_\mu u^\mu = -1$ [32] . After appropriate adaption the equations yield

$$\left(\frac{dt}{d\tau}\right) = \frac{H + \frac{f'(r)}{2r} s J_z}{\Pi_s(r)\Sigma_s(r) f(r)} \,, \tag{2.22}$$

$$\left(\frac{dr}{d\tau}\right) = \pm \frac{\sqrt{R_s(r)}}{\Pi_s(r)\Sigma_s(r)} \,, \tag{2.23}$$

$$\left(\frac{d\phi}{d\tau}\right) = \frac{\left(J_z - Hs\right)\left(1 - \frac{f''(r)}{2} s^2\right)}{\Pi_s(r)\Sigma_s(r)^2 r^2} \,. \tag{2.24}$$

Here $f(r)$ is defined in eq.(1.7), the prime denotes partial derivative with respect to r, and

$$\Pi_s(r) = 1 + \frac{\left(f''(r) - \frac{f'(r)}{r}\right)(J_z - Hs)^2 s^2}{2r^2\Sigma_s(r)^3}\,, \tag{2.25}$$

$$\Sigma_s(r) = 1 - \frac{f'(r)}{2r}s^2\,, \tag{2.26}$$

$$R_s(r) = \left(H - \frac{f'(r)}{2r}sJ_z\right)^2 - f(r)\left\{\Sigma_s(r)^2 + \frac{(J_z - Hs)^2}{r^2}\right\}\,. \tag{2.27}$$

Parametrisation of bound orbits

Again we are interested in bound motion, so we require two turning points r_a and r_p where $dr/d\tau = 0$, which corresponds to $R_s = 0$. We rescale, as before, $r \mapsto rM$, $J_z \mapsto J_zM$, $\Lambda \mapsto \Lambda M^{-2}$ and now also $s \mapsto sM$. Notice that for test particle motion our dimensionless spin parameter s necessarily satisfies the condition $-1 < s < 1$. The maximum absolute value that s can attain is estimated by considering the units it is measured in: Remember the spin being measured in units of Mm, i.e. in terms of the mass of the central body and that of the particle $s \to sMm = S$, where s is the unitless value we are using in our equations. Then, think of a rotating compact particle as a Kerr black hole of mass m which has for extremal rotation a spin value $\approx m^2$. Thus, we obtain for the estimation of the spin value $|s| = \frac{|S|}{Mm} = \frac{m^2}{Mm} = \frac{m}{M} < 1$, since in the testparticle limit the mass of the moving object is assumed to be smaller than that of the central body [36, 38]. Subsequently, we can choose values for s between -1 and 1.

Moreover, we substitute

$$L = J_z - Hs\,, \tag{2.28}$$

for mathematical convenience. Then $R_s(r)$ can be rewritten as

$$R_s(r) = \frac{\Lambda\left(1 + \frac{\Lambda}{3}s^2\right)^2}{3r^7}P_9(r) \tag{2.29}$$

where

$$P_9(r) = r^9 + ar^7 + br^6 + cr^5 + dr^4 + er^3 + gr + h \tag{2.30}$$

with

$$a = \frac{\left(H\left(1 + \frac{\Lambda}{3}s^2\right) + \frac{\Lambda}{3}Ls\right)^2 + \frac{\Lambda}{3}L^2}{\frac{\Lambda}{3}\left(1 + \frac{\Lambda}{3}s^2\right)^2} - \frac{3}{\Lambda}\,, \tag{2.31}$$

$$b = \frac{2}{\frac{\Lambda}{3}\left(1 + \frac{\Lambda}{3}s^2\right)}\,, \tag{2.32}$$

$$c = -\frac{L^2}{\frac{\Lambda}{3}\left(1+\frac{\Lambda}{3}s^2\right)^2}\,, \tag{2.33}$$

$$d = -\frac{2\left((L+Hs)^2-s^2\right)}{\frac{\Lambda}{3}\left(1+\frac{\Lambda}{3}s^2\right)} + \frac{2L\left(2L+Hs\right)}{\frac{\Lambda}{3}\left(1+\frac{\Lambda}{3}s^2\right)^2}\,, \tag{2.34}$$

$$e = -\frac{4s^2\left(1+\frac{\Lambda}{4}s^2\right)}{\frac{\Lambda}{3}\left(1+\frac{\Lambda}{3}s^2\right)^2}\,, \tag{2.35}$$

$$g = \frac{s^2\left((L+Hs)^2-s^2\right)}{\frac{\Lambda}{3}\left(1+\frac{\Lambda}{3}s^2\right)^2}\,, \tag{2.36}$$

$$h = \frac{2\,s^4}{\frac{\Lambda}{3}\left(1+\frac{\Lambda}{3}s^2\right)^2}\,. \tag{2.37}$$

The number of zeroes of $P_9(r)$ determines the types of motion possible in the corresponding spacetime. Finding the maximum number of positive real zeroes in this case is not so easy, though, since the signs of a and d are unclear. (The sign of g does not matter because the signs of e and h are already different.) In any case, from the Descartes' rule of sign we find that the number of positive real zeroes can only be 0, 2, 4 or 6.

Actually, it is possible to investigate the characteristics of the orbits by analysing the merging of two zeroes which can be found by solving the system

$$\begin{aligned}\frac{dr}{d\tau} &\equiv 0\\ \frac{d}{dr}\left(\frac{dr}{d\tau}\right) &\equiv 0\end{aligned}$$

resulting in expressions for H and L depending on the radial coordinate r. Physically, they correspond to the circular orbits, either stable or unstable, and mark the boundaries between different types of orbits. If the structure of the corresponding effective potential changes, it should be visible in terms of these boundaries plotted in a (H, L) - diagram. As it is shown in fig. 2.5 the shapes of the boundary lines for different combinations for values of Λ and s covering the range of allowed values (central row and bottom row), look very similar to those of a non-spinning particle moving in Schwarzschild-de-Sitter spacetime , cf. [21]. For comparison the top row shows the region for (non-) geodesic motion in Schwarzschild spacetime in the figure on the left (right). It is obvious that the spin has no influence on the general shape of the region of bound motion but only on the quantitative values of H and L, which is connected to the shift of the ISCO. However, it is important to note here, that the boundary at $H = 1$ results from the coefficients

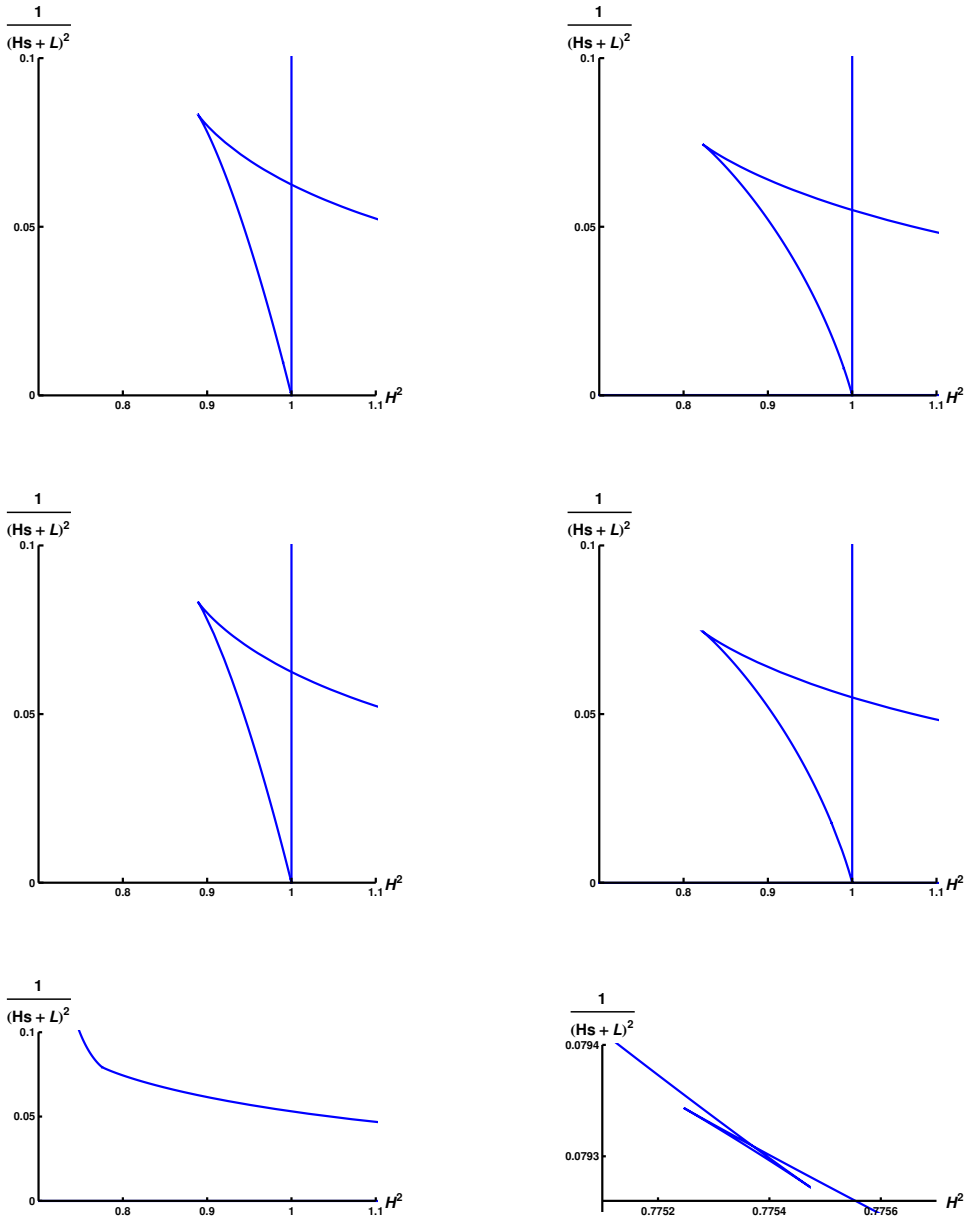

Figure 2.5: Top row: The left figure corresponds to parameter choice of $\Lambda = 0$ and $s = 0$, i.e. geodesic motion in Schwarzschild spacetime. The figure on the right shows the region of bound motion for $\Lambda = 0$ and $s = 1$. Central Row: The left figure corresponds to parameter choice of $\Lambda = 10^{-18}$ and $s = 10^{-5}$. The right figure corresponds to parameter choice of $\Lambda = 10^{-18}$ and $s = 1$. Bottom Row: Both figures correspond to a parameter choice of $\Lambda \approx \Lambda_{\text{crit}}$ and $s = 1$. The figure on the right is zoomed in.

in the polynomial in Schwarzschild spacetime while in Schwarschild-de Sitter spacetime this boundary corresponds to the merging of the two outer zeros ($r_a = r_2$), which is not necessarily restricted to $H = 1$, as we see in the plots in the bottom row. Since the maximal possible value for Λ changes with the value of the spin, the two figures on the bottom are computed with a value for Λ which approaches the associated critical value in the case of $s = 1$. The figure on the right clarifies that also for large Λ and s values the shape of the boundaries remain the same, i.e. no additional lines occur. If the spin is taken to be negative the qualitative picture does not change and the lines get merely shifted.

Each line corresponds to a merger of two zeroes and the region within the small triangles corresponds to parameter values for bound orbits. Since no additional boundary lines emerge, which would correspond to an additional merger of two zeros, we conclude that the three lines provide us with a good indication that we indeed have four positive real zeroes.

Now, we check the signs of the coefficients of the polynomial $P_9(r)$ presented in fig. 2.6. We observe, that within the relevant region in the vicinity of bound motion, the outstanding

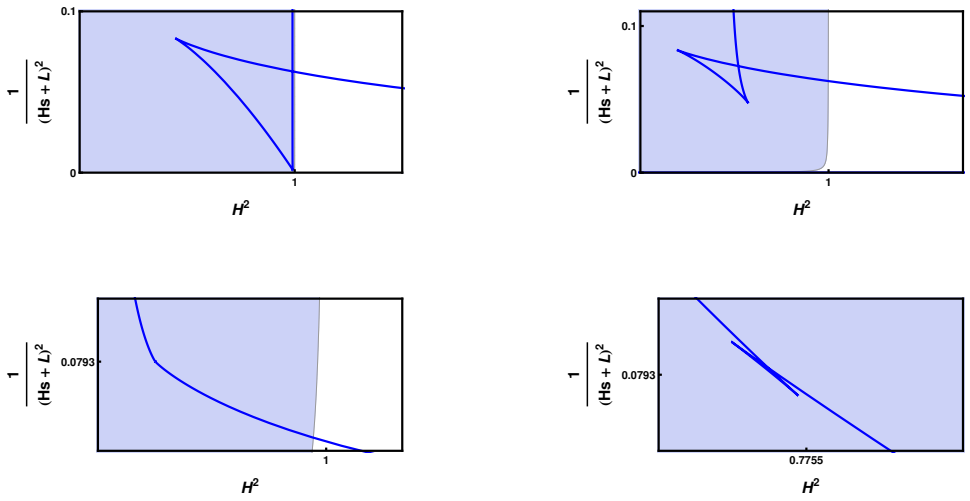

Figure 2.6: The figure shows the region where the coefficients of (2.30) satisfy $a < 0$ and $d > 0$ within the relevant region of bound motion. Top row: The left figure corresponds to parameter choice of $\Lambda = 0$ and $s = 0$, i.e. geodesic motion in Schwarzschild-de Sitter spacetime. The figure on the right shows the region of bound motion for a medium choice for Λ and s, i.e. parameter values that are far away from the allowed limits. Bottom Row: Both figures correspond to a parameter choice of $\Lambda \approx \Lambda_{\text{crit}}$ and $s = 1$. The figure on the right is zoomed in.

coefficients given in (2.30) satisfy $a < 0$ and $d > 0$ which is marked by the blue shaded area in the plots. Subsequently, we have six changes in signs of the coefficients in the polynomial. According to the rule of signs by Descartes, we can have at most six positive real zeroes.

The inspection of the merging of the zeroes, though, showed strong evidence for only four positive real zeroes, which means, that two non-real complex conjugate zeroes substitute the two missing positive real zeroes. Even if the absolute spin value is increased to large values and/or the value of the cosmological constant is varied, the qualitative picture does not change. Thus, it is justified that we can assume the polynomial to have four positive real zeroes, shown in fig.(2.7) for an appropriate choice of parameters.

Again, in order to consider bound motion we must have at least four positive real zeros. We argue that in this case eq. (2.30) can be written as

$$P_9\left(r\right) = (r-r_\gamma)(r-r_\beta)(r-r_\alpha)(r-r_1)(r-r_p)(r-r_a)(r-r_2)(r-r_I)(r-\bar{r}_I)\ , \quad (2.38)$$

with $r_\gamma < r_\beta < r_\alpha < 0$, $0 < r_1 < r_p < r_a < r_2$ and r_I, $\bar{r}_I$ being the non-real complex zero and its conjugate, respectively. Bound motion exists only between r_p and r_a. Since also for the spinning particle the motion is fully described by the parameters r_a and r_p, we find expressions for $H\left(r_p, r_a\right)$ and $L\left(r_p, r_a\right)$ by setting $R_s\left(r_p\right) = R_s\left(r_a\right) \equiv 0$. With the help of the relation (2.7) they are converted to $H(p,e)$ and $L(p,e)$.

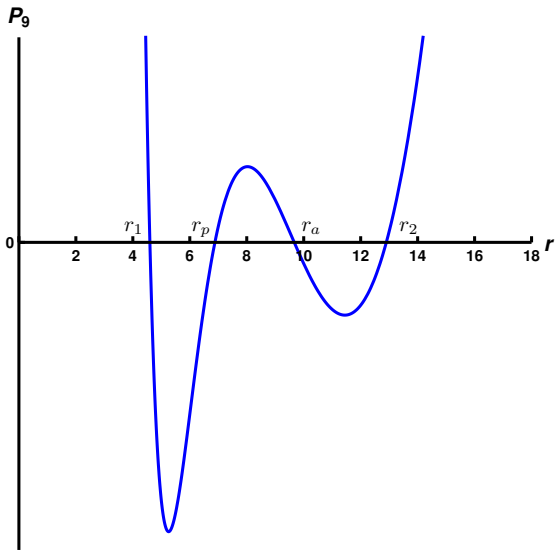

Figure 2.7: The polynomial $P_9(r)$ is plotted for the choice of the following parameters $H = 0.935$, $J_z = 3.394$, $\Lambda = 0.0005$, $s = 0.1$ and $M = 1$. It has four positive real zeroes r_1, r_p,r_a and r_2. Physical motion is possible for radial coordinates between 0 and r_1 (terminating orbits) , between r_p and r_a (bound orbits) and between r_2 and ∞ (escaping orbits).

The next task is to find the boundaries of the region of bound motion in the (p,e) - plane, i.e. the separatrices. As already mentioned the boundaries are given by the merging of the

zeroes, $r_1 = r_p$ or/and $r_p = r_a$ or/and $r_a = r_2$. Unfortunately, the explicit expressions for the zeroes are not as easily found as in the non-spinning case. But there is a way around: We simply exploit the fact that the values of H and L for the homoclinic orbits (i.e. the ones with non-vanishing eccentricity) are identical to the ones for the unstable circular orbits which they approach asymptotically. Having access to the values of H and L for circular orbits by solving

$$R_s(r) \equiv 0 \ ,$$

and

$$R_s'(r) \equiv 0 \ ,$$

the only computation needed is to find the intersection point of the lines of constant H and constant L in the (p, e)-plane. In this way we obtain the values for p and e of the homoclinic orbits corresponding to the separatrices.

In fig. 2.8 the region of bound motion is shown in a (p, e) - diagram for both a spinning particle and a non-spinning particle moving in Schwarzschild and Schwarzschild-de Sitter spacetime. Here, we have fixed the cosmological constant either to $\Lambda = 0$ or to $\Lambda = 0.0005$

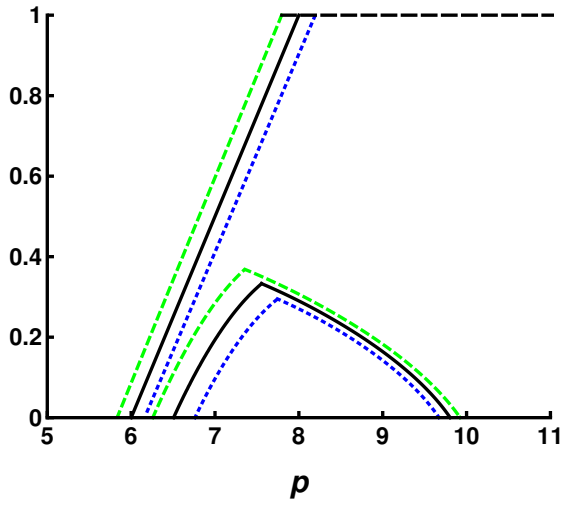

Figure 2.8: The figure presents the regions of bound motion in the (p, e)-plane for different values of s for $\Lambda = 0$ as well as $\Lambda = 0.0005$. The straight lines on the left correspond to $\Lambda = 0$ and the triangles on the right correspond to $\Lambda = 0.0005$. In either case, the (green) dashed line corresponds to $s = 0.1$, the black solid line to $s = 0$, and the (blue) dotted line to $s = -0.1$.

and varied the value of the spin parameter.

From fig. 2.8 we read that for a spinning particle in Schwarzschild spacetime the region of bound motion is infinitely large as it is for geodesic motion. The well-known shift of the ISCO due to the spin is visible, such that for positive spin it is moved inwards and

for negative spin outwards, cf. [31] and also [34, 106]. This reflects the coupling of the particle's spin to its orbital angular momentum. If they are parallel to each other, the resulting force is repulsive, while it is attractive if they are anti-parallel [31, 35]. Notice that the upper boundary is given by $e = 1$ which corresponds to parabolic orbits and marks the transition from bound motion to unbound orbits. The general shape of the separatrices resembles the one for non-spinning particles in Schwarzschild spacetime.

When a positive cosmological constant is considered, the value of the maximal eccentricity becomes smaller for negative and larger for positive spin. Correspondingly, the critical value of Λ is also shifted: for positive spin Λ_{crit} is bigger than for the spinless case and for negative spin it is smaller. The dependence of Λ_{crit} on the spin is shown in fig. 2.9.

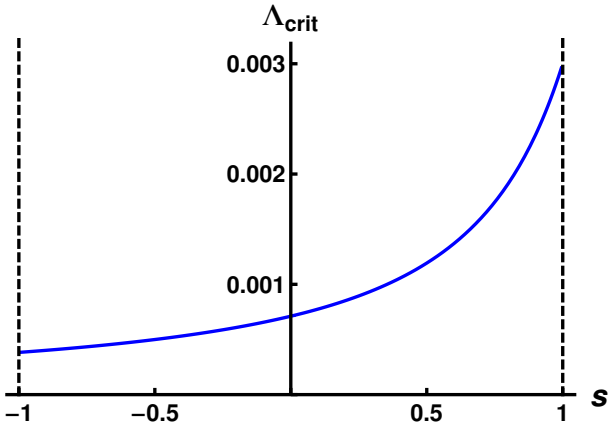

Figure 2.9: The figure presents the evolution of the critical values of Λ with respect to the spin parameter. It monotonically increases with the spin. The boundaries $s = -1$ and $s = 1$ are due to physical restrictions.

It reveals that for $\Lambda < \Lambda_{\text{crit}}(s = 0) = 4/5625$ bound motion is possible for all positive spin values but not for all negative spin values. This is the reason why for our particular choice of $\Lambda = 0.0005$ it is not possible to have bound orbits with spins that are smaller than ≈ -0.5. As soon as the chosen value of Λ drops below $\Lambda_{\text{crit}}(s = -1) \approx 0.0004$ bound motion is possible for all spin values $-1 < s < 1$.

The influence of the spin on the ISCO in the Schwarzschild-de Sitter spacetime is similar as in the Schwarzschild spacetime. Again we see that for positive spin parameters the ISCO gets shifted towards the centre and for negative spin parameters away from the centre. For the OSCO it is the other way around. By taking into account these two characteristics as well as the shift of the maximal eccentricity, it can be immediately seen that the region of bound orbits becomes smaller for negative spin and gets larger for positive spin.

One might think that a large positive spin is somehow able to destroy the existence of the heteroclinic orbit sitting at maximal eccentricity. However, even if the spin is chosen

to have its maximal value of 1, the shape of the region of bound motion does not change. The triangle survives and with it the heteroclinic orbit. If Λ approaches zero the maximal eccentricity goes to 1 and the OSCO to infinity, for any spin value. In this case the separatrix resembles the one of Schwarzschild, only shifted closer to the centre for $s > 0$ and farther away from the centre for $s < 0$.

2.3 The dynamics in the frequency domain

After having defined the region of bound orbits, we continue with the calculation of the frequencies. As mentioned before, observations of gravitational waves will provide access to the frequencies of the underlying dynamical system, such as EMRIs. In order to draw inferences from the measured gravitational waveforms about the source it is necessary to have a theoretical understanding of the system as detailed as possible. So far, the dynamical properties have rarely been investigated in terms of the system's frequencies. One reason may be, that it was long thought that the frequencies merely provide yet another unique parametrisation. Barack and Sago [26], though, observed that for bound orbits of spinless test particles in the Schwarzschild spacetime the transformation from the constants of motion H and J_z to the radial and azimuthal frequencies becomes degenerate in the highly relativistic regime. This means there exist physically distinct orbits which have the same pair of frequencies giving rise to new characteristic quantities by which a dynamical system can be described. We are curious about what happens to the degeneracy if we alter the system a little by including a positive cosmological constant Λ and then adding the particle's spin.

2.3.1 Non-spinning particles

We start with the geodesic motion in Schwarzschild-de Sitter spacetime. The frequencies are already defined in (2.8) - (2.11). From equations (2.13)-(2.18) we obtain:

$$T_r = 2\,H\sqrt{\frac{3}{\Lambda}}\int_{r_p}^{r_a}\frac{r^2 dr}{f(r)\sqrt{rP_5(r)}}\,, \tag{2.39}$$

$$\Delta\Phi = 2\,L\sqrt{\frac{3}{\Lambda}}\int_{r_p}^{r_a}\frac{1}{\sqrt{rP_5\,(r)}}dr\,. \tag{2.40}$$

with $f(r)$ given in (1.7) and $P_5(r)$ from eq. (2.17). In correspondence with our choice of units in the previous sections we rescale $\Omega_r \to \Omega_r M^{-1}$ and analogously $\Omega_\phi \to \Omega_\phi M^{-1}$. As the polynomial $rP_5\,(r)$ under the root in the denominator of the integrand is of order 6, the integral is of hyperelliptic type, which cannot be integrated in terms of elementary functions.

If we use, as before, the (p, e) parametrisation of the bound orbits, we may substitute the integration variable r in (2.39) and (2.40) according to

$$r = \frac{p}{1 + e\cos\chi} \ , \tag{2.41}$$

where the new integration variable χ is the relativistic anomaly. Then the boundary values of the integral change to 0 and π.

Since we want to compare the frequencies of different orbits we choose in analogy to Warburton *et al.* [39] the (Ω_ϕ, e) parametrisation for our analysis of bound orbits, which we are allowed to do, because Ω_ϕ monotonically decreases with p if the eccentricity is held fixed. In order to do this we have to deal with several obstacles. First, we cannot analytically invert the integral of Ω_ϕ to obtain p as a function of e and Ω_ϕ. To circumvent this hindrance the value for e is fixed in the integral for the frequency, so that the value for p can be computed using a root-finding method for any allowed Ω_ϕ. In this way we obtain the value for p for any given e and Ω_ϕ; that is to say we numerically acquire a function $p\left(\Omega_\phi, e\right)$. Hence the radial frequency can also be written as a function $\Omega_r\left(p\left(\Omega_\phi, e\right), e\right) = \Omega_r\left(\Omega_\phi, e\right)$ and we are able to plot contour lines for constant Ω_r into a (Ω_ϕ, e)-diagram. The advantage of this parametrisation is, that it connects the frequency domain with the orbital parameters so that conclusions on the shape of the orbit can be drawn just by looking at the properties of the parameter space for any given pair of frequencies.

Secondly, we encounter problems close to the separatrices. Both T_r and $\Delta\Phi$ diverge making it numerically challenging to perform the integration for the calculation of the frequencies close to the separatrices. Luckily, there exists an approximation scheme for hyperelliptic integrals developed by Sochnev in 1968 based on the approximation of irrational numbers by rational ones [133].

Approximation of hyperelliptic integrals according to Sochnev

First, we rewrite the integrals of (2.39) and (2.40) with the substitution

$$r \to \frac{(r_a + r_p) + (r_a - r_p)x}{2} \ , \tag{2.42}$$

to obtain

$$T_r = A(r_p, r_a, \Lambda) \int_{-1}^{1} \frac{V_t(x)}{\sqrt{V_r(x)}} dx \ , \tag{2.43}$$

$$\Delta\Phi = B(r_p, r_a, \Lambda) \int_{-1}^{1} \frac{1}{\sqrt{V_r(x)}} dx \ , \tag{2.44}$$

where $V_t(x)$ is a rational function whose denominator has no zeroes in the integration interval and

$$V_r(x) = (1-x^2)(1+k_1x)(1+k_2x)(1+k_3x)(1+k_4x) \ , \tag{2.45}$$

with

$$\begin{aligned} k_1 &= \frac{r_a - r_p}{r_a + r_p} \ , \\ k_2 &= \frac{r_a - r_p}{(r_a - r_0) + (r_p - r_0)} \ , \\ k_3 &= \frac{r_a - r_p}{(r_a - r_1) + (r_p - r_1)} \ , \\ k_4 &= -\frac{r_a - r_p}{(r_2 - r_a) + (r_2 - r_p)} \ , \end{aligned}$$

which satisfy $0 \le k_2 \le k_1 \le k_3 \le 1$ and $-1 \le k_4 \le 0$. If we get close to the separatrices, either k_3 or $-k_4$ approach 1. The equation (2.45) provides the basis for the approximation scheme developed by Sochnev [133] to be applied.

He based the method on the approximation of irrational functions by rational ones. In particular, the irrational function $c = \sqrt[m]{c_1c_2...c_m}$ can be approximated by the sequences $\{a_n\}$ and $\{b_n\}$ which are defined iteratively by

$$a_1 = \frac{c_1 + c_2 + ... + c_m}{m} \ , \qquad b_1 = \frac{c_1c_2...c_m}{a_1^{m-1}} \ , \tag{2.46}$$

and

$$a_{n+1} = \frac{(m-1)a_n + b_n}{m} \ , \qquad b_{n+1} = \frac{a_n^{m-1}b_n}{a_{n+1}^{m-1}} \ , \tag{2.47}$$

for $n \ge 1$. While $\{a_n\}$ approaches c from above, $\{b_n\}$ comes from below, i.e. $a_1 > a_2 > ... > a_n > c > b_n > ... > b_2 > b_1$, and their common limit for $n \to \infty$ is c.

Let us consider a specific example related to our problem of hyperelliptic integrals. The irrational function $\sqrt[m]{1+kx}$ with $|k| < 1$ is finite for $-1 < x < 1$. These boundaries become important when we consider the boundaries of the integrals. According to Sochnev, we can approximate this function by choosing $\sqrt[m]{1+kx} = \sqrt[m]{c_1c_2...c_m}$ with $c_1 = 1 + kx$ and $c_2 = c_3 = ... = c_m = 1$ and evaluating the sequences $\{a_n\}$ and $\{b_n\}$ within the defined range of x. In this way we approximate our irrational function by rational ones.

This method can be used for evaluating our hyperelliptic integrals in (2.43), (2.44) where $m = 2$. To that end we have to approximate the function $\sqrt{V_r(x)}$ where $V_r(x)$ is given by eq. (2.45).

If the absolute values of the k factors are far away from one, the procedure goes like this: First, we extract the factor $(1-x^2)$ out of the radicand, arrange the remaining factors

in decreasing order in the absolute values of the ks and group the terms of positive and negative ks. Then, we form subgroups with $m = 2$ elements within each group, where we supplement a factor of one when there are less than $m = 2$ elements in a subgroup, i.e.

$$\sqrt{V_r(x)} = \sqrt{1-x^2}\,\sqrt{(1-k_3x)(1+k_1x)}\,\sqrt{(1+k_2x)\cdot 1}\,\sqrt{(1+k_4x)\cdot 1}\ , \tag{2.48}$$

Now, we are able to compute the approximating sequences $\{a_n\}$ and $\{b_n\}$ for each subgroup up to arbitrarily high order in n, always resulting in a rational function. Consequently, the integral that has to be solved can be approximated by integrals of the form

$$\int_{-1}^{1} R\left(x, \sqrt{1-x^2}\right) dx\ ,$$

where $R\left(x, \sqrt{1-x^2}\right)$ denotes a rational function of x and $\sqrt{1-x^2}$. Using any of the three Euler substitutions or elementary transformations, which rearrange the form of the integral into tabulated ones, the integral can be solved in terms of elementary functions.

This gives a good approximation scheme as long as the absolute values of all ks are far away from one. However, we are interested in the frequencies close to the separatrices corresponding to absolute values close to one for either k_3 or k_4. Luckily, only a few modifications to the procedure are necessary to adapt it to this case.

To begin with the integrals in (2.43) and (2.44) are divided into two integrals, where one runs from -1 to 0 and the other from 0 to 1. In addition, it is not the factor $(1-x^2)$ that is extracted. Consider eq. (2.45) rewritten as

$$(1-x)(1+x)(1+k_3x)(1+k_1x)(1+k_2x)(1+k_4x)\ ,$$

where the k factors are already arranged in decreasing order in their absolute values and $(1-x^2)$ is rewritten as $(1+x)(1-x)$. In the first integral (from -1 to 0) the product $(1+x)(1+k_3x)$ is taken out where k_3 is the greatest of the positive coefficients k_i leading to

$$\int_{-1}^{0} \frac{dx}{\sqrt{(1+x)(1+k_3x)}\,\mathcal{A}(x,k_1,k_2,k_4)}\ ,$$

where $\mathcal{A}(x,k_1,k_2,k_3) = \sqrt{(1+k_1x)(1+k_2x)(1-x)(1+k_4x)}$ has to be approximated by the same procedure as explained above. The second integral (from 0 to 1) is rearranged in such a way that it yields

$$\int_{0}^{1} \frac{dx}{\sqrt{(1-x)(1+k_4x)}\,\mathcal{B}(x,k_1,k_2,k_3)}\ ,$$

with $\mathcal{B}(x,k_1,k_2,k_3) = \sqrt{(1+x)(1+k_3x)(1+k_1x)(1+k_2x)}$. Here, the factor $(1+k_4x)$

is pulled out together with $(1-x)$ because k_4 is the greatest of the negative coefficients k_i. Again, the remaining function is approximated resulting in a rational function in x. Therefore we obtain for our integral an approximation of the form

$$\int_{-1}^{0} \frac{R_1(x)dx}{\sqrt{(1+x)(1+k_3x)}} + \int_{0}^{1} \frac{R_2(x)dx}{\sqrt{(1-x)(1+k_4x)}}$$

the solution of which can be found in terms of elementary functions. In order to simplify the calculations further we may apply partial fraction decompositions to each of the rational functions providing us with the approximation of the integrals in eq. (2.43) and (2.44) in terms of elementary integrals

$$\int_{-1}^{0} \frac{1}{(1+a(k_1,k_2,k_4)x)\sqrt{(1+x)(1+k_3x)}}dx \ , \tag{2.49}$$

$$\int_{0}^{1} \frac{1}{(1+b(k_1,k_2,k_3)x)\sqrt{(1-x)(1+k_4x)}}dx \ . \tag{2.50}$$

It is worth to mention here, that the first iteration, $n=1$, from above, i.e. a_1, is sufficient in order to obtain satisfying results for the frequencies. More precisely, as we have a fraction of two hyperelliptic integrals in the azimuthal frequency in eq. (2.11) the difference between the results obtained on the basis of a_1 and b_1 is of order 10^{-5}. Since we are not aiming at making any quantitative statements, the accuracy of a_1 suffices for our purposes.

Isofrequency Pairing

Consequently, the frequencies close to the separatrix can be expressed in terms of elementary functions. Now, we have the tools we need to analyse the behaviour of the frequencies in the region of bound motion. In fig. 2.10 the region of bound orbits is shown in the (Ω_ϕ, e)-plane. It is the shape of this region that is striking. It looks no longer like a triangle but more like a trapezoid. The tip of the triangle is stretched out to a straight line at $e_{\max}$. In the (p,e)-representation the heteroclinic orbit must correspond to a single point – the tip of the triangle – since it has a uniquely defined pair (r_p, r_a). By contrast, the azimuthal frequency is not uniquely defined for the heteroclinic orbit. Note that the original definition of the frequencies is valid only within the region of bound orbits. On the boundaries, that is at the separatrices, the frequencies are defined only by a continuous extension, which assigns unique frequencies to the homoclinic orbits. However, in the case of the heteroclinic orbit the value of Ω_ϕ depends on how the orbit is approached, i.e. it depends on the characteristics of the orbits in its vicinity. This is the reason why the heteroclinic orbit is stretched out to a straight line in the (Ω_ϕ, e)-diagramm.

In order to physically understand this line we recall the zoom-whirl feature close to

separatrices. This has already been discussed in [20, 28] for homoclinic orbits in the

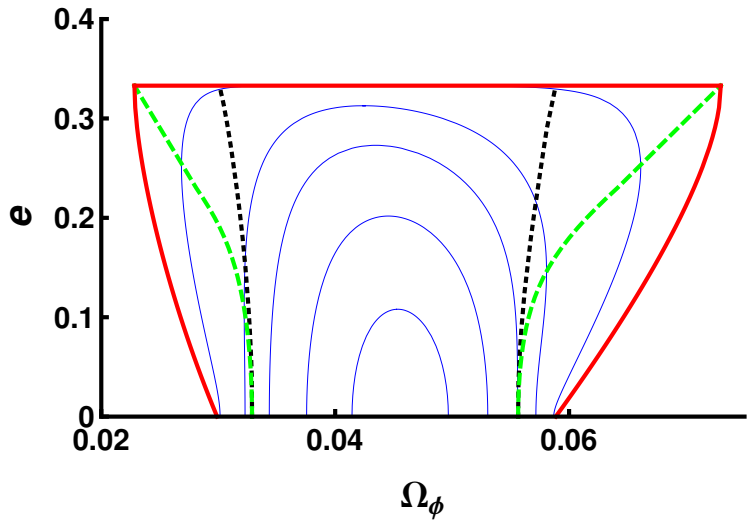

Figure 2.10: The figure depicts the phenomenon of isofrequency pairing for bound orbits in the (Ω_ϕ, e)-plane for a fixed $\Lambda = 0.0005$. The thick (red) boundary lines correspond to the separatrices and confine the region of bound motion. The (blue) solid lines inside this region correspond to constant values of Ω_r. The (green) dashed line represents the singular curve, i.e. the locus where the Jacobian determinant of the transformation from (p, e) to (Ω_r, Ω_ϕ) vanishes. The Circular Orbit Duals (COD), marking the boundary of the domain where isofrequency pairing occurs, is shown by the dotted black line.

Schwarzschild and Kerr geometry. The endpoints of the straight line in fig. 2.10 correspond to orbits that start at a maximal (minimal) radius and approach a circular orbit with radius $r_1 = r_p$ ($r_a = r_2$) without zooming out (or in) again. A highly probable explanation is the following: In-between these endpoints lie orbits that connect the two equilibrium points and exhibit the zoom-whirl property, e.g. an orbit starting at the inner circular orbit performs a certain number of revolutions before zooming out to the outer circular orbit and again whirls around for some time before zooming back again. Depending on the times spent at each equilibrium point the azimuthal frequency changes. Such a bound orbit could be called a "whirl-whirl orbit", because it periodically changes between a large number of whirls near its apastron and a large number of whirls near its periastron.

Close to the heteroclinic orbit, these zoom-whirl features should be observable by computational simulations. Although not connecting equilibrium points the periastron and apastron (r_p, r_a) of an orbit located in the vicinity of the heteroclinic orbit approach the values $(r_{p_{htcl}}, r_{a_{htcl}})$ and it depends on the location in the (Ω_ϕ, e) - diagram, whether the periastron gets closer to $r_{p_{htcl}}$ or the apastron gets closer to $r_{a_{htcl}}$. We stress here again, that if a representation in terms of Ω_ϕ is chosen, the heteroclinic orbit does not contract to one single point, but reveals the hidden characteristics of heteroclinic orbits in the frequency

domain.

The main property we are interested in is the isofrequency pairing. This phenomenon is easily seen in the diagram close to the two separatrices. Looking at a contour line for $\Omega_r =$ constant near one of the separatrices, we see that it has two intersection points with a contour line for $\Omega_\phi =$ constant, i.e. with a vertical line in this diagram. Since these intersection points correspond to orbits of different eccentricities, we conclude that there exist two geometrically distinct orbits with the same pair of frequencies. In mathematical terms this means that the transformation from the frequencies (Ω_r, Ω_ϕ) to (p, e) is not one-to-one. In order to prove this degeneracy it is sufficient to show that the Jacobi determinant

$$J = \left| \frac{\partial (\Omega_r, \Omega_\phi)}{\partial (p, e)} \right| , \tag{2.51}$$

becomes singular somewhere within the region of bound orbits. In fig. 2.10 these singular points can be found as the points where the tangents to the contour lines of $\Omega_r =$ constant become vertical. This happens along the two (green) dashed curves in fig. 2.10 which are called the *singular curves*. To verify that J does have two zeroes close to $e = 0$, one may perform a Taylor expansion of J about $e = 0$ up to first order,

$$J = \frac{e P_{10}(p)}{4p^4 \sqrt{p\left(\frac{\Lambda}{3}p^3 - 1\right)} \left(\frac{\Lambda}{3}p^3 - p + 2\right) \left(\frac{\Lambda}{3}(4p - 15)p^3 - p + 9\right)^{3/2}} + O(e^2)$$

with

$$\begin{aligned} P_{10}(p) = {} & 15\Lambda^3 p^{10} - 50\Lambda^3 p^9 + 30\Lambda^2 p^8 - 315\Lambda^2 p^7 + 9\Lambda(80\Lambda - 1)p^6 - 45\Lambda p^5 + 918\Lambda p^4 \\ & - 2241\Lambda p^3 + 108p^2 - 1053p + 2322 \ . \end{aligned}$$

Numerically one finds that the tenth order polynomial $P_{10}(p)$ has precisely two positive real zeros lying withing the allowed range of p values for bound motion, for all $0 < \Lambda < \Lambda_{\rm crit} = 4/5625$.

The isofrequency pairs lie on opposite sides of one of the singular curves, i.e. each orbit that is located between a separatrix and a singular curve has a partner orbit on the other side of the corresponding singular curve, which is geometrically different but has the same pair of frequencies. The regions where isofrequency pairing occurs are bounded by the so-called "Circular Orbit Dual" (COD) curves which are represented by the black dashed lines. A point on a COD curve corresponds to an orbit that has the same frequencies as a stable circular orbit situated between one of the singular curves and the corresponding separatrix.

Interestingly, the isofrequency pairs do not only occur in the strong field regime as in

Schwarzschild (or Kerr) spacetime, such as in [26, 39, 40], but also far away from the centre where the gravitational field becomes weak so that the dynamics can be approximated by Newtonian physics. In Schwarzschild geometry the orbits resemble Kepler ellipses with degenerate frequencies in the weak field, where the lines of constant radial frequency become almost vertical in the far field leading to the degenerate frequencies (Ω_r, Ω_ϕ). In the case of a positive cosmological constant the boundary of bound motion is not extended to infinity which means it has a finite distance represented by the OSCO. The smaller the value for Λ is chosen the closer it approaches infinity but it always stays finite. However, in the region far away from the centre the gravitational field becomes weak and Newtonian physics can be applied. Indeed, one can check that such an OSCO exists in Newtonian theory. Therefore it would be interesting to analyse the behaviour of the frequencies concerning the isofrequency pairing in a Newtonian background.

While we could read from fig. 2.4 how the ISCO radius, the OSCO radius and the maximal eccentricity depend on Λ, fig. 2.10 gives us information on the frequencies of bound motion. A quite interesting property is the existence of a maximal radial frequency. Although this feature is also present in the Schwarzschild geometry, it provides us with a method to compare different spacetimes, such as universes with different cosmological constants. From fig. 2.10 we observe that the lines of constant Ω_r have the shape of semicircles which become smaller in the centre of the diagram. The value of Ω_r varies between $\Omega_r = 0$ on the separatrices and a maximal value when the semicircle is contracted to just one single point. A parametric plot of the maximal value of Ω_r against p is shown

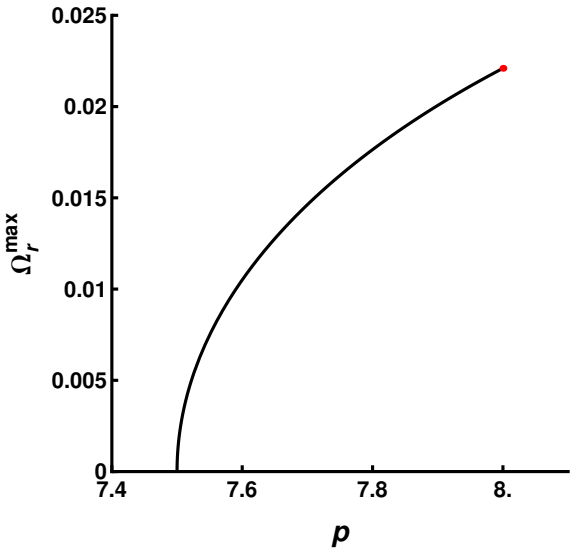

Figure 2.11: The figure shows the change of $\Omega_r^{\max}$ as well as in value as in position from the centre when the value of Λ is varied. The dot marks the Schwarzschild case with $\Lambda = 0$. Along the solid black line Λ increases up to its maximal value $4/5625$ when $\Omega_r^{\max}$ vanishes.

in fig. 2.11, where the parameter is the cosmological constant. As Ω_r takes its maximal value on the axis $e = 0$, i.e. for the limiting case of a circular orbit, p is the same as the radius coordinate.

The bold red point corresponds to the Schwarzschild case which yields the largest $\Omega_r^{\max}$ at $p = 8$. As soon as the cosmological constant is turned on both the values $\Omega_r^{\max}$ and the distance from the centre decrease. At $p = 7.5$ we reach the maximum value for $\Lambda = \Lambda_{\text{crit}} = 4/5625$ which also confines the region of bound orbits outside of which it does not make sense to define a radial frequency. Hence, the maximal radial frequency allows us to compare different dynamical systems and the inclusion of different types of properties, such as the spin of the particle or a rotating black hole, might change its behaviour, too.

Moreover, we can read from fig. 2.11 that the presence of a positive cosmological constant introduces another kind of degeneracy. Notice that $\Omega_r^{\max}$ decreases slightly when Λ is slightly increased. Transferring this change to fig. 2.10 we can think of the lines of constant Ω_r getting shifted towards the centre. Imagine that we have a frequency pair close to the right separatrix. Choose the outer contour line of $\Omega_r =$ constant and let some vertical line of constant Ω_ϕ intersect it twice and mark these two points. As described above, they are two orbits with the same frequencies. If the cosmological constant is changed a little bit the line of constant Ω_r gets shifted either to the right if Λ is reduced, or to the left if Λ is amplified. However, we would still have two intersection points with the vertical line representing the azimuthal frequency we have fixed before. If Λ is reduced the two intersection points diverge while for amplified Λ the intersection points approach one another, i.e. their eccentricities change. This means that infinitely many physically distinct pairs of orbits have the same frequencies as the originally fixed one if we allow the cosmological constant to take values in a certain interval.

Still, our description in terms of geodesic motion in Schwarzschild-de Sitter spacetime is a quite simple one and more realistic situations have further properties that should be considered. We have seen that the introduction of a cosmological constant into the geodesic equations of motion introduces a second region far away from the centre where isofrequency pairing occurs. As can be observed by simply watching the motion of the planets in our solar system, most astrophysical objects rotate and therefore possess a non-vanishing spin. Thus, it seems natural to ask what kind of influence the spin has on this degeneracy feature, i.e. what happens if the motion is non-geodesic.

2.3.2 Spinning particles

As before, we are interested in the influence of a particle's spin on its motion and dynamical properties. When considering the motion of spinning particles in Schwarzschild-de Sitter spacetime, we parametrised bound orbits by the orbital parameters p and e, which was the

most intuitive one. In the following, we change from this parametrisation to the frequency domain. This will allow us to discuss the phenomenon of isofrequency pairing. We have already seen that the inclusion of a cosmological constant leads to additional isofrequency pairs in the weak field limit. Now, we are interested in the influence of a particle's spin on its motion and dynamical properties.

The frequencies have been defined in eq. (2.9) and (2.11) and from equations (2.22) - (2.24) we obtain:

$$T_r = 2\sqrt{\frac{3}{\Lambda}}\int_{r_p}^{r_a}\frac{\tilde{V}_t^s(r)}{\sqrt{rP_9\left(r\right)}}dr\,, \tag{2.52}$$

$$\Delta\phi = 2L\sqrt{\frac{3}{\Lambda}}\int_{r_p}^{r_a}\frac{\tilde{V}_\phi^s(r)}{\sqrt{rP_9\left(r\right)}}dr\,, \tag{2.53}$$

with $P_9(r)$ given in (2.30) and

$$\tilde{V}_t^s(r) = \frac{r^2\left[H\left(r^3+\left(\frac{\Lambda}{3}r^3-1\right)s^2\right)+\left(\frac{\Lambda}{3}r^3-1\right)sL\right]}{\left(-\frac{\Lambda}{3}r^3+r-2\right)\left(1+\frac{\Lambda}{3}s^2\right)}\,, \tag{2.54}$$

$$\tilde{V}_\phi^s(r) = \frac{r^2\left(r^3+\left(\frac{\Lambda}{3}r^3+2\right)s^2\right)}{\left(r^3+\left(\frac{\Lambda}{3}r^3-1\right)s^2\right)\left(1+\frac{\Lambda}{3}s^2\right)}\,. \tag{2.55}$$

The order of the polynomial $rP_9\left(r\right)$ under the root in the denominator of the integrand is 10. Therefore we now have a considerably more difficult kind of hyperelliptic integral than in the spinless case.

Following the same procedure as for the non-spinning particle, we transform the integrals with the relation in (2.41) to obtain the resulting frequencies as functions of (p, e). Therewith, we are able to reparametrise the radial frequency, again, as a function of (Ω_ϕ, e) so that the comparison of different orbits and their frequencies is simplified. Since the inclusion of the spin does not make the system easier to be solved, we encounter the same numerical problems as before, i.e. the numerical inversion to $p(\Omega_\phi, e)$ and the divergencies close to the separatrices, as we have in the non-spinning case. Luckily, these problems can be tackled by the same method, only the expressions become more complicated.

Approximation of hyperelliptic integrals according to Sochnev

Employing Sochnev's approach of approximating hyperelliptic integrals we rewrite the integrals of (2.52) and (2.53) with the substitution given in (2.42) to obtain

$$T_r = A^s(r_p, r_a, \Lambda, s)\int_{-1}^{1}\frac{V_t^s(x)}{\sqrt{V_r^s(x)}}dx\,, \tag{2.56}$$

$$\Delta\phi = B^s(r_p, r_a, \Lambda, s) \int_{-1}^{1} \frac{V_\phi^s(x)}{\sqrt{V_r^s(x)}} dx \,, \tag{2.57}$$

where $V_t^s(x)$ and $V_\phi^s(x)$ are rational functions whose denominators have no zeroes in the integration interval and

$$\begin{aligned} V_r^s(x) &= (1-x^2)(1+k_1x)(1+k_2x)(1+k_3x)(1+k_4x)(1+k_5x)(1+k_6x) \\ &\quad \times (x-(a_I+ib_I))\,(x-(a_I-ib_I)) \ , \end{aligned} \tag{2.58}$$

with

$$\begin{aligned} k_1 &= \frac{r_a - r_p}{r_a + r_p} \ , \\ k_2 &= \frac{r_a - r_p}{(r_a - r_1) + (r_p - r_1)} \ , \\ k_3 &= -\frac{r_a - r_p}{(r_2 - r_a) + (r_2 - p_2)} \ , \\ k_4 &= \frac{r_a - r_p}{(r_a - r_\alpha) + (r_p - r_\alpha)} \ , \\ k_5 &= \frac{r_a - r_p}{(r_a - r_\beta) + (r_p - r_\beta)} \ , \\ k_6 &= \frac{r_a - r_p}{(r_a - r_\gamma) + (r_p - r_\gamma)} \ , \end{aligned}$$

which satisfy $0 \le k_6 \le k_5 \le k_4 \le k_1 \le k_2 \le 1$ and $-1 \le k_3 \le 0$. As in the non-spinning case, we employ Sochnev's method for evaluating these integrals near the separatrices.

Similar to the motion of the non-spinning particle, we have to evaluate the integrals (2.56) and (2.57), i.e. we have to approximate the function $\sqrt{V_r^s(x)}$ with $V_r^s(x)$ given by (2.58). It is convenient to treat the two non-real zeros and the real zeroes separately. Since

$$\sqrt{(x-(a_I+ib_I))\,(x-(a_I-ib_I))} \ ,$$

is a real-valued irrational function it is possible to approximate it by Sochnev's method leading to

$$\sqrt{(x-(a_I+ib_I))\,(x-(a_I-ib_I))} \to \left(\frac{r_a - r_p}{2} - a_I\right)\left(1 + \frac{r_a - r_p}{r_a + r_p - 2a_I}x\right) \ ,$$

in first approximation a_1 from above, which proves to be of sufficient accuracy for our purposes. Therewith, the remaining terms

$$\sqrt{(1-x^2)(1+k_1x)(1+k_2x)(1+k_3x)(1+k_4x)(1+k_5x)(1+k_6x)} \ ,$$

can be approximated analogously to the non-spinning case. Here, close to the separatrices either k_2 or $-k_3$ approaches 1, and the approximation only contains elementary integrals, which, after partial fraction decomposition, reduce to integrals of the form

$$\int_{-1}^{0} \frac{dx}{(1+a_s(k_1,k_2,k_4)x)\sqrt{(1+x)(1+k_2x)}}\,,$$
$$\int_{0}^{1} \frac{dx}{(1+b_s(k_1,k_2,k_3)x)\sqrt{(1-x)(1+k_3x)}}\,, \tag{2.59}$$

so that the frequencies in (2.9) and (2.11) are expressed in terms of elementary functions.

Isofrequency Pairing

In fig. 2.12 plots of the isofrequency pairing phenomenon for particles with two different spin values $(0.1, -0.1)$ moving in the same Schwarzschild-de Sitter spacetime with $\Lambda = 0.0005$ are shown.

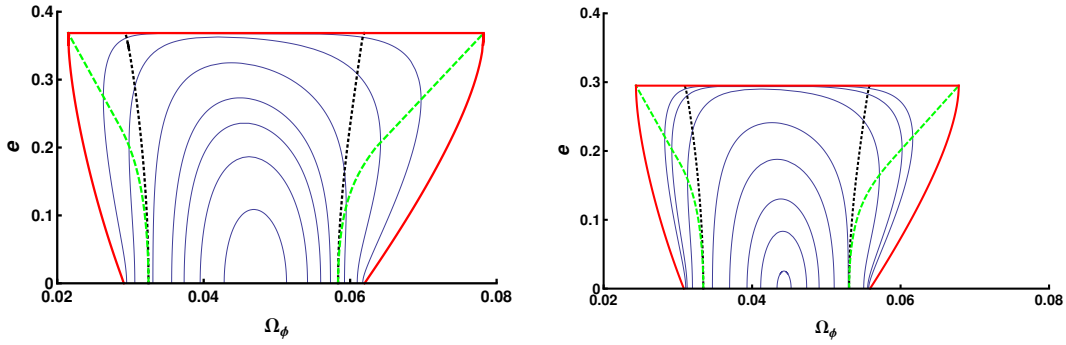

Figure 2.12: The figure depicts the phenomenon of isofrequency pairing for bound orbits in the (Ω_ϕ, e)-plane for a fixed $\Lambda = 0.0005$. The figure on the left shows the characteristics for $s = 0.1$ and the one on the right corresponds to $s = -0.1$. The thick (red) boundary lines correspond to the separatrices and confine the region of bound motion. The (blue) solid lines inside these regions coorespond to constant values of Ω_r. The (green) dashed line represents the singular curve, i.e. the locus where the Jacobian determinant of the transformation from (p, e) to (Ω_r, Ω_ϕ) vanishes. The Circular Orbit Duals (COD) marking the boundaries of the domains where isofrequency pairing occur are shown by the black dotted lines.

The qualitative shape of the region of bound motion is similar to that of a non-spinning particle. The quantitative differences become apparent in the characteristic features of bound motion and its boundaries. Some basic facts that we have already seen in the (p, e)-diagram are obvious, such as the shifts of the maximal eccentricity, of the ISCO and of the OSCO. However, what interests us is the impact on the domain, where isofrequency pairing occurs and the question of whether further degeneracies due to the spin emerge.

First, we qualitatively compare the size of the region, where isofrequent orbits exist. It can be characterised by the azimuthal frequency at the ISCO (OSCO) and the one at the intersection of the COD line with the horizontal axis. Only orbits having an azimuthal frequency within this range do have isofrequent partners. The size of the allowed frequency interval decreases if the spin is chosen to be negative and increases if the spin value is positive. Although the region shrinks for negative spin, it will never completely vanish as long as bound motion exists. Therefore, the spin does not destroy this degeneracy in the fundamental frequencies of the orbital motion.

Next, we compare the evolution of the maximal radial frequency for different spin values in fig. 2.13. We notice immediately the shift of the entire curve closer to the centre for

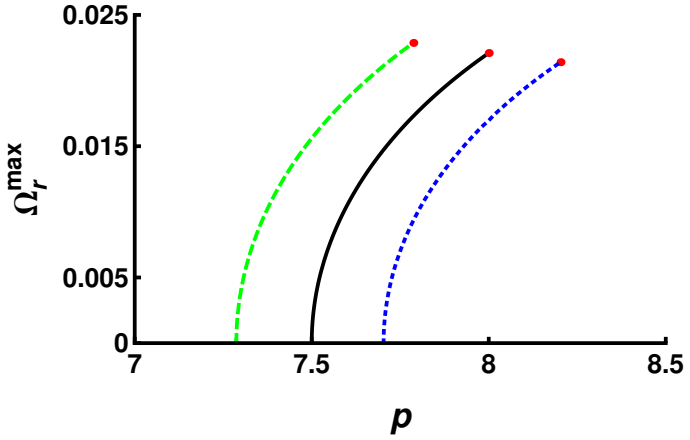

Figure 2.13: The figure shows the change of $\Omega_r^{\max}$ in value as well as in position from the centre when the value of Λ is varied. The (red) dots mark the Schwarzschild case with $\Lambda = 0$. Along each curve Λ increases up to its maximal value when $\Omega_r^{\max}$ vanishes. The black solid curve corresponds to $s = 0$, the (green) dashed one to $s = 0.1$ and the (blue) dotted one to $s = -0.1$.

positive spin and further away for negative spin values. This coincides with the trend of the shifts of the ISCO and OSCO. We also see the spin dependence of the value for $\Omega_r^{\max}$ for $\Lambda = 0$ (bold dots). More generally, if we choose a value for $\Omega_r^{\max}$ on the vertical axis and determine the intersection points with the three curves, not only the position differs but also the corresponding Λ is different for the distinct systems.

We will now investigate if the spin induces a further degeneracy in the sense that isofrequency pairs with different spin values may have the same frequencies. Indeed, we can deduce this from fig. 2.12. Choose a line of constant radial frequency that lies in the isofrequency range. Then draw a line of constant azimuthal frequency that corresponds to a circular orbit located outside the range between the ISCO and the OSCO and mark the two intersection points. We know from the analysis of Ω_r^{max} that the maximal radial frequency

increases with positive spin and decreases with negative spin, keeping the cosmological constant fixed. Now, imagine the line of constant Ω_r shrinking and spreading slowly for small negative and positive values for the spin parameter, respectively. The two intersection points will diverge for positive spin and approach one another for negative spin leading to six different orbits that have different eccentricities. For example, if the initial intersection points belong to a non-spinning particle and the spin is slightly changed to positive or negative values, there exist infinitely many physically distinct pairs of orbits having the same frequencies but different spin values. Even the spin direction is different in this example. If we allow both the cosmological constant and the spin parameter to vary we get two-parameter families of isofrequency pairs with the same frequencies, parametrised by (Λ, s).

It is now natural to ask whether these results are astrophysically relevant. It is true that the considered values for Λ and s in this work are much bigger than the ones expected from real astrophysical situations. Indeed, small spin values in the range of 10^{-4} in our units are expected to be realistic for the compact objects in our Universe, see e.g. [36]. However, as indicated, the qualitative picture does not change.

2.4 Discussion

In this chapter we investigated the characteristics of isofrequency pairing for both geodesic motion of a test particle and the non-geodesic motion of a spinning test particle moving in Schwarzschild-de Sitter spacetime. In contrast to the case without a cosmological constant, there exist *two* regions in the domain of bound orbits where isofrequency pairing occurs. More precisely, it is not only the strong field regime that exhibits such a feature but also a region close to the outermost stable circular orbit. Since the OSCO already appears in Newtonian physics it would be interesting to check whether the isofrequency pairing can also be predicted within this theory.

Generally, adding a cosmological constant and/or the spin leads to the emergence of additional degeneracies in the frequencies. This occurs already for arbitrary small values of the cosmological constant and the spin. At least in principle, this additional degeneracy is of relevance in view of gravitational wave data analysis. Here we may think of an EMRI, which, among all possible gravitational wave sources, is the closest physical realisation of the dynamical system considered here. Whenever isofrequency pairing occurs, knowledge of the fundamental frequencies alone does not determine the shape of the orbit, i.e. additional information on the spectrum has to be taken into account.

The most obvious plan for follow-up work would be to consider spinning particles that are not restricted to the equatorial plane but allow for more general motion. Then future studies should be devoted to more general spacetimes, such as the Kerr-de Sitter-NUT...

spacetime. Note that for a rotating black hole new features occur, such as precession of the particle's orbit outside the equatorial plane and the precession of the spin vector - even if we still restrict to motion in the equatorial plane with the spin perpendicular to this plane. Then we have three vectors (the orbital angular momentum of the particle, the spin of the particle and the spin of the black hole) which can be mutually parallel or anti-parallel. This will make the discussion of possible degeneracies more complicated. In addition, there are several other avenues for future studies on isofrequency pairing which we would like to mention briefly.

From a theoretical point of view isofrequency pairing is of relevance in view of perturbation techniques. For example, in order to use KAM theory for perturbed integrable systems, certain non-degeneracy conditions have to be satisfied. The simplest version of these non-degeneracy conditions is obviously violated if there is a degeneracy in the frequencies such that other, more complex or more restrictive, conditions have to be tested. To mention another example, the feature of isofrequency pairing and the occurrence of a singular curve can be used to compare different approaches to the general relativistic two-body problem, as it was already mentioned in [39]. Methods such as the effective-one-body approach or the post-Newtonian approximation can profit from the isofrequency pairing and its related characteristics.

Also from a theoretical point of view, it is an interesting question to ask if there are spacetimes, where three or more orbits with the same frequencies exist. In all examples treated so far there are only isofrequency pairs. (Here we are referring to the situation that all the parameters of the dynamical system have been fixed which means fixing Λ and s.) As an attempt to find a candidate for isofrequency triples one could start with a Bertrand spacetime and perturb it a little bit. Bertrand spacetimes, which were introduced in [134], are spherically symmetric and static spacetimes in which the ratio of the radial frequency and the azimuthal frequency is a constant rational number q for all bound orbits, so they show the same total degeneracy of the frequencies as the Kepler problem but now with $q \neq 1$. We are planning to search for isofrequency triples etc. in future work.

Another interesting feature, which we came across in our study, is the heteroclinic orbit, which we cannot assign a single azimuthal frequency to. Physically, this can be explained by the zoom-whirl feature connected to the presence of the separatrices. Since a well-established approach for the computations of gravitational radiation emitted by EMRIs uses the progression through orbits, the modeled particle has to cross the separatrices or homoclinic orbits at some point in order to plunge into the black hole [17, 20]. Thus, such a particle experiences the zoom-whirl orbits during the transition and it has been suggested that the zoom-whirl feature exhibits a distinct signal in the gravitational radiation signal [28, 29]. Since the heteroclinic orbit is no longer a single point in the frequency domain,

which is the accessible picture by gravitational wave observations, but a stretched line covering a whole range of azimuthal frequencies, it might be possible that the imprint of such a heteroclinic orbit is also visible in the waveforms and differs somehow from the ones obtained by the homoclinic orbits.

In conclusion, we stress that a non-vanishing spin and a positive cosmological constant have their impacts on isofrequency pairing. Both quantities add degeneracies in the frequency picture instead of destroying them. The cosmological constant gives rise to a heteroclinic orbit, which might be visible in the gravitational radiation. Future work may focus on the imprint of such orbits on gravitational waveforms.

Chapter 3

Numerical comparison of two supplementary conditions: T SSC & NW SSC [1]

The description of spinning particles relies on the definition of the centre of mass, i.e. the SSC. As we have seen in section 1.3.2 the spin supplementary conditions are in some sense arbitrary. In principle, we can choose any point within the body by choosing the appropriate SSC and follow its evolution by solving the MP equations. In other words, the observer, who sees this particular point as the object's centre of mass, changes if another point within the body is considered. Physically though, the dynamics should not depend on the selection of the reference worldline corresponding to a gauge choice. The supplementary condition fixes this gauge. Nevertheless, for each SSC we have a different worldline and hence, each SSC prescribes a different evolution of the MP equations, see e.g. [83]. But although this ambiguity appears to be a major issue in the modelling of an EMRI binary system, the difference in the evolution caused by different supplementary conditions has not yet received the adequate attention.

In order to compare the evolution of different SSCs we have chosen to investigate the motion of a spinning particle moving in Kerr spacetime given by eq. (1.8) described by the MP equations and supplemented with two different SSCs [1]. Since most of the astrophysical objects rotate, it is reasonable to assume that black holes possess a non-vanishing spin, which is why we have chosen a rotating black hole as the gravitating body.

Then, we have decided to analyse the T SSC and to compare it with the NW SSC. The T SSC has been widely used in the past and is so far the only supplementary condition, whose existence and uniqueness in the determination of the reference worldline has been

[1] This chapter is based on the work published in [1]

rigorously proven [90, 91, 92]. Moreover, it yields an explicit relation between the four-velocity and the four-momentum simplifying the numerical treatment. It therefore provides a good, robust and well understood reference worldline, which the results using the NW SSC are compared with.

Secondly, we have chosen the NW SSC, since it is the most promising supplementary condition within the Hamiltonian formalism as it leads to a canonical structure. In addition, it has been successfully implemented in the framework of the PN approximation, see e.g. [58, 116]. Compared to the T SSC the NW SSC is neither unique, since it depends on the four-velocity of the observer, nor does it yield an explicit relation between the particle's velocity and momentum. This implicit relation makes it numerically more challenging to integrate the equations of motion for such a reference worldline.

The next question would be how the comparison of the two worldlines can be performed. Usually the discussion about the transition between two different SSCs is based on the centre of mass worldline displacement, which leads to a shift in the value of the spin tensor as well as to a shift of the initial point in configuration space [58, 81, 83]. This treatment assumes just one and the same body and its centre of mass as seen by different observers. If the starting point, though, already differs at the very beginning, the initial situations are completely different from each other and their evolutions cannot be compared. Therefore, we employ another approach for our investigation. Namely, we require the two orbits to start at the very same point in configuration space, i.e. at the same point in spacetime. This means that both of the different corresponding observers see the centre of mass lying the same place, even if the SSCs are different. More precisely, we do not attempt to change the observer and analyse the shift of the centre of mass of one particle. The two observers may see different particles but with coinciding centres of mass. If the internal structure of the particles has an impact on their dynamical evolution, we expect the resulting worldlines to be different from each other, since they are two distinct particles. However, if the influence is small and the geodesic limit is approached, they should coincide. As a measure of the influence of the internal structure we choose the value of the spin.

3.1 Initial Conditions

The equations of motion of a particle with dynamical mass $\mathcal{M}$ and the spin tensor $S^{\mu\nu}$ in a given background gravitational field $g_{\mu\nu}$ are given by the MP equations in the pole-dipole approximation and stated in eq. (1.14) - (1.15). In order to simplify the numerical treatment we first define the constants of motion, which are useful for fixing the initial conditions and make them comparable for the two different settings depending on the SSCs. The conserved quantities for spinning particles moving in a stationary and axisymmetric spacetime are given by the two Killing vectors (∂_t, ∂_ϕ). They are computed with eq. (1.16)

to be the energy

$$E := -p_t + \frac{1}{2} g_{t\mu,\nu} S^{\mu\nu} \quad , \tag{3.1}$$

and the z-component of the total angular momentum

$$J_z := p_\phi - \frac{1}{2} g_{\phi\mu,\nu} S^{\mu\nu} \quad , \tag{3.2}$$

which both are preserved along the solutions of the MP equations. These two constants of motion exist independently of the choice of the supplementary condition and reflect the symmetries of the background spacetime.

As we have seen in the introduction of spinning particles a wise choice of SSC implies further conserved quantities. For instance, in the case of the T SSC the spin measure S^2 and the dynamical mass $\mathcal{M}$ are preserved along the evolved worldline and are used to set up the initial conditions. Then, the SSC has also to be preserved along the solutions of the MP equations fixing the relation between the u^μ and p^μ. While this relation is given in an explicit expression for the T SSC, eq. (1.30), in the case of NW SSC we merely have an implicit relation given in eq. (1.40). This hindrance can be overcome by employing numerical techniques to solve this initial value problem. Note that we selected the worldline parameter σ to be the proper time τ and normalised the velocity to $u^\nu \, u_\nu = -1$, guaranteeing the worldline of the particle to be timelike and therefore physically relevant. Then, there exist two possibilities for how the initial value problem addressing the implicit relation between u^μ and p^μ can be treated which are briefly introduced in Appendix A.

Having the relation between u^μ and p^μ at hand, we can now begin with the integration of the MP equations. Since we have to start at some point, the problem is an initial value problem. Expanding the covariant derivatives of p^μ and $S^{\mu\nu}$ we obtain for the system of equations that are to be solved

$$\begin{cases} \frac{\mathrm{d}\, x^\mu}{\mathrm{d}\tau} = u^\mu \quad , \\ \frac{\mathrm{d}\, p^\mu}{\mathrm{d}\tau} = -\frac{1}{2} \; R^\mu{}_{\nu\kappa\lambda} u^\nu S^{\kappa\lambda} - \Gamma^\mu_{\nu\kappa} u^\nu p^\kappa \quad , \\ \frac{\mathrm{d}\, S^{\mu\nu}}{\mathrm{d}\tau} = p^\mu \; u^\nu - u^\mu \; p^\nu + \Gamma^\mu_{\kappa\lambda} S^{\nu\kappa} u^\lambda - \Gamma^\nu_{\kappa\lambda} S^{\mu\kappa} u^\lambda \quad , \\ x^\mu(\tau = 0) = x^\mu_0 \quad , \\ p^\mu(\tau = 0) = p^\mu_0 \quad , \\ S^{\mu\nu}(\tau = 0) = S^{\mu\nu}_0 \quad . \end{cases} \tag{3.3}$$

with x^μ_0, p^μ_0, $S^{\mu\nu}_0$ being the initial conditions that have to be fixed beforehand. If one is looking naively at the equations, one may count twelve values that have to be chosen

initially. However, this is a very large number of values and the range of variations is way too big to cover the entire parameter space and to find the physically relevant or interesting solutions. Therefore, it is handy to include constraints in form of the constants of motion as well as the spin vector instead of the spin tensor in the fixing procedure of the initial conditions. Without loss of generality we choose to start at $t = \phi = 0$ and provide initial values for r, θ, p^r as well as the two spin components S^r and S^θ. The remaining initial conditions p^t, p^θ, p^ϕ, S^t and S^ϕ are then fixed by the constraints.

In the case of the T SSC those constraints are

$$E = -p_t - \frac{1}{2\mathcal{M}} g_{t\mu,\nu} \eta^{\mu\nu\gamma\delta} S_\gamma p_\delta \quad , \tag{3.4}$$

$$J_z = p_\phi + \frac{1}{2\mathcal{M}} g_{\phi\mu,\nu} \eta^{\mu\nu\gamma\delta} S_\gamma p_\delta \quad , \tag{3.5}$$

$$\mathcal{M}^2 = -g^{\mu\nu} p_\mu p_\nu \quad , \tag{3.6}$$

$$S^2 = g^{\mu\nu} S_\mu S_\nu \quad , \tag{3.7}$$

$$0 = g^{\mu\nu} S_\mu p_\nu \quad , \tag{3.8}$$

where we have substituted eq. (1.35) into the constants of motion (3.1), (3.2), and lowered the indices wherever needed. Thus, we specify an orbit by providing values for the physical quantities E, J_z, S^2, and $\mathcal{M}^2$ which are easier to relate to physically realistic situations. We then solve the system (3.4)-(3.8) for p_t, p_θ, p_ϕ, S_t, and S_ϕ with the help of the Newton-Raphson method, see Appendix A.

The next step is to find initial conditions for the choice of the NW SSC, which are as similar as possible to the ones defined for the system with T SSC, since we aim to compare the evolutions of the reference worldlines starting from the same initial setup. Therefore, we supply the MP equations supplemented by NW SSC with the same initial values for r, θ, p^r, S^r, S^θ, E, J_z, S^2 and $\mathcal{M}^2$. The initial conditions for p_t, p_θ, p_ϕ, S_t, and S_ϕ necessary to solve the system of differential equations (3.3) are then again computed using the constraints. Both the energy and the angular momentum are obtained by the Killing vector fields, which are independent of the choice of the SSC. Hence, we can use these relations also in the case of NW SSC.

Next, we use eq. (3.6) although the mass $\mathcal{M}$ is not preserved during the evolution for a reference worldline fixed by the NW SSC. For the measure of the spin, which is also not preserved, we use eq. (1.44) instead of (3.7). However, at this point we are interested neither in the behaviour of the spin measure nor in that of the mass during the evolution, but only in the starting situation so that we are able to use these equations in order to fix the initial setup. The last constraint is given, of course, by the NW SSC substituting (3.8). Thus, in total we have the following constraints for the NW SSC

$$E = -p_t - \frac{1}{2\mathcal{M}} g_{t\mu,\nu} \eta^{\mu\nu\gamma\delta} S_\gamma p_\delta \quad , \tag{3.9}$$

$$J_z = p_\phi + \frac{1}{2\mathcal{M}} g_{\phi\mu,\nu} \eta^{\mu\nu\gamma\delta} S_\gamma p_\delta \quad , \tag{3.10}$$

$$\mathcal{M}^2 = -g^{\mu\nu} p_\mu p_\nu \quad , \tag{3.11}$$

$$S^2 = -\frac{\mathcal{M}^2}{\zeta_\nu \zeta^\nu} \; S_\sigma \; S^\sigma \quad , \tag{3.12}$$

$$0 = g^{\mu\nu} S_\mu \zeta_\nu \quad , \tag{3.13}$$

which can be solved for p_t, p_θ, p_ϕ, S_t, and S_ϕ for the same provided r, θ, p^r, S^r, S^θ, E, J_z, S^2 and $\mathcal{M}^2$ as in the case of T SSC, we get what we referred to as similar initial conditions above. At last, by raising indices of the momenta and going from spin vectors to tensors with the help of the transformations (1.35) and (1.43), respectively, we get suitable data to start the computation with. The orbits are evolved through the eq. (1.14), (1.15). A more detailed discussion about the techniques we have applied to evolve the MP equations is provided in Appendix A.

As already explained in the previous section 1.3.2, the NW SSC does not provide a unique description of a reference frame. The observer's four-velocity ζ_μ depends on a timelike vector n_μ, which can be chosen at will. We adapt the definition of Barausse, Racine and Buonanno [53], since we aim to compare their formalism, which is linearised in the spin, to the MP approach later on in chapter 6. Implementing this choice from the very beginning, simplifies upcoming calculations. Thus, we set

$$n_\mu = e^{(t)}{}_\mu \; , \tag{3.14}$$

which refers to the timelike direction of an orthonormal local tetrad field defined on the background spacetime. An intuitive choice is the time gauge for this tetrad basis vector

$$e^{(t)}{}_\mu = \delta^t_\mu \sqrt{\frac{\Delta\Sigma}{\Lambda}} \quad , \tag{3.15}$$

based on the Boyer-Lindquist coordinates given in (1.8) and corresponding to a ZAMO observer. It fixes the direction of the timelike tetrad basis vector to be aligned with the coordinate time direction. The tetrad formalism has been introduced within the theory of measurement for general relativity. Each observer carrying such a tetrad measures the quantities that are projected onto this tetrad [95, 170]. Therefore, when the tetrad formulation is used, a relation to observable features can be established.

Now, we are ready to start the numerical analysis. As mentioned before we are interested in the influence of the inner structure onto the evolution of an orbit starting at the same spacetime point but corresponding to different particles. The inner structure is

parametrised by the measure of the spin of the particle, which we vary: the higher the spin the stronger the expected effects.

By adapting the convention that lengths and times are measured in units of the central object's mass and angular momenta in units of the particle's and the central object's mass, we set $M = 1$ and $\mathcal{M} = 1$ in the case of the T SSC (recall that the kinematical mass m has already been fixed by the normalisation condition $u_\mu u^\mu = -1$ in eq. (1.32)), i.e. we set $r \mapsto rM$, $J_z \mapsto J_z \mathcal{M} M$ and $S \mapsto SM\mathcal{M}$ (note that $\mathcal{M}$ is not conserved for the NW SSC and is therefore not suitable for a rescaling in this case) [2]. Indeed, we are just interested in the initial situation where we have to fix the initial conditions by setting up the values for the constants of motion. The maximal absolute value of the spin parameter given in these units is therewith obtained by an estimate for small compact spinning objects modeled by a Kerr black hole and amounts to 1 , see section 2.2.2 or [35, 36, 38]. So we start our numerical analysis with a large spin value $S = 1$.

3.2 Large Spin

First, the initial position of the orbit is chosen to be in the equatorial plane $\theta_0 = \pi/2$ at a radius of $r_0 = 11.7$ which is not too close to the centre that the particle plunges in but also not too far away so that the coupling between the spin and the gravitational field still matters. Moreover, the distance ensures the validity of the pole-dipole approximation, since the scale of curvature is much larger than the extension of the body, so that tidal forces can be neglected.

In order to analyse the properties of the evolution under the two different SSCs it is useful to maintain spin-curvature interaction during the evolution so that its influence can be investigated. The best way to ensure the coupling terms to be relevant is to examine a bound orbit. Therefore the remaining starting values are chosen appropriately: $p^r = 0.1$, $S = 1$, $S^r = 0.1S$, $S^\theta = 0.01S$, $E = 0.97$, $J_z = 3$ and $\mathcal{M} = 1$. The spin of the black hole a is fixed to be 0.5, since a variation of the Kerr spin does not change the qualitative picture, see Appendix C. Thus the MP equations can now be integrated for both the T SSC and the NW SSC. The resulting orbits are presented in fig. 3.1 in configuration space with

$$\begin{aligned} x &= r\cos(\phi)\sin(\theta) \ , \\ y &= r\sin(\phi)\sin(\theta) \ , \\ z &= r\cos(\theta) \ , \end{aligned}$$

[2] We refrain here from the notation we used in chapter 2 for the spin parameter s, since the spin vector is no longer restricted to be perpendicular to the orbital plane but allows for more general motion. In order to emphasise this difference we use different notations for the spin measure S.

as Cartesian coordinates. The evolution time is $\tau \approx 10^3$ and covers about three orbital revolutions.

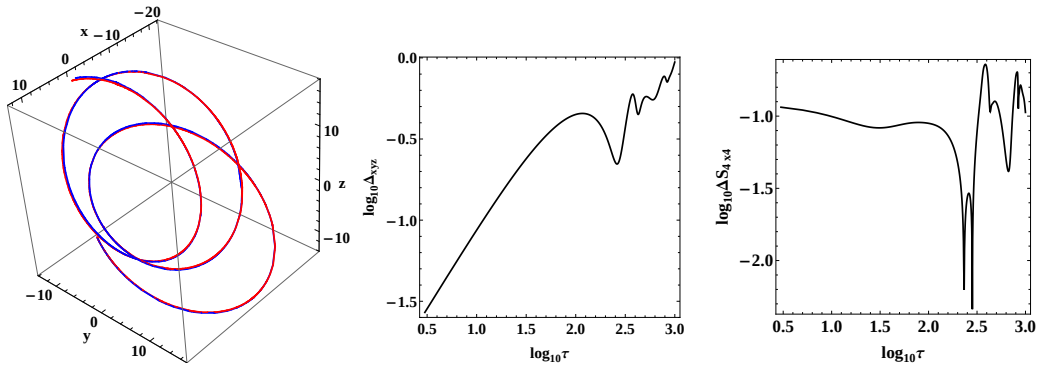

Figure 3.1: The left panel shows a MP orbit with T SSC (red) and a MP orbit with NW SSC (blue) in the configuration space x, y, z (Cartesian coordinates). The common parameters for these orbits are $a = 0.5$, $r = 11.7$, $\theta = \pi/2$, $p^r = 0.1$, $S = 1$, $S^r = 0.1\ S$, $S^\theta = 0.01\ S$, $E = 0.97$, $J_z = 3$, and $\mathcal{M} = 1$. The central panel shows the logarithm of the Euclidean distance in the configuration space between these two orbits as a function of the proper time. The right panel shows the logarithm of the difference $\Delta S_{4\text{x}4}$ between the spin tensors of these two orbits as a function of the proper time.

The divergence between the two orbits is barely visible in the left panel, but if we take the Euclidean norm

$$\Delta_{xyz} = \sqrt{(x_T - x_{NW})^2 + (y_T - y_{NW})^2 + (z_T - z_{NW})^2} \quad , \tag{3.16}$$

we see that at the end of our run, the separation between the two orbits is of the order one (central panel of fig. 3.1), while the radial distance from the central black hole is of the order ten (left panel of fig. 3.1). Even if the Möller radius is not an appropriate tool for our setup, because the worldlines do not necessarily correspond to the same particle, it is worthy to notice that the two orbits lie inside a Möller radius ($S/\mathcal{M} = 1$) for $\tau = 10^3$, even if their distance will grow out of this radius later on. This divergence in the orbit evolution follows the discrepancy in the spin space. To illustrate this, the norm of the difference between the spin tensor $S_T^{\mu\nu}$ of the T SSC and the spin tensor $S_{NW}^{\mu\nu}$ of the NW SSC,

$$\Delta S_{4\text{x}4} = \sqrt{\left| g_{\mu\nu} g_{\kappa\lambda} (S_T^{\nu\kappa} - S_{NW}^{\nu\kappa})(S_T^{\mu\lambda} - S_{NW}^{\mu\lambda}) \right|} \quad , \tag{3.17}$$

is displayed in the right panel of fig. 3.1. $\Delta S_{4\text{x}4}$ is one tenth of the spin measure right from the beginning, and stays at this level during the evolution. Thus, from an orbital dynamic point of view the choice of different SSCs leads to orbital evolutions, which diverge significantly with time, when the spin of the test particle is of order $S = 1$.

One thing that has to be discussed before we proceed is the meaning of a 'common' proper time, when two orbits with different SSCs are compared. Each SSC defines its own centre of reference, which implies that with each SSC the proper time that is measured along the above orbits is different, even if the orbits start with similar initial conditions. Another issue that arises here is how we can measure the distance between two 'nearby' orbits in a curved spacetime. Above, we use Euclidean norm, however the spacetime is not Euclidean. The same aspect arises when geodesic chaos is studied in curved spacetimes (see, e.g., [135, 136]). One of the suggestions in the aforementioned field is to use the two-nearby-orbits technique, i.e. to evolve two orbits with similar initial conditions and measure their distance when they reach the same proper time. This is in few words the approach we adapt in our study for the time issue.

For the issue of the distance in the configuration space between the two orbits, we have chosen to employ the Euclidean metric. We could employ the local $g_{\mu\nu}$ metric as well, even if the orbits depart from each other significantly (central panel of fig. 6.1). However, for the evolution time $\tau = 10^3$ the results coming from both approaches are almost identical, and therefore we went for the the simplest metric, which is the Euclidean.

To sum up, a large spin does indeed affect the evolution of the orbits of two particles confirming the deviation from a geodesic orbit. However, even though the spin is chosen to be big the effect is not so distinct that the discrepancy between the orbits exceeds the Möller radius at the end of our evolution time.

In the next step we analyse the convergence of the two orbits by considering the geodesic limit, i.e. reducing the value of the spin to 10^{-8}.

3.3 Small Spin

As already mentioned the geodesic limit is approached by setting the spin measure to $S = 10^{-8}$ while keeping the other parameters fixed. The resulting orbits look similar to the ones obtained by the previous setup. This outcome is expected, since merely the spin measure is changed. However, the distance between the two orbits has dropped significantly about eight orders of magnitude. The reason for this drop is the smaller impact of the spin on the shape of the particle's orbit. The smaller this influence is the smaller is the effect of the choice of the spin supplementary condition. Still, the level of divergence in the configuration space is again defined by the magnitude of the spin difference $\Delta S_{4\times4}$. Although the initial position in configuration space of the particles at the beginning are identical, during the evolution their orbits follow slightly different paths, which is due to the geodesic deviation caused by the internal structure. This is also reflected by the initial difference in the spin components $\Delta S_{4\times4} \approx 10^{-9}$, which is passed on to the configuration space resulting in the deviation of the two orbits.

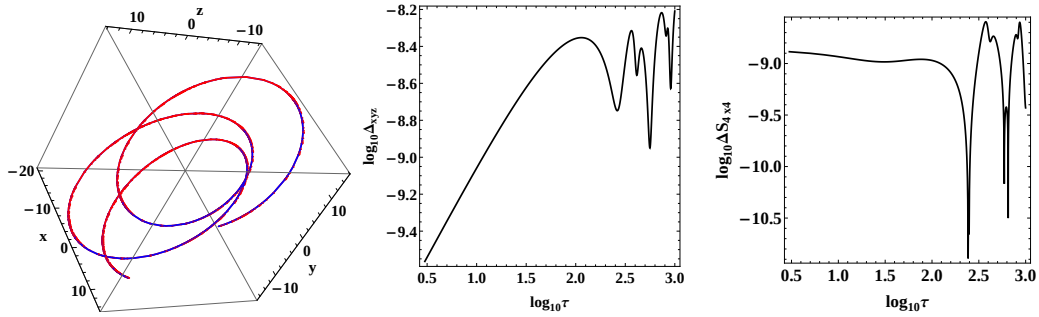

Figure 3.2: The left panel shows a MP orbit with T SSC (red) and a MP orbit with NW SSC (blue) in the configuration space $x,\ y,\ z$ (Cartesian coordinates). The common parameters for these orbits are $a = 0.5$, $r = 11.7$, $\theta = \pi/2$, $p^r = 0.1$, $S = 10^{-8}$, $S^r = 0.1\ S$, $S^\theta = 0.01\ S$, $E = 0.97$, $J_z = 3$, and $\mathcal{M} = 1$. The central panel shows the logarithm of the Euclidean distance in the configuration space between these two orbits as a function of the proper time. The right panel shows the logarithm of the difference $\Delta S_{4\text{x}4}$ between the spin tensors of these two orbits as a function of the proper time.

In order to assess the behaviour of the two orbits properly it is useful to have a look at the constants of motion.

3.4 Constants of Motion

Since both the energy and the angular momentum are conserved in both cases, it is interesting to check the difference in the behaviour of the particle's rest mass and the measure of the spin, which are only preserved in the case of T SSC. The preservation is checked by analysing the relative error of the four-momentum

$$\Delta\mathcal{M}^2 = \left|1 - \frac{\mathcal{M}^2(\tau)}{\mathcal{M}^2(0)}\right| \quad , \tag{3.18}$$

and the relative error of the spin measure S^2

$$\Delta S^2 = \left|1 - \frac{S^2(\tau)}{S^2(0)}\right| \quad , \tag{3.19}$$

where $\mathcal{M}^2(\tau)$, and $S^2(\tau)$ are calculated at time τ.

We see from fig. 3.3 that both the rest mass $\mathcal{M}^2$ and the spin length are conserved for the T SSC (red lines) as it was expected. On the other hand, in the case of the NW SSC (blue lines) the four-momentum scales with the magnitude of the spin S, while the square of the spin itself stays at the same level indifferently from the spin's magnitude. This scaling in the conservation of the mass is anticipated because, as $S \to 0$, the evolution

of the MP equations approaches that of the geodesic motion. In order to illustrate better the above mentioned scaling, we run several simulations with initial setups similar to the one of fig. 3.1 where we only change the measure of the spin, S. For every simulation,

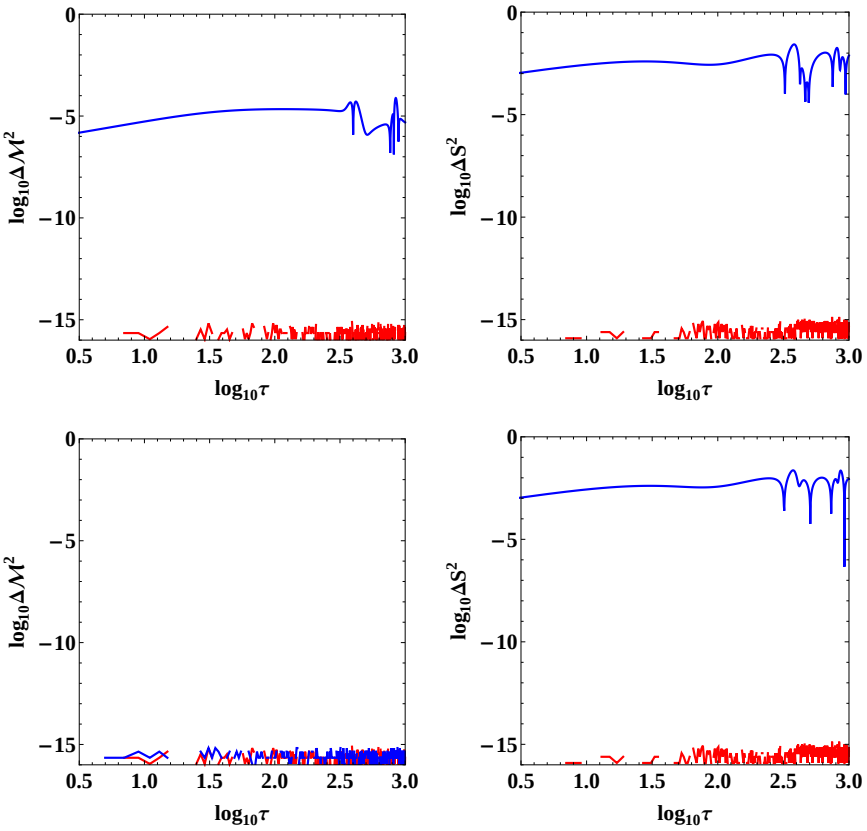

Figure 3.3: The top row of panels corresponds to the orbits of fig. 3.1, while the bottom row of panels corresponds to the orbits of fig. 3.2. The red lines represent the evolution of the MP equations with T SSC, while the blue lines represent the NW SSC. The left column of panels shows the relative error in the preservation of the four-momentum, while the right depicts the preservation of the spin.

we plot the maximum value of $\Delta\mathcal{M}^2$ along the trajectory against the initial spin measure shown in fig. 3.4. The resulting plot shows that, as we decrease S, the four-momentum for the NW SSC tends to be conserved up to the computational accuracy. There are two effects that shape this figure. One is the theoretical scaling of $\Delta\mathcal{M}^2$ as a function of S and the other is the finite computational accuracy. From a linear fit of our data we get for $S > 10^{-6}$ (dashed line in fig. 3.4) $\Delta\ \mathcal{M}^2\ \propto\ S^2$. For smaller spins a plateau appears because we reach the computational accuracy (in our runs we use double precision).

Since for T SSC the four-momentum is conserved and for the NW SSC the $\sqrt{\Delta\ \mathcal{M}^2}$ scales linearly with the spin, this scaling can be interpreted as the rate by which the two

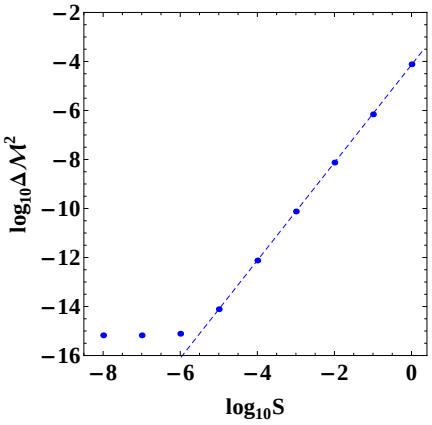

Figure 3.4: The relative error of the four-momentum $\Delta\mathcal{M}^2$ as a function of the spin measure S for the NW SSC. The black dots correspond to the maximum values of $\Delta\mathcal{M}^2$ during the evolution for each S. The dashed line is a linear fit of the form $\log_{10}\Delta\mathcal{M}^2 = a\log_{10}S + b$ for data with $S > 10^{-6}$, where $a = 1.996 \pm 0.004,\ b = -4.135 \pm 0.013$.

different SSC converge to each other. In fact, based on the laws of black hole dynamics the dynamical mass $\mathcal{M}$ of compact spinning objects can generally be expressed as a function of the spin measure $\mathcal{F}$ [137]

$$\mathcal{M}^2 = m_0^2 + \mathcal{F}\left(S^2\right) \ , \tag{3.20}$$

in the pole-dipole approximation, with m_0 as the irreducible mass. Indeed, if the observer is placed in the particle's rest frame, i.e. the worldline is fixed by the T SSC, then the conservation of $\mathcal{M}$ is recovered from eq. (3.20), because the contribution from the spin measure is constant. In the case of the NW SSC the spin measure is no longer preserved. Therewith, we obtain

$$\Delta\mathcal{M}^2 \quad = \quad \left|\frac{\mathcal{M}^2(\tau) - \mathcal{M}^2(0)}{\mathcal{M}^2(0)}\right| = \left|\frac{m_0^2 - \mathcal{M}^2(0)}{\mathcal{M}^2(0)} + \frac{\mathcal{O}(S^2)}{\mathcal{M}^2(0)}\right| \ ,$$

where the first term is not expected to depend on the spin measure leading to the scaling of $\Delta\mathcal{M}^2 \propto S^2$, which we found in our numerical analysis.

3.5 Discussion

We conclude that the numerical results for both choices of SSCs yield the outcome we expected from theoretical considerations providing the ansatz given in eq. (3.20) within the pole-dipole approximation.

The NW SSC conserves the mass at linear order in the particle's spin while the error in the spin measure stays at the same level. These characteristics complicate an intuitive

approach to the behaviour of the NW SSC.

Recall that the two orbits correspond to two spinning particles at the same point in configuration space. More precisely, we have two distinct particle's with internal structure characterised by the spin value, which start at the same position in configuration space. As the qualitative behaviour does not change if the value of the Kerr spin or the direction of the particle's spin vector is reversed, see Appendix C, the evolution of the worldline is indeed affected by the internal structure of the particle, i.e. it does depend on the value of the particle's spin. In fact, the deviation from geodesic orbits is assigned to spin-gravity interaction in the case of spinning particles, see e.g. [78, 97, 104, 138], such as spin-spin or spin-orbit coupling. Indeed, we observe slight quantitative changes in the Euclidean distances between the two orbits when the value of the Kerr spin or the sign of the spin parameter is varied. They do not affect the differences in the spin space or the behaviour of the constants of motion, which are used to determine the convergence of the two SSCs. Thus, their orbital evolution diverges and scales linear in the particle's spin, which is attributed to spin-curvature coupling. Astrophysically relevant spin values are estimated to be $S \leq 10^{-4}$ so that the motion of the particles in the pole-dipole approximation has a noticeable effect induced by the spin.

However, the orbit considered in this work is located at a distance of $r = 11.7$, at which the influence of curvature is not too strong. Thus, if one wants to thoroughly investigate the divergences in strong-field region, it is best to choose a circular orbit and shift it closer to the centre [103, 104, 139, 138]. One has to take care, though, for higher multipole moments, which become the more important the stronger the gravitational field. Otherwise, the pole-dipole approximation breaks down at some point [83].

After the examination of different SSCs and analysing the properties of the NW SSC, we apply the NW in a different setting. While the behaviour of the NW SSC is somewhat strange compared to the T SSC it offers a great advantage in the context of Hamiltonian mechanics: It provides a canonical formulation. In the next part we will focus on the Hamiltonian description of spinning particles, investigate a linearised in spin formulation and extend the Hamiltonian to higher orders in spin.

Part II

Lagrangian and Hamiltonian Mechanics of spinning particles

Lagrangian and Hamiltonian for spinning particles briefly reviewed

The second part of this thesis deals with two different formulations of classical dynamical systems: Lagrangian and Hamiltonian mechanics. In particular, the significance of a canonical Hamiltonian function for a spinning test particle linearised in spin is analysed by numerical comparison to the Lagrangian result. In addition, we search for criteria such a Hamiltonian has to satisfy in order to give physically relevant results in numerical computations. In order to improve the Hamiltonian formulation we generalise the Hamiltonian to all orders in the particle's spin within the pole-dipole approximation.

The Lagrangian as well as the Hamiltonian formalism are approached from different angles. Barker and O'Connell generalise the PN approximated Lagrangian to spinning particles and derive the corresponding Hamiltonian [113]. Mathematically sophisticated approaches are discussed in [93, 94, 140] giving explicit expressions for the Lagrangian for objects moving in external gravitational and electromagnetic fields. An extensive study on the action approach using the concept of tetrads and the variational principle is provided by Westpfahl *et al.* in the 1960s [69, 141, 142, 143], including special and general relativistic systems as well as electromagnetic fields. Shortly after that, Hanson and Regge [144] developed a Lagrangian approach to the special relativistic spherical top and established a canonical Hamiltonian formulation by imposing constraints according to Dirac's ansatz [71, 145]. Further action approaches are discussed by Bailey and Israel [146, 147] and in the context of PN theory by Porto [148]. The equations of motion are obtained from a covariant variation of an implicit action and match the MP equations.

A canonical formulation becomes important when Hamiltonian mechanics is considered. Tauber studied the canonical formalism for general relativistic spinning particles and presented the true conjugate momenta up to linear order in the particle's spin [149]. A sophisticated Hamiltonian formulation was provided by Arnowitt, Deser and Misner [49, 50, 51, 52] (ADM), which was extended to spinning particles by Steinhoff in the context of PN approximation very recently [58, 116]. Based on a different method Barausse, Racine and Buonanno developed a canonical Hamiltonian from a Legendre transformation

of an implicit Lagrangian [53] as a key ingredient for EOB theory. However, this Hamiltonian is only valid to linear order in the particle's spin and leads to constants of motion that exhibit unphysical behaviour in numerical computations. Thus, it is of interest to study this Hamiltonian in more detail.

In chapters 4 and 5 we give a brief overview of the Lagrangian formalism, the action principle and the Hamiltonian formulation in general relativity. Then, we numerically compare the linearised Hamiltonian by Barausse *et al.* to the MP equations and discuss the range of significance for the Hamiltonian in chapter 6. After that, in chapter 7, the reason for the unphysical behaviour of some constants of motion within the Hamiltonian evolution is examined. We improve the derivation and formulation of the Hamiltonian using a spin-gauge invariant action in chapter 8.

Chapter 4

Lagrangian Formalism

Before entering the Hamiltonian formalism we first give a short introduction into the Lagrangian formulation of classical mechanics, see e.g. [117, 150, 151]. Historically, the Lagrangian formalism has been developed before the Hamiltonian one, so that these two formulations can be connected to each other by starting from the Lagrangian.

4.1 The Action Principle

Generally in classical mechanics and flat spacetime, the Lagrangian formulation provides a convenient way to describe the dynamics of physical systems that may be subject to external forces. Moreover, constraints can be implemented via the Lagrangian multipliers. The heart of this formalism is the so called Hamilton's principle of extremal action implying the determination of the dynamics and thereby the equations of motion by a variational problem. The varied quantity is based either on a function $L(q, \dot{q})$ for single particles with generalised coordinates q and velocities $\dot{q}$, here the dot denotes the ordinary derivative with respect to time, or on a density $\mathcal{L}(\phi, \partial_\mu \phi)$ if the dynamical variable is a field $\phi(q)$ which depends on the generalised coordinates. Both L and $\mathcal{L}$ include all physical information necessary to fix the dynamics of the particle or the field.

Hamilton's principle then says that the system behaves in such a way that the corresponding action $\mathcal{S} = \int dt L$, for a system of discrete particles, or $\mathcal{S} = \int dt \int d^3x \mathcal{L}$, for fields, is required to be stationary. Using variational calculus we can find the extrema of the action making it stationary with which we obtain the equations of motion describing the dynamics of the considered system.

Applying this approach to general relativity we are able to define a Lagrangian that yields the Einstein equations as the resulting equations of motion. First, recall the gravitational field or metric $g_{\mu\nu}$ to be the dynamical variable and generalise through minimal coupling the formulae from special relativity to general relativity leading to

$$\mathcal{S} = \int \mathcal{L}\left(g_{\mu\nu}, \nabla_\alpha g_{\mu\nu}\right) d^4x \ ,$$

where the Lagrangian density $\mathcal{L}$ can be expressed as

$$\mathcal{L} = \sqrt{-g}\hat{\mathcal{L}} \ ,$$

with $\hat{\mathcal{L}}$ being a scalar and g the determinant of the spacetime metric $g_{\mu\nu}$. The prefactor $\sqrt{-g}$ makes sure that the integral is covariant, i.e. that it is independent of the choice of the coordinates by ensuring the volume element to be invariant under coordinate transformations [7]. Since we need a scalar function $\hat{\mathcal{L}}$ that depends on derivatives of the metric, it seems natural to choose the Ricci scalar (the Riemannian curvature scalar) so that the action is given by

$$\mathcal{S} = \int \sqrt{-g} R d^4x \ , \tag{4.1}$$

also known as the Einstein-Hilbert action. And indeed, applying the principle of least action and treating the gravitational field as the dynamical variable results in the Einstein equations as the equations of motion for the metric $g_{\mu\nu}$ [7].

Another example, where the variational principle can be used, is the geodesic equation. It is known that a freely falling testparticle always follows the path of maximal proper time. Therewith we can extremise the proper time functional

$$\tau = \int \sqrt{-g_{\mu\nu}\frac{dx^\mu}{d\sigma}\frac{dx^\nu}{d\sigma}} d\sigma \ ,$$

in order to obtain the corresponding equations of motion, i.e. the geodesic equation, describing the behaviour of such a particle freely propagating through a gravitational field.

The case of spinning particles is different, though. We have to deal with non-geodesic motion and include the degrees of freedom induced by the spin into the Lagrangian, see e.g. [58, 137, 143, 146, 148]. Therefore the motion of a spinning particle can be characterised by the evolution of a worldline, which has a tetrad $e_A{}^\mu$ attached at each point representing the eigenrotation of the body. This tetrad is assumed to be a set of orthonormal basis vectors satisfying the normalisation condition [6, 7]

$$\text{I. } \eta_{AB} \ = \ e_A{}^\mu e_B{}^\nu g_{\mu\nu} \ , \tag{4.2}$$

or equivalently

$$\text{II. } g^{\mu\nu} = e_A{}^\mu e_B{}^\nu \eta^{AB} \ , \tag{4.3}$$

with $\eta_{AB} = diag\left(-1, 1, 1, 1\right)$ as the Minkowski metric. Consequently, the spacetime metric is transformed to be flat within the body-fixed frame denoted by the capital latin indices

$A = 0 \ldots 3$ at each point. Since the tetrad is Lorentz covariant, endowing the particle with such a tetrad means that we can assign an element of the Poincaré group $(x^\mu(\sigma),\, e_A{}^\mu(\sigma))$ to the particle, which will give us the Lagrangian coordinates later. The spin angular velocity is related to the rotation of the tetrad while the particle that carries the tetrad moves along its worldline. Motivated by Newtonian theory we introduce the angular velocity as [58, 148]

$$\Omega^{\mu\nu} := e_A{}^\mu \frac{De^{A\nu}}{d\sigma} = e_A{}^\mu \left[\frac{de^{A\nu}}{d\sigma} + \Gamma^{\nu\mu}{}_\alpha u^\alpha \right] \ , \tag{4.4}$$

where $\Gamma^\mu{}_{\alpha\beta}$ is given in (1.4) and the tetrad $e_A{}^\mu(\sigma)$ is associated to the Newtonian time dependent spatial rotation matrix which we are acquainted with in the dynamics of a rigid body. The covariant derivative appears due to minimal coupling in the general relativistic context and considers the curvature of the spacetime along the particle's worldline.

Similar to the Newtonian case the angular velocity $\Omega^{\mu\nu}$ is antisymmetric, which can be deduced by the metric compatibility with the covariant derivative using the condition in eq. (4.3)

$$0 = \frac{D}{d\sigma} g^{\mu\nu} = \frac{De_A{}^\mu}{d\sigma} e^{A\nu} + e_A{}^\mu \frac{De^{A\nu}}{d\sigma} = \Omega^{\nu\mu} + \Omega^{\mu\nu} \ .$$

Notice that $\Omega^{\mu\nu}$ corresponds to an infinitesimal Lorentz transformation with six degrees of freedom, three Lorentz boosts and three spatial rotations. Thus, in order to translate the system into an ordinary physical system with the correct number of degrees of freedom, i.e. three spatial rotations, we have to get rid of the three Lorentz boosts. This is achieved by imposing constraints on the system, which we have already identified as the spin supplementary conditions in section 1.3.2.

To sum up, the Lagrangian coordinates are composed of the spacetime position x^μ, the four-velocity u^μ, the tetrad field $e_A{}^\mu$ and its velocity $\frac{De_A{}^\mu}{d\sigma} = \dot{e}_A{}^\mu$. Keeping it unspecified and generic we obtain for the Lagrangian scalar function [137]

$$L\left(g_{\mu\nu}, u^\mu, \Omega^{\mu\nu}\right) \ , \tag{4.5}$$

where we substituted the dependency on $e_A{}^\mu,\ \dot{e}_A{}^\mu$ by $\Omega^{\mu\nu}$ and the one on x^μ by $g_{\mu\nu}$. The equations of motion are then obtained by a reparametrisation invariant action principle

$$\delta S = \delta \int L\left(g_{\mu\nu}, u^\mu, \Omega^{\mu\nu}\right) d\sigma = 0 \ .$$

However, before we start the variation of the Lagrangian it is worth spending some time on the geometrical meaning of the variational principle. If the worldline is varied naively, the component values of tensors defined on the original worldline are not included in the variational procedure so that covariance is lost. A useful tool is provided by the covariant

variation introduced in the following section.

4.2 Infinitesimal covariant variation

A shift of the position can be obtained through a repeated infinitesimal variation of the action. Linear variations δ lead to the equations of motion in flat spacetime. However, such an approach may loose covariance during the variation procedure in curved geometry. In order to keep track and sustain the covariance it is useful to apply an approach that includes manifest covariance. In this context, a covariant variation of these quantities defined along a worldline z^α was introduced in [137, 152] as

$$\Delta := \delta + \Gamma^\mu{}_{\nu\alpha}\delta z^\alpha G^\nu{}_\mu \ , \tag{4.6}$$

where δz^α is the infinitesimal shift of the worldline. Here $G^\nu{}_\mu$ is a linear operator, which rearranges spacetime indices such that the covariant derivative ∇_α can be written in the abstract form

$$\nabla_\alpha := \partial_\alpha + \Gamma^\mu{}_{\nu\alpha}G^\nu{}_\mu \ . \tag{4.7}$$

For instance, $G^\nu{}_\mu$ operates on a tensor $T_\alpha{}^\beta$ as $G^\nu{}_\mu T_\alpha{}^\beta := \delta^\beta_\mu T_\alpha{}^\nu - \delta^\nu_\alpha T_\mu{}^\beta$. This implements an infinitesimal parallel transport in the variation Δ. In this notation, the covariant differential D reads

$$D := d + \Gamma^\mu{}_{\nu\alpha}dz^\alpha G^\nu{}_\mu \ . \tag{4.8}$$

Curvature is defined by the change of a vector that is parallel transported around a closed loop, which can be expressed as the commutator of covariant derivatives

$$[\nabla_\alpha, \nabla_\beta] = R^\mu{}_{\nu\alpha\beta}G^\nu{}_\mu \ ,$$

where our convention for the Riemann tensor is fixed by the definition in (1.3). It immediately follows that the commutator of the covariant differential and the corresponding variation involves curvature as well

$$[\Delta, D] = R^\mu{}_{\nu\alpha\beta}\delta z^\alpha dz^\beta G^\nu{}_\mu \ , \tag{4.9}$$

i.e. it does not vanish. Here we used the intermediate commutator of the linear operator $G^\nu{}_\mu$

$$[G^\nu{}_\mu, G^\beta{}_\alpha] = \delta^\beta_\mu G^\nu{}_\alpha - \delta^\nu_\alpha G^\beta{}_\mu \ . \tag{4.10}$$

In order to maintain the particle's properties during the worldline shift, we require them to be parallel transported along the geodesic that connects the two worldlines by setting

$$\Delta p_\mu = 0 \ , \qquad \Delta S_{\mu\nu} = 0 \ . \tag{4.11}$$

Although the geometrical objects p_μ and $S_{\mu\nu}$ remain unaltered, the variation implies that the numerical component values of the worldline quantities are transformed. However, as we already mentioned geometrically this is just a parallel transport and we refrain from denoting this change by a hat and regard them as geometrically unchanged. The variation of fields due to the variation of the worldline is given by

$$\Delta \equiv \delta z^\alpha \nabla_\alpha \ . \tag{4.12}$$

This geometric machinery allows a convenient, manifestly covariant, derivation of the equation of motion for the position.

4.3 Variation of the action

As the action as well as the Lagrangian are scalar quantities the ordinary variation can be interchanged with the covariant one, so that the principle of least action can be applied in a manifestly covariant manner

$$\delta L\left(g_{\mu\nu}, u^\mu, \Omega^{\mu\nu}\right) = \left.\frac{\partial L}{\partial u^\mu}\right|_\Omega \Delta u^\mu + \left.\frac{\partial L}{\partial \Omega^{\mu\nu}}\right|_u \Delta\Omega^{\mu\nu} \ ,$$

since the variation of the metric tensor field according to (4.12) $\Delta g_{\mu\nu} = \delta z^\alpha g_{\mu\nu;\alpha} = 0$ vanishes due to the metric compatibility with the covariant derivative. Defining the generalised momenta by

$$p_\mu := \frac{\partial L}{\partial u^\mu} \ , \qquad\qquad S := 2\frac{\partial L}{\partial \Omega^{\mu\nu}} \ , \tag{4.13}$$

where the linear momentum p_μ corresponds to the four-velocity u^μ and the spin tensor $S_{\mu\nu}$ to the angular velocity $\Omega^{\mu\nu}$, we obtain

$$\delta L\left(g_{\mu\nu}, u^\mu, \Omega^{\mu\nu}\right) = p_\mu \Delta u^\mu + \frac{1}{2} S_{\mu\nu} \Delta\Omega^{\mu\nu} \ ,$$

for the variation of the Lagrangian. At this point, we note that p_μ is not the canonical momentum to x^μ, since $\Omega^{\mu\nu}$ also depends on u^μ, which is held fixed for the definition of p_μ, though. When considering the variation of the velocities it is important to recall the dependence of $\Omega^{\mu\nu}$ on the body-fixed tetrad field and its normalisation condition given by(4.2) or (4.3). In particular, this means that the variation of the tetrad field is subject to constraints. They are taken into account by defining a new antisymmetric quantity [137, 144]

$$\Delta\Theta^{\mu\nu} = e^{A[\mu} \Delta e_A{}^{\nu]} \ ,$$

resulting from the metric compatibility and the normalisation condition for tetrads (4.3) and which is used to perform the variation with respect to the angular velocity or the tetrad field, respectively. Then, useful formulae for the variation of the velocities are given by [137]

$$\Delta u^{\mu} = \frac{D\delta z^{\mu}}{d\sigma} \ , \qquad \Delta\Omega^{\mu\nu} = \frac{D\left(\Delta\Theta^{\mu\nu}\right)}{d\sigma} + \Omega_{\alpha}{}^{[\mu}\Delta\Theta^{\nu]\alpha} + R^{\mu\nu}{}_{\alpha\beta}u^{\alpha}\delta z^{\beta} \ , \tag{4.14}$$

so that the varied Lagrangian results in

$$\delta L\left(g_{\mu\nu}, u^{\mu}, \Omega^{\mu\nu}\right) = p_{\mu}\frac{D\delta z^{\mu}}{d\sigma} + \frac{1}{2}S_{\mu\nu}\left(\frac{D\left(\Delta\Theta^{\mu\nu}\right)}{d\sigma} + \Omega_{\alpha}{}^{[\mu}\Delta\Theta^{\nu]\alpha} + R^{\mu\nu}{}_{\alpha\beta}u^{\alpha}\delta z^{\beta}\right) \ .$$

Applying the principle of least action and performing partial integration we arrive at

$$\delta S = \int\left(\left(-\frac{Dp_{\beta}}{d\sigma} + \frac{1}{2}S_{\mu\nu}R^{\mu\nu}{}_{\alpha\beta}u^{\alpha}\right)\delta z^{\beta} + \left(\frac{1}{2}S_{\mu\nu}\Omega_{\alpha}{}^{[\mu}\Delta\Theta^{\nu]\alpha} - \frac{1}{2}\frac{DS_{\mu\nu}}{d\sigma}\Delta\Theta^{\mu\nu}\right)\right)d\sigma \ ,$$

which already gives the equations of motion. Since the variations δz^{β} and $\Delta\Theta^{\mu\nu}$ are arbitrary and independent, we have

$$\frac{Dp_{\beta}}{d\sigma} = \frac{1}{2}S_{\mu\nu}R^{\mu\nu}{}_{\alpha\beta}u^{\alpha} \ , \qquad \frac{DS_{\mu\nu}}{d\sigma} = 2S_{\alpha[\mu}\Omega_{\nu]}{}^{\alpha} \ , \tag{4.15}$$

of which the first one can be rearranged in such a way that it recovers the equation of motion for the linear momentum as given by the MP equations in eq. (1.14). The second equation gives the equation of motion for the spin tensor.

In order to bring it into a recognisable expression we take advantage of the fact that the Lagrangian $L\left(g_{\mu\nu}, u^{\mu}, \Omega^{\mu\nu}\right)$ is a scalar and invariant under an infinitesimal coordinate transformation $x'^{\mu} = x^{\mu} - \xi^{\mu}$ [137, 146]. However, it depends on tensors which transform according to

$$\Psi'^{\mu_1\cdots\mu_k}{}_{\nu_1\ldots\nu_m} = \Psi^{\mu_1\cdots\mu_k}{}_{\nu_1\ldots\nu_m} - \left(\partial_{\alpha}\xi^{\beta}\right)G^{\alpha}{}_{\beta}\Psi^{\mu_1\cdots\mu_k}{}_{\nu_1\ldots\nu_m} \ ,$$

under such a coordinate transformation. For example, the transformed four-velocity results in

$$u'^{\mu} = u^{\mu} - u^{\alpha}\left(\partial_{\alpha}\xi^{\mu}\right) \ .$$

Thus, we expand the Lagrangian given as a function dependent on the transformed variables in the infinitesimal coordinate transformation and obtain

$$L\left(g'_{\mu\nu}, u'^{\mu}, \Omega'^{\mu\nu}\right) = L\left(g_{\mu\nu}, u^{\mu}, \Omega^{\mu\nu}\right) - \left(\frac{\partial L}{\partial u^{\mu}}u^{\alpha} + 2\frac{\partial L}{\partial\Omega^{\mu\nu}}\Omega^{\alpha\nu} - 2\frac{\partial L}{\partial g_{\mu\nu}}g_{\mu\nu}\right)\left(\partial_{\alpha}\xi^{\mu}\right) \ .$$

After exploiting the invariance of the Lagrangian, i.e. $L\left(g'_{\mu\nu}, u'^{\mu}, \Omega'^{\mu\nu}\right) = L\left(g_{\mu\nu}, u^{\mu}, \Omega^{\mu\nu}\right)$, the following identity is obtained

$$p_\mu u^\alpha + S_{\mu\nu}\Omega^{\alpha\nu} - 2\frac{\partial L}{\partial g_{\mu\nu}} g_{\mu\nu} \equiv 0 \ , \tag{4.16}$$

which allows us to substitute the term on the right-hand side in eq. (4.15). Due to the antisymmetry of $\Delta\Theta^{\mu\nu}$ the contribution of the symmetric metric tensor in eq. (4.16) vanishes, so that we are left with

$$p_\mu u_\nu - \frac{1}{2}\frac{DS_{\mu\nu}}{d\sigma} \quad = \quad 0 \ ,$$

which can be rewritten as

$$\frac{DS_{\mu\nu}}{d\sigma} = p_\mu u_\nu - p_\nu u_\mu \ , \tag{4.17}$$

due to the (anti-) symmetry properties of $S_{\mu\nu}$ and $\Theta^{\mu\nu}$. Therewith the equations of motion in eq. (4.15) and (4.17) obtained by the action principle of a general Lagrangian function for spinning particles recover the MP equations from eq. (1.14) and (1.15), which are obtained by the conservation of $T^{\mu\nu}$. Indeed, this shows the consistency of the action approach. It is worth to mention here that the equations of motion do not depend on the explicit form of the Lagrangian in terms of spin and momentum. The derivation merely uses the properties imposed on the Lagrangian in order for the description to be physically relevant.

As before the set of equations is underdetermined so that a supplementary condition has to be added. In principle the introduction of the tetrad implies another gauge freedom in the choice of the direction of its temporal basis vector, which, for instance, becomes important when the symplectic structure of the system's phase space is sought to be preserved in the Hamiltonian formulation in [53].

Although the Lagrangian offers a straightforward way to analyse the dynamical behaviour of mechanical systems, it usually implies differential equations of second order that have to be solved. On contrary, the Hamiltonian formulation translates the equations of motion in differential equations of first order. Therefore the next section focuses on the Hamiltonian formulation of spinning particles in general relativity.

Chapter 5

Hamiltonian Formalism

Despite the fact that the Hamiltonian formalism describes the dynamical problem in terms of first order differential equations, it also provides a natural approach to quantisation. Therefore, shortly after the discovery of quantum mechanics and general relativity between 1915 and 1930, the desire for a canonical formulation of general relativity was born. Today, the ideas of a Hamiltonian formulation of general relativity supply important contributions to both quantum gravity and numerical relativity [52, 153].

In classical mechanics the Hamiltonian formulation has been developed by R. Hamilton in 1834 as a reformulation of the description of dynamical systems [117, 154]. Instead of using the position and velocities as the generalised coordinates the Hamiltonian employs position and momenta as the dynamical variables. As we have seen in the previous chapter the momenta are defined as the derivatives of the Lagrangian with respect to the velocities

$$p^i = \frac{\partial \mathcal{L}}{\partial u^i} \ . \tag{5.1}$$

Generally, these relations are used to find an explicit relation between the velocities u^i and the momenta p^i. Therewith the Hamiltonian function or density is attained from the Lagrangian by a Legendre transformation

$$\mathcal{H}\left(x^i, p_i\right) = p_i u^i - \mathcal{L}\left(x^i, u^i\left(x^i, p_i\right)\right) \ ,$$

where the index i runs only over spatial dimensions 1...3. The Hamiltonian is often identified with the energy in the case of conservative dynamical systems. As well as the Lagrangian the resulting Hamiltonian contains all information on the dynamics of the system determining the dynamical behaviour. Since the Hamiltonian is defined on a phase space that is equipped with a symplectic structure, Darboux's theorem says that we can always find local canonical coordinates satisfying the fundamental Poisson bracket relations

$$\left\{x^i, x^j\right\} = 0 \qquad \{p_i, p_j\} = 0 \qquad \left\{x^i, p_j\right\} = \delta^i_j \ ,$$

with δ^i_j being the Kronecker delta. This canonical structure implies the equations of motion to be of the following form

$$\dot{x}^i \ = \ \frac{\partial \mathcal{H}}{\partial p_i} \ , \qquad \dot{p}_i = -\frac{\partial \mathcal{H}}{\partial x^i} \ ,$$

known as Hamilton's equations (the dot refers to ordinary differentiation with respect to time). It is important here to draw the attention to the different treatment of space and time in the Hamiltonian formulation because only time derivatives define the generalised momenta in eq. (5.1) leaving out the space derivatives. In general relativity, though, space and time are treated on an equal footing which is incompatible with the Hamiltonian description at first sight. This difference in the treatment is tackled by the introduction of a splitting of spacetime into spacelike hypersurfaces and the choice of a time evolution vector which is taken to be the basis of the Arnowitt-Deser-Misner (ADM) formalism [49, 50, 51, 52].

5.1 Spacetime Split in the context of the ADM Formalism

The major goal of the ADM approach is to find a Hamiltonian formulation of the Einstein-Hilbert action given in eq. (4.1) and therewith describe the Einstein equations in a canonical way. The idea can be summarised as follows: First foliate the spacetime manifold into spacelike hypersurfaces and a select a time direction. Then translate the variables of the Lagrangian into quantities characterising the spacetime foliation and define the corresponding conjugate momenta. In the end perform a variation of the Lagrangian in order to obtain the constraint and evolutionary equations resembling the Einstein field equations [155].

So let us start with the spacetime foliation. The spacetime manifold M equipped with a metric $g_{\mu\nu}$ is supposed to have a topological structure consisting of spacelike three-dimensional hypersurfaces Σ_t of constant time parameter $t \in \mathbb{R}$. In general relativity there are lots of ways to choose a time parameter so that we fix the direction of time derivatives by introducing a three-dimensional vector field t^i satisfying $t = t^i \nabla_i$ such that $t^i t_{;i} = 1$ on the spacetime manifold M representing the evolution of time through spacetime.

The geometry of each slice Σ_t is described by the intrinsic Riemannian structure defined by an induced spatial metric γ_{ij} which is a time-dependent three-dimensional tensor field living on the family of manifolds Σ_t. The corresponding tangent space is composed of a spatial tangent space characterised by the vector s^i and a timelike normal space characterised by the vector n^i imposing conditions on γ_{ij}:

$$\gamma_{ij} n^i \;=\; 0 \;, \qquad \gamma_{ij} = g_{ij} s^i \;,$$

yielding the induced metric

$$\gamma_{ij} = g_{ij} + n_i n_j \;,$$

where n_i is a unit normal vector field and s^j is tangent to some Σ_t. In order to be able to

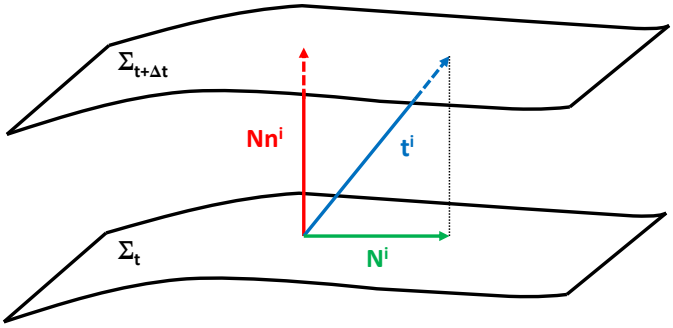

Figure 5.1: This figure shows the foliation of spacetime into spacelike hypersurfaces Σ_t of constant time. The decomposition of the time evolution vector $t^i = N n^i + N^i$ is visualised.

describe the dynamics in such a formulation it is necessary to know how the points on one hypersurface can be identified with points on another hypersurface, i.e. the time evolution of the coordinates has to be determined. Since the time direction does not necessarily have to be parallel to the direction of the normal vector, we can decompose the evolution of the coordinates in two pieces: the shift of the spatial coordinates tangential to Σ_t expressed by the shift vector N^i and the elapsed proper time when moving normal to Σ_t represented by the lapse function N, see fig. 5.1. Therewith the time evolution vector can be written as

$$t^i = N n^i + N^i \;.$$

Now, that we are able to describe the time evolution of each hypersurface by relating the coordinates from one to another hypersurface at different instants of time we can sew all the Σ_t together to obtain the initial spacetime M. Consequently, all information on the geometry of M described by $g_{\mu\nu}$ and quantities thereof is completely included in the induced spatial metric, the lapse function and the shift vector. Thus, by finding expressions relating the spacetime metric to γ_{ij}, N^i and N the Lagrangian is rewritten in terms of these variables and the corresponding velocities (remember γ_{ij} being time-dependent) as [153, 155]

$$\mathcal{L}\left(\gamma_{ij}, \dot{\gamma}_{ij}, N^i, \dot{N}^i, N, \dot{N}\right) \;.$$

Be careful with the velocities (the dot) in this context. We are still working in the framework of general relativity so that the Lagrangian should be independent of the choice of

coordinates including time. Therefore, we should differentiate to the local time, which is perpendicular to Σ_t at each point and given by the field that describes the time evolution. The corresponding time derivatives are realised by the Lie derivative along the time-evolution vector field t^i denoted by $\mathscr{L}_t$.

The time derivative of γ^{ij} is geometrically understood by means of the extrinsic curvature of Σ_t which measures how much the surface is curved in its embedding in spacetime. Put into different words, it is defined by the difference between an initially tangent vector that is parallel transported and and the one that remains tangent on M characterised by [155]

$$K_{ij} = \frac{1}{2}\mathscr{L}_n \gamma_{ij} \ , \tag{5.2}$$

where $\mathscr{L}_n$ is the Lie derivative along the unit normal vector. It provides a handy quantity to express the Lagrangian in a convenient way as a function of $\mathcal{L}\left(\gamma_{ij}, \dot{\gamma}_{ij}, N^i, N, \right)$ resulting in the following conjugate momenta

$$\Pi^{ij} = \frac{\partial \mathcal{L}}{\partial \dot{\gamma}_{ij}} \ , \qquad \Pi_N = \frac{\partial \mathcal{L}}{\partial \dot{N}} = 0 \ , \qquad \Pi^i_N = \frac{\partial \mathcal{L}}{\partial \dot{N}^i} = 0 \ .$$

Next it follows that the time derivatives of the conjugate momenta Π_N and Π^i_N have to vanish as well

$$\dot{\Pi}_N \ = 0 \ \ , \qquad\qquad \dot{\Pi}^i_N = 0 \ .$$

Then, emplyoing Hamilton's equations with the Hamiltonian function obtained by a Legendre transformation

$$H = \Pi^{ij}\dot{h}_{ij} - \mathcal{L} \ \ ,$$

gives the momentum and Hamilton's constraint

$$\dot{\Pi}_N \ = \ \frac{\partial H}{\partial N} \ \equiv 0 \ , \qquad\qquad \dot{\Pi}^i_N = \frac{\partial H}{\partial N^a} \equiv 0 \ ,$$

which are both primary constraints since they directly follow from the properties of the Lagrangian.

The remaining evolutionary equations are given by the variation of the Hamiltonian with respect to the induced metric. The number of the final equations is ten which is equivalent to the number of Einstein's field equations. An explicit computation shows indeed that this procedure yields the correct form of Einstein's equations in a consistent canonical formulation [155].

First applications focused on point masses and two-body systems with spin, see e.g. [58]. However the canonical treatment of dynamical systems consisting of a particle with

spin moving in a background gravitational field appears to be not that simple. This is why the next sections and chapters are devoted to the investigation of two different approaches to compute a Hamiltonian: the first is based on a Legendre transformation including the constraints by Dirac brackets, which we will explain in the following section. After that we analyse the properties of the resulting Hamiltonian before we describe the second approach which uses an action approach where the constraints enter via the Lagrange multipliers.

5.2 Hamiltonian for spinning testparticles in general relativity

In principle the two approaches considered in this thesis are not very different. Both strategies are developed on the basis of an action, the corresponding Lagrangian and a Legendre transformation to the Hamiltonian. The difference lies in the treatment of the constraints.

First, we will concentrate on the Hamiltonian as derived by E. Barausse, E. Racine and A. Buonanno and follow closely their work [53] .

5.2.1 Action Principle and Legendre Transformation

Starting from the general Lagrangian $L\left(g_{\mu\nu}, u^{\mu}, \Omega^{\mu\nu}\right)$ given in (4.5) we rewrite it as

$$L\left(x^{\mu}, u^{\mu}, e_{A}{}^{\mu}, \frac{de_{A}{}^{\mu}}{d\sigma}\right) \ ,$$

using the definition for the angular velocity $\Omega^{\mu\nu}$ in eq. (4.4). The orthonormal tetrad $e_{A}{}^{\mu}\left(x^{\mu}, \phi^{A}\right)$ characterising the body-fixed reference frame depends on the spatial coordinates x^{μ} as well as on six Lorentz parameters ϕ^{A} (three boosts, three spatial rotations) describing the orientation of the tetrad with respect to some background reference frame. Thus, it is related to a local tetrad $e_{a}{}^{\mu}\left(x^{\mu}\right)$ which serves as the reference frame covering the whole spacetime by a Lorentz transformation $\Lambda_{A}{}^{b}\left(\phi^{A}\right)$

$$e_{A}{}^{\mu}\left(x^{\mu}, \phi^{A}\right) = \Lambda_{A}{}^{b}\left(\phi^{A}\right) e_{b}{}^{\mu}\left(x^{\mu}\right) \ , \tag{5.3}$$

which satisfies the (flat spacetime) Lorentz matrix condition $\eta^{AB}\Lambda_{A}{}^{a}\Lambda_{B}{}^{b} = \eta^{ab}$. Therewith, the action yields

$$\mathcal{S} = \int L\left(x^{\mu}, u^{\mu}, \phi^{A}, \frac{d\phi^{A}}{d\sigma}\right) d\sigma \ .$$

Since we are not considering any fields but a particular particle with position variables, velocities and a finite number of degrees of freedom, the Lagrangian function is taken

instead of the Lagrangian density.

As already mentioned the action has to be invariant under a reparametrisation of the worldline parameter σ. Indeed, in order to obtain a Hamiltonian formulation the spacetime has to be splitted into $3+1$, so that we choose the coordinate time t to be the worldline parameter σ. Thus, we have $x^0 = t$, $u^0 = 1$ and define $v^i \equiv u^i = dx^i/dt$ with which we get

$$\mathcal{S} = \int L\left(x^i, v^i, \phi^A, \dot{\phi}^A \equiv \frac{d\phi^A}{dt}, t\right) dt \ ,$$

so that the configuration space is characterised by $\left(x^i, \phi^A\right)$. It has been discussed in section (4.3) that the momenta p_μ found by variation of $L\left(x^\mu, u^\mu, \Omega^{\mu\nu}\right)$ are not conjugate to the x^μ which, however, is desired to have. In order to redefine the momenta we first perform a variation of $L\left(x^i, v^i, \phi^A, \dot{\phi}^A, t\right)$

$$\delta L = \frac{\partial L}{\partial x^i}\delta x^i + \underbrace{\frac{\partial L}{\partial v^i}}_{P_i}\delta v^i + \frac{\partial L}{\partial \phi^A}\delta\phi^A + \underbrace{\frac{\partial L}{\partial \dot{\phi}^A}}_{P_{\phi^A}}\delta\dot{\phi}^A \ , \tag{5.4}$$

where we define the momenta P_i truly conjugate to x^i and the momenta P_{ϕ^A} which are the true conjugates to ϕ^A. Then, we compare eq. (5.4) with the variation of $L\left(x^i, v^i, \Omega^{\mu\nu}\right)$

$$\delta L = \left.\frac{\partial L}{\partial x^i}\right|_\Omega \delta x^i + \left.\frac{\partial L}{\partial v^i}\right|_\Omega \delta v^i + \left.\frac{\partial L}{\partial \Omega^{\mu\nu}}\right|_{x,v} \delta\Omega^{\mu\nu} \ , \tag{5.5}$$

using the variation of the angular velocity by considering its dependence on the set of variables $\left(x^i, v^i, \phi^A, \dot{\phi}^A\right)$

$$\delta\Omega^{\mu\nu} = \frac{\partial\Omega^{\mu\nu}}{\partial x^i}\delta x^i + \frac{\partial\Omega^{\mu\nu}}{\partial v^i}\delta v^i + \frac{\partial\Omega^{\mu\nu}}{\partial\phi^A}\delta\phi^A + \frac{\partial\Omega^{\mu\nu}}{\partial\dot{\phi}^A}\delta\dot{\phi}^A \ .$$

Therewith we obtain explicit expressions for the conjugate momenta P_i and P_{ϕ^A} as functions of the kinematical momenta p_i

$$\begin{aligned} P_i &= p_i + E_{i\mu\nu}S^{\mu\nu} \ , \\ P_{\phi^A} &= \frac{1}{2}S_{\mu\nu}\lambda_A{}^{ab}e_a{}^\mu e_b{}^\nu \ , \end{aligned} \tag{5.6}$$

with the tensors

$$\begin{aligned} E_{\alpha\mu\nu} &:= \frac{1}{2}\eta_{ab}e^a{}_\mu e^b{}_{\nu;\alpha} \ , \\ \lambda_A{}^{ab} &:= \Lambda_C{}^a\frac{\partial\Lambda^{Cb}}{\partial\phi^A} \ . \end{aligned} \tag{5.7}$$

Then we apply Euler's theorem on homogeneous functions to the Lagrangian, which is a homogeneous function of degree one in the velocities due to reparametrisation invariance, and arrive at

$$L = v^i p_i + p_t + \frac{1}{2} S_{\mu\nu}\Omega^{\mu\nu} \ ,$$

where we already implemented the worldline gauge $\sigma = t$ as well as the definition of p_μ and $S_{\mu\nu}$ from eq. (4.13). Then, a Legendre transformation is performed under the assumption that the Lagrangian is regular so that the Hamiltonian is given by [53]

$$\begin{aligned} H &= P_i v^i + P_{\phi^A}\dot{\phi}^A - L \\ &= -p_t - E_{t\mu\nu} S^{\mu\nu} \ . \end{aligned} \tag{5.8}$$

Strictly speaking this Hamiltonian is not yet related to a well defined Hamiltonian formalism, since the relation between the conjugate momenta and the velocities has not been established or fixed yet. This missing piece to the Hamiltonian refers to the ambiguity of the centre of mass in an extended body in general relativity, which is the reason for such a dynamical system to require a supplementary condition in order to be solvable. As a result, the MP equations can be derived from this general unconstrained Hamiltonian by computing the associated equations of motion [53]. Since the dynamical variables have a canonical structure, the equations of motion are simply Hamilton's equations.

To sum up, the canonical momenta have been found by the variation of a general Lagrangian that depends on independent variables. A comparison to the results of a Lagrangian containing the physical dynamical variables respecting the Poincaré invariance led to the canonical momenta. The next step concerns the inclusion of constraints in the phase space which supply the system with a relation between the velocities and the momenta.

5.2.2 Poisson and Dirac brackets

Generally, a Hamiltonian system lives in phase space which is equipped with a symplectic structure allowing to choose locally canonical coordinates [156, 157]. With the help of a bilinear differential operator, the Poisson bracket, the equations of motion are given by Hamilton's equations if the phase space variables are of canonical structure. If they are not canonical, their Poisson brackets yield more complicated expressions leading to a different formulation of the equations of motion. However, as long as the Poisson brackets of the phase space variables are known, the evolution of any dynamical quantity Q of the system can conveniently be expressed as

$$\frac{dQ}{dt} = \frac{\partial Q}{\partial t} + \{Q, H\} \ ,$$

where Q is some function on phase space.

So far the dynamics does not suffice any constraints. A quite straightforward way to impose constraints onto the phase space of a Hamiltonian system is provided by the substitution of the Poisson brackets by the so-called Dirac brackets [145, 158]. A condition that has to be satisfied in order for the approach to be applicable is that the matrix C_{ij} consisting of the set of constraints ξ_i

$$C_{ij} = \{\xi_i, \xi_j\} \ , \tag{5.9}$$

is not singular, classifying the constraints to be second class constraints[1]. The Dirac brackets are then calculated as [53, 145, 158]

$$\{Q, R\}_{DB} := \{Q, R\} - \{Q, \xi_i\} \left[C^{-1}\right]_{ij} \{\xi_j, R\} \ , \tag{5.10}$$

which suffices the same properties the Poisson bracket does: it is bilinear, antisymmetric, it satisfies the Leibniz rule and the Jacobi identity. By definition of the Dirac bracket it is easily seen that the Dirac brackets between the constraints ξ_i vanish. Then, the constraints can be used and included in the formalism, e.g. the Hamiltonian, before the Dirac brackets between any phase space variables or the Hamiltonian are actually computed. Thus the equations of motion of the constrained system are given by

$$\frac{dQ}{dt} = \frac{\partial Q}{\partial t} + \left\{Q, \bar{H}\right\}_{DB} \ , \tag{5.11}$$

with $\bar{H}$ as the Hamiltonian, which includes already the set of constraints ξ_i.

In the case of the general relativistic motion of a spinning particle we need a spin supplementary condition to fix the reference worldline within the extended body. Thus, this constraint is imposed according to the procedure we have just explained.

It is already known that the NW SSC leads to canonical variables in special relativity. Therefore, it is not very far fetched to guess that it also does in general relativity. So this should be a reasonable choice of a SSC. The general relativistic Newton-Wigner condition is given by eq. (1.39) and eq. (3.14) so that we define the first set of constraints by

$$Z^\mu := S^{\mu\nu} \left(p_\nu - \mathcal{M} e^{(t)}{}_\nu\right) = 0 \ ,$$

where $\mathcal{M}^2 = -p_\mu p^\mu$ is the dynamical mass, which contains contributions from the internal structure. It is worth noting here, that the mass is not necessarily conserved, even in the pole-dipole approximation, and is treated as a dynamical variable in order to keep track of all the dynamics.

[1] a more detailed overview on the classification on constraints is given in the section 8.1.

Since we have $Z^\mu \left(p_\mu - \mathcal{M} e^{(t)}{}_\mu\right) = 0$ due to the antisymmetry property of the spin tensor only three of the four constraints are independent. The spacetime split makes it reasonable to choose the three independent constraints to be the spatial ones. Then they can be viewed as constraints on P_{ϕ^A} because the map from the spin tensor to the momenta is one-to-one. However these constraints reduce the number of configuration variables by three which is not sufficient to maintain the symplectic structure of the phase space. Thus, an additional set of constraints on ϕ^A is required in order to equip the constrained hypersurface in phase space with the same number of configuration variables and corresponding conjugate momenta. A reasonable constraint follows from the choice of the time direction of the body-fixed frame to be aligned with the four-momentum [148]

$$\chi_\mu := e_{T\mu} - \frac{p_\mu}{\mathcal{M}} = 0 \ ,$$

which provides again three independent constraints on the phase space variables ϕ^A, which are chosen to be the spatial ones following the same argument as before. Therewith the set of constraints $\xi_i = \left(Z^i, \chi_i\right)$ is used to compute C_{ij}, its inverse and therewith the Dirac brackets. When the Dirac brackets between the position variables and the conjugate momenta are calculated the canonical structure is recovered [53]

$$\begin{aligned} \left\{x^i, x^j\right\}_{DB} &= \mathcal{O}\left(S^2\right) \ , \\ \left\{x^i, P_j\right\}_{DB} &= \delta^i_j + \mathcal{O}\left(S^2\right) \ , \\ \left\{P_i, P_j\right\}_{DB} &= \mathcal{O}\left(S^2\right) \ . \end{aligned} \tag{5.12}$$

The computations of the brackets involving the spin are simplified by using the spin projected onto the background tetrad

$$S^{(i)(j)} = S^{\mu\nu} e^{(i)}{}_\mu e^{(j)}{}_\nu \ , \tag{5.13}$$

with the flat spin vector

$$S^{(i)} = \frac{1}{2} \varepsilon^{(i)(j)(k)} S^{(j)(k)} \ , \tag{5.14}$$

recovering

$$\begin{aligned} \left\{x^i, S^{(j)}\right\}_{DB} &= \mathcal{O}\left(S^2\right) \ , \\ \left\{P_i, S^{(j)}\right\}_{DB} &= \mathcal{O}\left(S^2\right) \ , \\ \left\{S^{(i)}, S^{(j)}\right\}_{DB} &= \varepsilon_{(i)(j)(k)} S^{(k)} + \mathcal{O}\left(S^2\right) \ , \end{aligned} \tag{5.15}$$

which confirms the canonical structure of the phase space variables $\left(x^i,\, P_i,\, S^{(i)}\right)$ at linear

order in the particle's spin.

5.2.3 The Hamiltonian

The corresponding constrained Hamiltonian is obtained by inserting the constraints, in particular the solution to the mass shell condition $\mathcal{M}^2 + p_\mu p^\mu = 0$

$$p_t = -N^i p_i - N\,\sqrt{\mathcal{M}^2 + \gamma^{ij} p_i p_j}\ , \tag{5.16}$$

where the lapse function N, the shift vector N^i and the spatial metric γ^{ij} are already discussed in the context of the ADM formalism in section (5.1) and characterise the spacetime split needed for a Hamiltonian formulation; they are given by

$$N = \frac{1}{\sqrt{-g^{00}}}\ , \qquad N^i = \frac{g^{0i}}{g^{00}}\ , \qquad \gamma^{ij} = g^{ij} - \frac{g^{0i}g^{0j}}{g^{00}}\ . \tag{5.17}$$

Then, we obtain for the solution to the second constraint, the NW SSC given in eq. (1.39),

$$S^{(t)(i)} = \frac{S^{(i)(j)}\zeta_{(j)}}{\zeta_{(t)}}\ ,$$

which is plugged into the unconstrained Hamiltonian function (5.8) together with the result in (5.16), so that the new Hamiltonian can be expressed in terms of the canonical phase space variables offering the use of the Dirac brackets for the investigation of the dynamics. Now, the resulting Hamiltonian

$$\bar{H} = \bar{H}_{NS} + \bar{H}_S\ , \tag{5.18}$$

splits in two parts. Considering the linearisation in the particle's spin in the expression for the canonical momenta in eq. (5.6) and the solution to the mass shell constraint from eq. (5.16) the Hamiltonian for a non-spinning particle eventually yields

$$\bar{H}_{NS} = -P_t = N^i P_i + N\,\sqrt{\mathcal{M}^2 + \gamma^{ij} P_i P_j}\ , \tag{5.19}$$

where P_i are the canonical momenta conjugate to x^i of the Hamiltonian in (5.18). The second part of the Hamiltonian,

$$\bar{H}_S = -\left(N^i F_i^{(k)} + F_0^{(k)} + \frac{N\ \gamma^{ij} P_i\ F_j^{(k)}}{\sqrt{\mathcal{M}^2 + \gamma^{ij} P_i P_j}}\right) S_{(k)}\ , \tag{5.20}$$

describes the contribution of the spin of the particle to its motion, with

$$F_{\mu}^{(k)} = \left(2E_{\mu(t)(i)} \frac{\bar{\zeta}_{(j)}}{\bar{\zeta}_{(t)}} + E_{\mu(i)(j)} \right) \epsilon^{(i)(j)(k)} \ , \tag{5.21}$$

and

$$\begin{aligned}
\bar{\zeta}_a &= \bar{\zeta}_\nu \ e_a{}^\nu \ , \\
\bar{\zeta}_\nu &= \bar{P}_\nu - \mathcal{M} \ e^{(t)}{}_\nu \ , \\
\bar{P}_i &= P_i \ , \\
\bar{P}_0 &= -N^i \ P_i - N\sqrt{\mathcal{M}^2 + \gamma^{ij} P_i P_j} \ , \\
\bar{\zeta}_{(t)} &= \bar{P}_\nu \ e_{(t)}{}^\nu - \mathcal{M} \ , \\
\bar{\zeta}_{(j)} &= \bar{P}_\nu \ e_{(j)}{}^\nu \ .
\end{aligned} \tag{5.22}$$

where we changed the quantities to the local frame if they are related to the spin. Therefore, the equations of motion for any quantity Q are calculated according to (5.11) where we know Q as a function of the phase space variables. Indeed, it can be shown that the mass $\mathcal{M}$ is conserved up to linear order in the particle's spin

$$\left\{ \mathcal{M}^2, H \right\}_{DB} = \mathcal{O}\left(S^2\right) \ ,$$

which is consistent within the Hamiltonian formalism so that it is treated as a constant of motion. Thereby Hamilton's equations of motion yield the evolution equations for the phase space variables

$$\frac{dx^i}{dt} = \left\{ x^i, H \right\} = \frac{\partial H}{\partial P_i} \ , \qquad \frac{dP_i}{dt} = \{ P_i, H \} = -\frac{\partial H}{\partial x^i} \ , \tag{5.23}$$

$$\frac{dS_{(i)}}{dt} = \left\{ S_{(i)}, H \right\} = \epsilon_{(i)(j)(k)} \frac{\partial H}{\partial S_{(j)}} S^{(k)} \ . \tag{5.24}$$

Although a Hamiltonian formalism implies many advantages for the dynamical and/or numerical examination of the motion of spinning particles as well as for applications in the effective-one-body theory (EOB), this formalism is only valid at linear order in spin. Certainly, this approximation appears to be reasonable if the spin terms at quadratic and higher orders are considered to become important when the quadrupole or higher order multipole moments are taken into account, since the MP equations neglect all contributions from higher order multipoles than the dipole [54]. This statement is generally assumed and not rigorously proven, see e.g [55]. Moreover, Costa *et al.* [55] showed that the contributions from the quadratic terms in the pole-dipole approximation do matter when the particle

is assumed to be nearly spherical, i.e. when the influence of the quadrupole moment is ignored. In this sense, the approximation at linear order in the particle's spin corresponds to the assumption that the spin is supposed to be small. Consequently, it is of interest to know what effects this approximation in the Hamiltonian has on the resulting motion of a spinning particle compared to the solutions given by the MP equations.

Chapter 6

Numerical comparison: Lagrangian vs. Hamiltonian [1]

In the following, we compare the evolutions of a spinning particle moving around a rotating Kerr black hole given in eq. (1.8) obtained by the Hamiltonian formalism presented in the preceding section with the one gained by the MP equations supplemented by the NW SSC given in eq. (1.14), (1.15) with (1.39). The procedure and the challenges how to numerically integrate the MP equations are already discussed in chapter 3 and appendix A .

Thus, we focus on the integration procedure in the Hamiltonian formalism before we compare the resulting orbits. The main difference between the two approaches is the evolution parameter resulting from the spacetime split needed within a Hamiltonian formalism. While the worldline is parametrised by proper time τ in the MP equations it is coordinate time t for the Hamiltonian. In order to compare the two resulting worldlines we either have to rewrite the MP equations with respect to the coordinate time or find a way to relate the proper times to the coordinate times. Luckily, the coordinate times, at which our quantities were calculated in the MP simulations, were given as output anyway. Hence, the Hamiltonian is evolved at constant coordinate time steps $t_{i-1}, t_i, t_{i+1}, ...$ where $\Delta t = (t_{i+1} - t_i) = \text{constant}$. Then, we are given a coordinate time by the output of the MP equations t_{out} at which we would like to know the quantities given by the Hamiltonian formalism. Assume the required time lies within an interval given by t_i and t_{i+1}. Employing the interpolation property of collocation schemes we can compute an interpolation polynomial which stays close to the exact solution of the equations of motion and also to the numerically calculated trajectory. Therewith we obtain our solution at t_{out} by evaluating the interpolation function at the required time coordinate and the parametrisation

[1] This chapter is based on the work published in [1]

problem is solved.

Secondly, in order to numerically integrate Hamilton's equations of motion the integrator should be based on structure preserving algorithms respecting the geometric properties of the exact flows of differential equations. As an example, according to Liouville's theorem the flow of a Hamiltonian system is area preserving which is required to be true also after a long integration time. The differential equations of a Hamiltonian system are defined on a symplectic phase space which gives rise to the application of symplectic integrators, a subclass of geometric integrators [159]. They already have been successfully implemented for simulations in various fields in general relativity, see e.g. [160, 161, 162, 163].

6.1 Initial Set-Up

Another aspect is the use of canonical variables in the Hamiltonian formalism. Of course, they simplify the appearance and the computations of the equations of motion but they exacerbate the comparison to a Lagrangian based formalism. Therefore, the canonical variables $\left(x^i, P_i, S^{(i)}\right)$ are transformed to the dynamical ones $(x^\mu, p_\mu, S^{\mu\nu})$ or vice versa, in order to start both the MP equations and the corresponding Hamilton's equations with exactly the same initial setup. Then, since the canonical spin variables are projected onto a local Lorentz frame, it is important to fix the corresponding tetrad beforehand

$$\begin{aligned} e^{(t)}{}_\mu &= \delta^t_\mu \sqrt{\frac{\Delta\Sigma}{\Lambda}} \ , \\ e^{(1)}{}_\mu &= \delta^r_\mu \sqrt{\frac{\Sigma}{\Delta}} \ , \\ e^{(2)}{}_\mu &= \delta^\theta_\mu \sqrt{\Sigma} \ , \\ e^{(3)}{}_\mu &= -\delta^t_\mu \frac{2aMr\sin\theta}{\sqrt{\Lambda\Sigma}} + \delta^\phi_\mu \sin\theta \sqrt{\frac{\Lambda}{\Sigma}} \ , \end{aligned} \tag{6.1}$$

by adapting the tetrad basis vectors to the ones given by the Boyer-Lindquist coordinate system. The timelike tetrad vector enters the NW SSC in (1.39) so that we simultaneously choose an observer, that coincides with a ZAMO observer, i.e. $u_\phi = 0$, by setting up this tetrad.

The initial conditions are set up in the same way as in section 3.1 given by eq. (3.9) - (3.13). Then they are converted to Hamiltonian variables so that it is ensured that both formulations start from exactly the same state of the system (initial spin state, position in configuration space, etc.).

Before showing the results it is worth to say a few words on the physical interpretation. When the numerical comparison of two supplementary conditions within the same formalism was performed in chapter 3, the resulting worldlines did not necessarily correspond

to the same particle. This is caused by the choice of two different SSCs and the requirement that the orbits start at the same position in configuration space. Now, we no longer have two distinct supplementary conditions but two formalisms. Both formalisms, the MP equations as well as the Hamiltonian formalism, satisfy the NW SSC. Thus, we describe the dynamical evolution of one and the same spinning particle by two different approaches. Physically, the resulting worldlines in configuration space should be the same. However, since the Hamiltonian considers only terms up to linear order in spin in contrast to the MP equations, we expect deviations that become stronger if the spin value is increased.

Again, we measure lengths and times in units of the central object's mass M which is tantamount to $M = 1$. Since both the dynamical mass and the spin measure have proven to be not conserved during the evolution of the MP equations in the case of the NW SSC, we start with a value of $\mathcal{M} = 1$ and deduce the allowed range of values for the spin parameter according to the same reasoning as in section 3.1. The maximal absolute value of the spin is therewith obtained by an estimate for small compact spinning objects modeled by a Kerr black hole and amounts to 1. So let us start with the comparison for large spin $S = 1$.

6.2 Large spin

Using the initial conditions for the NW SSC within the MP formalism given in fig. 3.1, we have evolved the orbit by solving Hamilton's equations. The motion of the corresponding orbit in the configuration space is shown in the left panel of fig. 6.1 (black solid curve) together with the orbit evolved through the MP equations (blue dashed line).

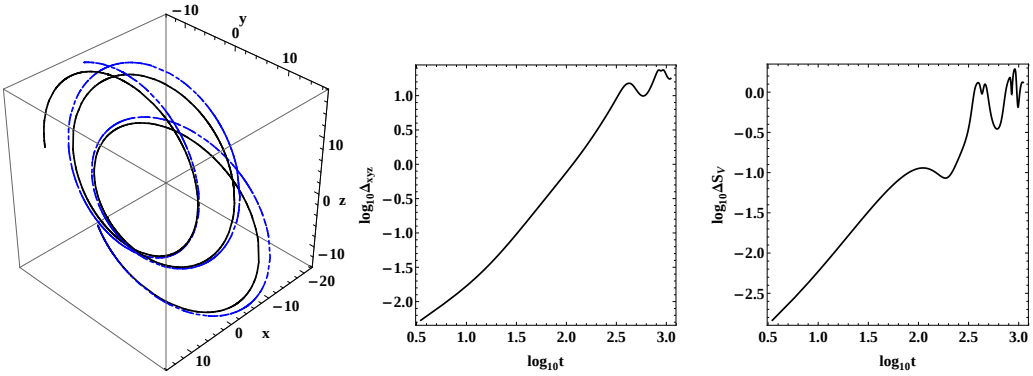

Figure 6.1: The left panel shows how the orbit evolves through the MP equations (blue dashed line) and through the Hamilton's equations (black solid curve) in the configuration space x, y, z, when we use the initial conditions given in fig. 3.1. The central panel shows the logarithm of the Euclidean distance in the configuration space between these two orbits as a function of the coordinate time. The right panel shows the logarithm of the Euclidean norm of the difference between the spin vectors of these two orbits as a function of the coordinate time.

Even if the two orbits start with the same initial conditions they depart from each other quite quickly. This is seen more clearly in the central panel of fig. 6.1, where the Euclidean distance between the two orbits

$$\Delta_{xyz} = \sqrt{(x_H - x_{MP})^2 + (y_H - y_{MP}) + (z_H - z_{MP})^2}\,, \tag{6.2}$$

is displayed as a function of the coordinate time. Close to the end of the calculation, the distance Δ_{xyz} is almost as large as the radial distance of the particle from the central black hole. From the appearance of the left panel of fig. 6.1 one might wonder whether the divergence between the orbits is a "synchronization" issue. However, since both schemes use the same SSC, i.e. the NW SSC, and since the initial conditions for both schemes are exactly the same, i.e. the orbits correspond to the same particle, the proper time for both orbits has to tick at the same rate. Thus, it is reasonable to claim that this divergence results from the fact that the Hamiltonian is valid up to the linear order in the particle spin, and since the spin here is large $S = 1$, such a divergence should be expected. Nevertheless, it is impressive that the orbits corresponding to the same particle evaluated with different schemes, i.e. the MP equations and the corresponding Hamiltonian, give a divergence that is of one order of magnitude greater than the divergence of the MP equations with different SSC (left panel of fig. 3.1 in section 3.2).

Here, it is now natural to check the value of the Möller radius, since we are looking at only one particle. Therefore, the separation of the two worldlines should not be greater than this radius if both formalisms do indeed describe the same particle. The distance between the two orbits though exceeds the diameter of the disc of centres of mass that is defined by the Möller radius $\frac{S}{\mathcal{M}}$. Hence, according to this criterion the orbits could not correspond to the same particle. Therefore, we can say that the Hamiltonian formalism does not agree with the MP equations for large spin values as expected.

The spin in the Hamiltonian formalism is given by the projection vector (5.13) and eq. (5.14). The Euclidean norm of the difference between the spin vector $S_H^{(i)}$ calculated by Hamilton's equations and the $S_{MP}^{(i)}$ calculated by the MP equations

$$\Delta S_{\mathrm{v}} = \sqrt{\sum_{i=1}^{3} \left(S_H^{(i)} - S_{MP}^{(i)}\right)^2}\,, \tag{6.3}$$

is plotted as a function of the coordinate time in the right panel of Fig. 6.1. This plot shows that the difference is quite high, even if the spin values are identical at first, and thus reflects the differences of the two formalisms. When decreasing the value of the spin, the two formalisms should converge. Since they are both describing spinning particles, we expect a convergence before they reach the geodesic limit. So, the next step is to consider

orbits of particles with small spins.

6.3 Small Spin

By decreasing the measure of the particle's spin to the level of $S = 10^{-8}$, we get the initial setup given in fig. 3.2 used for the MP equations.

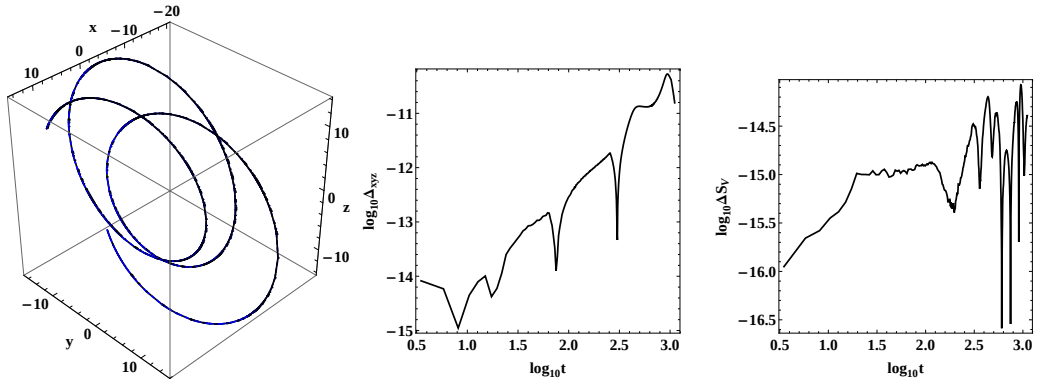

Figure 6.2: The left panel shows how the orbit evolves through the MP equations (blue dashed line) and through the Hamilton's equations (black solid curve) in the configuration space $x,\ y,\ z$, when we use the initial conditions given in fig. 3.2. The central panel shows the logarithm of the Euclidean distance in the configuration space between these two orbits as a function of the coordinate time. The right panel shows the logarithm of the Euclidean norm of the difference between the spin vectors of these two orbits as a function of the coordinate time.

The Euclidean distance between the evolutions of the MP equations and the Hamiltonian equations (central panel of fig. 6.2) drops to a level which is near the precision of our simulations. Therefore, practically, the two orbits should not discern. This seems to be the picture we get from the Euclidean norm of the difference between the spin vectors as well (right panel of fig. 6.2). Moreover, it is also evident that the distance between the two orbits does not exceed the diameter of the disc of centres of mass defined by the Möller radius for the coordinate time we have computed. Hence, it is reasonable to say that the two orbits obtained by two different formalisms do correspond to the same particle and thus infer that the Hamiltonian is indeed valid for small spin values as expected.

However, this picture might be a little bit illusive. The order of the spin is $S = 10^{-8}$, and thus what we see is in fact that the relative difference, i.e. $\Delta S_{\rm v}/S \approx 10^{-8}$ is of the order of the spins' magnitude. In other words, in the spin space the evolution of the two orbits do not agree completely. The reason that in the configuration space the orbits appear to be identical, while in the spin space the agreement is not at the same level, is that we are in the geodesic limit, and the evolution of the orbits is almost independent from the spins.

The bottom row of fig. 6.3 supports the claim that when $S = 10^{-8}$, we are at the geodesic limit, and the evolution does not depend on the spins. In the left panel of the bottom row in fig. 6.3, the relative errors of the Hamiltonian function,

$$\Delta H = \left| 1 - \frac{H(t)}{H(0)} \right| \quad , \tag{6.4}$$

lie at the computation precision level for both the MP orbit (gray line) and the Hamiltonian orbit (black line), while the level of the relative error (3.19) in the measure of the spin vectors,

$$S^2 = S_{(i)} S^{(i)} \quad , \tag{6.5}$$

is not as well preserved for the MP case (gray line) as for the Hamiltonian case (black line in the right panel of the bottom row in fig. 6.3). Notice that, as stated above, in the case of the MP equations, we can get the value of the Hamiltonian function H and of the square of the spin measure S^2 by transforming the set of kinematical variables $\{x^\mu, p^\mu, S^{\mu\nu}\}$ into the set of canonical variables $\{x^i, P^i, S^{(i)}\}$ and substituting the transformed set into eq. (5.18) and eq. (6.5) respectively. The remaining question now is, which values of spin is the Hamiltonian valid for. In order to answer this question it is easiest to investigate the convergence by examining the behaviour, i.e. the scaling, of the constants of motion.

6.4 Constants of Motion

When we raise the measure of the particle spin to $S = 10^{-4}$, then the relative error of the MP spin defined in eq. (6.5) remains practically at the same level (gray line in the right panel of the middle row in fig. 6.3) as in the $S = 10^{-8}$ case. This does not hold for the relative error of the Hamiltonian function (gray line in the left panel of the middle row in fig. 6.3) which is not at the computation precision level anymore. This shows that the motion is no longer in the geodesic limit. However, both ΔS^2 and ΔH for the MP orbit lie at acceptable levels, which show that for this magnitude of the particle spin, the MP equations and the Hamiltonian equations seem to be in agreement.

This agreement breaks when $S = 1$. The top row of fig. 6.3 shows that when $S = 1$, the relative errors, ΔH and ΔS^2 are at the same quite high level for the MP orbit. These relatively large values confirm the departure between the MP equations and the corresponding Hamiltonian that we see in fig. 6.1.

The black lines for all panels of fig. 6.3 are at the highest accuracy the computation accuracy allows, which means that apart from round-off error, the Gauss scheme we applied integrates accurately the system of Hamilton's equations, but also that the interpolation scheme we applied to match the coordinate times works quite well.

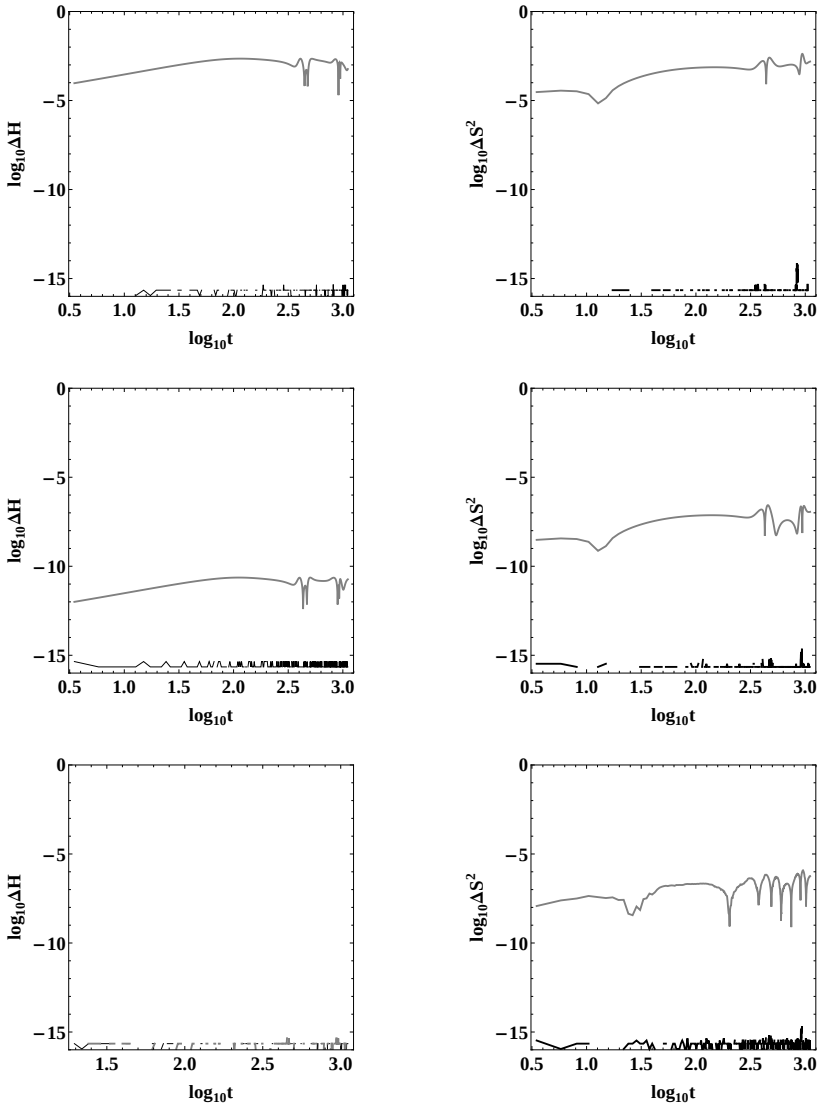

Figure 6.3: The top row of panels corresponds to the orbits of fig. 6.1, while the bottom row of panels corresponds to the orbits of fig. 6.2. The middle row of panels corresponds to initial conditions similar to fig. 3.1 only instead of spin measure $S = 1$ we set $S = 10^{-4}$. The gray lines represent the evolution of the MP equations, while the black lines the evolution of the Hamilton equations. The left column of panels shows the relative error in the preservation of the Hamiltonian function, while the right the preservation of the spin.

As at the end of the chapter 3, we can investigate the scaling of the constants of motion with the spin in more detail by taking the maxima of their relative errors for different values of the measure of the particle's spin. The result is shown in fig. 6.4. Again, as in the fig. 3.4, the precision of our computations and the scaling due to the spin measure shape the figure. We see a plateau at the left panel of fig. 6.4 for ΔH due to the computational

precision, while in the right panel of fig. 6.4 we see that ΔS^2 increases, which is due to to the smallness of the spin components. Even if we had applied a special integration scheme respecting these small quantities, this scheme could not follow below a threshold either. This threshold is in our case at $S = 10^{-6}$. When the scaling with the spin dominates ($S > 10^{-6}$), the linear fits show that $\Delta H \propto S^2$, while $\Delta S^2 \propto S$. These proportionalities are expected as we explain next.

By construction the Hamiltonian function H of a spinning particle is accurate up to linear order of the particle spin. Hence, when compared with the value of the Hamiltonian function yielded from the evolution of the MP equations $H_{MP}(t)$, the difference between the two Hamiltonian function values should differ by terms of the order $\mathcal{O}(S^2)$, i.e.,

$$H_{MP}(t) \approx H(t) + \mathcal{O}(S^2) \quad . \tag{6.6}$$

However, since we have chosen the same initial conditions for both evolution schemes, it holds that $H_{MP}(0) = H(0)$. Thus, the relative error from eq. (6.4) for the MP equations reads

$$\begin{aligned} \Delta H &= \left| \frac{H_{MP}(t) - H_{MP}(0)}{H_{MP}(0)} \right| \\ &\approx \left| \frac{H(t) - H(0)}{H(0)} + \frac{\mathcal{O}(S^2)}{H(0)} \right| \quad . \end{aligned} \tag{6.7}$$

Since we do not expect the relative error $\frac{H(t)-H(0)}{H(0)}$ to depend on the value of the particle's spin, and this expectation is confirmed by the numerical findings (black lines in the left column of fig. 6.3), we get the scaling $\Delta H \propto S^2$ of fig. 6.4.

In order to explain the scaling of the relative error ΔS^2, we use a similar way of reasoning. The preservation of the spin for the Hamiltonian formalism given in (6.5) is S^2. Thus a reasonable expectation is that for the MP case we should get values ${S^2}_{MP}(t)$ from eq. (6.5) which differ from the Hamiltonian case at order $\mathcal{O}(S^3)$, i.e.

$${S^2}_{MP}(t) \approx S^2(t) + \mathcal{O}(S^3) \quad . \tag{6.8}$$

Furthermore, we have ${S^2}_{MP}(0) = S^2(0)$. Thus, the relative error (3.19) for the MP equations reads

$$\begin{aligned} \Delta S^2 &= \left| \frac{{S^2}_{MP}(t) - {S^2}_{MP}(0)}{{S^2}_{MP}(0)} \right| \\ &\approx \left| \frac{S^2(t) - S^2(0)}{S^2(0)} + \frac{\mathcal{O}(S^3)}{S^2(0)} \right| \quad , \end{aligned} \tag{6.9}$$

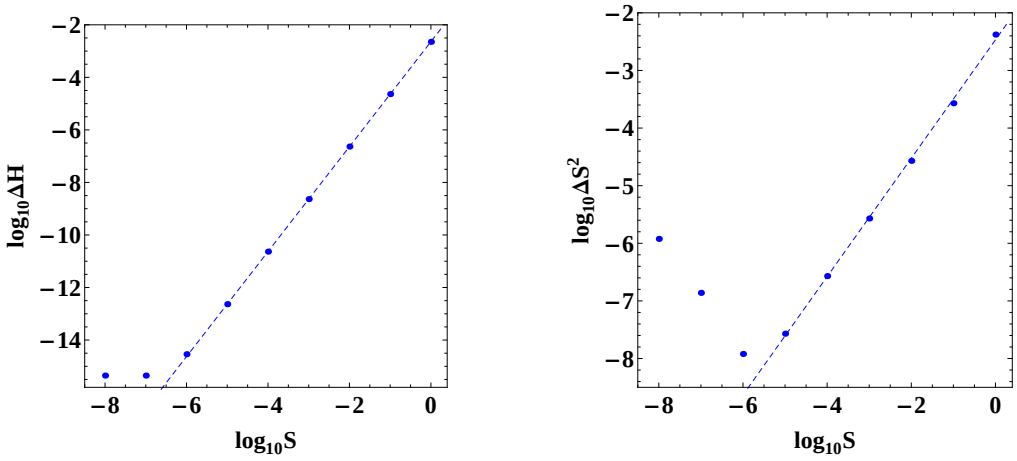

Figure 6.4: The left panel shows the relative error of the Hamiltonian ΔH of orbits evolved through the MP equations for different spin measures S of the particle, while the right panel shows the corresponding preservation of the measure of the 3-vector ΔS^2. The black dots correspond to the maximum values of ΔH, ΔS^2 respectively for each S. The dashed lines are linear fits of the form $\log_{10}\Delta H = a\log_{10} S + b$, and
$\log_{10}\Delta S^2 = c\log_{10} S + d$ respectively for data with $S > 10^{-6}$, where $a = 1.998 \pm 0.003$, $b = -2.642 \pm 0.003$, and
$c = 1.027 \pm 0.016$, $d = -2.469 \pm 0.048$.

which explains why we see that $\Delta S^2 \propto S$ in the right panel of fig. 6.4.

If we take as a criterion the convergence of the constants of motion shown in fig. 6.4, and consent that a relative error of the level of 10^{-6} is adequate to state that the different formalisms have converged, then from our comparison the Hamiltonian formalism is in agreement with the MP equations for the NW SSC when the measure of the particle's spin is $S < 10^{-4}$. When we reach $S \approx 10^{-6}$, the effect of the spin appears not to be important anymore, and the orbit evolves like a geodesic, i.e. it does not depend significantly on the spin. This characteristic behaviour is qualitatively not affected by a change of the Kerr spin a, or the sign of the spin value (see Appendix C for results for different values of a, and Appendix D for negative spin).

6.5 Discussion

To sum up we compared orbits given by the MP equations with orbits obtained via the Hamiltonian formalism of Barausse *et al.* [53] both supplemented by NW SSC. The difference between the respective orbits, which is quite significant for large spins of the order of one, decreases linearly as a function of the square of the test particle's spin, i.e. $\Delta H \propto S^2$, which agrees with the analysis given in [53].

According to our analysis, the Hamiltonian formalism of the spinning particle appears to be relevant in the range $10^{-6} < S < 10^{-4}$. For values of the spin smaller than 10^{-6} we can ignore the part of the Hamiltonian describing the spin evolution and keep the non-spinning part, which describes geodesic motion. For spin values greater than 10^{-4} our numerical results show that the Hamiltonian formalism is not in good agreement with the MP equations. Anyhow, the aforementioned range, where the Hamiltonian formalism is relevant, is appropriate for astrophysical binary systems of extreme mass ratio. Moreover, our simulations show that the CPU effort for the Hamilton equations of motion is far smaller than the computational cost for the MP equations (see Appendix B), so we find the use of these equations for simulations of test particles with small spins appropriate. When, in addition, favourable numerical methods, such as the one presented in this work, are applied, reliable results can be obtained within a short period of time. However, if one uses this Hamiltonian formalism, one has to be careful what kind of tetrads and/or coordinate systems the computation relies on. The effects evoked by a bad choice of tetrad and/or coordinate system are presented in the next chapter.

Chapter 7

Comparing Hamiltonians of a spinning test particle for different tetrad fields [1]

As we have seen earlier in this thesis, the behaviour of the MP equations supplemented by the T SSC and by the NW SSC is compared in chapter 3. In a second step, we compared the evolution of the system as described by the MP equations supplemented by the NW SSC to the corresponding evolution given by Hamilton's equations derived in [53] based on the same NW SSC in chapter 6. Therein, we focus on the latter, i.e. on a canonical Hamiltonian formalism which should be equivalent to the MP equations up to the linear order of the test particle spin. The corresponding results are published in [1]

In contrast to the T SSC the NW SSC, which is used within the framework of the Hamiltonian formalism, does not provide a unique choice of reference frame. It rather defines an entire class of observers, each characterised by a different tetrad field. Thus, the Hamiltonian formalism proposed in [53] depends on the choice of a reference basis given by such a tetrad field. Each choice of a tetrad field basically determines the form and the properties of the resulting Hamiltonian function. Although the tetrad basis vectors can geometrically be defined independently of any coordinate system, they are eventually expressed in some fixed coordinate system. Consequently, the description of the dynamical system in this Hamiltonian formalism is based on the coordinates. The question here is, whether the choice of a tetrad and also that of the coordinates influences the outcome obtained by (numerically) solving Hamilton's equations.

Before we start our discussion on the choices of coordinate systems and different tetrads, we shortly summarise the characteristic properties of the Hamiltonian formalism relevant

[1] This chapter is based on the work published in [3]

for our analysis. The Hamiltonian function is stated in (5.18) and is expressed in terms of canonical variables $\left(x^i,\, P_i\right)$ of which the conjugate momenta are given in (5.6) as functions of the kinematical momenta. Generally, the symplectic phase space of a Hamiltonian system is equipped with a binary operation, the Poisson bracket. If the dynamical system is subject to (secondary) constraints, as it is for general relativistic spinning particles, the Poisson bracket has to be replaced by the Dirac bracket (5.10) which respects these constraints [53, 145]. Consequently, the canonical structure of the phase space variables provided in eq. (5.12) and (5.15) within the linearised Hamiltonian formalism introduced in section (5.2) is given by

$$\begin{aligned}\left\{x^i, P_j\right\}_{DB} &= \delta^i_j \quad , \\ \left\{S^{(i)}, S^{(j)}\right\}_{DB} &= \epsilon^{(i)(j)(k)} S^{(k)} \quad .\end{aligned}$$

All other bracket relations between the variables vanish. Thus, the equations of motion for the canonical variables as a function of coordinate time t read simply Hamilton's equations stated in eq. (5.23) - (5.24). The general time evolution of any function on phase space is determined by eq. (5.11), which implies vanishing Dirac brackets for a conserved quantity I

$$\{I, H\}_{DB} = 0 \quad . \tag{7.1}$$

This means if a quantity is truly preserved, the Dirac bracket between I and H should be exactly zero, as long as the calculations are done consistently at the approximated level. For instance, the spatial spin measure

$$S^2 = S_{(i)} S^{(i)} \ , \tag{7.2}$$

yields

$$\left\{S^2, H\right\}_{DB} = 0 \ ,$$

so that S^2 is a constant of motion.

The mass $\mathcal{M}^2 = -p_\nu p^\nu$ considered as a function of the kinematical momenta is generally not a constant of motion for the exact MP equations with NW SSC but scales quadratically in the particle's spin, see section 3.4. Since the mass appears to be preserved at first order in the spin, a linearised Hamiltonian formalism is expected to conserve $\mathcal{M}$ at linear order

$$\{\mathcal{M}, H\}_{DB} = \mathcal{O}\left(S^2\right) \quad ,$$

where the higher order terms are dropped in the linearised case. This is consistent with the Hamiltonian approach and discussed in [53]. Thus, in the context of the Hamiltonian

formulation the mass is a conserved quantity in agreement with the linearised MP equations supplemented with NW SSC.

The formulation provided up to this point is general, in the sense that it does not depend on a specific coordinate system or on a specific tetrad field. These two factors, however, are essential for the Hamiltonian function (5.18). In particular, the non-spinning part of the Hamiltonian function (5.19) depends on the coordinate system which the metric is written in, while the spinning part (5.20) depends on the tetrad we choose.

In the following sections 7.1 and 7.2, we present three different combinations tetrad $\leftrightarrow$ coordinates for the Kerr spacetime background and discuss the advantages and shortcomings of the respective setups. Let us motivate our search for suitable tetrad and coordinate choices by discussing the advantages and the drawbacks of Hamiltonian functions arising from tetrad fields already proposed in [47, 53].

7.1 The Hamiltonian Function in Boyer-Lindquist coordinates compared with Cartesian Isotropic coordinates

It appears to be natural and it actually is quite common to use Boyer-Lindquist coordinates for an examination of dynamical systems in Kerr spacetime. Indeed, its axial symmetry naturally suggests these coordinates. However, it is not always the best choice, in particular if numerical calculations are involved as we will show in the subsequent analysis.

7.1.1 A tetrad in Boyer-Lindquist coordinates

The Hamiltonian formalism developed by E. Barausse, E. Racine and A. Buonanno [53] is already presented in section 5.2, which the reader is referred to for more information on the Hamiltonian. They also introduced the Hamiltonian function for Kerr spacetime in Boyer-Lindquist coordinates (BL) and gave explicit expressions, so that the continuation of further computations is made very easy. The line element of the Kerr spacetime in BL coordinates is given in (1.8) and the corresponding background tetrad field used in [53] reads

$$
\begin{aligned}
e^{(t)}{}_{\mu} &= \delta^t_{\mu}\sqrt{\frac{\Delta\Sigma}{\Lambda}}\,, & e^{(1)}{}_{\mu} &= \delta^r_{\mu}\sqrt{\frac{\Sigma}{\Delta}}\,,\\
e^{(2)}{}_{\mu} &= \delta^{\theta}_{\mu}\sqrt{\Sigma}\,, & e^{(3)}{}_{\mu} &= -\delta^t_{\mu}\frac{2aMr\sin\theta}{\sqrt{\Lambda\Sigma}} + \delta^{\phi}_{\mu}\sin\theta\sqrt{\frac{\Lambda}{\Sigma}}\,,
\end{aligned}
\tag{7.3}
$$

where for the small indices the numbers have been replaced with the corresponding coordinates, i.e. $t,\ r,\ \theta,\ \phi$ stand for $0,\ 1,\ 2,\ 3$, respectively. Recall, that the indices

written in parenthesis are associated to the local Lorentz basis. The proposed tetrad corresponds to a stationary observer in the zero-angular-momentum frame (ZAMO), i.e. $u_\phi = 0$, which intuitively yields a reasonable tetrad choice. Moreover, the coordinate system is based on the spherical coordinates in flat spacetime and respects the symmetries of the Kerr spacetime.

In the Schwarzschild limit the above tetrad field reduces to ($a \to 0$)

$$\begin{aligned} e^{(t)}{}_\mu &= \delta^t_\mu \sqrt{f(r)} \ , & e^{(1)}{}_\mu &= \delta^r_\mu \sqrt{f(r)^{-1}} \ , \\ e^{(2)}{}_\mu &= r \ \delta^\theta_\mu \ , & e^{(3)}{}_\mu &= r \ \sin\theta \ \delta^\phi_\mu \ . \end{aligned} \tag{7.4}$$

where $f(r)$ is given in (1.6). Then, in the flat spacetime limit ($M \to 0$, $a \to 0$) we get

$$\begin{aligned} e^{(t)}{}_\mu &= \delta^t_\mu \ , & e^{(1)}{}_\mu &= \delta^r_\mu \ , \\ e^{(2)}{}_\mu &= r \ \delta^\theta_\mu \ , & e^{(3)}{}_\mu &= r \ \sin\theta \ \delta^\phi_\mu \ , \end{aligned} \tag{7.5}$$

which simply yields the space dependent coordinate basis vectors in spherical coordinates in flat spacetime.

Now, we have a closer look at the dynamics in Schwarzschild spacetime. The corresponding metric in Schwarzschild spacetime is given in (1.5) with (1.6) and the associated tetrad field is defined in (7.4). Therewith, the Hamiltonian can be computed according to (5.18)-(5.22) as

$$H = H_{NS} + H_S \ ,$$

and is expressed in terms of the new canonical phase space variables

$$\left(r, \theta, \phi, P_r, P_\theta, P_\phi, S^{BL}{}_{(i)}\right) \ ,$$

where $S^{BL}{}_{(i)}$ stands for the spin projected onto the spatial background tetrad in spherical coordinates (reduced from the Boyer-Lindquist coordinates). All told, we have

$$\begin{aligned} H = & \frac{1}{\sqrt{f\,(r)}}\sqrt{Q} + \frac{M}{r^3\left(1+\sqrt{Q}\right)}\left(P_\theta S^{BL}{}_{(3)} - \frac{P_\phi}{\sin\,(\theta)} S^{BL}{}_{(2)}\right) \\ & - \frac{f\,(r)}{r^2\sqrt{Q}}\left(\frac{\cos\,(\theta)}{\sin^2\theta\sqrt{f\,(r)}} P_\phi S^{BL}{}_{(1)} - \frac{P_\phi}{\sin\,(\theta)} S^{BL}{}_{(2)} + P_\theta S^{BL}{}_{(3)}\right) \ , \end{aligned} \tag{7.6}$$

where

$$Q = \mathcal{M}^2 + f\,(r)\,P_r^2 + \frac{1}{r^2}P_\theta^2 + \frac{1}{r^2\sin^2\,(\theta)}P_\phi^2 \ .$$

A criterion in order to check whether the choice of coordinates is a "good" one, is provided by the behaviour of the Hamiltonian in flat spacetime. Ideally, the contributions

from the spin to the Hamiltonian H_S vanish, since we no longer have curvature which the spin could couple to and the trajectory of the spinning particle should simply be the one of a straight line. Thus, the motion of the particle should be completely independent of the spin.

However, in the case of spherical coordinates the contribution from the spin part in the Hamiltonian given by (7.6) does not vanish and represents an evolution of the spin in the absence of spin-orbit coupling or any other external forces, as was noted in [53]. This implies a coordinate effect which affects the analysis of the equations of motion for this choice of tetrad. Indeed, the basis vectors are coordinate dependent, since they are oriented along the direction of the coordinate basis vectors in spherical coordinates. Therefore, they introduce an additional evolution to the dynamical system which affects the equations of motion for the spinning particle, i.e. the equations of motion do not only contain the physical dynamics of the spinning object but also the unphysical coordinate dynamics. As a result, this coordinate dependence makes it harder to gain insights into the physical behaviour of the particle's motion, in particular if we have to rely on numerical calculations. In such situations, it is not so easy to distinguish between coordinate effects and physical effects in the outcome. Therefore, it is important to thoroughly think about the choice of coordinates before starting a numerical analysis.

Next, a solid check whether numerical calculations provide reliable results is connected to the preservation of the constants of motion during the evolution of a dynamical system. Generally, according to Noether's theorem each spacetime symmetry is related to a conserved quantity. In the case of spinning particles moving in a particular spacetime geometry equipped with a symmetry described by a Killing vector ξ_μ, the associated quantity conserved by the MP equations is stated in (1.16). In Schwarzschild spacetime we have three spatial Killing vectors corresponding to spherical symmetry yielding the three components of the total angular momentum [35]

$$\begin{aligned}
J_x =& -p_\theta \sin(\phi) - p_\phi \cot(\theta)\cos(\phi) + r^2 S^{\theta\phi}\sin(\theta)^2\cos(\phi) + rS^{\phi r}\sin(\theta)\cos(\theta)\cos(\phi) \\
& - rS^{r\theta}\sin(\phi) \quad , \\
J_y =& \; p_\theta \cos(\phi) - p_\phi \cot(\theta)\sin(\phi) + r^2 S^{\theta\phi}\sin(\theta)^2\sin(\phi) + rS^{\phi r}\sin(\theta)\cos(\theta)\sin(\phi) \\
& + rS^{r\theta}\cos(\phi) \quad , \\
J_z =& \; p_\phi - r\sin(\theta)^2\left(S^{\phi r} - rS^{\theta\phi}\cot(\theta)\right) \quad ,
\end{aligned}$$

where p_i are the kinematical momenta and S^{ij} the spin components written in the coordinate basis. In order to check whether the components of the total angular momentum are constants of motion within the Hamiltonian formulation we have to transform these expressions to the canonical variables P_i and $S^{BL}{}_{(i)}$ using the relations given in (5.6) and

(5.13). Therewith we obtain

$$
\begin{aligned}
J_x &= \cos(\phi)(S^{BL}{}_{(1)}\csc(\theta) - P_\phi\cot(\theta)) - P_\theta\sin(\phi) \ , \\
J_y &= P_\theta\cos(\phi) + \sin(\phi)(S^{BL}{}_{(1)}\csc(\theta) - P_\phi\cot(\theta)) \ , \\
J_z &= P_\phi \ ,
\end{aligned}
$$

for the components of the total angular momentum, with which we may now compute the evolution equations for J_i via the Dirac brackets with the Hamiltonian, given in (5.11). Then, they result in

$$
\begin{aligned}
\{J_x, H\}_{DB} &= \mathcal{O}\left(S^2\right) \ , \\
\{J_y, H\}_{DB} &= \mathcal{O}\left(S^2\right) \ , \\
\{J_z, H\}_{DB} &= 0 \ ,
\end{aligned}
$$

and the measure of the time evolution of the total angular momentum yields

$$
\left\{J_x^2 + J_y^2 + J_z^2, H\right\}_{DB} = \mathcal{O}\left(S^2\right) \ .
$$

Although we consistently keep the linearisation in the Hamiltonian and the corresponding bracket structure, we find that the Dirac brackets for J_x, J_y and J_z contain contributions from higher orders in the particle's spin. Indeed, J_x and J_y start oscillating when the Hamiltonian system corresponding to the tetrad field (7.4) is numerically evolved through the equations of motion (5.23)-(5.24). It is visible from the relative error

$$
\Delta J_i = |1 - \frac{J_i(t)}{J_i(0)}| \quad i = x, y \ , \tag{7.7}
$$

at time t of the J_x and J_y (grey line) in Fig. 7.1, that the Hamiltonian function resulting from the tetrad (7.4) apparently violates the symmetry properties of the Schwarzschild spacetime. Consequently, the total angular momentum J^2 is not preserved, because the x and y components of the total angular momentum exhibit inappropriate behaviour. On the other hand, the respective evolution using the MP equation supplemented with NW SSC, instead, shows the expected preservation of the angular momentum components (black curves in Fig. 7.1). This shows that even in the above linear in spin Hamiltonian approximation a quantity is a constant of motion only when its Dirac brackets with the Hamiltonian are exactly zero, while when the brackets have contributions from the higher spin orders, the quantities show no constancy. It is true, however, that the relative error of the J_x and J_y components scale with S^2, i.e. when the spin measure S is reduced the

relative errors are reduced accordingly.

Again, we measure the spin in units of the masses $\mathcal{M}M$ in our numerical calculations and set both masses to 1, so that the spin parameter S is dimensionless. Since we do not intend to derive astrophysical implications from our results but concentrate on the general dynamical properties of the Hamiltonian formalism, we choose the limit $S = 1$, as it is explained in [36].

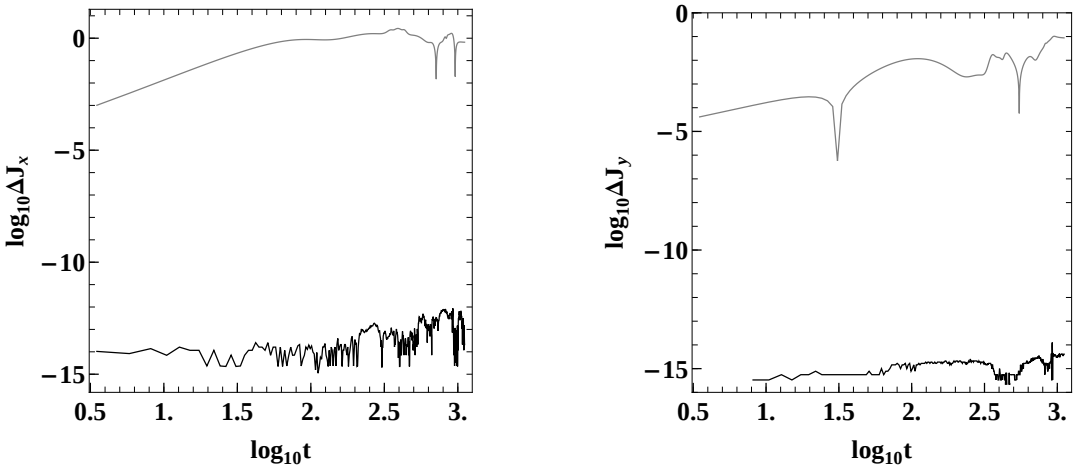

Figure 7.1: The left panel shows the relative error ΔJ_x, and the right of ΔJ_y as a function of time in logarithmic scale for the Schwarzschild background. The grey lines show the relative error of these quantities when the system is evolved using the Hamiltonian function corresponding to the tetrad (7.4), while the black lines show the relative error of these quantities when the system is evolved using the respective MP equations. Both evolutions share the same initial conditions conditions, where $a = 0$, $M = m = 1$, and $S = 1$.

Moreover, we find that the measure of the orbital angular momentum is also preserved up to linear order in spin

$$\left\{L_x^2 + L_y^2 + L_z^2, H\right\}_{DB} = \mathcal{O}\left(S^2\right) \quad ,$$

with the components given by

$$\begin{aligned} L_x &= -p_\theta \sin(\phi) - p_\phi \cot(\theta)\cos(\phi) \ , \\ L_y &= p_\theta \cos(\phi) - p_\phi \cot(\theta)\sin(\phi) \ , \\ L_z &= p_\phi \ , \end{aligned}$$

which also have to be rewritten in terms of the canonical momenta P_i (5.6) before computing the Dirac bracket. The conservation of the measure of the orbital angular momentum of

the linearised in spin MP equation in the case of the Schwarzschild spacetime background has been thoroughly discussed in [101] for the P SSC.

When the measure of the spin $S^2 = S_{(i)}S^{(i)}$ and the total angular momentum J^2 are preserved, the integral of motion L^2 is equivalent to the conservation of $\vec{L}\cdot\vec{S}$, which will be used in the investigation of the dependence of the preservation of the constants of motion on the choice of coordinates and/or tetrads. However, as we have already seen for the total angular momentum in this setting, we recover the same numerical problems for the measure of the orbital angular momentum showing some kind of oscillating behaviour. These two kinds of oscillations can be traced back to the coordinate dependence of the basis vectors in the spherical coordinate system, as we will see in the next section 7.1.2.

So far, these coordinate effects have been investigated in Schwarzschild spacetime. Since the Schwarzschild spacetime is the non-rotating limit of the Kerr spacetime, we would like to ensure that such coordinate effects can be eliminated in the non-rotating limit, i.e. the coordinate effects should vanish for non-rotating or slowly rotating black holes. Thus, we are wondering whether there are more suitable choices of coordinate systems and of a tetrad for rotating black holes which do not show any unphysical coordinate effects in the Schwarzschild limit. Subsequently, the question arises as to which coordinates are best used.

Therefore, in the rest of section 7.1 we study the Hamiltonian formulation in an isotropic coordinate systems for the same kind of observer (ZAMO), as it was introduced by [47].

7.1.2 The Hamiltonian function in isotropic Cartesian coordinates

A revised Hamiltonian function for the Kerr spacetime background in BL coordinates has been provided in [47]. The formulation starts in Cartesian quasi-isotropic coordinates. The line element in these coordinates for an axisymmetric stationary metric reads

$$\begin{aligned} ds^2 &= g_{tt}\, dt^2 + 2\, g_{tX} dX\, dt + 2\, g_{tY} dY\, dt + 2\, g_{XY} dX\, dY + g_{XX}\, dX^2 + g_{YY}\, dY^2 \\ &\quad + g_{ZZ}\, dZ^2 \quad , \end{aligned}$$

with

$$\begin{aligned} g_{tt} &= e^{-2\beta}\left[B^2\omega^2(X^2+Y^2) - e^{4\beta}\right] \quad , & g_{tX} &= e^{-2\beta}\omega B^2 Y \quad , \\ g_{tY} &= -e^{-2\beta}\omega B^2 X \quad , & g_{XY} &= -\frac{(e^{-2\beta}B^2 - e^{2\alpha})XY}{X^2+Y^2} \quad , \\ g_{XX} &= \frac{e^{2\alpha}X^2 + e^{-2\beta}B^2\, Y^2}{X^2+Y^2} \quad , & g_{YY} &= \frac{e^{2\alpha}Y^2 + e^{-2\beta}B^2\, X^2}{X^2+Y^2} \quad , \\ g_{ZZ} &= e^{2\alpha} \quad , \end{aligned} \tag{7.8}$$

and the coefficients are expressed by

$$B=\frac{\sqrt{\Delta}}{R},\qquad e^{2\beta}=\frac{\Delta\Sigma}{\Lambda},\qquad e^{2\alpha}=\frac{\Sigma}{R^2},\qquad \omega=\frac{2Mar}{\Lambda}\ ,$$

where the quantities (Δ, Σ, Λ) are provided in (1.10). They can be expressed as functions of (X, Y, Z) using the transformation properties between the Cartesian quasi-isotropic coordinates and the BL coordinate system

$$X=R\left(r\right)\sin\theta\cos\phi\ \ ,\qquad Y=R\left(r\right)\sin\theta\sin\phi\ \ ,\qquad Z=R\left(r\right)\cos\theta\ \ ,$$

where

$$R\left(r\right)\ \ =\ \ \frac{1}{2}(r-M+\sqrt{\Delta})\ \ . \tag{7.9}$$

The above relation between r and R holds only outside the black hole's horizon [2].

For this coordinate system the authors propose the tetrad field

$$\begin{aligned}
e^{(t)}{}_{\mu}&=e^{\beta}\delta^{t}_{\mu}\ \ ,\quad e^{(1)}{}_{\mu}=\frac{B\ \omega\ Y}{e^{\beta}}\delta^{t}_{\beta}+\frac{e^{\alpha}X^2+e^{-\beta}B\ Y^2}{X^2+Y^2}\delta^{X}_{\mu}+\frac{(e^{\alpha}-e^{-\nu}B)XY}{X^2+Y^2}\delta^{Y}_{\beta}\ \ ,\\
e^{(3)}{}_{\mu}&=e^{\alpha}\delta^{Z}_{\mu}\ \ ,\quad e^{(2)}{}_{\mu}=-\frac{B\ \omega\ X}{e^{\beta}}\delta^{t}_{\beta}+\frac{(e^{\alpha}-e^{-\beta}B)XY}{X^2+Y^2}\delta^{X}_{\mu}+\frac{e^{\alpha}Y^2+e^{-\beta}B\ X^2}{X^2+Y^2}\delta^{Y}_{\mu}\ \ ,
\end{aligned} \tag{7.10}$$

which also corresponds to a ZAMO observer. Notice, this tetrad becomes Cartesian, i.e. $e^{(t)}{}_{\mu}=1$, $e^{(1)}{}_{\mu}=\delta^{(i)}_{\mu}$, in the flat spacetime limit.

When we approach limit of the Schwarzschild spacetime where $a\to 0$,

$$ds^2=-f(R)dt^2+h(R)(dX^2+dY^2+dZ^2), \tag{7.11}$$

the tetrad (7.10) reduces to the isotropic tetrad given in [53]:

$$\begin{aligned}
e^{(t)}{}_{\mu}&=\sqrt{1-\frac{2M}{r}}\delta^{t}_{\mu}=\sqrt{f\left(R\right)}\delta^{t}_{\mu}\ \ ,\qquad & e^{(1)}{}_{\mu}&=\frac{r}{R}\delta^{X}_{\mu}=\sqrt{h\left(R\right)}\delta^{X}_{\mu}\ ,\\
e^{(2)}{}_{\mu}&=\frac{r}{R}\delta^{Y}_{\mu}=\sqrt{h\left(R\right)}\delta^{Y}_{\mu}\ , & e^{(3)}{}_{\mu}&=\frac{r}{R}\delta^{Z}_{\mu}=\sqrt{h\left(R\right)}\delta^{Z}_{\mu}\ ,
\end{aligned} \tag{7.12}$$

with

$$r=R\left(1+\frac{M}{2R}\right)^2\ \ ,\qquad f(R)=\frac{\left(2R-1\right)^2}{\left(2R+1\right)^2}\ ,\qquad h\left(R\right)=\left(1+\frac{M}{2R}\right)^4\ \ .$$

[2] The general relation between r and R is $r=R+M+\dfrac{M^2-a^2}{4\ R}$

In order to check the behaviour of these so called isotropic Cartesian coordinates (X, Y, Z) we analyse the conservation of the constants of motion given by the symmetries of the system. The spherical symmetry of the spacetime can be described in Cartesian-like coordinates x^μ by the three Killing vectors

$$\xi_k^\mu = \epsilon^{klm} x^l \delta_m^\mu. \tag{7.13}$$

Using (1.16) we thus get the three conserved components of the total angular momentum as a combination of kinematical momentum p_μ and components of spin tensor $S^{\mu\nu}$. On the other hand, in the canonical description, the conservation of the components of the total angular momentum

$$J_k = \epsilon^{kij} x^i P_j + S_{(k)} \ , \tag{7.14}$$

is demonstrated by vanishing Dirac brackets

$$\{J_k, H\}_{DB} = 0, \tag{7.15}$$

which is the preferred result we would like to have for numerical calculations. Contrary to the previous expressions for the components of the total angular momentum obtained by the Killing vectors (7.13) and the conserved quantity for spinning particles (1.16), the canonical momenta P_i and tetrad components of the spin appear in this formula (7.14). The relations between the two sets of quantities, the kinematical and the canonical ones, are given by (5.6) and (5.13). By computing the difference of the projection of (1.16) and (7.14) it can be shown, that if the Lie derivatives of the three spatial tetrad vectors obey the Cartesian-like rule

$$\left(\xi_k e_{(i)}{}^\mu\right) e_{(j)\mu} = \epsilon_{kij} \quad \wedge \quad \xi_k^0 \equiv 0 \ , \tag{7.16}$$

the two conserved quantities, one in kinematical variables (1.16) and the other in canonical ones (7.14), are identical. Indeed, this formula holds in flat Minkowski spacetime for Cartesian tetrad $e_\mu{}^a = \delta_\mu^a$, which naturally leads to the intuition, that a tetrad, that reduces to a Cartesian one in flat spacetime, is a good tetrad choice. In (7.16) the fact that the time component of the Killing vectors is required to vanish is explicitly stated, since it is written as a covariant, coordinate independent formula, but it was derived using this coordinate assumption.

The general condition (7.16) can now be applied to the particular case of the Schwarzschild limit (7.11). As Lie derivatives can be written using partial rather then covariant derivatives, one can easily check, that the tetrad field (7.12) satisfies (7.16).

Yet, as an example, that the equivalence between the components of the total angu-

lar momentum expressed in kinematical and canonical variables is not so obvious, let us consider a symmetry of the Schwarzschild spacetime with respect to a rotation along the z-axis

$$\xi_z^\mu = [0, -Y, X, 0]. \tag{7.17}$$

It yields the related component of the total angular momentum

$$J_z = Xp_y - Yp_x + S^{xy}\left(h\left(R\right) + \frac{\left(h\left(R\right)\right)'}{2R}\left(X^2+Y^2\right)\right) - \frac{\left(h\left(R\right)\right)'}{2R} Z\left(XS^{yz} + YS^{zx}\right) \quad .$$

Here, p_i represent the kinematical MP momenta and S^{ij} the coordinate spin components, the prime denotes the ordinary partial derivative with respect to R. In the Hamiltonian approach we use the canonical momenta P_i and the projected spin components $S^{(i)}$, so it is necessary to perform a transformation from $\left(p_i, S^{ij}\right)$ to $\left(P_i, S^{(i)}\right)$ using the relations given in eq. (5.6) and (5.13). With these, terms proportional to $h'(R)$ get absorbed into P_x and P_y and the corresponding component of the total angular momentum can indeed be written as

$$J_z = XP_y - YP_x + S_{(3)} \quad . \tag{7.18}$$

In order to check the conservation of J_x, J_y and J_z we have to express the Hamiltonian in terms of the canonical variables and isotropic coordinates. Then the Dirac brackets can be computed to obtain the time evolution of the total angular momentum. The corresponding Hamiltonian in these coordinates, cf. [53], reads

$$H = H_{NS} + H_S \ ,$$

with

$$H_{NS} = \frac{1}{\sqrt{f\left(R\right)}}\sqrt{Q} \ , \tag{7.19}$$

$$H_S = \frac{1 - \frac{M}{2R} + 2\left(1 - \frac{M}{4R}\right)\sqrt{Q}}{\left(1+\frac{M}{2R}\right)^6 R^3 \sqrt{Q}\left(1+\sqrt{Q}\right)} \frac{M}{\mathcal{M}}\left(\vec{L}\cdot\vec{S}\right) \ , \tag{7.20}$$

and $Q = \mathcal{M}^2 + \frac{1}{h(R)}\vec{P}^2$. The term H_S contains the contribution to spin-orbit coupling $\vec{L}\cdot\vec{S}$ influencing the motion of spinning particles in Schwarzschild spacetime. Notice, that setting $M \to 0$, i.e. no gravitational field, we indeed obtain that the spin part of the Hamiltonian H_S becomes zero and the spin-orbit coupling vanishes, as it should in Minkowskian spacetime.

Next, we can easily compute the evolution equations for J_x, J_y and J_z as

$$\{J_x, H\}_{DB} = 0 \ ,$$
$$\{J_y, H\}_{DB} = 0 \ ,$$
$$\{J_z, H\}_{DB} = 0 \ ,$$

which is thus also true for the measure of the total angular momentum J^2. Then, using the argument stated above, we know that $\left\{L^2, H\right\} = 0$ holds, since we can write $H = H\left(|\vec{r}|^2, |\vec{P}|^2, \vec{r}\cdot\vec{P}, \vec{L}\cdot\vec{S}\right)$ with $\vec{L}\cdot\vec{S}$ the only terms containing the spin part. $L^2 = L_x^2 + L_y^2 + L_z^2$ is the measure of the orbital angular momentum and its respective components are defined in canonical coordinates as

$$L_i = \varepsilon_{ijk} q^j P^k \ , \tag{7.21}$$

with $q^i = (X, Y, Z)$ and $P^i = (P_x, P_y, P_z)$.

In fact, since a Hamiltonian system of a spinning particle linearised in spin given by (5.20) has five independent degrees of freedom, the five constants of motion

$$(J_z, \ J^2, \ L^2, S^2, \ H)$$

in involution holding in the Schwarzschild limit make the system integrable, implying the motion of the particle to be regular at linear order in spin. The integrability for the Schwarzschild background seems to result from the linearised in spin Hamiltonian approximation, since in [35] it has been shown that for the full MP equations with T SSC in the Schwarzschild background chaos appears. As for the Kerr spacetime, the degree of symmetry is reduced because of the rotation of the black hole. For the geodesic motion in Kerr spacetime there exist enough constants of motion in order to make the system integrable, thanks to the Carter constant. Introducing the spin generally destroys the conservation of Carter's constant. However, it was shown in [85, 86] that if the MP equations supplemented by the T SSC are linearised in the spin, an integral of motion C^S associated with a Killing-Yano tensor appears, usually linked with the Carter constant in Kerr spacetime.

This led to the impression that, up to linear order in the particle's spin, the motion of a spinning particle is generally integrable, too [48]. However, a thorough analysis reveals that even with the additional constant of motion in the linearised case, the number of constants of motion in involution is not sufficient to make the system integrable. The motion of a spinning particle in Kerr spacetime also needs at least five constants of motion in involution but we are aware of only four,

$$(J_z,\ C^S,\ S^2,\ H)\ .$$

Indeed, according to our numerical calculations, this seems to be the case for the Hamilto-

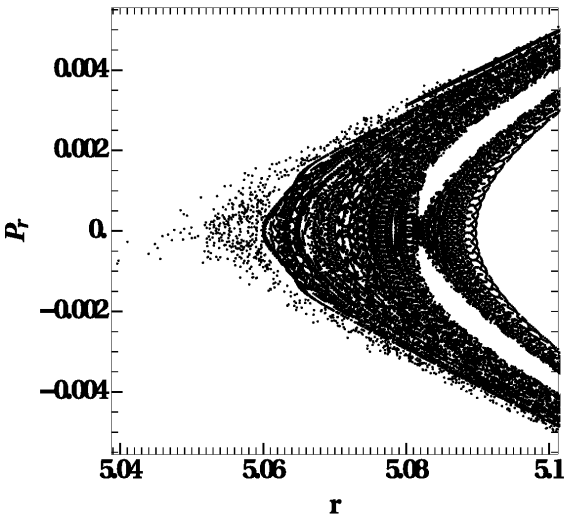

Figure 7.2: A detail from the surface of section $\theta = \pi/2$, $P_\theta > 0$. The parameters of the orbits are $H = 0.9449111825230683$, $J_z = 3.5$, $S = M = \mathcal{M} = 1$, $a = 0.1$, the common initial conditions are $\phi = 0$, $P_r = 0$, $S_1 = 0$, while by solving numerically the system $P_\theta = -S_2$, $J_z = P_\phi$, and $S = \sqrt{S_2^2 + S_3^2}$ we define the rest.

nian formalism depending on the NW SSC. In particular, in the case of the Kerr spacetime a Poincaré surface of section $\theta = \pi/2$, $P_\theta > 0$ indicates chaotic behaviour (scattered dots in fig. 7.2), which suggests the non-integrability of the system. The appearance of chaos in the Kerr background case is not just a confirmation of previous studies, see e.g. [36, 37], it further shows that the linearised in spin Hamiltonian function given in [47] is non-integrable as well. Thus, the above results match exactly the expectations we had from the symmetries. A more thorough analysis of chaotic motion for spinning particles by means of Hamiltonian methods is in progress.

In this section we have investigated the properties of a ZAMO tetrad in spherical and Cartesian coordinates in Schwarzschild spacetime. We found that in order to be a good choice of tetrad the corresponding numerical results should reflect the symmetries of the dynamical system, i.e. preserve the integrals of motion, and avoid any coordinate effects evoked by coordinate dependent tetrad basis vectors. Therewith, both the reduction to the Cartesian tetrad in flat spacetime as well as the vanishing of the spin dependent Hamiltonian are promising indicators for a suitable tetrad choice. Two questions arise with this statement: First, are there other coordinates we may choose providing us with "good" tetrads, and second, since we have been focusing on a ZAMO tetrad, we ask whether a

non-ZAMO tetrad yields the same properties if the coordinate basis is not changed. We expect the properties of the tetrad to depend on the choice of the coordinates, so that in the following we change the coordinates to Kerr-Schild coordinates and analyse two tetrads, one ZAMO and one non-ZAMO tetrad.

7.2 The Hamiltonian function in Kerr-Schild coordinates

Kerr-Schild coordinates have the great advantage that they are horizon penetrating so that they are well behaved in the vicinity of the horizon which simplifies numerical calculations in this domain, probably improving the numerical treatment compared to isotropic coordinates for events in the strong field. In particular, this may be of interest for the numerical simulations of gravitational waves of which the sources are expected to lie in the strong field regime of black holes.

Here we shall introduce a Hamiltonian function using the Kerr-Schild (KS) coordinates $(\bar{t}, \bar{x}, \bar{y}, \bar{z})$. The line element in KS coordinates reads [62]

$$ds^2 \;=\; g_{\mu\nu} d\bar{x}^\mu d\bar{x}^\nu \quad \text{, with } g_{\mu\nu} = \eta_{\mu\nu} + f\ l_\mu\ l_\nu \quad , \tag{7.22}$$

where $(0, 1, 2, 3)$ correspond to $(\bar{t}, \bar{x}, \bar{y}, \bar{z})$,

$$l_{\bar{t}} = -1 \quad , \qquad l_{\bar{x}} = -\frac{\bar{r}\ \bar{x} + a\ \bar{y}}{\bar{r}^2 + a^2} \quad , \qquad l_{\bar{y}} = -\frac{\bar{r}\ \bar{y} - a\ \bar{x}}{\bar{r}^2 + a^2} \quad , \qquad l_{\bar{z}} = -\frac{\bar{z}}{\bar{r}} \quad , \tag{7.23}$$

and

$$f = \frac{2\ M\ r^3}{r^4 + a^2\ z^2} \quad , \qquad \bar{r} = \sqrt{\frac{\bar{\rho}^2 + \sqrt{\bar{\rho}^4 + 4a^2\ z^2}}{2}} \quad , \qquad \bar{\rho}^2 = \bar{x}^2 + \bar{y}^2 + \bar{z}^2 - a^2 \quad . \tag{7.24}$$

Independently of the tetrad field the choice of coordinates implies the non-spinning part of the Hamiltonian

$$H_{NS} = \alpha f\ l_i P_i + \alpha \sqrt{\mathcal{M}^2 + P_i P_i - f\alpha^2 (l_i P_i)^2} \ , \tag{7.25}$$

where $l_i P_i = \delta^{ij} l_i P_j$ and

$$\alpha = \frac{1}{\sqrt{1+f}} \ . \tag{7.26}$$

The independence of the non-spinning Hamiltonian on the tetrad is obvious: As we have seen in section 4.1 the tetrad is introduced in order to describe spin degrees of freedom of the particle. Consequently, the tetrad notion is redundant when the particle has no spin.

As soon as we have non-vanishing spin, the spin part of the Hamiltonian is characterised by the choice of the tetrad introduced by the NW SSC. More precisely, the NW SSC leads

to an entire class of observers that are physically equivalent, i.e. the change of an observer should have no influence on the physics of the spinning particle. In particular, if the coordinate system is retained we should not encounter any coordinate effects smearing the intrinsic dynamical behaviour. Nevertheless, it is worth to examine the impact of different frames based on the same coordinate system on the Hamiltonian description and check whether different types of observers do indeed lead to equivalent (numerical) results at the qualitative level.

7.2.1 ZAMO Tetrad

In the previous section, we focused on a tetrad field associated to the observers with vanishing momentum $u_\phi = 0$, i.e. zero angular momentum observers (ZAMO), in two different coordinate systems, isotropic Cartesian and Boyer-Lindquist coordinates. Therefore, it is reasonable to first consider such an observer in KS coordinates as well. Here, we choose a tetrad corresponding to an observer infalling with the radial velocity $u^r = e_{(t)}{}^r = (\partial r/\partial \bar{x}^\mu)\, e_{(t)}{}^\mu = -\alpha f$:

$$e^{(t)}{}_\mu = \alpha\, \delta^0_\mu \ , \qquad e^{(i)}{}_\mu = \delta^i_\mu + \left(\alpha^{-1} - 1 - \alpha f\right) l_i\, \delta^0_\mu + \left(\alpha^{-1} - 1\right) l_i l_\mu \ .$$

Again, this tetrad becomes Cartesian, i.e. $e^{(t)}{}_\mu = \delta^t_\mu$, $e^{(i)}{}_\mu = \delta^i_\mu$, in the flat spacetime limit, which is a first indication for being a good tetrad and coordinate choice.

The next step is to analyse the behaviour in the Schwarzschild limit $a \to 0$. Then, following the procedure introduced in section 5.2, we obtain the Hamiltonian $\bar{H}^{\rm Schw} = \bar{H}^{\rm Schw}_{NS} + \bar{H}^{\rm Schw}_{S}$ with

$$\bar{H}^{\rm Schw}_{NS} = \alpha \left(\overline{m} - \frac{2M\alpha}{r^2}\, \vec{r}\cdot\vec{P} \right) \ , \tag{7.27}$$

$$\bar{H}^{\rm Schw}_{S} = \frac{M}{\overline{m}} \left[\frac{2\alpha^2}{\alpha+1} - \frac{\alpha^5 + 3\alpha^3}{r} \frac{\vec{r}\cdot\vec{P}}{\omega_T} - \alpha^4 \frac{\overline{m}}{\omega_T} \right] \frac{\vec{L}\cdot\vec{S}}{r^3} \ , \tag{7.28}$$

where

$$\overline{m} = \sqrt{\mathcal{M}^2 + \vec{P}^2 - \frac{f\alpha^2}{r^2} \left(\vec{r}\cdot\vec{P}\right)^2} \ , \qquad \omega_T = -\mathcal{M} - \overline{m} \ . \tag{7.29}$$

Therewith the total Hamiltonian is obtained as merely a function of certain scalar combinations of $\left(\vec{r}, \vec{P}, \vec{S}\right)$ where $\vec{r} = (\bar{x}, \bar{y}, \bar{z})$. Namely, we write $\bar{H} = \bar{H}\left(|\vec{r}|^2, |\vec{P}|^2, \vec{r}\cdot\vec{P}, \vec{L}\cdot\vec{S}\right)$ with L_i given in eq. (7.21) with $\vec{q} \equiv \vec{r}$, so we can deduce that

$$\left\{ \vec{L} + \vec{S}, H \right\}_{DB} = 0 \ , \tag{7.30}$$

by using the canonical structure of the variables. Moreover, we would like to stress here again, that the conservation of L^2 in Schwarzschild spacetime is equivalent to the conservation of $\vec{L}\cdot\vec{S}$, since both S^2 and J^2 are preserved. Thus, it suffices to express the Hamiltonian in terms of $\vec{L}\cdot\vec{S}$ in order to show (7.30). In fact, it reflects the integrability of the system at linear order in spin.

However, we cannot simply infer that $\vec{J}=\vec{L}+\vec{S}$ is valid in the new canonical coordinates. The expression for the constant of motion is already given by (1.16) and with the Killing vectors stated in (7.13) of the Schwarzschild spacetime we arrive at

$$J_i = \tilde{L}_i + S_i \ , \tag{7.31}$$

where the tilde denotes the quantities to be written in terms of the kinematical momenta p_i $\left(\tilde{L}_i=\varepsilon_{ijk}r^j p^k\right)$ and the index i in S_i refers to the coordinate basis. This relation is valid in KS coordinates, independent of the tetrad choice.

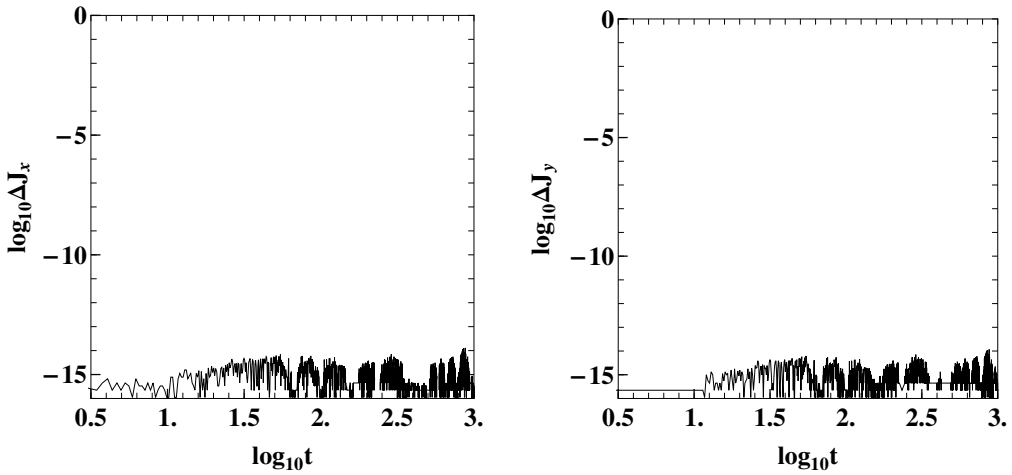

Figure 7.3: The left panel shows the relative error of J_x, and the right of J_y as a function of time in logarithmic scale for the ZAMO tetrad in KS coordinates as evolved by the Hamiltonian with $a=0$, $M=m=1$, and $S=1$.

In order to relate the conserved quantities to the canonical momenta P_i and the tetrad components of the spin $S_{(i)}$, we have to perform a transformation from (p_i, S_i) to $\left(P_i, S_{(i)}\right)$ using the relations given in (5.6) and (5.13). Therewith, we indeed find the components J_i to be given by (7.18) and the corresponding evolution equations can now be computed by

$$\{J_i, H\}_{DB} = 0 \ ,$$

which yields vanishing Dirac brackets for each component of the total angular momentum.

In order to support this statement we performed a numerical check shown in fig. (7.3). It is immediately obvious that the conservation of these components is ensured up to numerical errors which do not accumulate over the integration time but stay at the same level. These results are similar to the ones obtained in isotropic Cartesian coordinates, so that the quality of the outputs is comparable. Therefore, if one can choose between KS and isotropic Cartesian coordinates, there is no preferred choice between those two in Schwarzschild spacetime. However, if the dynamics of plunging orbits is considered in a Kerr spacetime background, it may be more sensible to change to KS coordinates, since they are horizon penetrating and avoid numerical divergences close to the horizon.

Finally, we consider the contribution from the spin part of the Hamiltonian in flat spacetime. From (7.28) we easily see that for $M \to 0$ the contributions from H_S vanish as it should. Hence, also additional coordinate effects, which arise in spherical coordinates, are avoided, further supporting such a choice of tetrad.

7.2.2 Non-ZAMO tetrad

Although the ZAMO tetrad appears to be intuitively a good tetrad choice, we are interested in the effects a different kind of observer has on the Hamiltonian description. One major benefit is the simplification of the Hamiltonian in KS coordinates when we change to another tetrad field, which is not required to be a ZAMO observer. In particular, we take advantage of the fact that for certain observers no square roots appear due to the normalisation of the tetrad vectors

$$e_\mu{}^{(t)} = \left[1 - \frac{f}{2},\ \frac{f}{2}l_{\bar{x}},\ \frac{f}{2}l_{\bar{y}},\ \frac{f}{2}l_{\bar{z}}\right] \quad , \tag{7.32}$$

$$e_\mu{}^{(1)} = \left[-\frac{f}{2}l_{\bar{x}},\ 1 + \frac{f}{2}l_{\bar{x}}l_{\bar{x}},\ \frac{f}{2}l_{\bar{x}}l_{\bar{y}},\ \frac{f}{2}l_{\bar{x}}l_{\bar{z}}\right] \quad , \tag{7.33}$$

$$e_\mu{}^{(2)} = \left[-\frac{f}{2}l_{\bar{y}},\ \frac{f}{2}l_{\bar{y}}l_{\bar{x}},\ 1 + \frac{f}{2}l_{\bar{y}}l_{\bar{y}},\ \frac{f}{2}l_{\bar{y}}l_{\bar{z}}\right] \quad , \tag{7.34}$$

$$e_\mu{}^{(3)} = \left[-\frac{f}{2}l_{\bar{z}},\ \frac{f}{2}l_{\bar{z}}l_{\bar{x}},\ \frac{f}{2}l_{\bar{z}}l_{\bar{y}},\ 1 + \frac{f}{2}l_{\bar{z}}l_{\bar{z}}\right] \quad , \tag{7.35}$$

where we use the definitions from above, cf. eqs. (7.23)-(7.24).
This is the tetrad of an infalling 'non-ZAMO' observer, as the observer's specific angular momentum as measured from infinity

$$-u_\phi = e_{\phi(t)} = \left(\frac{\partial}{\partial\phi}\right)^\mu e_{\mu(t)} = -\frac{1}{2}\,\frac{fa}{r}\,\frac{x^2+y^2}{r^2+a^2} \neq 0 \ , \tag{7.36}$$

does not vanish and the observer's radial coordinate velocity

$$u^r = e^r{}_{(t)} = \left(\frac{\partial r}{\partial x^\mu}\right) e^\mu{}_{(t)} \ = -\frac{f}{2} < 0 \ ,$$

is directed towards the central object. Thus, we again compute the Hamiltonian in canonical coordinates up to linear order in spin given by eq. (5.18) - (5.21)

$$H = H_{NS} + H_{SO} + H_{SS}, \tag{7.37}$$

where H_{NS} is given by (7.25), the spin-orbit coupling is expressed as

$$H_{SO} = \alpha f \frac{Mm - 2\widetilde{m}(M - fr)}{2M\ \overline{m}\ \omega_T}\ \frac{r\ \epsilon^{ij(k)} l_i p_j S^{(k)}}{r^2 + a^2 l_z^2}\ , \tag{7.38}$$

and the spin-spin coupling by

$$\begin{aligned} H_{SS} = &- \frac{af}{4\,\omega_T\ M\overline{m}\ (a^2 l_{\bar{z}}^2 + r^2)} \times \Bigg\{ \Big[4\, f l_{\bar{z}}\, \widetilde{m}\, ((\overline{m} - \alpha f \widetilde{m}) r + \alpha \widetilde{m} M) - \\ &- 2M\, l_{\bar{z}} \left(\overline{m}\mathcal{M} + \alpha \mathcal{M}^2\right) + 2\,\alpha\, [(M + 2\,r)\mathcal{M} f l_{\bar{z}} + (3M - 2fr) P_z]\, \widetilde{m} \Big] S^{(i)} l_i + \\ &+ 2\,\alpha\,(\mathcal{M} + \widetilde{m}) \left[M l_{\bar{z}}\ S^{(i)} P_i - \widetilde{m}\,(2\,fr - 3M)\, S^{(3)} \right] - 2\,\frac{a l_{\bar{z}}\, \widetilde{m}}{r^2} \times \\ &\times \left(3\,Mr - a^2 f {l_{\bar{z}}}^2 - 3\,fr^2\right) \left[\alpha (S^{(1)} P_y - S^{(2)} P_x) - (\alpha \mathcal{M} + \overline{m} - \alpha f \widetilde{m})\, (S^{(1)} l_{\bar{y}} - S^{(2)} l_{\bar{x}}) \right] \Bigg\} \ . \end{aligned} \tag{7.39}$$

Here, instead of (7.29), we use

$$\begin{aligned} \overline{m} &= \sqrt{\mathcal{M}^2 + P_i P_i - f\alpha^2 (l_i P_i)^2}\ , \\ \widetilde{m} &= \alpha \overline{m} - \alpha^2 P_i l^i\ , \\ \omega_T &= -\mathcal{M} - \frac{\overline{m}}{\alpha} + \frac{f}{2}\widetilde{m}\ , \end{aligned} \tag{7.40}$$

which, together with the usage of the components of l^μ instead of the coordinates, significantly shortened expressions for H_{SO} and H_{SS}. All vector components are grouped in such a way that the relation $\left\{L_3 + S_{(3)}, H\right\}_{DB} = 0$ is obvious.

Again, the conservation of the total angular momentum is restored in the Schwarzschild limit. Since $\bar{H}_{NS}$ only depends on the chosen coordinate basis, it is still given by (7.27). The spinning part

$$\bar{H}_S = \left[\alpha \frac{M}{\overline{m}} \left(1 - \frac{M + 2r}{r\,(r + 2M)} \frac{\vec{r}\cdot\vec{P}}{\omega_T} \right) - \frac{M}{\omega_T} \frac{1 - \frac{M}{r}}{1 + \frac{2M}{r}} \right] \frac{\vec{L}\cdot\vec{S}}{r^3}\ , \tag{7.41}$$

where $\bar{m}$ and ω_T are given by (7.40), can again be written as a function

$$\bar{H} = \bar{H}\left(|\vec{r}|^2, |\vec{P}|^2, \vec{r}\cdot\vec{P}, \vec{L}\cdot\vec{S}\right) \ ,$$

so that we can follow the reasoning of the preceding section to obtain the vanishing Dirac brackets (7.30). Therefore, we only have to check the equations for the components of the total angular momentum J_i in canonical coordinates $\left(P_i, S_{(i)}\right)$. Using the expressions for the total angular momentum with respect to the coordinate basis (7.31), we again perform a transformation to the tetrad basis and the canonical momenta and recover relation (7.18). Thus, in the Schwarzschild limit, the non-ZAMO tetrad in KS coordinates has the same numerical properties as the ZAMO tetrad, as it is also visible in Fig. (7.4). Consequently,

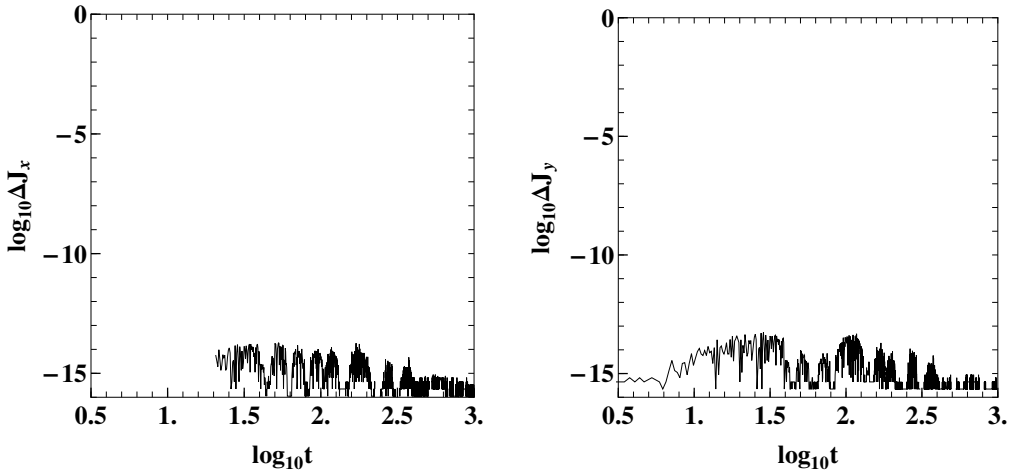

Figure 7.4: The left panel shows the relative error of J_x, and the right of J_y as a function of time in logarithmic scale for the non-ZAMO tetrad in KS coordinates as evolved by the Hamiltonian with $a = 0$, $M = m = 1$, and $S = 1$.

it seems to be a good choice of coordinate system for numerical investigations.

It is of course also possible to rewrite the coefficients of the tetrad basis vectors in terms of any coordinates without changing the general properties of the Hamiltonian system as long as the tetrad basis vectors remain oriented along the isotropic-Cartesian coordinate basis vectors. In [53], it was already mentioned that the coordinate effects can be avoided by choosing the directions of the tetrad basis vectors along a Cartesian coordinate system. However, if the tetrad corresponds to a Cartesian frame, the spin variables remain Cartesian whereas the position and momentum variables are spherical ones. This approach is used in EOB theory or PN methods in order to compare the dynamical contributions, such as spin-orbit or spin-spin coupling, from different orders in spin, (see e.g., [53, 148]) and may in fact also be used for the computation of the equations of motion from the Hamiltonian. Nevertheless, in that case, it is more sensible to be consistent in the choice of coordinates and spin variables so that the Dirac brackets can be used for the calculation of the equations

of motion. Generally, it is very useful to choose a coordinate system and corresponding basis vectors that do not imply coordinate effects if one aims at an analysis of the equations of motion. This coordinate system does not necessarily adapt to the symmetries of the spacetime as we have seen.

7.3 Discussion

In this chapter, we have studied the dependence of the linearised Hamiltonian formalism introduced by Barausse *et al.* [53] on the coordinate system one chooses in order to express the tetrad field or the Hamiltonian function, which has been mentioned in [53]. Using the Dirac brackets to check the integrals of motion, we found that an unfortunate choice of the coordinate system can lead to a non-preservation of quantities in numerical integration which should, according to the symmetries of the system and the linearised MP equations, be conserved. Since a change of tetrad is associated to a canonical transformation of the phase space variables, we find that the type of tetrad, i.e. whether the observer is ZAMO or follows some other worldline which does not correspond to a ZAMO, does not affect the general dynamical properties of the constants of motion as expected. In fact, we have examined both kinds of tetrads and found no difference in their ability to be numerically applied, i.e. they possess the same properties with respect to numerical computations. However, the formulae for the spinning part of the Hamiltonian can be simplified and compactified, which we think is worth to be mentioned.

In order to obtain Hamiltonian systems without coordinate effects smearing the actual physical behaviour in numerical solutions and which are still reliable in the vicinity of the central object's horizon, two new horizon penetrating Hamiltonian functions were introduced. Both of them were constructed on tetrad fields which were expressed in Kerr-Schild coordinates. When spinning particles are considered in strong gravitational fields, the limits of the pole-dipole approximation have to be taken into account, though [87, 83]. For instance, tidal effects coming from higher order multipoles become more important for large curvature gradients so that the description of the motion of a spinning particle has to be extended to higher order multipoles. Nevertheless, the Kerr-Schild coordinates avoid the appearance of coordinate effects and the non-ZAMO tetrad allows us to express the Hamiltonian both in Schwarzschild and Kerr spacetime in a simple and compact form. Future (numerical) work may profit from this explicit Hamiltonian, even in the pole-dipole approximation.

While studying the Dirac brackets in the Schwarzschild limit, we have shown that in this limit the Hamiltonian functions are integrable. In particular, the system's five degrees of freedom admit five independent and in involution integrals of motion. On the other hand, a numerical example in the Kerr background reveals the appearance of chaos. This suggests

that the Hamiltonian system is non-integrable for this more general setting. As chaos and perturbation theory, such as Poincaré sections or recurrence plots, frequently include approaches based on Hamiltonian formalisms future numerical works may profit from this explicit Hamiltonian. Indeed, in order to answer the question for chaos thoroughly, a detailed analysis of the motion of spinning particles in Kerr spacetime described by the Hamiltonian is in progress.

So far, the investigated Hamiltonian has been linearised in the spin and was found by applying Dirac's approach for (secondary class) constraints which replaces the Poisson bracket by the Dirac bracket. However, there exists another method which considerably simplifies the implementation of constraints and therewith the extension to higher orders in spin. In the next chapter we concentrate on this alternative approach, the action approach, and compute a canonical Hamiltonian up to quadratic order in the particle's spin.

Chapter 8

Action approach[1]

8.1 The Dirac Hamiltonian: An Action Approach

In section 5.2 we have seen how (second class) constraints are imposed on a Hamiltonian system by the substitution of the Poisson brackets by the Dirac brackets. The explicit computations are hideous, which does not make this approach very attractive to include the constraints in this way. Again, Dirac proposed to first ignore the inability of applying a Legendre transformation. Indeed, a Legendre transformation from a Lagrangian L is performed and the constraints C^i are imposed alternatively with the help of Lagrange multipliers λ_i, such that a Dirac Hamiltonian H_D can be defined as the sum of the so-called canonical Hamiltonian, i.e. the Legendre transformed Hamiltonian, and the constraints [71, 145, 158, 164]:

$$H_D = H_{\text{can}} + \lambda_i C^i \ , \tag{8.1}$$

where $H_{\text{can}} = \dot{q}^i \frac{\partial L}{\partial \dot{q}^i} - L$. Subsequently, the resulting action is obtained as

$$\mathcal{S} = \int \left(p_i \dot{q}^i - H_D \right) dt \ , \tag{8.2}$$

which the variational principle can be applied to in order to find the equations of motion. The momenta p_i are the generalised momenta $\frac{\partial L}{\partial \dot{q}^i}|_{\dot{q}^j (j \neq i) = \text{const}}$. Moreover, the system's Hamiltonian does not coincide with H_D because the momenta have to satisfy constraints in this formalism, which in turn leads to momenta that are not the true conjugates to the position variables. For instance, in the case of spinning particles we have seen that the angular velocity $\Omega^{\mu\nu}$ depends on the linear velocity u^μ, cf. (4.4), which reflects the ambiguity in the choice of the worldline associated with the mass shell constraint. Such relations are then fixed by the constraints included in H_D. Subsequently the velocity terms

[1] This chapter is based on work which is in preparation with J. Vines, T. Hinderer and J. Steinhoff [4]

are combined in the action in order to read off the Hamiltonian [58].

Before focusing on the search for the Hamiltonian it is worth spending some time on the classification of constraints, how they are treated and what their physical interpretation is [58, 145, 158, 164]. Consider a set of constraints

$$C^i(q,p) \approx 0 \ , \tag{8.3}$$

where $\approx$ stands for "weakly equal" introduced by Dirac [71, 145]. More precisely, it means that the constraints define hypersurfaces in phase space where the dynamics takes place. As the Poisson brackets are defined on the unconstrained phase space, the equation (8.3) is treated to be unsatisfied until the Poisson brackets have been computed. Then, the constraints are actually imposed. The reason for that lies in the classification of the constraints, which is defined by the structure of the Poisson brackets between the constraints. In order to accurately examine the relation between the constraints they have to be considered as unsatisfied until the Poisson brackets have been calculated.

The constraints entering the action at this stage via the Lagrange multipliers λ_i are *primary constraints*. They directly result from the Lagrangian. Correspondingly, the Lagrange multipliers represent additional degrees of freedom which may be fixed by the consistency requirement. All primary constraints have to satisfy such a consistency requirement, which means that they have to be preserved under the time evolution given by the Hamiltonian. Therewith, further constraints, the *secondary constraints*, as well as linear equations for the Lagrange multipliers may follow. Subsequently, the secondary constraints also have to fulfill the consistency requirement which may lead to even further constraints, and so on. In the end we are provided with a complete set of constraints and linear equations for the Lagrange multipliers. The latter are usually used to eliminate certain linear combinations of λ_i from the equations of motion. In special cases it is even possible to uniquely fix the Lagrange multipliers. More generally, though, combinations of or single Lagrange multipliers can remain undetermined, which means that their corresponding degrees of freedom are physically irrelevant and relate to gauge freedom. Thus, those multipliers can be chosen arbitrarily.

Instead of characterising the degrees of gauge freedom by the number of unfixed Lagrange multipliers, which includes some lengthy computations, it is more convenient to classify the constraints in two more groups: the *first class* and the *second class constraints*. A first class constraint is defined to have vanishing Poisson brackets with all other constraints. Under second class constraints we put the remaining ones, i.e. the ones that have non-vanishing Poisson brackets. Therewith, the gauge degrees of freedom are given by the number of independent primary first class constraints. They can be multiplied by arbitrary functions, which are associated with the Lagrange multipliers, and are ad-

ded to the Hamiltonian without changing the physical properties of the system. Indeed, both primary and secondary first class constraints are related to gauge symmetries. These degrees of gauge freedom are usually fixed in advance.

In order to implement second class constraints we have to introduce a new structure, the Dirac bracket, which projects the Poisson bracket onto the constrained phase space. Since the second class constraints have non vanishing Poisson brackets, we are able to define an invertible matrix C_{ij} consisting of the Poisson brackets between the second class constraints, see eq. (5.9). Therewith the Dirac brackets are computed, eq. (5.10), and give the correct equations of motion together with the total Hamiltonian, which is obtained by a Legendre transformation using the true conjugate momenta to the position variables and contains already the solutions to the second class constraints, such as it was done in section 5.2 and in [53].

As we have briefly broached, the computation of the Hamiltonian can be approached by employing the action and imposing the constraints differently. As an example, we first investigate the action of point masses [58]. The corresponding action of point masses moving in an external gravitational field is given by

$$\mathcal{S} = \int L d\sigma = \int -m\sqrt{-g_{\mu\nu}u^\mu u^\nu}d\sigma \ ,$$

with the worldline parameter σ , the four-velocity $u^\mu = dx^\mu/d\sigma$ and rest mass m. Generally, it does not matter which parameter σ is chosen to parametrise the trajectory of the particle. Therefore, the action should be invariant under reparametrisation. Applying the variational principle on this general action the corresponding equations of motion are obtained, which still depend on the gauge choice for σ. At this stage we already know that there exists a gauge symmetry implied in the Lagrangian. Computation of the generalised momenta yields

$$p_\mu = \frac{\partial L}{\partial u^\mu} = m\frac{u_\mu}{\sqrt{-g_{\mu\nu}u^\mu u^\nu}} \ ,$$

and gives rise to

$$L = \frac{\partial L}{\partial u^\mu}u^\mu = p_\mu u^\mu \ . \tag{8.4}$$

The last relation actually is a consequence of the required reparametrisation invariance. Any Lagrangian which is invariant under reparametrisation has to be a homogenous function of degree one in the velocities. According to Euler's theorem the Lagrangian function can then be written as the sum of the products of the generalised momenta and the velocities (8.4). Thus, if we now perform a Legendre transformation we arrive at

$$H_{\text{can}} = p_\mu u^\mu - L = 0 \ ,$$

yielding a vanishing canonical Hamiltonian. Indeed, the canonical Hamiltonian generally vanishes in the case of reparametrisation invariant Lagrangians, which is usually assumed in general relativistic systems [58]. But, if the Hamiltonian vanishes where does the information on the system's dynamics go? Dirac proposed a way around by saying that the time evolution is given by the constraints. Recall the gauge freedom we have in the choice of the worldline parameter. This ambiguity represents the inability to uniquely define a relation between the four-velocity and the four-momentum. It depends on the gauging of σ which is encoded in the mass shell constraint

$$p_\mu p^\mu + m^2 \approx 0 \ , \tag{8.5}$$

which has to be added to the Dirac Hamiltonian with a Lagrange multiplier

$$H_D = H_{\text{can}} + \lambda \left(p_\mu p^\mu + m^2\right) = \lambda \left(p_\mu p^\mu + m^2\right) \ ,$$

and leads, according to eq. (8.2), to the following action

$$\mathcal{S} = \int \left(p_\mu u^\mu - \lambda \left(p_\mu p^\mu + m^2\right)\right) d\sigma \ .$$

Notice that we have not yet fixed the gauge for σ. By looking at the action we deduce that with respect to an arbitrary worldline parameter the Hamiltonian is of the form $\lambda \left(p_\mu p^\mu + m^2\right)$ generating the time evolution of the particle's motion. Variation of the action therewith fixes the Lagrange multiplier and gives the equations of motion.

If, on the other hand, the gauge is fixed at the level of the action the Hamiltonian can be read off directly for this specific gauge. By solving the mass shell constraint in eq. (8.5) to

$$-p_t = N^i p_i + N \sqrt{m^2 + \gamma^{ij} p_i p_j} \ ,$$

with N^i, N and γ^{ij} as quantities describing a spacetime split given in (5.17) and fixing the gauge to proper time $\tau \approx x^t$ or $u^t \approx 1$ the action yields

$$\mathcal{S} = \int \left(p_i u^i + p_t\right) d\tau = \int \left(p_i \dot{x}^i + p_t\right) d\tau \ ,$$

characterised by the only independent variables x^i and p_i. Notice indeed that x^t is no longer interpreted as a variable but as a time parameter characterising the dynamics. It can also be understood as some kind of way to split spacetime into space and time because through the gauge fixing procedure we degraded the time coordinate to the status of a parameter. At this point it becomes obvious that a Hamiltonian formalism in general relativity requires a spacetime split.

Now we can distinguish the terms that contain velocities from the ones that are independent of velocities in the action. The latter is identified to be the Hamiltonian

$$H = -p_t \ ,$$

containing all information on the evolution of the dynamical system of a freely falling test particle moving in an external gravitational field. On top of that the Poisson brackets are encoded in the action as well, showing that p_i and x^i are indeed of canonical structure. Thus the equations of motion equal the famous Hamilton's equations. Unfortunately, in the general case the variables do not have to be canonical yielding a complicated structure for the Poisson brackets, which remain to be still implied in the action though, see section 8.6.

As this approach is based on the action, an explicit Lagrangian is an essential ingredient. However, when we considered spinning particles so far, we never actually had to choose a particular Lagrangian in order to continue our investigations, in particular to derive the unconstrained equations of motion. Nevertheless, there exist a few works in both special and general relativity using an explicit Lagrangian function for the investigation of the dynamics of spinning bodies [58, 93, 94, 144, 165, 166]. In all these studies the reference worldline has been chosen beforehand so that the specific form of the Lagrangian and therewith the form of the action only fits to this particular supplementary condition or constraint, respectively. Of course it is possible to shift the chosen worldline in such a way that the resulting variables correspond to another supplementary condition. Thus, a change of the choice of the observer cannot be performed at the level of the action but only by a coordinate shift in a given Lagrangian belonging to a first observer.

8.2 Spin-gauge invariant Action

If the subject is regarded from the physical point of view the dynamics of the particle should not change if the observer goes to a different reference frame. Each description given by different observers should yield the same physical results. Consequently we would expect an action to exist that is invariant under the transformation from one observer to another, i.e. the action should be invariant under the change of the supplementary condition. Due to the physical irrelevance of the supplementary condition the latter can be transferred into a spin gauge constraint which leads to a Lagrangian respecting this gauge symmetry [59]. The spin gauge constraint is given by [59]

$$C_\mu := S_{\mu\nu}\omega^\nu \approx 0 \ , \tag{8.6}$$

with

$$\omega^\nu := \frac{p^\nu}{p} + e_T{}^\nu \ ,$$

and $e_T{}^\nu$ being the time direction of the body-fixed frame. Applying a Lorentz boost the time direction of the body-fixed frame is transformed in such a way that it is aligned with the particle's linear momentum. Therefore, all the physical information concerning the orientation of the particle are encoded in the remaining rotational degrees of freedom. It is worth to remark here, that C_μ is not a spin supplementary condition and does not correspond to a particular choice of an observer but merely parametrises the full range of possible choices by a gauge field $e_T{}^\nu$. In addition to the spin gauge constraint we surely still have the freedom to choose any arbitrary parameter for the worldline without changing the dynamics of the particle. More precisely, the action should be invariant under reparametrisation which is represented by the mass shell constraint

$$T := p_\mu p^\mu + \mathcal{M}^2 \approx 0 \ , \tag{8.7}$$

where $\mathcal{M}$ corresponds to the dynamical mass. In general, the dynamical mass $\mathcal{M}$ is a function of the dynamical variables. It can contain nonminimal couplings to the curvature tensor, which account for higher multipoles (quadrupole etc), see [132, 137]. We will therefore keep $\mathcal{M}$ generic for most of the derivations. It is worth to stress here again, that in the case of spinning particles the linear momentum is no longer aligned with the particle's velocity so that we distinguish between the dynamical mass $\mathcal{M}$ and the kinematical mass m, cf. (1.18).

Previously we have already introduced the use of the Dirac Hamiltonian (8.1) which is composed of the canonical Hamiltonian and the given constraints in terms of Lagrange multipliers. Naturally, the canonical Hamiltonian vanishes because of the reparametrisation invariance so that the action for a spinning particle results in

$$\mathcal{S} = \int \left(p_\mu u^\mu + \frac{1}{2} S_{\mu\nu} \Omega^{\mu\nu} - H_D \right) d\sigma \ , \tag{8.8}$$

where $H_D = \lambda_1 T + \lambda_2^\mu C_\mu$ and p_μ and the spin tensor $S_{\mu\nu}$ are the generalised momenta (4.13). However, because of the particle's spin these momenta are not the conjugate momenta to the position variables so that the structure of their Poisson brackets differs from the canonical ones. This is visible from eq. (8.12) since $\Omega^{\mu\nu}$ is a function of the four-velocity and subsequently, at this stage, the Hamiltonian cannot be read off from the action. At the moment, though, our main purpose is not the Hamiltonian but the form of the action.

We would like to have the action invariant under the transformation of the reference worldline, i.e. under different choices for the supplementary condition. Treating this sym-

metry as well as the reparametrisation invariance as gauge degrees of freedom the corresponding constraints have to be first class constraints. Their Lagrange multipliers cannot be fixed by the consistency requirements but reflect the arbitrariness in the choice of an observer and of the worldline parameter. It can be checked that the constraints C_μ leads to the correct spin gauge constraint fulfilling all the properties we wish: first it generates the shift of the representative worldline and the appropriate shift in the spin tensor and it has indeed vanishing Poisson brackets [59]. Therefore, the physical as well as the mathematical requirements are perfectly satisfied.

Since the Hamiltonian is not only composed of the spin gauge constraint but also of the mass shell constraint, the latter must also be made invariant under spin gauge transformations. In particular this means that it should have vanishing Poisson brackets with C_μ. Although the momenta p_μ are not affected by the change of the SSC [59], the dynamical mass $\mathcal{M}\left(x^\mu,\, p_\mu,\, S_{\mu\nu},\, \Lambda_i{}^\mu\right)$ is, since it depends on the position, the spin and therewith on the Lorentz matrix. Hence in order to make $\mathcal{M}$ invariant under spin gauge transformations we find a position $\tilde{x}^\mu$, a spin $\tilde{S}^{\mu\nu}$ and a Lorentz matrix $\tilde{\Lambda}_i{}^\mu$ which are invariant, i.e. which have weakly vanishing Poisson brackets with the gauge constraint C_μ. The solution is obtained by a projection of the quantities $(x^\mu,\, S_{\mu\nu},\, \Lambda_i{}^\mu)$ onto the particle's rest-frame. Then we can construct an invariant mass out of all the invariant variables. It is important to note here, that the dynamical mass contains all field interactions of the spinning particle, such as tidal forces, which have to be taken at the invariant position variable. Therefore, it appears to be reasonable to shift the worldline of the action x^μ to this new invariant position variable $\tilde{x}^\mu$. One has to be careful, though: the switch cannot be applied to the spin tensor or the Lorentz matrix because the corresponding transformation includes projections onto the spatial hypersurface of the local Lorentz frame, $\tilde{\Lambda}_i{}^\mu p_\mu = 0$. Therefore we keep $\Lambda_i{}^\mu$ and $S_{\mu\nu}$ as the fundamental variables of the action. After coupling to the gravitational field we arrive at [59]

$$\mathcal{S} = \int d\sigma \left(-p_\mu \tilde{u}^\mu - S^{\mu\nu} \frac{p_\nu}{p_\alpha p^\alpha} \frac{Dp_\mu}{d\sigma} - \frac{1}{2} S_{\mu\nu} \Omega^{\mu\nu} - H_D \right) \,, \tag{8.9}$$

which is the explicit action whose form is invariant under spin gauge transformations and valid to all orders in spin. Thus, we can choose any observer or reference worldline within the particle we like at the level of the action. We no longer have to adjust the terms of the Lagrangian in order to fit the supplementary condition or, the other way around, search for the correct spin constraint for a given Lagrangian.

Compared to (8.8) a new term appears in the spin gauge invariant action which includes a covariant derivative of the four-momentum

$$\frac{Dp_\mu}{d\sigma} = \dot{p}_\mu - p_\rho \Gamma^\rho{}_{\mu\nu} u^\nu \,, \tag{8.10}$$

where the dot denotes the ordinary derivative with respect to the worldline parameter σ. It resembles the acceleration term in the action used in [167] which was interpreted as the contribution from the special relativistic Thomas precession. Here, we may think of this term as the Fermi-Walker transport of the spin vector along the non-geodesic worldline of the spinning test particle. It ensures that the particle follows the worldline defined by its rest frame.

As before, the spin of the particle is characterised by an orthonormal tetrad $e_A{}^\mu$ where the capital latin indices refer to the body-fixed Lorentz basis and the greek ones to the coordinate basis. In curved spacetime an orthonormal tetrad has to satisfy the normalisation condition given in (4.2). This motivates us to introduce a tetrad gravitational field $e^a{}_\mu$, which also satisfies the normalisation condition $\eta^{ab} e_a{}^\mu e_b{}^\nu = g^{\mu\nu}$, so we can define a Lorentz matrix $\Lambda_A{}^a = e^a{}_\mu e_A{}^\mu$, such as in (5.3), to define the orientation between the two tetrads with respect to each other. In order to make sure that the physical spin is represented by the spatial tetrad field of the spinning particle the body-fixed tetrad is Fermi-Walker transported. Then, the angular velocity is defined by (4.4).

It turns out to be useful to write the term containing the spin tensor and the angular velocity in the action (8.9) in the local frame,

$$\begin{aligned} S_{\mu\nu}\Omega^{\mu\nu} &= S_{\mu\nu}\Lambda_A{}^a e_a{}^\mu \frac{D(\Lambda^{Ab} e_b{}^\nu)}{d\sigma} \\ &= S_{ab}\left(\Lambda_A{}^a \dot{\Lambda}^{Ab} + \omega_\mu{}^{ab} u^\mu\right) \ , \end{aligned} \tag{8.11}$$

where $S_{ab} = e_a{}^\mu e_b{}^\nu S_{\mu\nu}$, and $\omega_\mu{}^{ab} = e^{a\nu}{}_{,\mu} e^b{}_\nu + e^b{}_\nu e^{a\rho}\Gamma^\nu{}_{\rho\mu}$. Here, we have used the angular velocity from eq. (4.4) with the Lorentz transformation introduced in eq. (5.3) in the form

$$\Omega^{\mu\nu} = \Lambda_A{}^a e_a{}^\mu \frac{D(\Lambda^{Ab} e_b{}^\nu)}{d\sigma} \ . \tag{8.12}$$

The four-velocity u^μ is based on an ordinary derivative, as usual. The $\omega_\mu{}^{ab}$ are called Ricci rotation coefficients [168] or the spin connection [7] and serve as the connection coefficients in the local Lorentz basis, e.g. the covariant derivative for some vector X^a in the local Lorentz basis is computed as

$$\nabla_\mu X^a = \partial_\mu X^a + \omega_\mu{}^a{}_b X^b \ .$$

Although the name "spin connection" has its roots in the expression of the Dirac equation within a curved spacetime geometry, it fits perfectly into the subject of a classical spinning particle in general relativity. Keeping with Dirac's notation we repeat the Dirac Hamiltonian given by the gauge constraints described above

$$H_D = \frac{\lambda}{2}\mathcal{T} + \chi^a \mathcal{C}_a \ , \tag{8.13}$$

where λ and χ^μ are the Lagrange multipliers corresponding to the constraints. As explained above, the mass shell constraint (8.7) reflects the invariance under reparametrisation of the worldline parameter.

The second constraint in the Dirac Hamiltonian is the spin-gauge constraint (8.6) which can be rewritten in the local frame as [59]

$$0 \approx \mathcal{C}_a := S_{ab}\left(\frac{p^b}{\sqrt{-p_\rho p^\rho}} + \Lambda_T{}^b\right) \ , \tag{8.14}$$

where $p^a = e^{a\mu}p_\mu$. The following choices for the gauge "field" $\Lambda_T{}^a$ turn the spin gauge constraint (8.14) into various familiar SSCs:

$$\Lambda_0{}^a \approx \frac{p^a}{\sqrt{-p_\rho p^\rho}} \qquad \Rightarrow \quad \mathcal{C}_a = S_{ab}p^b \approx 0 \tag{8.15}$$

$$\Lambda_0{}^a \approx \delta_0^a \qquad \Rightarrow \quad \mathcal{C}_a = S_{ab}\left(p^b + \sqrt{-p_\rho p^\rho}\delta_0^b\right) \approx 0 \tag{8.16}$$

$$\Lambda_0{}^a \approx \frac{2p^0\delta_0^a - p^a}{\sqrt{-p_\rho p^\rho}} \qquad \Rightarrow \quad \mathcal{C}_a = S_{a0} \approx 0 \tag{8.17}$$

Indeed, the first choice represents the widely known and very popular T SSC and the third one refers to the P SSC. The second condition leads to the NW SSC and is probably most useful in an action approach, since it removes the temporal components from the kinematic term (notice that also $\Lambda_A{}^{(t)} \approx \delta_A^T$)

$$\frac{1}{2}S_{ab}\Lambda_A{}^a\dot{\Lambda}^{Ab} = \frac{1}{2}S_{(i)(j)}\Lambda^{K(i)}\dot{\Lambda}^{K(j)} \ . \tag{8.18}$$

Moreover, the NW SSC is the only one known to lead to canonical variables in special relativity [56, 57]. Recently, canonical variables up to linear order in spin have been found in a general relativistic system supplemented with the NW SSC [53].

8.3 Coordinate Transformation

By construction, the variables apparent in the action 8.9 correspond to the worldline describing the centre of mass in the rest frame of the particle, i.e. to the reference worldline which would be fixed by the T SSC. However, it is not the SSC which makes sure that the particle follows this worldline but the term of Fermi-Walker transport in the action. Consequently, since we have not yet fixed the spin gauge symmetry, we are allowed to shift the worldline by a transformation of the position variables in such a way that a canonical

formulation is obtained. This shift is not necessarily related to a change of the SSC, but rather corresponds to a change of coordinates that describe the behaviour of the particle.

However, if this is approached naively, then one might loose manifest covariance. Instead, geometric objects defined on the worldline, like the spin, must then be transported to the new worldline in a geometric manner, i.e. by parallel transport. Then, the procedure of infinitesimal covariant variation, as it is presented in section 4.2, can be applied to a complete shift of the worldline representing the evolution of the spinning body while taking care for the proper entrainment of the dynamical properties of the particle which are usually defined with respect to the chosen reference worldline. Hence, the covariance is maintained when the variation of the action is performed so that we now focus on the finite covariant variation which yields a finite shift of the worldline [137].

Finite covariant variation

We want to express a function (or functional) f of the old worldline z^μ in terms of the new worldline $\hat{z}^\mu$. This expansion reads

$$f(z^\alpha) = \sum_n \frac{\delta^n f(\hat{z}^\alpha)}{n!} = f(\hat{z}^\alpha) + \frac{\partial f(\hat{z}^\alpha)}{\partial \hat{z}^\mu}\delta\hat{z}^\mu + ... \quad . \tag{8.19}$$

It should be noted that this is an expansion around the *new* worldline $\hat{z}^\mu$. Then $\delta\hat{z}^\mu$ is pointing from $\hat{z}^\mu$ to z^μ, which is indicated by the hat on $\delta\hat{z}^\mu$. Therefore, we understand that the new worldine coordinate is used in all formulas provided in the last section from now on. It is important to notice that the action is a scalar, so that the ordinary variation δ and the covariant one Δ can be used interchangeably. This allows us to switch to the covariant variation

$$S_{\rm PP}[z^\mu] = \sum_n \frac{\delta^n S_{\rm PP}[\hat{z}^\mu]}{n!} = \sum_n \frac{\Delta^n S_{\rm PP}[\hat{z}^\mu]}{n!} \equiv e^{\Delta} S_{\rm PP}[\hat{z^\mu}], \tag{8.20}$$

and perform the shift of the worldline in a manifestly covariant manner.

Since $\delta\hat{z}^\mu$ cannot be considered as an infinitesimal any more, it can not directly provide a coordinate difference. Instead, it is a tangent vector on the new worldine $\hat{z}^\mu$. The coordinate difference is given by a refinement in the form of *non-vanishing* $\delta^n\hat{z}^\mu$ in eq. (8.19),

$$z^\mu = \sum_n \frac{\delta^n \hat{z}^\mu}{n!}. \tag{8.21}$$

In order to give this expansion a geometric meaning, we require that it approaches a spacelike geodesic connecting $\hat{z}^\mu$ and z^μ, which fixes the $\delta^n\hat{z}^\mu$. For this purpose, we introduce an affine parameter λ for the geodesic $y^\mu(\lambda)$. The geodesic equation is the parallel transport

of the tangent vector along itself,

$$0 = \frac{dy^\nu}{d\lambda}\nabla_\nu \frac{dy^\mu}{d\lambda} = \frac{d^2y^\mu}{d\lambda^2} + \Gamma^\mu{}_{\nu\rho}\frac{dy^\nu}{d\lambda}\frac{dy^\rho}{d\lambda} \tag{8.22}$$

with the initial conditions $y(0) = \hat{z}^\mu$, $dy^\mu(0)/d\lambda = \delta\hat{z}^\mu$ and the searched-for final value $z^\mu := y^\mu(1)$. Thus this geodesic equation geometrically maps the tangent vector $\delta\hat{z}^\mu$ (initial condition) to the coordinate difference $z^\mu - \hat{z}^\mu$. Since the old worldline z^μ is understood to be the solution to the geodesic equation at $\lambda = 1$ with given initial conditions, this is equivalently true for eq. (8.21) to be a series solution of the geodesic equation expanded around $\lambda = 0$ and evaluated at $\lambda = 1$. Therewith we can write the nth-order variation of z^μ as the nth total derivative of the geodesic with respect to λ evaluated at $\lambda = 0$

$$\delta^n\hat{z}^\mu = \left.\frac{d^n y^\mu}{d\lambda^n}\right|_{\lambda=0} . \tag{8.23}$$

For $n = 2$, this reads explicitly

$$\delta^2\hat{z}^\mu = -\Gamma^\mu{}_{\nu\rho}\delta\hat{z}^\nu\delta\hat{z}^\rho. \tag{8.24}$$

or

$$\Delta\delta\hat{z}^\mu = 0, \tag{8.25}$$

which means that the initial tangent vector $\delta\hat{z}^\mu$ is parallel transported along itself. This is of course just a restatement of the geodesic equation. It is straightforward to see that the higher order variations follow from $0 = \delta^{n-1}\Delta\delta z^\mu = \Delta^n\delta z^\mu$. Similarly, the higher variations of the other worldline quantities add up to a finite parallel transport, which will be calculated below.

The covariant differential and covariant variation are given by the equations (4.6) and (4.8). Therewith the shift is performed in a manifestly covariant manner

$$\hat{S} = \sum_n \frac{\delta^n S}{n!} = \sum_n \frac{\Delta^n S}{n!}$$

where we interchanged the ordinary variation δ and the covariant one Δ, since the action S is a scalar.

The action is given in (8.9) and contains the Lagrangian L and the Dirac Hamiltonian H_D. As for linear variations we can interchange the covariant variation with the integral, since the boundaries are independent of the variables. Indeed, we can restrict our analysis to the Lagrangian, since H_D merely consists of the gauge constraints which are independent of a worldline shift (by construction). Thus, we perform a shift from the old worldline z^μ

to the new worldline $\hat{z}^\mu$ and obtain a new Lagrangian which we denote by $\hat{L}$. However, we start at the new worldline and take the variation around $\hat{z}^\mu$ where we have to consider that $\delta\hat{z}^\mu$ has the opposite sign of δz^μ : Then the Lagrangian is expressed in terms of the new coordinates with $\hat{u}^\mu = \dot{\hat{z}}^\mu$ as the tangent to the new worldline

$$\begin{aligned}\hat{L} =& p_\mu \hat{u}^\mu + \frac{1}{2} S_{\mu\nu}\Omega^{\mu\nu} - \frac{p_\mu S^{\mu\nu}}{p_\rho p^\rho}\frac{Dp_\nu}{d\sigma} + \Delta\left(p_\mu \hat{u}^\mu\right) + \Delta\left(\frac{1}{2} S_{\mu\nu}\Omega^{\mu\nu}\right) - \Delta\left(\frac{p_\mu S^{\mu\nu}}{p_\rho p^\rho}\frac{Dp_\nu}{d\sigma}\right) \\ &+ \frac{1}{2}\Delta^2\left(p_\mu \hat{u}^\mu\right) + \ldots \ . \end{aligned} \tag{8.26}$$

Choosing the shift $\delta\hat{z}^\mu$ appropriately we can transform the coordinates to canonical ones.

8.4 Hamiltonian to linear order in spin

Starting with the computation of the Hamiltonian at linear order in spin, we show that the action approach yields the same results as in section 5.2 or [53]. First, we compute the Lagrangian shifted to the new worldline given in (8.26)

$$\hat{L} = p_\mu \hat{u}^\mu + \frac{1}{2} S_{\mu\nu}\Omega^{\mu\nu} - \frac{p_\mu S^{\mu\nu}}{p_\rho p^\rho}\frac{Dp_\nu}{d\sigma} + \Delta\left(p_\mu \hat{u}^\mu\right) + \mathcal{O}\left(S^2\right) \ , \tag{8.27}$$

where all orders higher than linear in spin are neglected. Using the commutator relation between the covariant differential and the variation in (4.9) as well as the shift of the four-velocity (4.14) results in

$$\Delta(p_\mu \hat{u}^\mu) = p_\mu \frac{D\delta\hat{z}^\mu}{d\sigma} = -\frac{Dp_\mu}{d\sigma}\delta\hat{z}^\mu + \frac{d(p_\mu \delta\hat{z}^\mu)}{d\sigma} \ , \tag{8.28}$$

where the last term amounts to a divergence which vanishes when the integral is computed (by definition of the variational approach). However, we keep track of this term in the next calculations. Therewith we obtain for the Lagrangian

$$\hat{L} \ = \ p_\mu \hat{u}^\mu + \frac{1}{2} S_{\mu\nu}\Omega^{\mu\nu} - \frac{p_\mu S^{\mu\nu}}{p_\rho p^\rho}\frac{Dp_\nu}{d\sigma} - \frac{Dp_\mu}{d\sigma}\delta\hat{z}^\mu + \mathrm{div} + \mathcal{O}\left(S^2\right) \ .$$

In order to get canonical coordinates the time derivative of p_μ has to vanish. Notice, that we can cancel the time derivative of p_μ if we choose the worldline shift appropriately. Hence, by setting

$$\delta\hat{z}^\mu = \frac{S^{\mu\nu}p_\nu}{p_\rho p^\rho} \ , \tag{8.29}$$

the relation between the old and the new worldline results in

$$z^\mu = \hat{z}^\mu + \frac{S^{\mu\nu}p_\nu}{p_\rho p^\rho} \ , \tag{8.30}$$

resembling the worldline shift known from special relativity, see e.g. [58, 144]. Thus, the action of a spinning particle at linear order in spin is given by

$$S_{\rm PP} = \int d\sigma \left[p_\mu \hat{u}^\mu + \frac{1}{2} S_{\mu\nu}\Omega^{\mu\nu} - H_D \right] \ . \tag{8.31}$$

The same form of action can be obtained from special relativity as it was worked out in [144] by minimal coupling, which is allowed only up to linear order in the particle's spin. Fortunately, higher orders can be worked out in a straightforward manner using the approach from the preceding section. Notice that the momenta p_μ are not the true conjugate momenta to the position variable $\hat{z}^\mu$ since $\Omega^{\mu\nu}$ depends on $\hat{u}^\mu$, so that these variables do not have a canonical structure.

At the same time, it is worth to mention here, that this action does not yet provide us with the correct Hamiltonian, though, but only with the unconstrained Dirac Hamiltonian H_D. So far we have ignored the (gauge) constraints which reduce the degrees of freedom or rather respect the free degrees of freedom and fix the dependent ones. Thus the strategy to derive the reduced or constrained Hamiltonian is to fix the gauges for the worldline parameter and the spin, solve the constraints (together with the gauge conditions) for the dependent variables, and insert the solutions into the action. This leaves us with an action containing only the independent or reduced variables. It also implies that $H_D = 0$ after solving the constraints. However, a new Hamiltonian will arise from the kinematic terms in the action, as we have seen in section 8.1.

8.4.1 Solving the constraints

We start with the worldline gauge which we choose to be $\sigma \approx \hat{t}$, or $\hat{u}^0 \approx 1$, so that

$$p_\mu \hat{u}^\mu = p_i \dot{\hat{z}}^i + p_t \ . \tag{8.32}$$

The solution to the mass shell constraint (8.7) reads

$$p^t = \frac{1}{N}\sqrt{\mathcal{M}^2 + \gamma^{ij}p_i p_j}, \tag{8.33}$$

$$p_t = -N\sqrt{\mathcal{M}^2 + \gamma^{ij}p_i p_j} + N^i p_i. \tag{8.34}$$

with N as the lapse function, N^i the shift vector and γ^{ij} the spatial metric given in (5.17). For the Lorentz matrix, we use the gauge $\Lambda_0{}^a \approx \delta_0^a$, or $\Lambda_A{}^0 \approx \delta_A^0$, corresponding to a reference worldline fixed by the NW SSC so that we arrive at

$$\begin{aligned}\frac{1}{2}S_{\mu\nu}\Omega^{\mu\nu} &= \frac{1}{2}S_{ab}\Lambda_A{}^a\dot{\Lambda}^{Ab} + \frac{1}{2}S_{ab}\omega_\mu{}^{ab}\hat{u}^\mu \\ &= \frac{1}{2}S_{(i)(j)}\Lambda^{K(i)}\dot{\Lambda}^{K(j)} + \frac{1}{2}S_{ab}\omega_i{}^{ab}\dot{\hat{z}}^i + \frac{1}{2}S_{ab}\omega_t{}^{ab} \ , \end{aligned} \tag{8.35}$$

for the spin dependent term in the action. Since we have fixed the reference frame by the NW SSC which reads

$$S_{ab}(p^b + \mathcal{M}\delta^b_{(t)}) \approx 0 \ , \tag{8.36}$$

we solve for the mass dipole $S^{(t)(i)}$

$$S_{(t)(i)} = \frac{S_{(i)(j)}e^{(j)\mu}p_\mu}{e^{(t)\nu}p_\nu + \mathcal{M}} \ . \tag{8.37}$$

Moreover, we notice from (8.36) that

$$S^{ab}p_b = S^{a(t)}\mathcal{M} \ . \tag{8.38}$$

Therewith, the second term in (8.35) can be rewritten as

$$\begin{aligned}\frac{1}{2}S_{ab}\omega_\mu{}^{ab} &= \frac{1}{2}S_{(i)(j)}\omega_\mu{}^{(i)(j)} + S_{(t)(i)}\omega_\mu{}^{(t)(i)} \\ &= \frac{1}{2}S_{(i)(j)}\omega_\mu{}^{(i)(j)} + \frac{\omega_\mu{}^{(t)(i)}S_{(i)(j)}e^{(j)\mu}p_\mu}{e^{(t)\nu}p_\nu + \mathcal{M}} \ . \end{aligned} \tag{8.39}$$

In addition, the NW SSC implies a further gauge choice, namely, the orientation of the background tetrad that has to be fixed. It seems natural to choose the timelike tetrad vector to point into the coordinate time direction with its length equal to the elapsed time N when moving along the particle's trajectory. Thus, the time gauge (TG) for the tetrad

$$e^{(t)}{}_\mu = N\delta^t_\mu \ , \tag{8.40}$$

is very useful and implies also $e_a{}^t = \delta^t_a/N$. For instance, it simplifies $S_{(t)(i)}$,

$$S_{(t)(i)} = \frac{S_{(i)(j)}e^{(j)k}p_k}{Np^t + \mathcal{M}} \quad \text{(in TG)}. \tag{8.41}$$

yielding

$$\frac{1}{2}S_{ab}\omega_\mu{}^{ab} = \frac{1}{2}S_{(i)(j)}\omega_\mu{}^{(i)(j)} + \frac{\omega_\mu{}^{(t)(i)}S_{(i)(j)}e^{(j)k}p_k}{Np^t + \mathcal{M}} \quad \text{(in TG)}. \tag{8.42}$$

The SSC reads

$$S^{\mu\nu}(p_\nu - \mathcal{M}N\delta^t_\nu) \approx 0 \quad \text{(in TG)}. \tag{8.43}$$

Leaving the time gauge again, the term appearing in the Lagrangian can finally be written as

$$\frac{1}{2}S_{\mu\nu}\Omega^{\mu\nu} = \frac{1}{2}S_{(i)(j)}\Lambda^{K(i)}\dot{\Lambda}^{K(j)} + \left(\frac{1}{2}S_{(j)(k)}\omega_i{}^{(j)(k)} + \frac{\omega_i{}^{(t)(j)}S_{(j)(k)}e^{(k)\mu}p_\mu}{e^{(t)\nu}p_\nu + \mathcal{M}}\right)\dot{\hat{z}}^i + \\ + \frac{1}{2}S_{(j)(k)}\omega_t{}^{(j)(k)} + \frac{\omega_t{}^{(t)(j)}S_{(j)(k)}e^{(k)\mu}p_\mu}{e^{(t)\nu}p_\nu + \mathcal{M}}$$

and can now be implemented into the action.

8.4.2 Hamiltonian and Poisson brackets

After the evaluation of the constraints we plug them into the action. Since we now have solved the constraints, the Dirac Hamiltonian H_D vanishes. However, a new Hamiltonian emerges as we will see in the following. We now separate the action into a part containing first-order ordinary time derivatives, which encodes the Poisson/Dirac brackets, and a part containing no time derivatives, which is identified as the Hamiltonian. Hence, after implementing the solutions to the constraints into the action given in (8.31), it holds

$$S_{\text{PP}} = \int d\hat{t}\left[(p_i + A_i)\dot{\hat{z}}^i + \frac{1}{2}S_{(i)(j)}\Lambda^{K(i)}\dot{\Lambda}^{K(j)} - H\right], \tag{8.44}$$

with the Hamiltonian

$$\begin{aligned} H &= -p_t - \frac{1}{2}S_{ab}\omega_t{}^{ab} \\ &= -p_t - \frac{1}{2}S_{(i)(j)}\omega_t{}^{(i)(j)} - \frac{\omega_0{}^{(t)(i)}S_{(i)(j)}e^{(j)\mu}p_\mu}{e^{(t)\nu}p_\nu + \mathcal{M}}\,, \end{aligned} \tag{8.45}$$

and the abbreviation

$$\begin{aligned} A_k &= \frac{1}{2}S_{ab}\omega_k{}^{ab} \\ &= \frac{1}{2}S_{(i)(j)}\omega_k{}^{(i)(j)} + \frac{\omega_k{}^{(t)(i)}S_{(i)(j)}e^{(j)\mu}p_\mu}{e^{(t)\nu}p_\nu + \mathcal{M}}\,. \end{aligned} \tag{8.46}$$

Here we still need to insert (8.33) and (8.34) in order to have the fully explicit expression, however, we keep p_t and p^t as abbreviations in the following. We can absorb the factor $(p_i + A_i)$ of the velocities $\dot{\hat{z}}^i$ by defining a new momentum

$$\hat{p}_i = p_i + A_i\,. \tag{8.47}$$

Then the Poisson brackets of the variables $\hat{z}^i$, $\hat{p}_i$, $\Lambda^{K(i)}$, and $S_{(i)(j)}$ are standard canonical.

In the time gauge we have

$$H = -p_0 - \frac{1}{2} S_{(i)(j)} \omega_t{}^{(i)(j)} - \frac{\omega_t{}^{(t)(i)} S_{(i)(j)} e^{(j)k} p_k}{N p^t + \mathcal{M}} \qquad \text{(in TG). ,} \tag{8.48}$$

$$A_k = \frac{1}{2} S_{(i)(j)} \omega_k{}^{(i)(j)} + \frac{\omega_k{}^{(t)(i)} S_{(i)(j)} e^{(j)l} p_l}{N p^t + \mathcal{M}} \qquad \text{(in TG).} \tag{8.49}$$

These expressions agree with [53] and therefore also the explicit expressions for the Hamiltonians agree. In order to see this, first notice that $E_{\lambda\mu\nu}$ used in [53] is connected to our notation by

$$\omega_\lambda{}^{ab} = 2 e^{a\mu} e^{b\nu} E_{\lambda\mu\nu}. \tag{8.50}$$

Then eq. (5.8) agrees with (8.45) and (5.6) agrees with (8.47) and (8.46). However, the important point of our approach is that the Poisson/Dirac brackets follow from an "inspection" of the action. Variation of the action implies variation of the Lagrangian

$$\hat{L} = \hat{p}_i \dot{\hat{z}}^i + \frac{1}{2} S_{(i)(j)} \Lambda^{K(i)} \dot{\Lambda}^{K(j)} - H$$

which gives the well-known canonical structure for the phase space variables $\left(\hat{z}^i, \hat{p}_i, S_{(i)(j)}\right)$.

8.5 Hamiltonian at quadratic order in spin

In a numerical study in chapter 6 we found that the Hamiltonian valid at linear order in spin yields comparable results to the Lagrangian formalism, i.e. the MP equations, if the spin value is small - between $10^{-4} - 10^{-6} M\mathcal{M}$. For lower values, the influence of the spin on the motion of the particle is negligible and the motion approaches the geodesic limit. However, spin values within the mentioned range of $10^{-4} - 10^{-6} M\mathcal{M}$ are indeed of astrophysical relevance match the expectations for realistic spin values in astrophysical systems. Then, a Hamiltonian formalism is of great interest, since it offers approaches to analyse the dynamics of spinning extended bodies in a different manner to the Lagrangian formalism. In particular chaos and perturbation theory make use of a Hamiltonian formalism. Moreover, in our study the numerical evaluation of the Hamiltonian system needed less computational costs than the MP equations. Within the Hamiltonian formulation we only have to solve first-order differential equations which is another advantage over the Lagrangian one. Thus, we are interested in higher contributions from the spin within the pole-dipole approximation and use the action approach to compute the Hamiltonian at quadratic order in spin. In many fields of research canonical variables provide a great advantage compared to the non-canonical ones. Therefore, we perform a coordinate transformation in the action yielding

these canonical variables.

8.5.1 Shift to quadratic order

Higher orders in spin include further effects, that can be attributed to the dynamical mass. The contributions from field interactions or nonminimal couplings to curvature are included in the dynamical mass and can be expressed as $\mathcal{M} = m + \mathcal{O}\left(S^2\right)$, which we have to take into account when approximating the equations at quadratic order in spin.

Again, we start with the computation of the Lagrangian shifted to the new worldline

$$\begin{aligned}\hat{L} =& p_\mu \hat{u}^\mu + \frac{1}{2} S_{\mu\nu}\Omega^{\mu\nu} - \frac{p_\mu S^{\mu\nu}}{p_\rho p^\rho}\frac{Dp_\nu}{d\sigma} + \Delta\left(p_\mu \hat{u}^\mu\right) + \Delta\left(\frac{1}{2} S_{\mu\nu}\Omega^{\mu\nu}\right) - \\ &- \Delta\left(\frac{p_\mu S^{\mu\nu}}{p_\rho p^\rho}\frac{Dp_\nu}{d\sigma}\right) + \frac{1}{2}\Delta^2\left(p_\mu \hat{u}^\mu\right) + \mathcal{O}\left(S^3\right) \end{aligned} \tag{8.51}$$

where all orders higher than quadratic in spin are neglected. Then, the variational terms are computed using the commutator relation between the covariant differential and the covariant variation in eq. (4.9) as well as the shift of the four-velocity from eq. (4.14) and of the angular velocity in eq. (**??**) which yields

$$\begin{aligned}\Delta\left(p_\mu \hat{u}^\mu\right) &= -\frac{Dp_\mu}{d\sigma}\delta\hat{z}^\mu + \text{div} \\ \Delta\left(\frac{1}{2} S_{\mu\nu}\Omega^{\mu\nu}\right) &= \frac{1}{2} S_{\mu\nu} R^{\mu\nu}{}_{\beta\alpha}\left(\delta\hat{z}^\alpha\right)\left(\hat{u}^\beta\right) \\ \Delta\left(\frac{p_\mu S^{\mu\nu}}{p_\rho p^\rho}\frac{Dp_\nu}{d\sigma}\right) &= -R^\gamma{}_{\nu\beta\alpha}\hat{u}^\beta p_\gamma \frac{S^{\alpha\mu}p_\mu}{p_\rho p^\rho}\delta\hat{z}^\nu \\ \Delta^2\left(p_\mu \hat{u}^\mu\right) &= -R^\gamma{}_{\mu\beta\alpha}\hat{u}^\beta p_\gamma \delta\hat{z}^\alpha \delta\hat{z}^\mu \end{aligned}$$

Therewith we obtain for the Lagrangian

$$\begin{aligned}\hat{L} &= p_\mu \hat{u}^\mu + \frac{1}{2} S_{\mu\nu}\Omega^{\mu\nu} - \frac{p_\mu S^{\mu\nu}}{p_\rho p^\rho}\frac{Dp_\nu}{d\sigma} - \frac{Dp_\mu}{d\sigma}\delta\hat{z}^\mu + \frac{1}{2} S_{\mu\nu} R^{\mu\nu}{}_{\beta\alpha}\left(\delta\hat{z}^\alpha\right)\left(\hat{u}^\beta\right) + \\ &+ R^\gamma{}_{\nu\beta\alpha}\hat{u}^\beta p_\gamma \frac{S^{\alpha\mu}p_\mu}{p_\rho p^\rho}\delta\hat{z}^\nu - \frac{1}{2} R^\gamma{}_{\nu\beta\alpha}\hat{u}^\beta p_\gamma \delta\hat{z}^\alpha \delta\hat{z}^\nu + \text{div} + \mathcal{O}\left(S^3\right)\end{aligned}$$

In order to obtain a canonical structure between the spatial variables of $\hat{z}^\mu$ we have to find the corresponding true conjugate momenta requiring the time derivative of p_μ to vanish. Notice, that we can cancel the time derivative of p_μ if we choose the worldline shift appropriately. Hence, by setting

$$\delta\hat{z}^\mu = \frac{S^{\mu\nu}p_\nu}{p_\rho p^\rho}. \tag{8.52}$$

the relation between the old and the new worldline results in

$$z^\mu = \hat{z}^\mu + \frac{S^{\mu\nu}p_\nu}{p_\rho p^\rho}, \tag{8.53}$$

resembling the worldline shift in special relativity, again. The approach is very similar to the one for linear order in spin. If one extends the formulation to higher order than quadratic in spin the procedure has to be changed. Further difficulties are encountered, since covariant derivatives of the worldline shift appear which can be eliminated by adapting the covariant shift of the position variable.

In the quadratic case the Lagrangian is therefore rewritten as

$$\begin{aligned}\hat{L} &= p_\mu\hat{u}^\mu + \frac{1}{2}S_{\mu\nu}\Omega^{\mu\nu} + \frac{1}{2}S_{\mu\nu}R^{\mu\nu}{}_{\beta\alpha}\left(\delta\hat{z}^\alpha\right)\left(\hat{u}^\beta\right) + \frac{1}{2}R^\gamma{}_{\nu\beta\alpha}\hat{u}^\beta p_\gamma\delta\hat{z}^\alpha\delta\hat{z}^\nu \\ &\quad +\text{div} + \mathcal{O}\left(S^3\right) \ .\end{aligned}$$

Hence, the action of a spinning particle at quadratic order in spin is given by

$$S_{\text{PP}} = \int d\sigma\left[\hat{p}_\mu\hat{u}^\mu + \frac{1}{2}S_{\mu\nu}\Omega^{\mu\nu} - H_D\right] \tag{8.54}$$

where we already combined the terms involving the four-velocity $\hat{u}^\mu$ to a new momentum variable $\hat{p}_\mu$

$$\hat{p}_\mu := p_\mu + \frac{1}{2}S_{\beta\nu}\,R^{\beta\nu}{}_{\mu\alpha}\,\delta\hat{z}^\alpha + \frac{1}{2}R^\gamma{}_{\nu\mu\alpha}\,p_\gamma\,\delta\hat{z}^\alpha\delta\hat{z}^\nu \ . \tag{8.55}$$

However, as before, this cannot be the true conjugate momentum to the position variable, since $\Omega^{\mu\nu}$ depends on $\hat{u}^\mu$.

Thus, this action does not yet provide us with the correct Hamiltonian, though, but only with the unconstrained Hamiltonian H_D. So the next step is to solve the constraints and the gauge conditions in order to establish the true Hamiltonian.

8.5.2 Solving the constraints

Rewrite the Lagrangian given in (8.54)

$$\hat{L} = \hat{p}_\mu\hat{u}^\mu + \frac{1}{2}S_{\mu\nu}\Omega^{\mu\nu} \ ,$$

in the local Lorentz basis, use (8.35) and neglect terms that are of cubic or higher order

$$\hat{L} \;=\; \tilde{p}_\mu \hat{u}^\mu + \frac{1}{2}\Lambda_A{}^a \dot{\Lambda}^{Ab} S_{ab} + \mathcal{O}\left(S^3\right) \;,$$

with the new defined momentum

$$\tilde{p}_\mu := p_\mu + \frac{1}{2}\omega_\mu{}^{bc} S_{bc} - \frac{1}{2} S_{bc} R^{bc}{}_{\mu d}\, \delta\hat{z}^d - \frac{1}{2} R^b{}_{c\mu d}\, p_b\, \delta\hat{z}^c \delta\hat{z}^d \;. \tag{8.56}$$

We choose the worldline gauge in such a way that the coordinate time equals proper time $\sigma \approx t$ or $u^0 \approx 1$, so that we arrive at

$$\tilde{p}_\mu \hat{u}^\mu = \tilde{p}_0 + \tilde{p}_i \hat{u}^i \;,$$

where latin indices in parenthesis are associated with the local Lorentz basis. Solving the corresponding mass shell constraint yields

$$\tilde{p}_0 = -N\sqrt{\tilde{m}^2 + \gamma^{ij}\tilde{p}_i\tilde{p}_j} + N^i \tilde{p}_i \;, \tag{8.57}$$

where $\tilde{m}^2 = -\tilde{p}_a\tilde{p}^a$ is the mass with respect to $\tilde{p}^a$. Thus, using (8.56) the mass $\tilde{m}^2$ is given by

$$\begin{aligned} \tilde{m}^2 \;&=\; -\tilde{p}_a\tilde{p}^a = \mathcal{M}^2 - S_{bc}\omega_a{}^{bc}\left(\tilde{p}^a - \frac{1}{2}\omega^{abc}S_{bc}\right) + \frac{1}{4}\omega_a{}^{bc}\omega^{ade}S_{bc}S_{de} \\ &\quad -R_{bcad}\,\tilde{p}^b\tilde{p}^a\delta\hat{z}^d\delta\hat{z}^c - R^{bc}{}_{ad}S_{bc}\,\tilde{p}^a\delta\hat{z}^d + \mathcal{O}\left(S^3\right) \;, \end{aligned} \tag{8.58}$$

at quadratic order in spin where $\tilde{p}_a = e_a{}^\mu \tilde{p}_\mu$. Simplifying the terms involving the Riemann curvature tensor it turns out to be convenient to express $\tilde{m}^2$ in terms of the electric and magnetic parts of the Weyl tensor, which is regarded to be equivalent to the Riemann tensor for vacuum spacetimes. Therefore, we first reproduce the split of the Riemann tensor into electric and magnetic components.

8.5.2.1 Weyl/Riemann tensor components

Since we are only interested in vacuum spacetimes, such as Schwarzschild or Kerr spacetimes, in classical general relativity with four spacetime dimensions, the Riemann tensor can be split into an electric $E(v)_{\mu\nu}$ and a magnetic part $B(v)_{\mu\nu}$ with respect to a timelike vector v^μ as

$$\begin{aligned} R_{\alpha\beta\mu\nu} \;&=\; (G_{\alpha\beta\rho\delta}G_{\mu\nu\gamma\phi} - \eta_{\alpha\beta\rho\delta}\eta_{\mu\nu\gamma\phi})E^{\delta\phi}\frac{v^\rho v^\gamma}{-v^2} - \\ &\quad -(\eta_{\alpha\beta\rho\delta}G_{\mu\nu\gamma\phi} + G_{\alpha\beta\rho\delta}\eta_{\mu\nu\gamma\phi})B^{\delta\phi}\frac{v^\rho v^\gamma}{-v^2} \;, \end{aligned} \tag{8.59}$$

where $G_{\alpha\mu\beta\nu} = g_{\alpha\beta}g_{\mu\nu} - g_{\alpha\nu}g_{\beta\nu}$. It holds

$$E(v)_{\mu\nu} = R_{\mu\alpha\nu\beta}\frac{v^\alpha v^\beta}{-v^2}, \qquad B(v)_{\mu\nu} = \frac{1}{2}\eta_{\mu\alpha\rho\sigma}R_{\nu\beta}{}^{\rho\sigma}\frac{v^\alpha v^\beta}{-v^2}, \tag{8.60}$$

where $\eta_{\mu\nu\alpha\beta} = \sqrt{-g}\epsilon_{\mu\nu\alpha\beta}$ is the volume form. These tensors have the properties

$$E_{\mu\nu} = E_{\nu\mu}, \qquad E_{\mu\nu}g^{\mu\nu} = 0, \qquad E_{\mu\nu}v^\nu = 0, \tag{8.61}$$

$$B_{\mu\nu} = B_{\nu\mu}, \qquad B_{\mu\nu}g^{\mu\nu} = 0, \qquad B_{\mu\nu}v^\nu = 0, \tag{8.62}$$

which make $E_{\mu\nu}$ and $B_{\mu\nu}$ much easier to handle compared to $R_{\mu\nu\alpha\beta}$.

In order to reformulate the contributions from the Riemann curvature tensor in (8.58) in terms of $E_{\mu\nu}$ and $B_{\mu\nu}$ we find that a useful relation is

$$R_{\alpha\beta\mu\nu}\, p^\alpha \delta\hat{z}^\beta \tilde{S}^{\mu\nu} = 2\mathcal{M}B(p)_{\alpha\beta}\tilde{S}^\alpha \delta\hat{z}^\beta, \tag{8.63}$$

where we introduced the definition of the spin four-vector $\tilde{S}_\alpha$

$$\tilde{S}_\alpha = -\frac{1}{2}\eta_{\alpha\beta\mu\nu}\frac{p^\beta}{\mathcal{M}}\tilde{S}^{\mu\nu}. \tag{8.64}$$

with

$$\tilde{S}_{ab} = P_a{}^c P_b{}^d S_{cd}\ , \tag{8.65}$$

and the projector

$$P_a{}^c = \delta_a^c + \frac{p_a p^c}{\mathcal{M}^2}\ , \tag{8.66}$$

which projects the quantities onto the particle's rest frame, as we will see below. Keep in mind that $\tilde{S}_{ab}$ is just used in intermediate expressions here, since it fulfills the simple condition

$$\tilde{S}_{ab}p^b = 0. \tag{8.67}$$

Notice the resemblance to the T SSC (1.29) and recall that the T SSC defines the reference worldline to be the centre of mass of the particle within the rest frame of the spinning body. Thus, the projector $P_a{}^c$ yields indeed the spin components as the projections onto the rest frame of the particle, denoted by a $\sim$.

Therewith the terms involving $R_{\mu\nu\alpha\beta}$ can be expressed in terms of the electric E_{ab} and the magnetic part B_{ab} of the Riemann tensor as

$$\begin{aligned} R_{bcad}\,\tilde{p}^b\tilde{p}^a\delta\hat{z}^d\delta\hat{z}^c &= \mathcal{M}^2 E\left(\tilde{p}\right)_{ab}\delta\hat{z}^a\delta\hat{z}^b\ , \\ R_{adbc}\,\tilde{p}^a\delta\hat{z}^d S^{bc} &= 2\mathcal{M}B\left(\tilde{p}\right)_{ab}\tilde{S}^a\delta\hat{z}^b - 2\mathcal{M}^2 E\left(\tilde{p}\right)_{ab}\delta\hat{z}^a\delta\hat{z}^b\ , \end{aligned}$$

and amount to

$$\begin{aligned}\tilde{m}^2 &= \mathcal{M}^2 - S_{bc}\omega_a{}^{bc}\tilde{p}^a + \frac{1}{4}\omega_a{}^{bc}\omega^{ade}S_{bc}S_{de} - 2\mathcal{M}B\left(\tilde{p}\right)_{ab}\tilde{S}^a\delta\hat{z}^b + \\ &\quad + \mathcal{M}^2 E\left(\tilde{p}\right)_{ab}\delta\hat{z}^a\delta\hat{z}^b + \mathcal{O}\left(S^3\right) \ . \end{aligned} \tag{8.68}$$

As part of solving the constraints we fix the gauge of the tetrad, i.e. we choose an orientation for the basis vectors of the local frame, since such a choice often simplifies the handling of the equations involving the spin.

8.5.2.2 The Carter frame and its rotation coefficients

Instead of using the time gauge, as we did in the linear case, the calculations involving curvature terms can be greatly simplified if we choose to go to the Carter frame

$$\left(e^a{}_\mu\right) = \begin{pmatrix} \sqrt{\frac{\Delta}{\Sigma}} & 0 & 0 & -\sqrt{\frac{\Delta}{\Sigma}}a\sin^2\theta \\ 0 & \sqrt{\frac{\Sigma}{\Delta}} & 0 & 0 \\ 0 & 0 & \sqrt{\Sigma} & 0 \\ -\frac{a\sin\theta}{\sqrt{\Sigma}} & 0 & 0 & \frac{\sin\theta}{\sqrt{\Sigma}}(a^2+r^2) \end{pmatrix}, \tag{8.69}$$

$$\left(e_a{}^\mu\right) = \begin{pmatrix} \frac{r^2+a^2}{\sqrt{\Delta\Sigma}} & 0 & 0 & \frac{a}{\sqrt{\Delta\Sigma}} \\ 0 & \sqrt{\frac{\Delta}{\Sigma}} & 0 & 0 \\ 0 & 0 & \frac{1}{\sqrt{\Sigma}} & 0 \\ \frac{a\sin\theta}{\sqrt{\Sigma}} & 0 & 0 & \frac{1}{\sqrt{\Sigma}\sin\theta} \end{pmatrix}, \tag{8.70}$$

with Σ, Δ, and ϖ^2 given in (1.10). This tetrad corresponds to a stationary observer rotating with angular velocity $\frac{a}{r^2+a^2}$ with respect to the rest frame at infinity , see e.g. [170, 169]. It should be mentioned here that the local tetrad is adapted to a Kerr background spacetime so that we restrict our following analysis to the motion of a spinning particle in the gravitational field of a Kerr black hole of mass M and spin a. All expressions in the local frame will thus be associated with the tetrad based on Kerr spacetime.

Consequently, with the abbreviations $\tilde{\omega}_{a(i)} = \frac{1}{2}e_a{}^\mu\omega_\mu{}^{(k)(l)}\epsilon_{(k)(l)(i)}$ and $\hat{\omega}_{a(i)} = e_a{}^\mu\omega_{\mu(0)(i)}$,

the components of the Ricci rotation coefficients are given by

$$\left(\tilde{\omega}_{a(i)}\right) = \frac{\sqrt{\Delta}}{\Sigma^{3/2}} \begin{pmatrix} a_1 & a_2 & 0 \\ 0 & 0 & -a_1 a_2/r \\ 0 & 0 & r \\ \omega_3 r & -r & 0 \end{pmatrix}, \tag{8.71}$$

$$\left(\hat{\omega}_{a(i)}\right) = \frac{\sqrt{\Delta}}{\Sigma^{3/2}} \begin{pmatrix} \omega_0 r - a_2^2/r & a_1 a_2/r & 0 \\ 0 & 0 & a_2 \\ 0 & 0 & a_1 \\ a_2 & -a_1 & 0 \end{pmatrix}, \tag{8.72}$$

where we defined

$$\omega_0 = \frac{M}{r\Delta}\left(r^2 - a^2\cos^2\theta\right) \tag{8.73}$$

$$\omega_3 = \frac{r^2 + a^2}{r\sqrt{\Delta}}\cot\theta \tag{8.74}$$

and a vector associated to the spin of a Kerr black hole

$$\vec{a} = a \begin{pmatrix} \cos\theta \\ -\sin\theta\, r/\sqrt{\Delta} \\ 0 \end{pmatrix} \quad . \tag{8.75}$$

Moreover, the spin interaction terms can be clearly structured with the flat vectors

$$\vec{\tilde{p}} = \begin{pmatrix} \tilde{p}_{(1)} \\ \tilde{p}_{(2)} \\ \tilde{p}_{(3)} \end{pmatrix}, \qquad \vec{S} = \begin{pmatrix} S_{(1)} \\ S_{(2)} \\ S_{(3)} \end{pmatrix} \quad , \tag{8.76}$$

with $S_{(i)} = \frac{1}{2}\epsilon_{ijk}S_{(j)(k)}$ which subsequently lead to an intuitive interpretation of the results. We combine the solution of the NW SSC as well as the radial coordinate to a vector

$$\vec{S}_0 = \left(S_{(t)(i)}\right) = \frac{\vec{p}\times\vec{S}}{p^{(0)} + \mathcal{M}}, \qquad \vec{r} = \begin{pmatrix} r \\ 0 \\ 0 \end{pmatrix} = r\vec{n} \tag{8.77}$$

and define

$$\vec{\omega} = (0, 0, \omega_3) \ ,$$

simplifying the structure of the spin interaction so that it can be written as a vector

equation. Therefore, the spin interaction reads

$$\frac{1}{2}\tilde{p}_c e^{c\mu}\omega_{\mu ab}S^{ab} = \frac{\sqrt{\Delta}}{\Sigma^{3/2}}[\tilde{p}^{(0)}(h_{0S}+h_{0aS}+h_{0a^2S})+\vec{\tilde{p}}\cdot(\vec{h}_S+\vec{h}_{aS}+\vec{h}_{a^2S})] \tag{8.78}$$

where we split the spin coupling terms as

$$h_{0S} = -\omega_0\,\vec{r}\cdot\vec{S}_0, \tag{8.79}$$
$$h_{0aS} = \vec{a}\cdot\vec{S}, \tag{8.80}$$
$$h_{0a^2S} = -\frac{1}{r}\vec{n}\cdot[\vec{a}\times(\vec{a}\times\vec{S}_0)], \tag{8.81}$$
$$\vec{h}_S = -\vec{r}\times\vec{S}+\vec{r}\cdot\vec{S}\,\vec{\omega}, \tag{8.82}$$
$$\vec{h}_{aS} = \vec{a}\times\vec{S}_0+2\vec{a}\cdot(\vec{n}\times\vec{S}_0)\vec{n}, \tag{8.83}$$
$$\vec{h}_{a^2S} = \frac{1}{r}\vec{n}\cdot\vec{a}\,\vec{a}\cdot(\vec{n}\times\vec{S})\vec{n}. \tag{8.84}$$

Then the spin-spin coupling can be expressed as

$$\frac{1}{4}\omega_{\mu ab}S^{ab}\omega^{\mu}{}_{cd}S^{cd} = \frac{\Delta}{\Sigma^3}[-(h_{0S}+h_{0aS}+h_{0a^2S})^2+(\vec{h}_S+\vec{h}_{aS}+\vec{h}_{a^2S})^2]. \tag{8.85}$$

Now we expand the solution of the NW SSC in terms of the canonical momenta up to quadratic order in the particle's spin in order to be consistent within the computation and obtain

$$\vec{S}_0 = \left[1-\frac{\sqrt{\Delta}}{\Sigma^{3/2}(\tilde{p}^{(0)}+m)}(h_{0S}+h_{0aS}+h_{0a^2S})\right]\frac{\vec{\tilde{p}}\times\vec{S}}{\tilde{p}^{(0)}+m} - \\ -\frac{1}{\tilde{p}^{(0)}+m}\frac{\sqrt{\Delta}}{\Sigma^{3/2}}(\vec{h}_S+\vec{h}_{aS}+\vec{h}_{a^2S})\times\vec{S}+\mathcal{O}(S^3) \tag{8.86}$$

where $m = \text{const} = \mathcal{M}+\mathcal{O}(S^2)$. The remaining terms in (8.68) involve curvature interactions which is why we first compute the curvature combinations in the Carter frame.

8.5.2.3 Curvature combinations in the Carter frame

First, we compute the electric and magnetic Weyl tensor with respect to the time vector of our frame $e_{(0)}{}^{\mu}$. The result in vector notation yields

$$E(e)_{(i)(j)} = \frac{E(e)}{\sqrt{6}}(\delta_{ij}-3\delta^1_i\delta^1_j), \tag{8.87}$$
$$B(e)_{(i)(j)} = \frac{B(e)}{\sqrt{6}}(-\delta_{ij}+3\delta^1_i\delta^1_j) \tag{8.88}$$

with

$$E(e) := \sqrt{E(e)_{\mu\nu}E(e)^{\mu\nu}} = \frac{\sqrt{6}M}{\Sigma^3} r(r^2 - 3a^2\cos^2\theta)$$
$$B(e) := \sqrt{B(e)_{\mu\nu}B(e)^{\mu\nu}} = \frac{\sqrt{6}M}{\Sigma^3} a\cos\theta(3r^2 - a^2\cos^2\theta) \ ,$$

where the time components vanish.

Based on this, we can obtain $E(p)_{ab}$ and $B(p)_{ab}$ by first computing $R_{\alpha\beta\mu\nu}$ using eq. (8.59) and then forming $E(p)_{(i)(j)} \equiv R_{acbd}\, p^c p^d/\mathcal{M}^2$ etc, with the result

$$\begin{aligned} E(p)_{ab} &= \frac{E(e)}{\sqrt{6}\mathcal{M}^2}[\mathcal{M}^2\eta_{ab} + p_a p_b - 12p^c\delta^1_{[c}\delta^0_{a]}p^d\delta^1_{[d}\delta^0_{b]} + 3\epsilon_{01ia}p_{(i)}\epsilon_{01jb}p_{(j)}] - \\ &\quad - \frac{\sqrt{6}B(e)}{\mathcal{M}^2}[\epsilon_{01ia}p_{(i)}p^c\delta^1_{[c}\delta^0_{b]} + (a \leftrightarrow b)] \ , \end{aligned} \tag{8.89}$$

$$\begin{aligned} B(p)_{ab} &= -\frac{B(e)}{\sqrt{6}\mathcal{M}^2}[\mathcal{M}^2\eta_{ab} + p_a p_b - 12p^c\delta^1_{[c}\delta^0_{a]}p^d\delta^1_{[d}\delta^0_{b]} + 3\epsilon_{01ia}p_{(i)}\epsilon_{01jb}p_{(j)}] - \\ &\quad - \frac{\sqrt{6}E(e)}{\mathcal{M}^2}[\epsilon_{01ia}p_{(i)}p^c\delta^1_{[c}\delta^0_{b]} + (a \leftrightarrow b)] \ , \end{aligned} \tag{8.90}$$

where we used the Levi-Civita tensor density $\eta_{\mu\nu\alpha\beta} = \sqrt{-g}\epsilon_{\mu\nu\alpha\beta}$ and the convention for the Levi-Civita Symbol $\epsilon_{0123} = 1$. Notice that $\eta_{abcd} = \epsilon_{abcd}$ and $\epsilon^{0123} = -1$.

Moreover, we express the full frame-components of the Riemann tensor as

$$R_{(0)(i)(0)(j)} = -\frac{E(e)}{\sqrt{6}} 3n_{<ij>}, \tag{8.91}$$
$$R_{(0)(i)(j)(k)} = \frac{B(e)}{\sqrt{6}} 3n_{<il>}\epsilon_{jkl}, \tag{8.92}$$
$$R_{(i)(j)(k)(l)} = \frac{E(e)}{\sqrt{6}} 3n_{<pq>}\epsilon_{ijp}\epsilon_{klq}, \tag{8.93}$$

where $3n_{<ij>} = 3n_i n_j - \delta_{ij} = 3\delta^1_i\delta^1_j - \delta_{ij}$. The components of $E(p)_{ab}$ and $B\,(p)_{ab}$ can also be written in this framework and yield

$$E(p)_{(0)(0)} = -\frac{E(e)}{\sqrt{6}} 3n_{<ij>}p^{(i)}p^{(j)}, \tag{8.94}$$
$$E(p)_{(0)(i)} = \frac{E(e)}{\sqrt{6}} 3n_{<ij>}p^{(j)}p^{(0)} + \frac{B(e)}{\sqrt{6}}\epsilon_{ijk}3n_{<kl>}p^{(j)}p^{(l)}, \tag{8.95}$$
$$\begin{aligned} E(p)_{(i)(j)} &= \frac{E(e)}{\sqrt{6}}\Big[- 3n_{<ij>}p^2_{(0)} + \epsilon_{ikp}\epsilon_{jlq}3n_{<pq>}p^{(k)}p^{(l)}\Big] \\ &\quad - \frac{B(e)}{\sqrt{6}}\Big[3n_{<il>}\epsilon_{jkl}p^{(k)}p^{(0)} + (i \leftrightarrow j)\Big], \end{aligned} \tag{8.96}$$

where the components of $B(p)_{ab}$ are likewise with $E(e) \to -B(e)$ and $B(e) \to E(e)$. Therewith we can compute the remaining terms in $\tilde{m}^2$

$$E(p)_{ab}\delta\hat{z}^a\delta\hat{z}^b = E(p)_{00}\delta\hat{z}^0\delta\hat{z}^0 + 2E(p)_{0i}\delta\hat{z}^0\delta\hat{z}^i + E(p)_{ij}\delta\hat{z}^i\delta\hat{z}^j, \tag{8.97}$$

$$B(p)_{ab}\tilde{S}^a\delta\hat{z}^b = B(p)_{00}\tilde{S}^0\delta\hat{z}^0 + B(p)_{0i}\tilde{S}^0\delta\hat{z}^i + B(p)_{i0}\tilde{S}^i\delta\hat{z}^0 + B(p)_{ij}\tilde{S}^i\delta\hat{z}^j, \tag{8.98}$$

and express the variations in terms of the canonical momenta as

$$\delta\hat{z}_0 = \frac{\vec{S}_0\,\vec{\tilde{p}}}{-m^2} + \mathcal{O}\left(S^2\right) = \mathcal{O}\left(S^2\right) \ , \tag{8.99}$$

$$\delta\vec{\hat{z}} = -\frac{\vec{\tilde{p}}\times\vec{S} - \vec{S}_0\,\tilde{p}^0}{m^2} + \mathcal{O}\left(S^2\right) \ . \tag{8.100}$$

Since the expressions in eq. (8.97) and (8.98) appear always in products with another spin term, we neglect here already the terms of second order in spin. Moreover, the projected spin vector $\tilde{S}^a$ is written as

$$\vec{\tilde{S}} = \vec{S} + \frac{\vec{p}(\vec{p}\cdot\vec{S})}{\mathcal{M}(p^{(0)}+\mathcal{M})} + \mathcal{O}\left(S^2\right) \ , \tag{8.101}$$

$$\tilde{S}^0 = \frac{\vec{p}\cdot\vec{S}}{\mathcal{M}} = \frac{\vec{\tilde{p}}\vec{S}}{\mathcal{M}} + \mathcal{O}\left(S^2\right) \ , \tag{8.102}$$

and

$$-\tilde{S}^0\vec{p} + p^{(0)}\vec{\tilde{S}} = p^{(0)}\vec{S} - \frac{\vec{p}(\vec{p}\cdot\vec{S})}{p^{(0)}+\mathcal{M}} \ , \tag{8.103}$$

with $\vec{\tilde{S}}^T = \left(\tilde{S}_{(1)}, \tilde{S}_{(2)}, \tilde{S}_{(3)}\right)$, $p_a\tilde{S}^a = 0$ and $\tilde{S}_a\tilde{S}^a = \vec{S}^2$ and the solution to the NW SSC given in (8.102). The electric and magnetic part of the curvature tensor can also be calculated with respect to the canonical momentum. However, since they also appear only in combinations with terms quadratic in spin, we can simply replace the momenta p_a by the kinematical momenta $\tilde{p}_a$. Therewith we write the curvature interactions as

$$\begin{aligned} E(p)_{ab}\delta\hat{z}^a\delta\hat{z}^b = {} & \frac{E(e)}{\sqrt{6}\mathcal{M}^2}\left[\mathcal{M}^2\delta\vec{\hat{z}}^2 - 3p_{(0)}^2(\vec{n}\cdot\delta\vec{\hat{z}})^2 + 3\left(\vec{n}\cdot(\vec{p}\times\delta\vec{\hat{z}})\right)^2\right] + \\ & + \frac{\sqrt{6}B(e)}{\mathcal{M}^2}p^{(0)}(\vec{n}\cdot\delta\vec{\hat{z}})\left(\vec{n}\cdot(\vec{p}\times\delta\vec{\hat{z}})\right), \end{aligned}$$

$$
\begin{aligned}
B(p)_{ab}\tilde{S}^a\delta\hat{z}^b &= \frac{\sqrt{3}B(e)}{\sqrt{2}\mathcal{M}^2}(\vec{n}\cdot\delta\vec{\hat{z}})\left[(2p_{(0)}^2-\mathcal{M}^2)(\vec{n}\cdot\vec{S})-\frac{2p^{(0)}+\mathcal{M}}{p^{(0)}+\mathcal{M}}(\vec{n}\cdot\vec{p})(\vec{p}\cdot\vec{S})\right] \\
&\quad+\frac{\sqrt{3}B(e)}{\sqrt{2}\mathcal{M}^2}\Bigg[\left(\vec{n}\cdot(\vec{p}\times\delta\vec{\hat{z}})\right)\left(p^{(0)}(\vec{n}\cdot\vec{S})-\frac{(\vec{n}\cdot\vec{p})(\vec{p}\cdot\vec{S})}{p^{(0)}+\mathcal{M}}\right)+ \\
&\quad+p^{(0)}(\vec{n}\cdot\delta\vec{\hat{z}})\left(\vec{n}\cdot(\vec{p}\times\vec{S})\right)\Bigg],
\end{aligned}
$$

where we have used $\vec{p}\cdot\delta\vec{\hat{z}}=0=\vec{S}\cdot\delta\vec{\hat{z}}$. Hence, when we plug in all the constraints, i.e. the worldline gauge (8.57) and the NW SSC (8.102), the mass term in (8.58) is completely expressed as a function of the canonical momenta $\vec{\tilde{p}}$ and the spatial spin vector $\vec{S}$ in a local basis adapted to Kerr spacetime.

8.5.3 Hamiltonian and Poisson brackets

After having solved the constraints, the Hamiltonian is obtained via the action

$$
\hat{S}=\int dt\left[\hat{L}-H_D\right]
$$

where we used the worldline gauge $\sigma=t$. Inserting all constraints ($H_D=0$) leads to

$$
\begin{aligned}
\hat{S} &= \int dt\left(\tilde{p}_a\hat{u}^a+\frac{1}{2}\Lambda_A{}^a\dot{\Lambda}^{Ab}S_{ab}+\mathcal{O}\left(S^3\right)\right) \\
&= \int dt\left(\tilde{p}_{(i)}\hat{u}^{(i)}+\frac{1}{2}S_{(i)(j)}\Lambda^{K(i)}\dot{\Lambda}^{K(j)}-H+\mathcal{O}\left(S^3\right)\right) \qquad (8.104)
\end{aligned}
$$

with the Hamiltonian $H=-\tilde{p}_{(t)}$ given by

$$
H=-\tilde{p}_{(t)}=N\sqrt{\tilde{m}^2+\gamma^{(i)(j)}\tilde{p}_{(i)}\tilde{p}_{(j)}}-N^{(i)}\tilde{p}_{(i)}\ .
$$

Notice the dependence of $\tilde{m}^2$ on $\tilde{p}_{(t)}$ implying that the solution for $\tilde{p}_{(t)}$ has to be used iteratively until the terms containing $\tilde{p}_{(t)}$ become of higher order than second order in the particle's spin.

The Poisson bracket relation can easily be deduced from the action (8.104) yielding a canonical structure for the phase space variables $\left(\hat{z}^i,\tilde{p}_i,S^{(i)(j)}\right)$

$$
\begin{aligned}
\left\{\hat{z}^i,\tilde{p}_j\right\} &= \delta^i_j+\mathcal{O}\left(S^3\right) \\
\\
\left\{S_{(i)(j)},S_{(k)(l)}\right\} &= S_{(l)(i)}\delta^k_j-S_{(l)(j)}\delta^k_i+S_{(k)(j)}\delta^k_i-S_{(k)(i)}\delta^l_j+\mathcal{O}\left(S^3\right)
\end{aligned}
$$

and all other bracket relations between the variables vanish.

8.6 Hamiltonian to all orders in spin

Previously, we aimed at a canonical formulation of the dynamics in the action. When constructing these canonical variables we introduce a shift of the reference worldline which eliminates the contribution from the Fermi-Walker transport of the momentum vector induced by the spin of the particle. In principle, we can extend the canonical formalism up to arbitrary order in the spin by taking into account the contributions from the higher orders to the dynamical mass $\mathcal{M}$. However, as we have seen the canonical momentum becomes more complicated if we consider higher orders in spin. In addition to that, this expansion will always be an approximation within an approximation, even in the pole-dipole formalism. One of the approximation properties can be avoided by giving up on the canonical formulation. Therewith, a Hamiltonian is obtained that is exact in the particle's spin within the pole-dipole approximation. The computation is similar to the previous cases, i.e. the ones where we truncated the series at linear and quadratic orders in the particle's spin. Instead of eliminating the derivative of the momentum it is now kept in the action. In order to ensure that Poisson brackets can be associated to the variables, the action may contain at most one time derivative in every term. Then, the equations of motion can be calculated as usual by the Poisson bracket relations between the searched for variables and the Hamiltonian.

The action is given in (8.9) and is repeated once more for the reader's convenience

$$\mathcal{S} = \int d\sigma \left(p_\mu u^\mu + \frac{1}{2} S_{\mu\nu}\Omega^{\mu\nu} - \frac{p_\mu S^{\mu\nu}}{p_\rho p^\rho}\frac{Dp_\nu}{d\sigma} - H_D \right) .$$

Notice, that the additional term considering the time derivative of the momentum only contains the connection, not the curvature, so the calculation should not be much more involved compared to the previous cases. Indeed, using the relation in (8.11) and the directional derivative the third term in the action is rewritten in the local frame and yields

$$\frac{1}{2} S_{\mu\nu}\Omega^{\mu\nu} - \frac{p_\mu S^{\mu\nu}}{p^2}\frac{Dp_\nu}{d\sigma} = \frac{1}{2} S_{ab}\Lambda_A{}^a \dot{\Lambda}^{Ab} + \frac{1}{\mathcal{M}} S^{ab} p_a \dot{p}_b + \frac{1}{2} S_{ab}\omega_\mu{}^{ab} u^\mu + \tag{8.105}$$

$$+ \frac{1}{\mathcal{M}} S_{ab} p^a p_c \omega_\mu{}^{cb} u^\mu \tag{8.106}$$

In the following we will compute this expression subject to the constraints, the worldline as well as the spin gauge constraints.

8.6.1 Solving the constraints

First, we start with the spin gauge constraint which we choose to be the NW SSC. Using the NW SSC through the relations (8.18) and (8.38), we arrive at

$$\frac{1}{2}S_{\mu\nu}\Omega^{\mu\nu} - \frac{p_\mu S^{\mu\nu}}{p^2}\frac{Dp_\nu}{d\sigma} = \frac{1}{2}S_{(i)(j)}\Lambda^{K(i)}\dot{\Lambda}^{K(j)} + S^{(t)(i)}\frac{d(e_{(i)}{}^\mu p_\mu)}{dt} + \frac{1}{2}\tilde{S}_{ab}\omega_\mu{}^{ab}u^\mu \tag{8.107}$$

where we introduced the abbreviation $\tilde{S}_{ab}$ in eq. (8.65). The solution of the corresponding T SSC-like condition in eq. (8.67) is given by

$$\tilde{S}_{(t)(i)} = \frac{\tilde{S}_{(i)(j)}e^{(j)\mu}p_\mu}{e^{(t)\nu}p_\nu} \ , \tag{8.108}$$

and corresponds to the mass dipole with respect to the particle's rest frame. However, the spin variable in the action is not the projected spin $\tilde{S}_{ab}$which satisfies the T SSC. Therefore, we have to express $\tilde{S}_{ab}$ in terms of the original spin variables which are subject to the NW SSC. Considering the spin supplementary condition in (8.36) and its solution (8.37) we arrive at

$$\tilde{S}_{(i)(j)} \quad = \quad S_{(i)(j)} - 2\frac{e_{[(i)}{}^\mu S_{(j)](k)}e^{(k)\nu}p_\mu p_\nu}{\mathcal{M}\left(e^{(t)\mu}p_\mu + \mathcal{M}\right)} \ , \tag{8.109}$$

Contraction with $\frac{p^j}{p^0}$ gives the simple relation

$$\frac{\tilde{S}_{(i)(j)}e^{(j)\mu}p_\mu}{e^{(t)\nu}p_\nu} \quad = \quad S_{(i)(j)}\frac{e^{(j)\mu}p_\mu}{\mathcal{M}} \ ,$$

so that we obtain for the projected mass dipole a function of the spatial spin components in the local basis

$$\tilde{S}_{(t)(i)} \quad = \quad \frac{S_{(i)(j)}e^{(j)\nu}p_\nu}{\mathcal{M}} \ . \tag{8.110}$$

In the time gauge, given in eq. 8.40, the subsequent calculation simplifies considerably, for instance

$$\tilde{S}_{(t)(i)} = \frac{S_{(i)(j)}e^{(j)k}p_k}{\mathcal{M}} \qquad \text{(in TG)} \tag{8.111}$$

by removing the time-components of the four-momentum vector and

$$\tilde{S}_{(i)(j)} = S_{(i)(j)} - 2\frac{e_{[(i)}{}^{l} S_{(j)](k)} e^{(k)m} p_l p_m}{\mathcal{M}\left(Np^t + \mathcal{M}\right)} \qquad \text{(in TG)}. \tag{8.112}$$

Therewith we express the term containing a time derivative appearing in (8.107) as

$$S^{(t)(i)}\frac{d(e_{(i)}{}^{\mu} p_\mu)}{dt} = -\frac{S_{(i)(l)} e^{(l)m} p_m}{\mathcal{M}\left(Np^t + \mathcal{M}\right)}\left(e^{(i)j}\dot{p}_j + e^{(i)j}{}_{,k} p_j \dot{z}^k + e^{(i)j}{}_{,t} p_j \dot{z}^t\right) \qquad \text{(in TG)},$$

where we have used the solution to the NW SSC $S^{(t)(i)}$ given in (8.37) as well as the time gauge, eq. 8.40. Lastly, considering (8.108) we have

$$\begin{aligned}\frac{1}{2}\tilde{S}_{ab}\omega_\mu{}^{ab} u^\mu &= \frac{1}{2}\tilde{S}_{(i)(j)}\Bigg(\left(\omega_t{}^{(i)(j)} + 2\frac{\omega_t{}^{(t)(i)} e^{(j)k} p_k}{Np^t}\right)\dot{z}^0 + \\ &\quad + \left(\omega_k{}^{(i)(j)} + 2\frac{\omega_k{}^{(t)(i)} e^{(j)l} p_l}{Np^t}\right)\dot{z}^k\Bigg) \qquad \text{(in TG)},\end{aligned}$$

where the projected spin can be eliminated by the relation in (8.109) or (8.112) yielding an expression dependent on the dynamical variables in the local frame. As before, we choose the worldline gauge such that proper time equals the coordinate time, i.e. $\sigma = t$. Then, the time component of the four-velocity becomes $\dot{z}^t = 1$. Again, z^t has been degraded from a spacetime variable to a time parameter characterising the motion providing the required spacetime split for a Hamiltonian formalism, where space and time are not treated at an equal footing.

8.6.2 The Hamiltonian and the equations of motion

Inserting the constraints provided in the last section, i.e. the NW SSC and the worldline gauge, into the Lagrangian and combining the time derivatives of the variables we obtain for the Lagrangian

$$L = \frac{1}{2}S_{(i)(j)}\Lambda^{K(i)}\dot{\Lambda}^{K(j)} + B^j\dot{p}_j + (p_j + A_j)\dot{z}^j - H\ , \tag{8.113}$$

with the abbreviations

$$\begin{aligned}A_k &= \frac{1}{2}S_{(i)(j)}\omega_k{}^{(i)(j)} + \frac{S_{(i)(j)}p^{(j)}}{\mathcal{M}(p^{(t)} + \mathcal{M})}e^{(i)l}\Gamma^m{}_{lk}p_m + \frac{S_{(i)(j)}p^{(j)}\omega_k{}^{(t)(i)}}{\mathcal{M}}\ , \\ B^j &= -\frac{e^{(i)j}S_{(i)(k)}p^{(k)}}{\mathcal{M}\left(p^{(t)} + \mathcal{M}\right)}\ .\end{aligned}$$

Since all the gauges have been fixed, the dynamical system is completely determined and has as many independent variables as degrees of freedom. According to Dirac's approach to constrained dynamical systems the Hamiltonian is read off from the Lagrangian as the remaining terms which do not contain any time derivatives

$$H = -p_0 - \frac{1}{2} S_{(i)(j)} \omega_t{}^{(i)(j)} + \frac{S_{(i)(j)} p^{(j)}}{\mathcal{M}(p^{(t)} + \mathcal{M})} \gamma^{kl} p_l e^{(i)m} (N_{k;m} - N K_{km}) - \frac{S_{(i)(j)} p^{(j)} \omega_t{}^{(t)(i)}}{\mathcal{M}} \ ,$$

which contains all information on the evolution of the dynamics of a spinning particle in the pole-dipole approximation to all orders in the particle's spin. The spin connection coefficients are given by

$$\omega_t{}^{(t)(i)} = -\omega_t{}^{(i)(t)} = -e^{(i)k} \left(N_{,k} - N^j K_{kj} \right) \ , \qquad \omega_i{}^{(t)(j)} = K_{ki} e^{(j)k} \ ,$$

$$\omega_t{}^{(i)(j)} = e^{(i)k}{}_{,0} e^{(j)}{}_k + e^{(j)k} e^{(i)l} (-N K_{kl} + N_{k;l}) \ , \quad \omega_i{}^{(j)(k)} = e^{(j)m}{}_{,i} e^{(k)}{}_m + e^{(k)l} e^{(j)m} \Gamma_{lmi} \ ,$$

where N is the lapse function, N^i the shift vector and K_{ij} corresponds to the extrinsic curvature. All these quantities have been introduced within the context of the ADM formalism in section 5.1 and are connected to the spacetime split.

Variation of the action with respect to its variables $\left(z^i,\, p_i,\, S_{(i)(j)},\, \Lambda^{K(i)} \right)$ gives the equations of motion. In contrast to the previous variation where we have used a manifestly covariant approach we can restrict ourselves to the ordinary variation δ, here. The worldline gauge, the solutions to the mass shell constraint and the NW SSC allow us to remove all the temporal components from the Hamiltonian. Putting the remaining terms into the local frame we locally have a flat geometry where the covariant variation reduces to the ordinary variation. When performing the variation of $\Lambda^{K(i)}$, though, we have to take into account the (flat) Lorentz matrix condition which is given in spatial components by

$$\Lambda^{K(i)} \Lambda^{K(j)} = \delta^{ij} \ .$$

Thus, we use an auxiliary antisymmetric quantity $\theta^{(l)(i)}$ and express the corresponding variation as $\delta \Lambda^{K(i)} = \Lambda^{K(l)} \delta \theta^{(l)(i)}$. Hence, the following relations are obtained when Hamilton's principle of least action and is applied:

- Variation of $\Lambda^{K(i)}$

$$\begin{aligned} \delta L &= \frac{1}{2} \left(-\dot{S}_{(l)(j)} - S_{(i)(j)} \Omega_{(l)(i)} + S_{(i)(l)} \Omega_{(j)(i)} \right) \delta \theta^{(l)(i)} \\ 0 &= -\frac{1}{2} \dot{S}_{(i)(j)} + S_{(k)[(i)} \Omega_{(j)](k)} \ , \end{aligned}$$

- Variation of S_{ij}

$$\begin{aligned}\delta L &= \left(\frac{1}{2}\Omega^{(i)(j)} + \frac{\partial B^l}{\partial S_{(i)(j)}}\dot{p}_l + \frac{\partial A_l}{\partial S_{(i)(j)}}\dot{z}^l - \frac{\partial H}{\partial S_{(i)(j)}}\right)\delta S_{(i)(j)} \\ 0 &= \frac{1}{2}\Omega^{(i)(j)} + \frac{\partial B^l}{\partial S_{(i)(j)}}\dot{p}_l + \frac{\partial A_l}{\partial S_{(i)(j)}}\dot{z}^l - \frac{\partial H}{\partial S_{(i)(j)}}\ ,\end{aligned}$$

- Variation of p_i

$$\begin{aligned}\delta L &= \left(\left(\frac{\partial B^j}{\partial p_i} - \frac{\partial B^i}{\partial p_j}\right)\dot{p}_j + \left(\delta_i^j + \frac{\partial A_j}{\partial p_i} - \frac{\partial B^i}{\partial z^j}\right)\dot{z}^j - \frac{\partial B^i}{\partial S_{(k)(l)}}\dot{S}_{(k)(l)} - \frac{\partial H}{\partial p_i}\right)\delta p_i \\ 0 &= \left(\frac{\partial B^j}{\partial p_i} - \frac{\partial B^i}{\partial p_j}\right)\dot{p}_j + \left(\delta_i^j + \frac{\partial A_j}{\partial p_i} - \frac{\partial B^i}{\partial z^j}\right)\dot{z}^j - \frac{\partial B^i}{\partial S_{(k)(l)}}\dot{S}_{(k)(l)} - \frac{\partial H}{\partial p_i}\ ,\end{aligned}$$

- Variation of z^i

$$\begin{aligned}\delta L &= -\left(\left(\delta_i^j - \frac{\partial B^j}{\partial z^i} + \frac{\partial A_i}{\partial z^i}\right)\dot{p}_j - \left(\frac{\partial A_j}{\partial z^i} - \frac{\partial A_i}{\partial z^j}\right)\dot{z}^j + \frac{\partial A_i}{\partial S_{(k)(l)}}\dot{S}_{(k)(l)} + \frac{\partial H}{\partial z^i}\right)\delta z^i \\ 0 &= \left(\delta_i^j - \frac{\partial B^j}{\partial z^i} + \frac{\partial A_i}{\partial z^i}\right)\dot{p}_j - \left(\frac{\partial A_j}{\partial z^i} - \frac{\partial A_i}{\partial z^j}\right)\dot{z}^j + \frac{\partial A_i}{\partial S_{(k)(l)}}\dot{S}_{(k)(l)} + \frac{\partial H}{\partial z^i}\ .\end{aligned}$$

The variational principle therewith provides us with a complete set of the equations of motion

$$\begin{aligned}\dot{z}^i &= -\left(\mathcal{A}_z\dot{p}_j + \mathcal{B}_z\dot{z}^j - \frac{\partial B^i}{\partial S_{(k)(l)}}\dot{S}_{(k)(l)} - \frac{\partial H}{\partial p_i}\right)\ , \\ \dot{p}_i &= \left(\mathcal{A}_p\dot{p}_j + \mathcal{B}_p\dot{z}^j - \frac{\partial A_i}{\partial S_{(k)(l)}}\dot{S}_{(k)(l)} - \frac{\partial H}{\partial z^i}\right)\ , \\ \dot{S}_{(i)(j)} &= 4S_{(l)[(j)}\left(\frac{\partial B^k}{\partial S_{(i)](l)}}\dot{p}_k + \frac{\partial A_k}{\partial S_{(i)](l)}}\dot{z}^k - \frac{\partial H}{\partial S_{(i)](l)}}\right)\ ,\end{aligned}$$

with

$$\mathcal{A}_z = \left(\frac{\partial B^j}{\partial p_i} - \frac{\partial B^i}{\partial p_j}\right)\ , \qquad \mathcal{A}_p = \left(\frac{\partial B^j}{\partial z^i} - \frac{\partial A_i}{\partial z^j}\right)\ ,$$

and

$$\mathcal{B}_z = \left(\frac{\partial A_j}{\partial p_i} - \frac{\partial B^i}{\partial z^j}\right)\ , \qquad \mathcal{B}_p = \left(\frac{\partial A_j}{\partial z^i} - \frac{\partial A_i}{\partial z^j}\right)\ ,$$

where we immediately notice that the variables are not of canonical structure so that the equations of motion do not coincide with Hamilton's equations.

8.6.3 Poisson brackets

In order to obtain the time evolution of any phase space quantity generated by the Hamiltonian the Poisson bracket relations between the phase space variables are needed. These brackets can be calculated according to the following procedure.

Consider an action containing at most first order derivatives in time. Thus using some sophisticated approach we can write the action in the following form

$$S = \int dt \left[B_I(q^J)\, \dot{q}^I - H(q^J) \right], \tag{8.114}$$

where I, J label the dynamical variables q_I. The equations of motion read

$$M_{IJ}\dot{q}^J = \partial_I H, \quad M_{IJ} := \partial_I B_J - \partial_J B_I. \tag{8.115}$$

where $\partial_I = \partial/\partial q^I$, or

$$\dot{q}^I = M^{IJ}\partial_J H, \quad M^{IJ} := M^{-1}_{IJ} \tag{8.116}$$

This can be written using Poisson brackets

$$\dot{X} = \{H, X\} + \frac{\partial X}{\partial t}, \tag{8.117}$$

if we set

$$\{X, Y\} = M^{-1}_{JI}\partial_I X \partial_J Y. \tag{8.118}$$

We conclude, that the Poisson bracket relations are encoded in the action, which, however, may exhibit a complicated form if the phase space variables are not of canonical structure. Consequently, the equations of motion cannot simply be computed by Hamilton's equations, as we have seen. Since the symplectic structure of the phase space is retained, it is in principle possible to find local canonical coordinates according to Darboux's theorem.

Alternatively, we have derived the equations of motion using Hamilton's principle of stationary action. The result is a system of equations for the time derivatives of the variables, which is not obviously solvable, though. Nevertheless, the equations are exact in the particle's spin and take into account that the dynamical mass $\mathcal{M}$ is not necessarily conserved but may be treated as a dynamical variable.

8.7 Discussion

This chapter focused on the Hamiltonian formulation of spinning particles based on an action approach by Dirac. We recovered the linearised Hamiltonian which was first derived in a complicated manner by [53] and gained confirmation for our approach. Since the use

of the spin gauge invariant action simplifies the procedure considerably, we extended the formulation to higher orders and obtained a canonical Hamiltonian at quadratic order in the particle's spin. Indeed, the desire for the inclusion of higher orders in the particle's spin is an up-to-date topic within the framework of EOB. As the mapping from the realistic situation consisting of two spinning equal-mass objects to the effective problem of a spinning test particle moving in a Kerr background deals with open questions, higher interaction terms in the test particle limit may help to further develop this theory. Moreover, we are planning to check the influence of the quadratic spin terms on EOB relevant quantities, such as the periastron shift or the ISCO frequency, that are needed to calibrate the approach with respect to numerical relativity.

Another approach is provided by the PN approximation valid at slow velocities in weak gravitational fields. We are currently working on a PN expansion for the Hamiltonian function at quadratic order in spin in order to confirm the result further.

In addition we discarded the canonical structure and derived a Hamiltonian that is valid to all orders in the spin within the pole-dipole approximation and stated its associated equations of motion which are different from the usual form. This means, that although the Hamiltonian is not of canonical form, it provides an exact approach to analyse the dynamical behaviour in general relativity within the Hamiltonian formalism and its characteristic methods. In particular, it can be useful for the investigation of chaos, since a large group of methods is based on a Hamiltonian formulation and the dynamics in phase space. For instance, the recurrence plots are based on the recurrence theorem which employs the characteristics of trajectories in phase space and analyses the dynamical properties subject to chaotic behaviour. The evolution of these trajectories is determined by the Hamiltonian function living in phase space.

Moreover, a Hamiltonian formalism may provide numerical advantages, as we have seen in our previous study. The computation is faster than for the Lagrangian equations and saves costs and time so that a first insight in the dynamics is provided on quite a short time scale. Future work may also include a numerical comparison, such as the one we did in the linearised framework, both for the quadratic and the exact Hamiltonian. The range of validity should increase the higher the order of the spin is and the results for the exact formulation should be equivalent to the MP equations up to numerical errors.

Summary and Outlook

Chapter 9

Summary and Outlook

In this thesis we explored the theoretical fundamental description of the dynamics of binary systems and examined the corresponding dynamical behaviour with regard to implications and improvements for gravitational wave astronomy.

The first part of this thesis addressed the dynamics of spinning particles in the pole-dipole approximation as characterised by the Mathisson-Papapetrou equations.
First, we analysed the isofrequency pairing phenomenon in Schwarzschild-de Sitter spacetime for a spinning particle moving in the equatorial plane with a perpendicular spin vector. Although this configuration is very special it reveals characteristic features attributed to the cosmological constant and the spin. In contrast to Schwarzschild and Kerr spacetime we found a second region where isofrequency pairing occurs which is located far away from the central region in the weak field regime. It would be interesting to check whether Newtonian or Post-Newtonian theory predict the isofrequency pairing as well.
Moreover, in addition to the homoclinic orbits, which define the separatrices in Schwarzschild and Kerr spacetimes, we found a further structure in Schwarzschild-de Sitter spacetime: the heteroclinic orbit. In the frequency picture this heteroclinic orbit is stretched out to a straight line covering a whole range of azimuthal frequencies. A well established approach to model extreme-mass-ratio inspirals and the emission of gravitational radiation is based on the progression through orbits [17, 19], so that at some point the particle has to cross the boundary from bound to unbound motion before it eventually plunges into the central object. Indeed, it has been suggested that the zoom-whirl feature close to homoclinic orbits has a distinct signal on the gravitational wave spectrum [28, 29]. As the heteroclinic orbit marks an additional boundary in the frequency picture it might be possible that it also has a distinct imprint visible in the gravitational waveform and differs somehow from the ones obtained by the homoclinic orbits.
On a more fundamental level, it is an interesting question to ask if there are spacetimes

where three or more orbits with the same frequencies exist. As an attempt to find a candidate for isofrequency triples one could start with the Bertrand spacetime and perturb it a little bit. Bertrand spacetimes, which were introduced in [134], are spherically symmetric and static spacetimes in which the ratio of the radial frequency and the azimuthal frequency is a constant rational number q for all bound orbits, so they show the same total degeneracy of the frequencies as the Kepler problem but now with $q \neq 1$. We are planning to search for isofrequency triples etc. in future work.
Also from a theoretical point of view the investigation of isofrequent orbits gives rise to an invariant structure of the dynamical system, namely the singular curve, which can be used to compare different approaches to the general relativistic two-body problem. In particular, the modelling of binary systems requires the calibration of different methods, such as numerical relativity, post-Newtonian approximations and the effective-one-body formulation, and can profit from isofrequency pairing and its related properties in the future.

In the context of EOB and PN methods treating the dynamics of spinning particles the NW SSC is of great interest for a Hamiltonian formalism describing the dynamics of binary systems. In order to better understand the behaviour and the properties of the NW SSC, we compared two orbits of spinning particles moving in Kerr spacetime obtained by the NW SSC and T SSC in the framework of the MP equations. We found that the NW SSC preserves the mass at linear order in spin while the error of the spin measure remains to be at the same level, which appears to be a somewhat complicated condition for an intuitive approach in the framework of MP equations.
Instead of considering one and the same particle where two different SSCs represent two different observers, we analysed the behaviour of two different particles that started at one and the same point in configuration space. We found that the discrepancies between the two orbits scale linear in the particle's spin and are caused by spin-gravity couplings, see e.g. [78, 103, 104, 139].
However, we considered only a non-circular bound orbit at a radial distance of $11.7M$ which is not strongly influenced by spacetime curvature and restricted the analysis to two initial configurations for the orientation of the spin vector with respect to the angular momentum and the Kerr spin vector respectively. In order for a more detailed understanding of the differences of the motion of two spinning particles future studies should cover a larger range of initial conditions and examine a circular orbit that is closer to the centre and experiences a strong gravitational field [138, 139]. As the pole-dipole approximation breaks down when the curvature gradient becomes too large, higher multipoles, such as the quadrupole [173], should be included. Moreover, a comparison with further SSCs is also of interest in the sense that the impact of the influence of the internal structure depends on the chosen SSC,

i.e. in our work on the two particles.

In the second part of this thesis we investigated Lagrangian and Hamiltonian mechanics for general relativistic spinning particles. We focused on a Hamiltonian function developed by E. Barausse, E. Racine and A. Buonanno in 2009 [53], which is linearised in the particle's spin and supplemented by NW SSC. By considering spinning particles in Kerr spacetime and comparing the worldlines obtained by Hamilton's equations to the ones resulting from the MP equations both supplemented with NW SSC, we found that the orbits converge linearly as a function of the square of the particle's spin in agreement with [53], $\Delta H \propto S^2$. According to our results the relevant range of test particle spin values appears to be $10^{-4}M\mathcal{M} > S > 10^{-6}M\mathcal{M}$. This range is indeed thought to be appropriate for astrophysical binary systems, see e.g. [36, 37]. For spins that are smaller than 10^{-6} the influence of the spin on the orbital evolution can be neglected approaching the geodesic limit and for spin values greater than 10^{-4} the Hamiltonian formulation show large discrepancies from the MP equations.
However, due to the linearisation in the particle's spin in this Hamiltonian formalism a bad choice of coordinates and corresponding tetrads evokes an unphysical behaviour of some constants of motion in numerical computations. We studied the behaviour of constants of motion in Schwarzschild and Kerr spacetime for Boyer-Lindquist, quasi-isotropic and Kerr-Schild coordinate systems as well as for zero-angular-momentum and non-zero-angular-momentum observers. The conservation of the preserved quantities is checked using the Dirac brackets which impose the constraints, such as the SSC or the worldline gauge, on the Hamiltonian [53]. We found that a good choice of tetrad and coordinates should reduce the tetrad to the Cartesian one in flat spacetime. Except for the Boyer-Lindquist coordinates the quasi-isotropic as well as the Kerr-Schild coordinates satisfy this requirement. Indeed, the type of tetrad, i.e. whether ZAMO or not, does not appear to have a strong influence on the numerical results. They equally lead to physically reasonable properties of the Hamiltonian function, i.e. they both preserve the constants of motion in numerical studies when the coordinate system is chosen appropriately. Indeed, the non-ZAMO observer in Kerr-Schild coordinates allows us to express the Hamiltonian in both Schwarzschild and Kerr spacetime in a simple and compact form.
Moreover, while investigating the symmetries of the systems and analysing the corresponding conserved quantities we have shown that the linearised Hamiltonian in Schwarzschild spacetime is integrable. As soon as the black hole starts to rotate a numerical analysis and the investigation of the symmetries indicate the presence of chaos. A thorough analysis of chaotic motion of spinning particles in Kerr spacetime as described by the linearised Hamiltonian is in progress [174].

In fact, chaos and perturbation theory often rely on the Hamiltonian formalism. In order to further investigate the appearance of chaos and characterise the dynamics of spinning particles with regard to chaotic behaviour several methods can be employed, such as Poincaré sections, the KAM theorem or recurrence plots. Since they often draw on numerical computations it is important to take into account the choice of coordinates in order to avoid unphysical behaviour of the solutions of the corresponding Hamilton's equations smearing the actual physics.

Finally, we improved the Hamiltonian description by using an action approach based on a spin-gauge invariant action and extended the Hamiltonian formulation to higher orders in the particle's spin. We keep canonical coordinates up to second order in the particle's spin and derived a Hamiltonian that is valid to all orders in spin within the pole-dipole approximation. Particularly with regard to applications in EOB and PN theory such a Hamiltonian is of great interest. Therefore we plan to compute the periastron shift and ISCO frequency so that the extended Hamiltonian can be compared to the linearised one in order to examine the influence of the higher orders in the particle's spin on the invariant quantities used to calibrate the EOB to PN and NR. However, since the framework of EOB aims at describing the process of coalescing binary systems, in particular the late stages of the inspiral and the merger phases, the dynamics becomes highly relativistic. In this regime tidal effects cannot be neglected any more, so that contributions from higher orders in the spin have to be taken into account when the conservative Hamiltonian is set up. The first step is of course to integrate higher orders within the pole-dipole approximation, which we have done here. As quadrupole effects enter at the quadratic spin order, it is of interest to include the quadrupole moment into the formulation, i.e. go beyond the pole-dipole approximation, in order to increase the accuracy in the analytical description. Moreover we intend to expand the Hamiltonian in PN orders and compare the results with existing approximations. Therewith we can confirm our formulation.
Although we have chosen the NW SSC we have not succeeded so far to establish a canonical formulation to all orders in the particle's spin. Thus it is worth to think of implementing a different SSC which probably will not lead to canonical coordinates either, but which might simplify the derivation of an exact Hamiltonian.
Apart from analytical theories numerical methods can also profit from this formulation. Future work may use the Hamiltonian, either at quadratic order or the exact one, for the investigation of chaos by means of Poincaré sections or recurrence plots. A comparison to the MP equations may also be of interest.

All in all, this thesis focused on the theoretical understanding and fundamental de-

scription on binary systems, both equal and extreme-mass ratios, which are thought to be promising sources for gravitational wave emission. Future work may use and include our results in order for a better way of modelling gravitational waves. In particular, we identified a heteroclinic orbit caused by the accelerated expansion of our Universe which might be visible in the frequency spectrum of gravitational waves, such as the homoclinic orbits. However, this to be checked is left for future studies. Moreover, we improved the Hamiltonian formulation with regard to applications in EOB and PN theory which are essential tools in modelling general binary systems and simulating gravitational waves. More precisely, the EOB theory still has problems in mapping the two real spins to the effective description. A different approach and an improved Hamiltonian for spinning particles may help to solve this problem in the future.

As binary systems may exhibit chaotic behaviour we analysed the physical behaviour of a linearised Hamiltonian in this context, since it serves as a good starting point for numerical methods to detect chaos, such as Poincaré sections or recurrence plots. Chaos may impede the analysis of gravitational waves so that it is important to properly investigate the dynamical behaviour of binary systems with regard to chaotic behaviour in the future. A detailed understanding of the fundamental dynamics of binary system provides the key ingredients for the data analysis of gravitational waves. The theoretical description, though, becomes the more complicated the more inner structure is added to the objects. In fact, we have seen that the system has to be simplified in order to obtain analytical results. On the other hand, numerical studies should be aware of possible unphysical effects arising from the construction of the set up to characterise the spinning particle.

Thus, there is a lot of work to do in the theoretical framework of binaries in the future, but it hopefully will soon blaze the way to gravitational waves, the sound of our Universe.

Appendix

Appendix A: Numerical integration of the MP equations[1]

Seen from a numerical point of view, the initial value problem (3.3) reads

$$\frac{\mathrm{d}\mathbf{y}}{\mathrm{d}\tau} = f(\mathbf{y}) \quad , \tag{A-1}$$

$$\mathbf{y}(\tau = 0) = \mathbf{y}_0 \quad . \tag{A-2}$$

with $\mathbf{y} = (t, r, ..., S^{\theta\phi}, S^{\theta\theta})^T \in \mathbb{R}^{24}$ and $f : \mathbb{R}^{24} \to \mathbb{R}^{24}$. If this system was of Hamiltonian canonical form, symplectic integration schemes would be the most natural choice for their numerical solution. They almost exactly preserve a differential equation's constants of motion and, unless for standard integration schemes, their overall numerical error grows only slowly as a function of the total integration time even for larger step sizes. Therefore, simulations over long time spans can be carried out efficiently. Unfortunately, the MP equations are not of Hamiltonian canonical form. But, they can be interpreted as the Euler-Lagrange equations of a suitable Lagrangian action, see, e.g., [143, 146, 148]. What then saves the day is that the flow of symplectic integration schemes can be interpreted as the solution of the Euler-Lagrange equations of a discretisation of the Lagrangian action. Schemes with this property are called *variational integrators* and they only rely on the existence of a Lagrangian structure for their favorable behaviour. For example they are known to exactly preserve an equation of motion's first integrals which are quadratic in the phase space variables. This implies that a variational integration scheme applied to the MP equations with T SSC will conserve the four-momentum $\mathcal{M}^2$ and the spin length S^2 up to numerical round-off errors. An extensive discussion of this topic can be found in the monograph [159], chapter VI.6. One prominent example of variational integrators are Gauss Runge-Kutta methods which have been shown to be the most efficient and accurate integrators in many general relativistic applications, see, e.g. [161], [160]. Motivated by these results, we choose this kind of variational integrators for the solution of the MP equations. Here we briefly summarize some of their properties.

An s-stage Gauss Runge-Kutta scheme is a collocation method, i.e. an implicit Runge-Kutta scheme

$$\mathbf{y}_{n+1} = \mathbf{y}_n + h \sum_{i=1}^{s} b_i f(\mathbf{Y}_i) \quad , \tag{A-3}$$

$$\mathbf{Y}_i = \mathbf{y}_n + h \sum_{j=1}^{s} a_{ij} f(\mathbf{Y}_j), \quad i = 1, ..., s \quad , \tag{A-4}$$

with coefficients

[1] This appendix has been written by J. Seyrich and appeared in [1].

$$a_{ij} = \int_0^{c_i} l_j(t)dt \quad , \tag{A-5}$$

$$b_j = \int_0^1 l_i(t)dt \quad , \tag{A-6}$$

where the stages $c_1, ..., c_s$ are chosen as

$$c_i = \frac{1}{2}(1 + \tilde{c}_i) \quad , \tag{A-7}$$

with $\tilde{c}_i$ being the roots of the Legendre-polynomial of degree s. Here, h denotes the time step size, Y_i, $i = 1, ..., s$, are the so-called inner stage values and $\mathbf{y}_n$ denotes the numerical approximation to the solution $\mathbf{y}$ at time $\tau = nh$. The functions $l_i(t)$ are the Lagrange-polynomials of degree s,

$$l_i(t) = \prod_{i \neq j} \frac{t - c_j}{c_i - c_j} \quad . \tag{A-8}$$

Gauss Runge-Kutta methods have a convergence order $\mathcal{O}(h^{2s})$ which is the highest possible order among collocation schemes, e.g. [171]. When integrating a time step with a Gauss Runge-Kutta scheme, one first solves the system of implicit equations (A-4) via a fixed-point iteration

$$\mathbf{Y}_i^{k+1} = \mathbf{y}_n + h \sum_{j=1}^{s} a_{ij} f(\mathbf{Y}_j^k) \quad . \tag{A-9}$$

This, of course, requires more calculations per time step than an explicit scheme with the same number of stages. But, this extra effort is more than offset by the high accuracy of Gauss collocation methods which allows to apply them with a much larger step size. Detailed information on their implementation is given in [160], section 7, and [159], chapters VIII.5 and VIII.6.

To illustrate the favourable behaviour of Gauss collocation methods, we compare the performance of a 4-stage scheme with step size $h = 1$ and a standard 5-th order explicit Cash-Karp scheme as proposed in [172] with a step size $h = 0.1$, when applied to the MP equations with T SSC (eq. (3.3) with (3.4)-(3.8)) and initial data given by $E = 0.95$, $J_z = 3.0$, $S = 1$, $M = 1$ $\mathcal{M} = 1$, $a = 0.9$, $r = 6.7$, $\theta = \frac{\pi}{2} + 0.1$, $p_r = 0.1$, $S_r = 0.1$, $S_\theta = 0.01$. In fig. 9.1, we plot for both integrators the relative error in the energy,

$$\Delta E(\tau) = \frac{|E(\tau) - E(0)|}{|E(0)|} \quad , \tag{A-10}$$

and the corresponding relative error in the z-component of the total angular momentum

ΔJ_z as a function of integration time τ. We observe that the Gauss Runge-Kutta method, which is also faster, gives much preciser results.

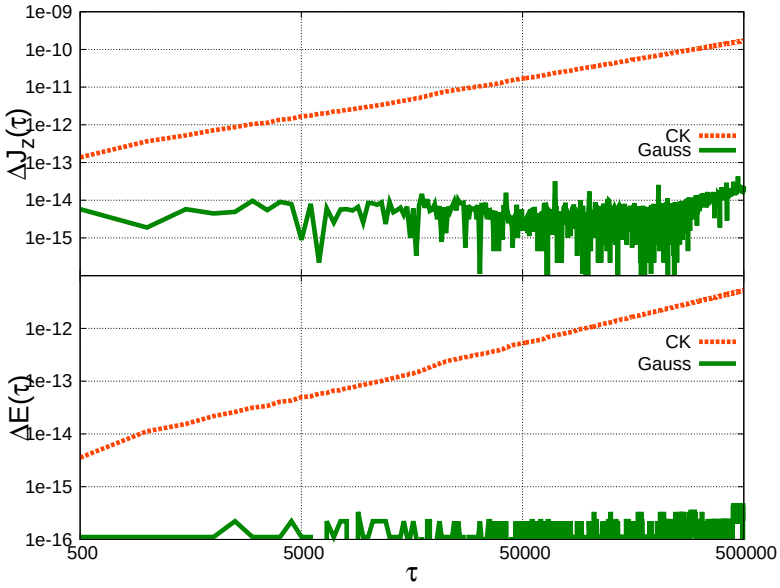

Figure 9.1: The relative error of the z-component of the total angular momentum, ΔJ_z, (top panel) and the relative error of the energy, ΔE, (bottom panel) against integration time τ for the 4-stage Gauss scheme with step size $h = 1$ and the 5-th order Cash-Karp scheme with step size $h = 0.1$ applied to the initial value problem (3.3) with initial data as stated in the text. CPU-time was 214.1s for the Gauss Runge-Kutta scheme and 422.7s for the Cash-Karp scheme.

An additional obstacle for simulations in the NW SSC case is that the tangential velocity u^μ is only given implicitly by eq. (1.40). (N.b.: Apart from the apparent u^ν in the first term on the right hand side, the covariant derivative of ω_ν implies a linear dependence on u^ν in the second term on the rhs as well, i.e. $\dfrac{D\,\zeta_\nu}{d\tau} = \dot{\zeta}_\nu - \Gamma^\kappa_{\nu\mu}\zeta_\kappa v^\mu$.) Setting $\vec{u} := (u^t, u^r, u^\phi, u^\theta)^T \in \mathbb{R}^4$, the implicit equation for u^μ is qualitatively given by

$$\vec{u} = A(x^\mu, p^\mu, S^{\mu\nu})\vec{u} \tag{A-11}$$

for a certain matrix $A \in \mathbb{R}^{4\times 4}$. Theoretically there are two possibilities to cope with the implicitness in the velocities, which we will describe now.

- Denoting the first four components of Y_i and $f(Y_i)$ by Y_i^x and $f^x(Y_i)$, and the other components by Y_i^p, Y_i^S, $f^p(Y_i)$, and $f^S(Y_i)$ we can augment the system of implicit equations (A-4) by adding the implicitly given quantity $\vec{u}_i$ which denotes the tangential velocity v^μ at the inner stage Y_i. This yields the system

$$\begin{pmatrix} \vec{u}_i \\ \mathbf{Y}_i^x \\ \mathbf{Y}_i^p \\ \mathbf{Y}_i^S \end{pmatrix} = \begin{pmatrix} A(Y_i^x, Y_i^p, Y_i^S)\vec{u}_i \\ \mathbf{y}_n^x + h\sum_{j=1}^s a_{ij}\vec{u}_i \\ \mathbf{y}_n^p + h\sum_{j=1}^s a_{ij} f^p(Y_i^x, Y_i^p, Y_i^S, \vec{u}_i) \\ \mathbf{y}_n^S + h\sum_{j=1}^s a_{ij} f^S(Y_i^x, Y_i^p, Y_i^S, \vec{u}_i) \end{pmatrix} \quad ,$$
$$i = 1, ..., s \quad , \tag{A-12}$$

to which, again, a fixed-point iteration can be applied. However, for this iteration to converge, it needs to satisfy

$$|| \begin{pmatrix} \vec{u}_i^{k+2} \\ Y_i^{k+2} \end{pmatrix} - \begin{pmatrix} \vec{u}_i^{k+1} \\ Y_i^{k+1} \end{pmatrix} || \leq || \begin{pmatrix} \vec{u}_i^{k+1} \\ Y_i^{k+1} \end{pmatrix} - \begin{pmatrix} \vec{u}_i^{k} \\ Y_i^{k} \end{pmatrix} || \quad , \tag{A-13}$$

which cannot be guaranteed when $A(Y_i^x, Y_i^p, Y_i^S)$ is of large norm. Numerical tests have shown that there are indeed problems with the convergence. Hence, for all its conceptual beauty, the approach of an augmented implicit system is of no practical use.

- With I denoting the 4×4 identity matrix, we can rewrite the implicit equation for the velocities (A-11) as

$$0 = (I - A)\vec{u} =: B\vec{u} \quad . \tag{A-14}$$

Thus, from an algebraical point of view, the vector consisting of the components of the 4-velocity is an element of the nullspace $\mathrm{Ker}(B)$ of the matrix B which here is a one-dimensional subspace. Consequently, we can determine the tangential velocity at an internal stage by the following procedure

1. Calculate
   $B(Y_i^x, Y_i^p, Y_i^S) = I - A(Y_i^x, Y_i^p, Y_i^S)$.
2. Calculate the singular-value-decomposition of B, i.e.,

$$B = V\Sigma U^T \quad , \tag{A-15}$$

   with $\Sigma = \mathrm{diag}(\sigma_1, \sigma_2, \sigma_3, \sigma_4)$ and $V^T V = U^T U = \delta_{ij}$, $i, j = 1, ...4$ (For more information on the singular value decomposition, see, e.g. [172], chapter 2.6). The nullspace of B is then spanned by the column of the orthonormal matrix $U_{.,i}$ that corresponds to the only singular value σ_i which is equal to 0.
3. The tangential velocity is now obtained by renormalising $U_{.,i}$ in order to have $u^\mu u_\mu = -1$.

This procedure is very robust and the computational cost for the calculation of the matrix B and the singular value decomposition is far less than the computational cost for the calculation of the other quantities which are needed anyway. This could be confirmed experimentally when comparing CPU times for simulations with T SSC and NW SSC for similar initial values. For all the simulations done in the preparation for this work, the CPU times in the NW SSC case where only slightly higher than those for the T SSC case where the velocities could be determined explicitly via eq. (1.30).

Now, we turn to the numerical integration of the Hamiltonian formalism in the next section.

Appendix B: Numerical integration of the Hamiltonian equations[2]

The Hamiltonian equations considered in this study have a so-called *Poisson structure*, that is, with $\mathbf{y} = (P_r, P_\theta, P_\phi, r, \theta, \phi, S_1, S_2, S_3)^T \in \mathbb{R}^9$, they can be written as

$$\dot{\mathbf{y}} = B(\mathbf{y})\nabla H(\mathbf{y}) \quad , \tag{B-1}$$

where $B : \mathbb{R}^9 \to \mathbb{R}^{9\times 9}$ is a skew-symmetric matrix-valued function. In our case, this function $B(\mathbf{y})$ is given by

$$B(\mathbf{y}) = \begin{pmatrix} 0 & -I_{3\times 3} & 0 \\ I_{3\times 3} & 0 & 0 \\ 0 & 0 & B_1(\mathbf{y}) \end{pmatrix} \quad , \tag{B-2}$$

with

$$I_{3\times 3} = \begin{pmatrix} 1 & 0 & 0 \\ 0 & 1 & 0 \\ 0 & 0 & 1 \end{pmatrix} \quad , \tag{B-3}$$

$$B_1(\mathbf{y}) = \begin{pmatrix} 0 & -S_3 & S_2 \\ S_3 & 0 & -S_1 \\ -S_2 & S_1 & 0 \end{pmatrix} \quad . \tag{B-4}$$

For such $B(\mathbf{y})$, there exists a smooth transformation to new coordinates $\mathbf{z}$, for which the equations of motion are of symplectic form

$$\dot{\mathbf{z}} = J^{-1}\nabla H(\mathbf{z}) \quad , \tag{B-5}$$

$$J = \begin{pmatrix} 0 & I_{4\times 4} \\ -I_{4\times 4} & 0 \end{pmatrix} \quad , \tag{B-6}$$

see [136, 160]. The idea how to find this transformation is based on the conservation of the spin length $S = \sqrt{S_1^2 + S_2^2 + S_3^2}$ by the eqs. (B-1). Thus, the three dimensional spin $\mathbf{S} = (S_1, S_2, S_3)^T$ can be given as a function of two variables α and ξ via

[2] This appendix has been written by J. Seyrich and appeared in [1]

$$\mathbf{S} = S \begin{pmatrix} \sqrt{1-\xi^2}\cos(\alpha) \\ \sqrt{1-\xi^2}\sin(\alpha) \\ \xi \end{pmatrix} \quad . \tag{B-7}$$

One can then show that

$$\dot{\xi} = -\frac{\partial H}{\partial \alpha} \quad , \tag{B-8}$$

$$\dot{\alpha} = \frac{\partial H}{\partial \xi} \tag{B-9}$$

hold, see, e.g. [160]. Hence, for the variables $\mathbf{z} = (P_r, P_\theta, P_\phi, \xi, r, \theta, \phi, \alpha)$, the equations of motion indeed take the form (B-5). Whenever a system can be smoothly transformed to symplectic form, it can be evolved by symplectic integration schemes. Therefore, for our studies of the Hamiltonian formalism of [53], we follow [160] and use Gauss Runge-Kutta schemes which have already been presented in the last section [3]. In order to show their favourable behaviour, we evolve the Hamiltonian system (eq. (5.23) - (5.24)) for a Kerr background with initial data $M = 1$, $\mathcal{M} = 1$, $a = \frac{1}{10}$, $r = 15$, $\theta = \frac{\pi}{2}$, $\phi = 0$, $P_r = 0$, $P_\theta = 3.69336$, $P_\phi = J_z = 3.8$, $S_1 = \frac{1}{\sqrt{2}}$, $S_2 = \frac{1}{\sqrt{3}}$, $S_3 = \frac{1}{\sqrt{6}}$ and plot, in fig. B-1, the relative error of the Hamiltonian (6.4) once for the Gauss Runge-Kutta method with $s = 4$ inner stages and once for the 5th order explicit Cash-Karp scheme. For the explicit method we observe a linear growth in the error while there is no significant error during the whole simulation for the Gauss scheme. This is in spite of the latter's much smaller CPU time. With regard to the computational effort, we also notice that it is much smaller than in the case of the full MP equations, although both cases were tested on the same machine. This gives another practical reason to consider the Hamiltonian approximation.

In our comparison of the orbits given by the MP equations with those of the Hamiltonian formalism, the concerning simulations have to produce output for the same coordinate times. To avoid having to reformulate the MP equations for the coordinate time as evolution parameter, we proceed as follows. In the simulation of the MP equations, output is produced at uniform distances in the evolution parameter proper time. The output also comprises the corresponding coordinate times. These are then fed as input to the Hamiltonian simulations -for example under the name $t_{\text{output required}}$. Now, if in the simulation with uniform steps in the evolution parameter coordinate time t, between times t_i and t_{i+1} say, one passes one of the prescribed times for which output is required, $t_{\text{output required}}$, one can take use of the interpolation property of the collocation schemes to comfortably obtain output at no computational extra cost. It is well known that the interpolation polynomial

[3] As opposed to the approach in [160] we did not bother to rewrite the system in the variables z, because in the present case the additional cost of the one extra variable is negligible in comparison to the other computational effort.

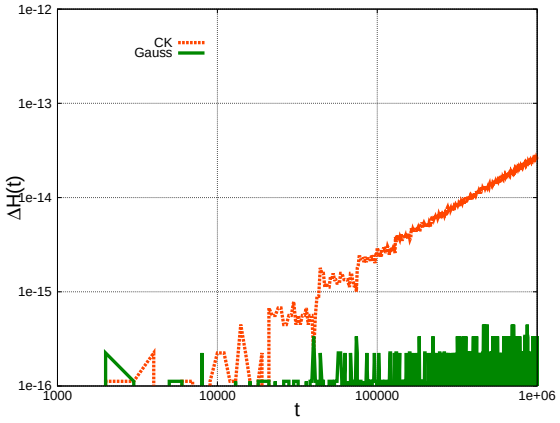

Figure B-1: The relative error of the Hamiltonian, ΔH against integration time t for the 4-stage Gauss scheme with step size $h = 2$ and the 5-th order Cash-Karp scheme with step size $h = 0.2$ applied to the initial value problem (B-1) with initial data as stated in the text. CPU-time was 7.83s for the Gauss Runge-Kutta scheme and 24, 7s for the Cash-Karp scheme.

$\mathbf{p}(t)$ through the points $(0, \mathbf{y}_n)$, $(c_i, \mathbf{Y}_i)$, $i = 1, ..., s$, stays $\mathcal{O}(h^s)$ close to the exact solution of the equation of motion, and, hence, also to the numerical calculated trajectory, see, e.g. [171]. We thus only have to evaluate $\mathbf{p}(t)$ at time $t_{\text{output required}} - t_i$ which yields an approximation of the solution at time $t_{\text{output required}}$ which is exact up to an error of $\mathcal{O}(h^s)$. The interpolation polynomial itself can be calculated very quickly with the so-called Horner scheme

$$\begin{aligned}
\mathbf{p}(t) &= \mathbf{y}_i + (t-0)\left(\delta^1[0, hc_1] + (t - hc_1)\left(\delta^2[0, hc_1, hc_2]\right.\right. \\
&\quad \left.\left. + (t - hc_2)\left(...(t - hc_{s-1})\delta^s[0, hc_1, ..., hc_s]\right)...\right)\right) \quad , \\
\delta^1[0, hc_1] &= \frac{\mathbf{Y}_1 - \mathbf{y}_i}{hc_1 - 0} \quad , \\
\delta^k[0, hc_1, ..., hc_k] &= \frac{\delta^{k-1}[hc_1, ..., hc_k] - \delta^{k-1}[0, hc_1, ..., hc_{k-1}]}{hc_k - 0} \quad .
\end{aligned}$$

The more intricate way of producing output at the desired times would be

- When having passed an output time $t_{\text{output required}}$ between t_i and t_{i+1}, go back to t_i.
- Change $h \to h_{\text{new}} = t_{\text{output required}} - t_i$.
- Evolve the system until $t = t_{\text{output required}}$ with step size h_{new} and produce output.
- Go back to t_i and go on integrating with step size h. (Note that this is necessary as the scheme would loose its symplectic structure when applied with different step sizes, see, e.g. [159], chapter VIII.)

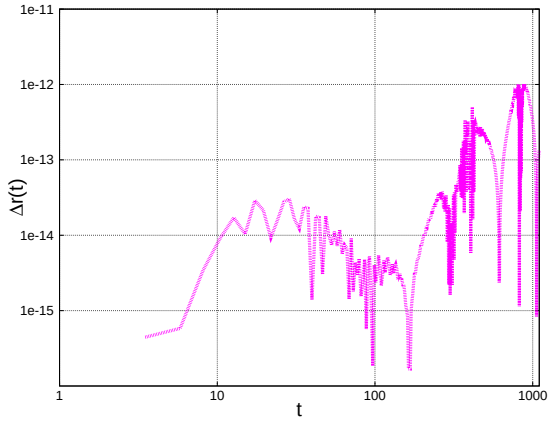

Figure B-2: The relative difference, Δr, between the radial distance calculated with the interpolation method and the radial distance calculated via the cumbersome method with extra integration steps plotted against output time t.

In order to illustrate that this cumbersome procedure is not worth the additional effort, we again consider the data which yielded Fig. 6.1 and, for every coordinate time t, for which Δ_{xyz} was plotted in the central panel of that figure, we plot the relative difference in the radial distance at those times between the interpolation method and the cumbersome method,

$$\Delta r(t) = \frac{|r_{\text{interpolation}}(t) - r_{\text{cumbersome}}(t)|}{r} \quad . \tag{B-10}$$

In Fig. B-2, we can observe that the difference is negligible.

Appendix C: Numerical Comparison of two SSCs: Complementary Figures

In chapter 3 we numerically compared the evolution of spinning test particles given by the MP equations supplemented by two different spin condition. Since the results are independent of the magnitude of the black hole spin we restricted the presentation of the figures to $a = 0.5$. In the following we show complementary figures for $a = 0.1$ and $a = 0.9$. The initial conditions are the same as in fig. 3.1.:

C1: Positive Spin

C1-1: Orbital Evolution

- **Large Spin** $S = 1$

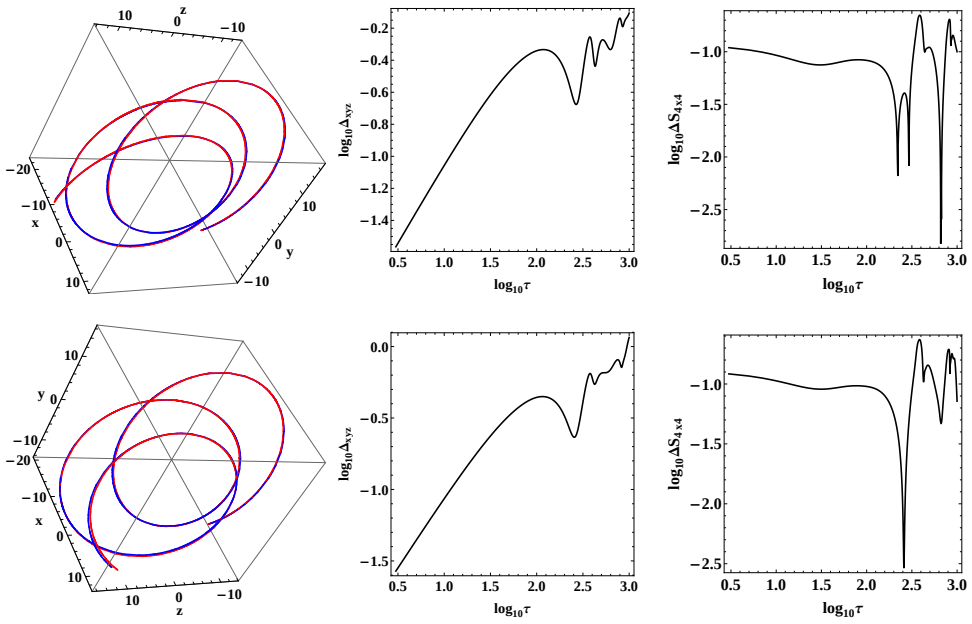

Figure C-1: Left panel: MP orbit with T SSC (red dots) and NW SSC (blue dots) in configuration space x, y, z (Cartesian coordinates). Central panel: Logarithm of the Euclidean distance in configuration space between these two orbits as a function of the proper time. Right panel: Logarithm of the difference $\Delta S_{4\text{x}4}$ between the spin tensors of these two orbits as a function of the proper time. Top Row: $a = 0.9$. Bottom Row: $a = 0.1$.

- **Medium Spin** $S = 10^{-4}$

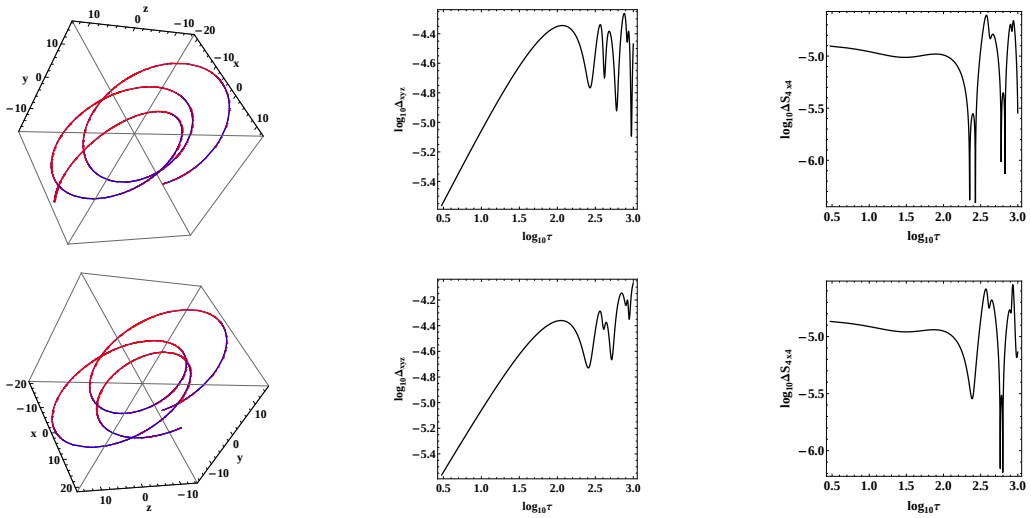

Figure C-2: see caption of fig. C-1.

- **Small Spin** $S = 10^{-8}$

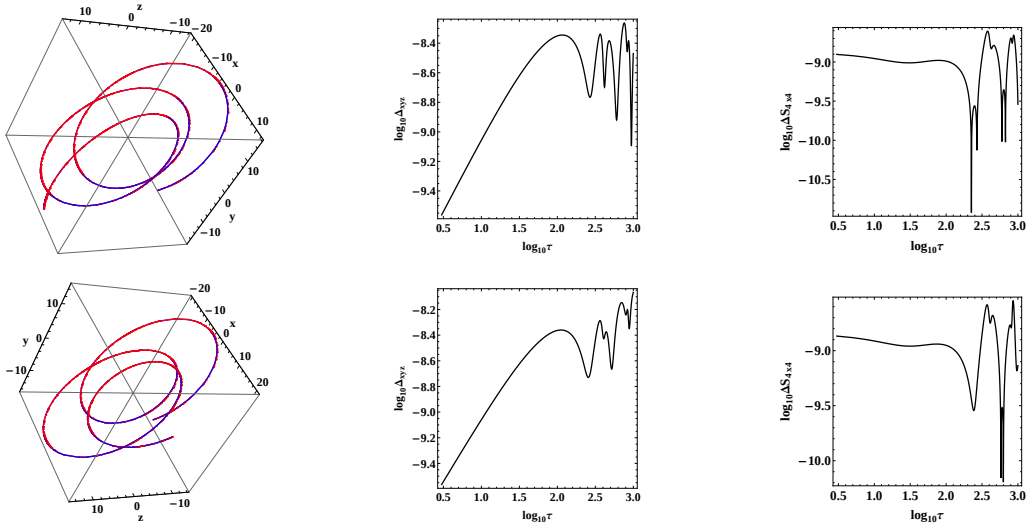

Figure C-3: see caption of fig. C-1.

C1-2: Constants of Motion

- **The evolution of the constants of motion for a black hole spin of** $a = 0.9$**:**

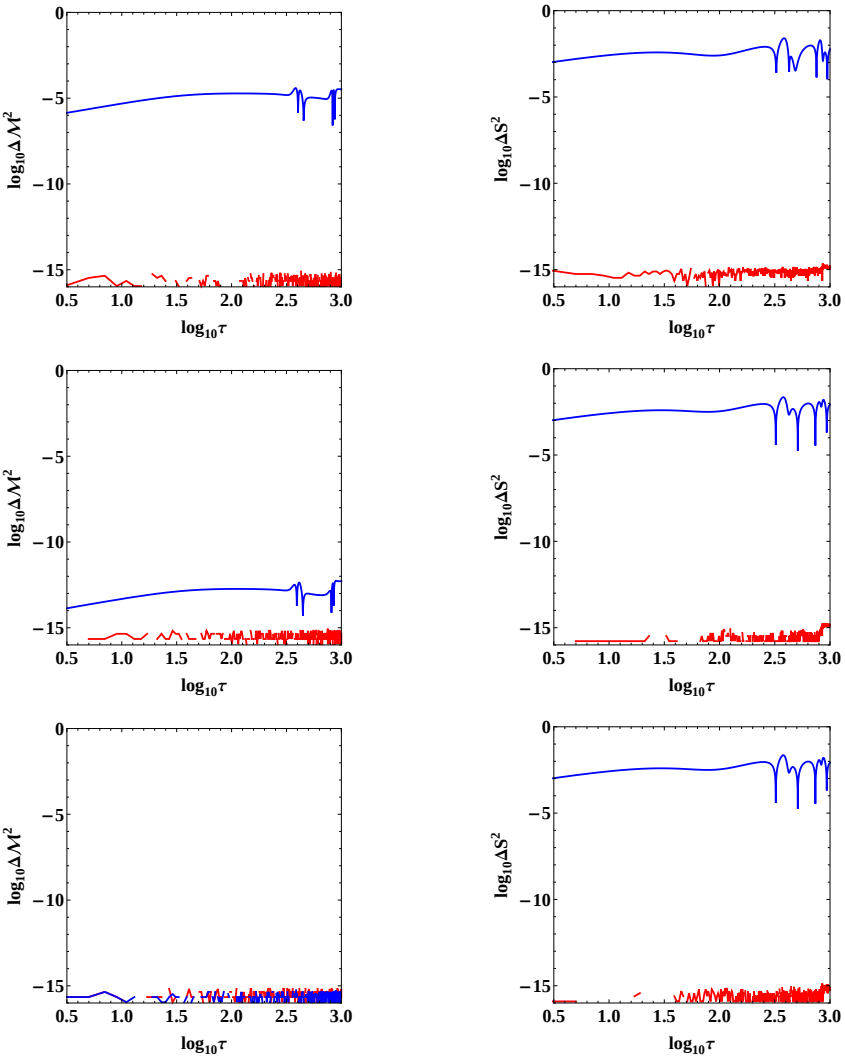

Figure C-4: Evolution of the MP equations with T SSC (red lines) and NW SSC (blue lines). Left column: relative error in the preservation of the four-momentum; Right column: relative error in the preservation of the spin. Top Row: $S = 1$, Middle Row: $S = 10^{-4}$, Bottom Row: $S = 10^{-8}$.

The corresponding relative error of the four-momentum as a function of the spin measure:

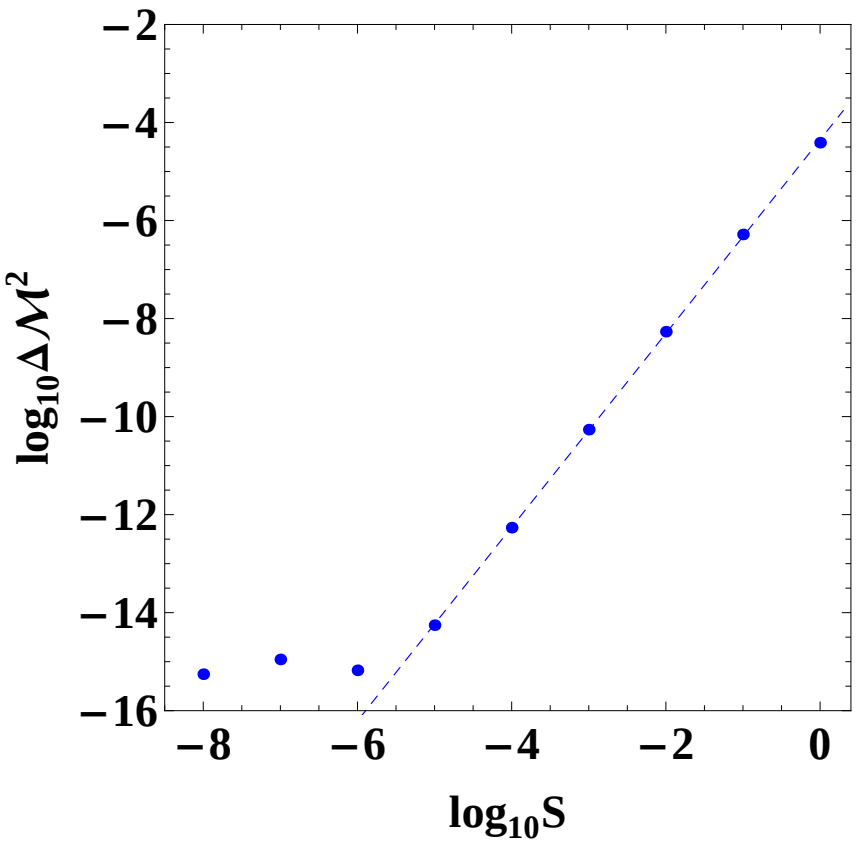

Figure C-5: The relative error of the four-momentum $\Delta\mathcal{M}^2$ as a function of the spin measure S for the NW SSC. The black dots correspond to the maximum values of $\Delta\mathcal{M}^2$ during the evolution for each S. The dashed line is a linear fit of the form $\log_{10}\Delta\mathcal{M}^2 = a\log_{10}S + b$ for data with $S > 10^{-6}$, where $a = 1.996 \pm 0.004$, $b = -4.135 \pm 0.013$.

- **The evolution of the constants of motion for a black hole spin of $a = 0.1$:**

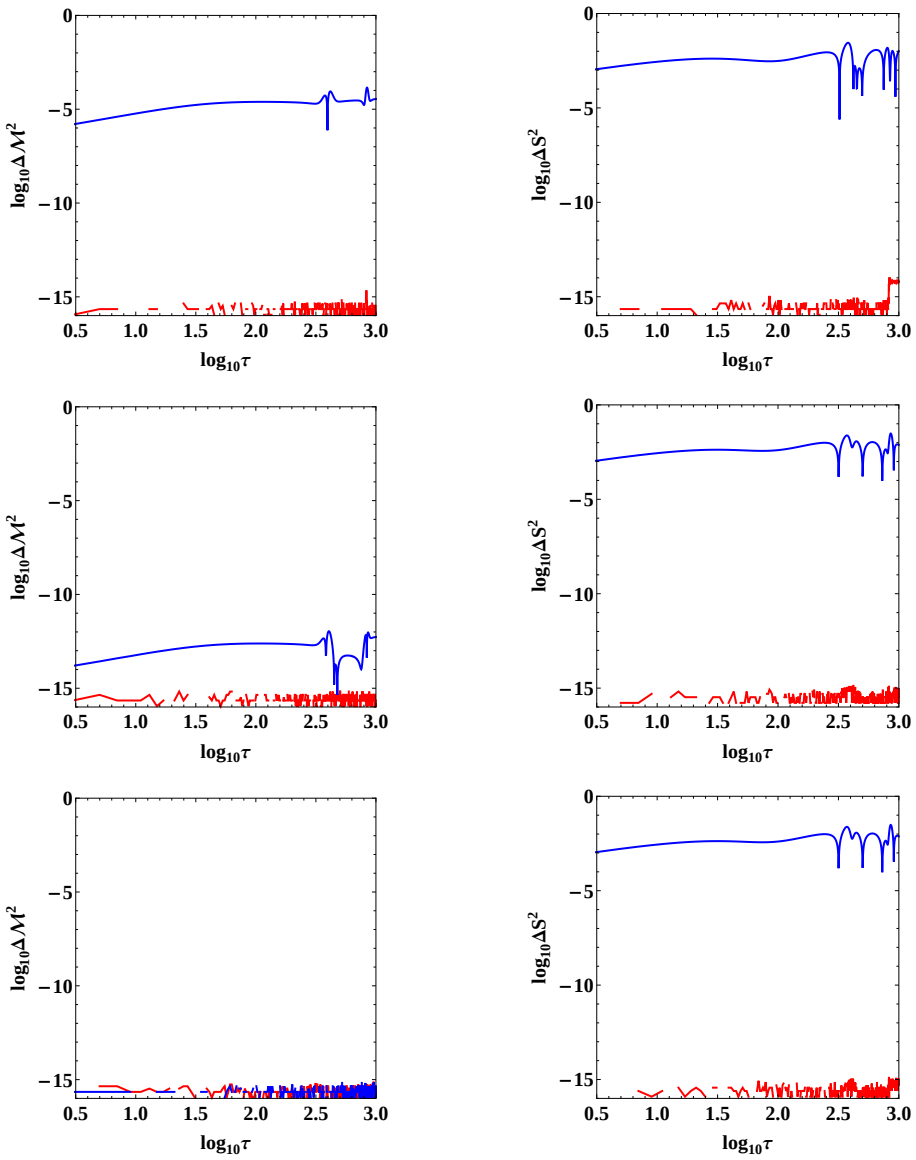

Figure C-6: Evolution of the MP equations with T SSC (red lines) and NW SSC (blue lines). Left column: relative error in the preservation of the four-momentum; Right column: relative error in the preservation of the spin. Top Row: $S = 1$, Middle Row: $S = 10^{-4}$, Bottom Row: $S = 10^{-8}$.

The corresponding relative error of the four-momentum as a function of the spin measure:

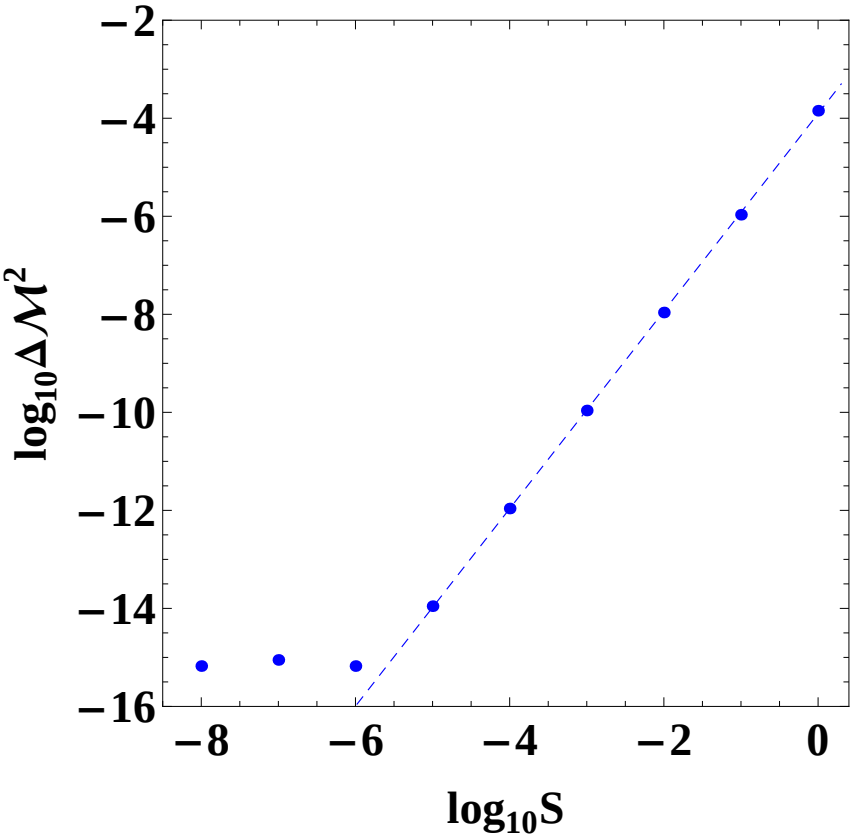

Figure C-7: The relative error of the four-momentum $\Delta\mathcal{M}^2$ as a function of the spin measure S for the NW SSC. The black dots correspond to the maximum values of $\Delta\mathcal{M}^2$ during the evolution for each S. The dashed line is a linear fit of the form $\log_{10}\Delta\mathcal{M}^2 = a\log_{10}S + b$ for data with $S > 10^{-6}$, where $a = 2.015 \pm 0.010,\ b = -3.906 \pm 0.031$.

C2: Negative Spin

The initial conditions are given by $a = 0.5$, $r = 11.7$, $\theta = \pi/2$, $p^r = 0.1$, $S = 0.1\ S$, $S^\theta = 0.08\ S$, $E = 0.97$, $J_z = 3$, and $\mathcal{M} = 1$.

C1-1: Orbital Evolution

- **Large Spin (absolute value)** $S = -1$

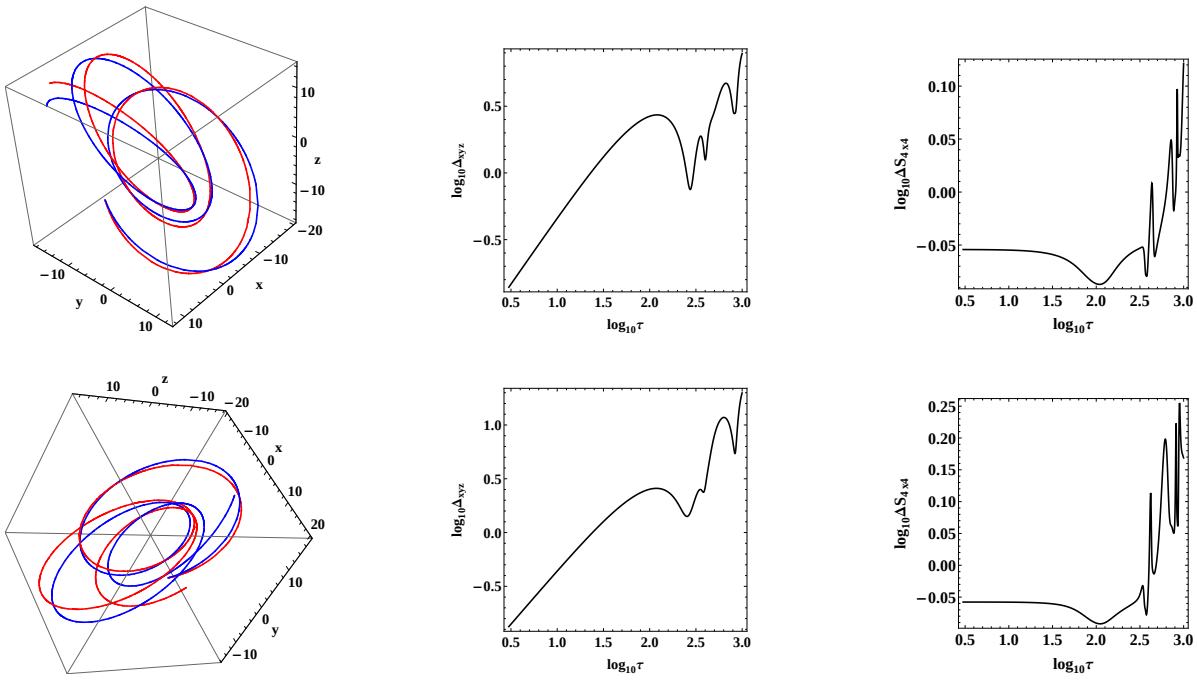

Figure C-8: Left panel: MP orbit with T SSC (red dots) and NW SSC (blue dots) in configuration space x, y, z (Cartesian coordinates). Central panel: Logarithm of the Euclidean distance in configuration space between these two orbits as a function of the proper time. Right panel: Logarithm of the difference $\Delta S_{4\text{x}4}$ between the spin tensors of these two orbits as a function of the proper time. Top Row: $a = 0.9$. Bottom Row: $a = 0.1$.

- **Medium Spin** $S = -10^{-4}$

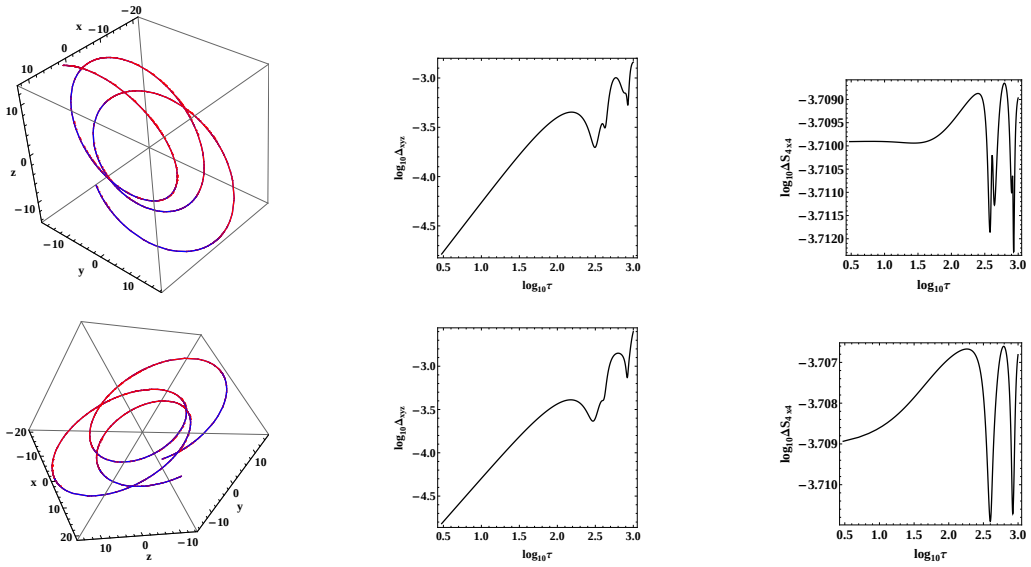

Figure C-9: see caption of fig. C-8.

- **Small Spin** $S = -10^{-8}$

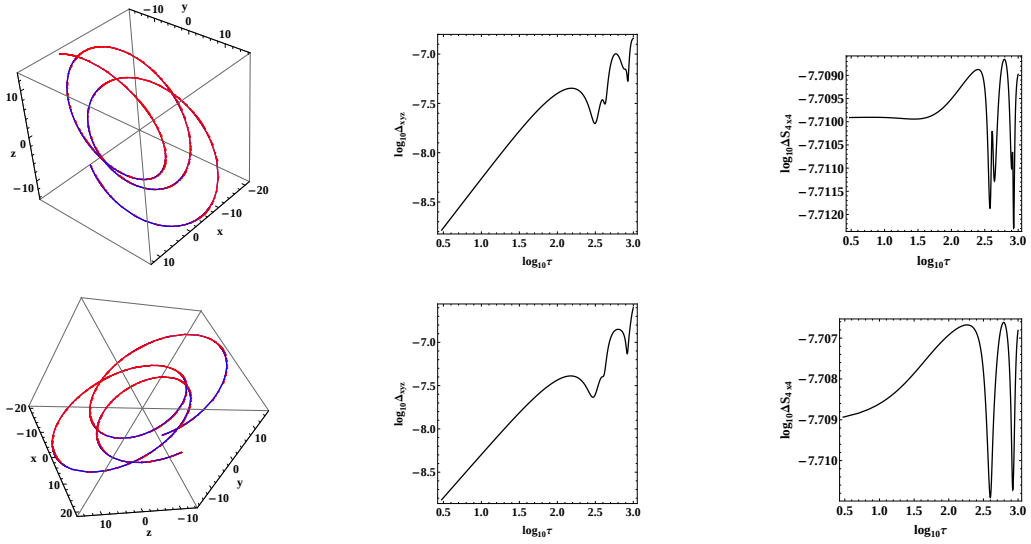

Figure C-10: see caption of fig. C-8.

C2-2: Constants of Motion

- **The evolution of the constants of motion for a black hole spin of** $a = 0.9$**:**

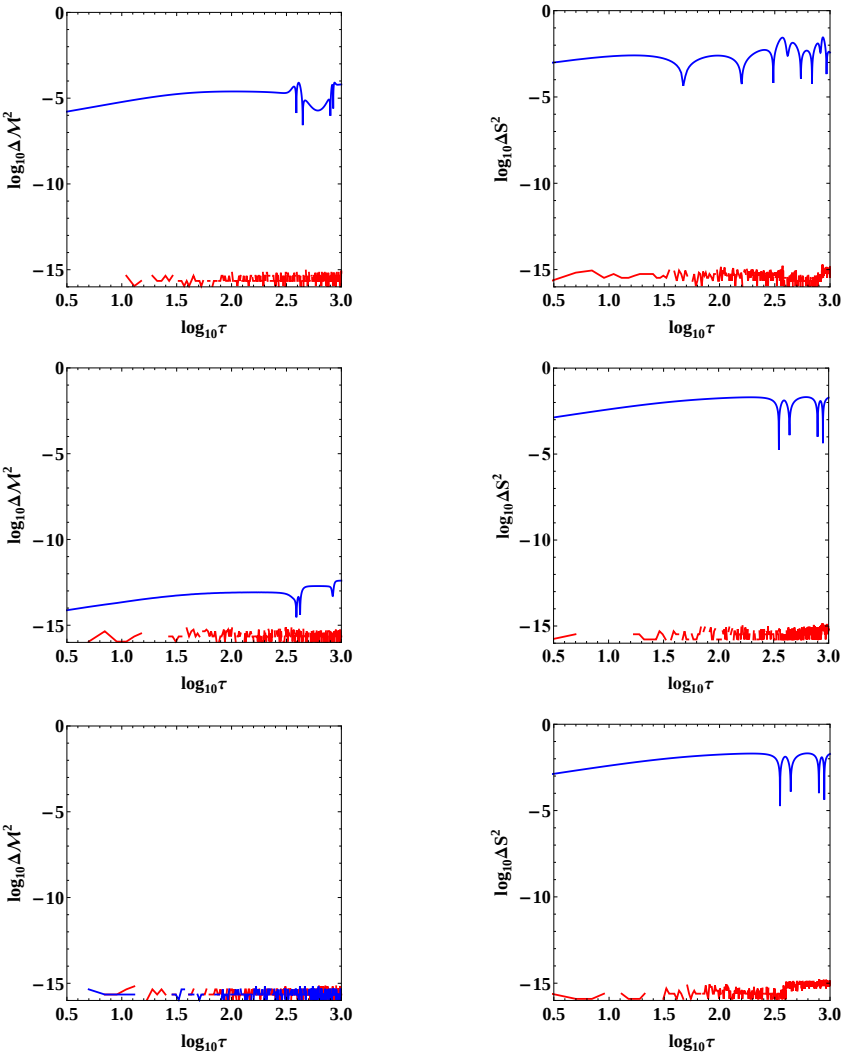

Figure C-11: Evolution of the MP equations with T SSC (red lines) and NW SSC (blue lines). Left column: relative error in the preservation of the four-momentum; Right column: relative error in the preservation of the spin. Top Row: $S = 1$, Middle Row: $S = 10^{-4}$, Bottom Row: $S = 10^{-8}$.

The corresponding relative error of the four-momentum as a function of the spin measure:

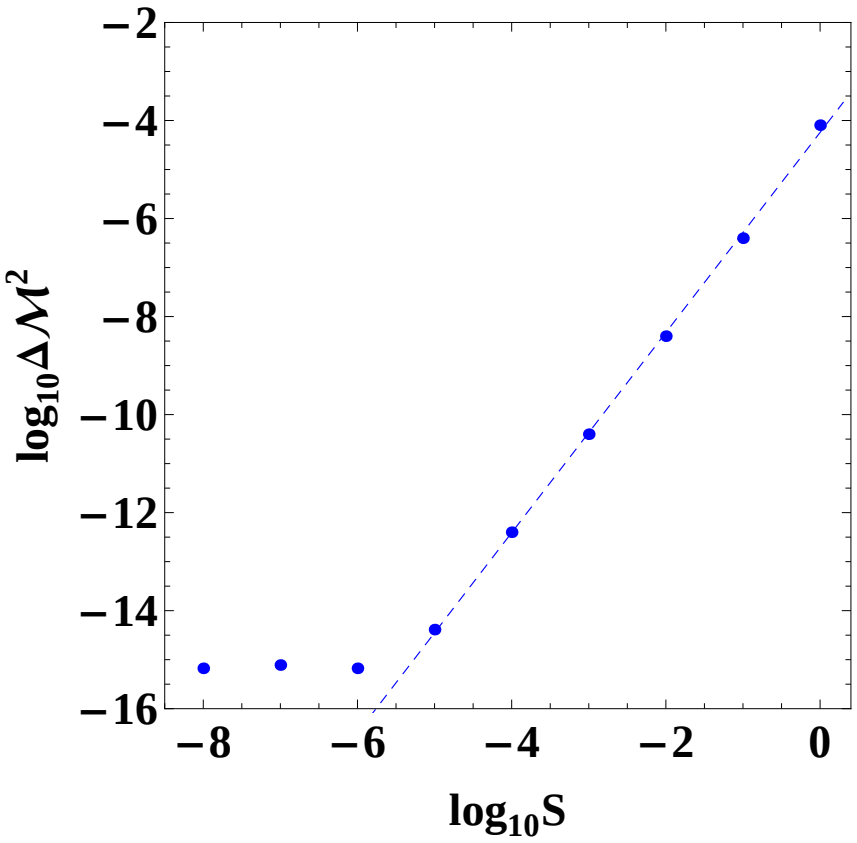

Figure C-12: The relative error of the four-momentum $\Delta\mathcal{M}^2$ as a function of the spin measure S for the NW SSC. The black dots correspond to the maximum values of $\Delta\mathcal{M}^2$ during the evolution for each S. The dashed line is a linear fit of the form $\log_{10}\Delta\mathcal{M}^2 = a\log_{10}S + b$ for data with $S > 10^{-6}$, where $a = 2.041 \pm 0.026$, $b = -4.243 \pm 0.078$.

- **The evolution of the constants of motion for a black hole spin of $a = 0.1$:**

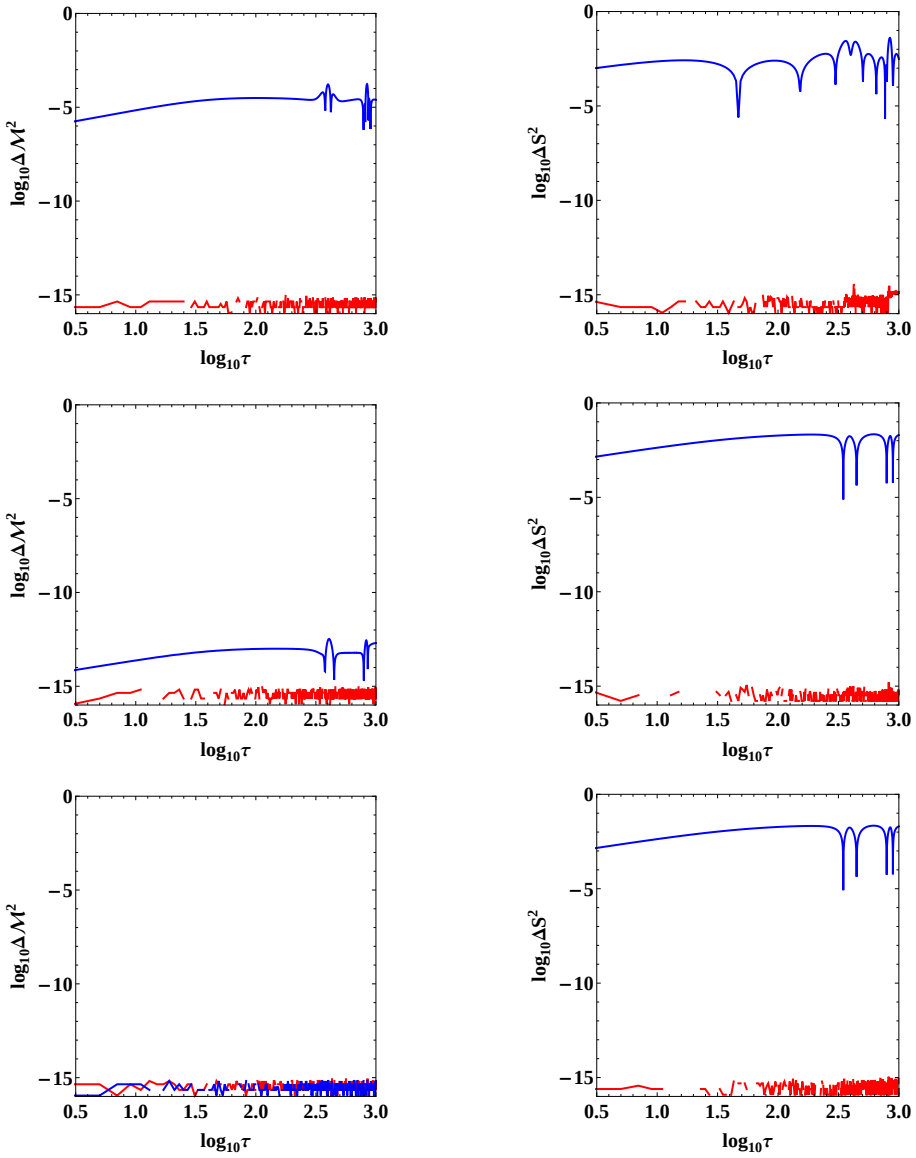

Figure C-13: Evolution of the MP equations with T SSC (red lines) and NW SSC (blue lines). Left column: relative error in the preservation of the four-momentum; Right column: relative error in the preservation of the spin. Top Row: $S = 1$, Middle Row: $S = 10^{-4}$, Bottom Row: $S = 10^{-8}$.

The corresponding relative error of the four-momentum as a function of the spin measure:

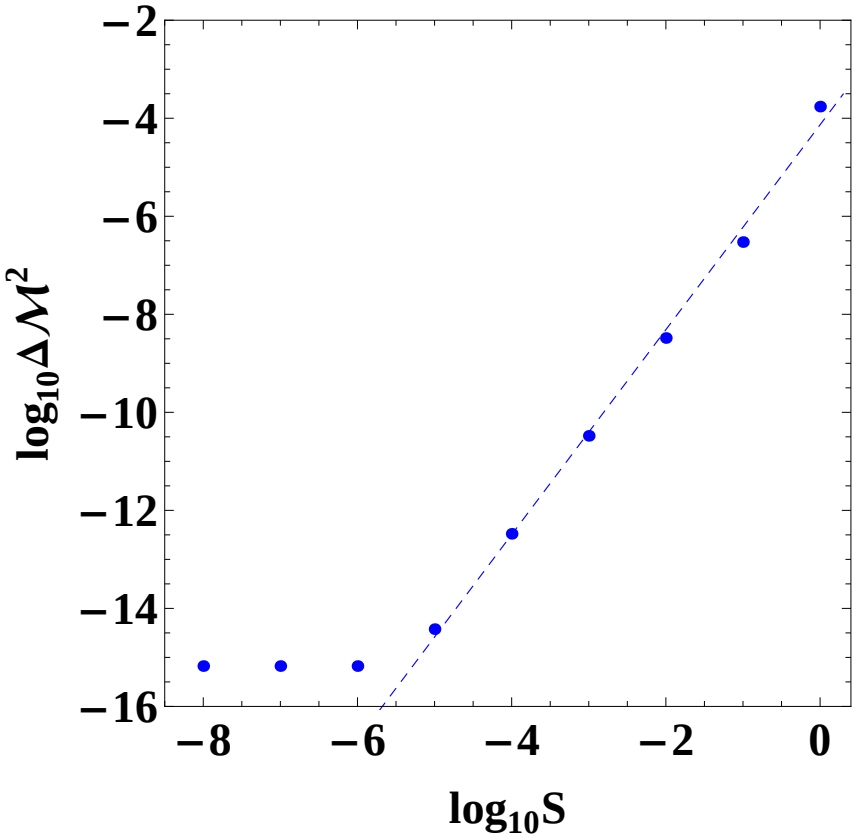

Figure C-14: The relative error of the four-momentum $\Delta\mathcal{M}^2$ as a function of the spin measure S for the NW SSC. The black dots correspond to the maximum values of $\Delta\mathcal{M}^2$ during the evolution for each S. The dashed line is a linear fit of the form $\log_{10}\Delta\mathcal{M}^2 = a\log_{10}S + b$ for data with $S > 10^{-6}$, where $a = 2.090 \pm 0.064,\ b = -4.133 \pm 0.195$.

Appendix D: Numerical Comparison two Formalisms: Complementary Figures

In chapter 6 we numerically compared the evolution of spinning testparticles given by the MP equations and the Hamiltonian formalism presented in [53]. Since the results are independent of the magnitude of the black hole spin, we restricted the presentation of the figures to $a = 0.5$. In the following we show complementary figures for $a = 0.1$ and $a = 0.9$. The initial conditions are the same as in fig. 3.1:

D1: Positive Spin

D1-1: Orbital Evolution

- **Large Spin** $S = 1$

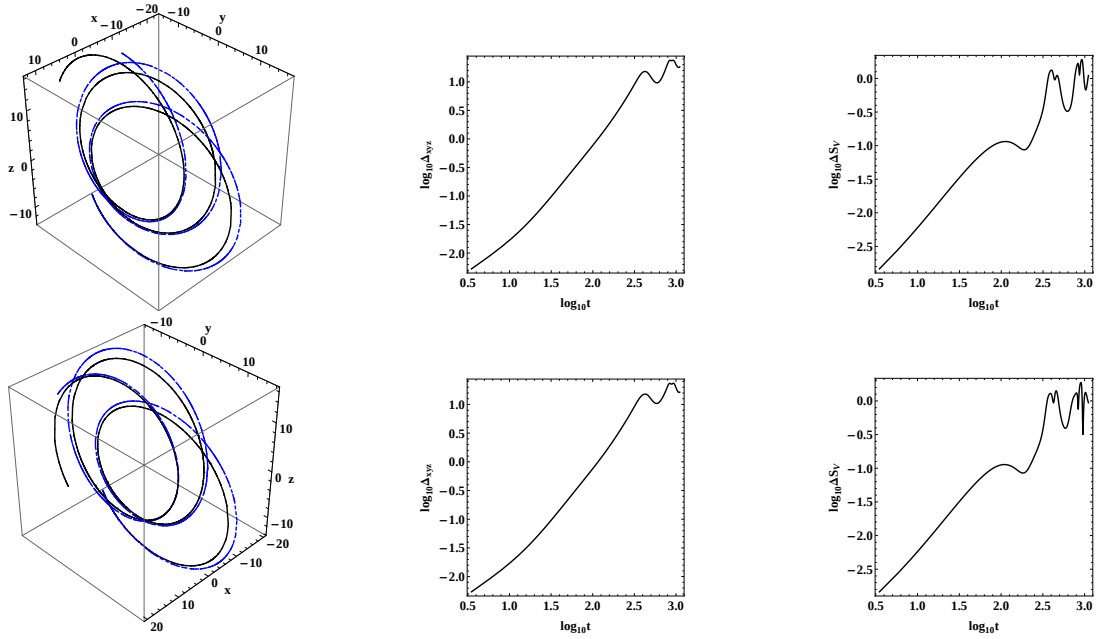

Figure D-1: Left panel: Orbit by MP equations (blue dots) and Hamilton's equations (black dots) in configuration space x, y, z (Cartesian coordinates). Central panel: Logarithm of the Euclidean distance in configuration space between these two orbits as a function of the proper time. Right panel: Logarithm of the difference ΔS_V between the spin vectors of these two orbits as a function of coordinate time. Top Row: $a = 0.9$. Bottom Row: $a = 0.1$.

- **Medium Spin** $S = 10^{-4}$

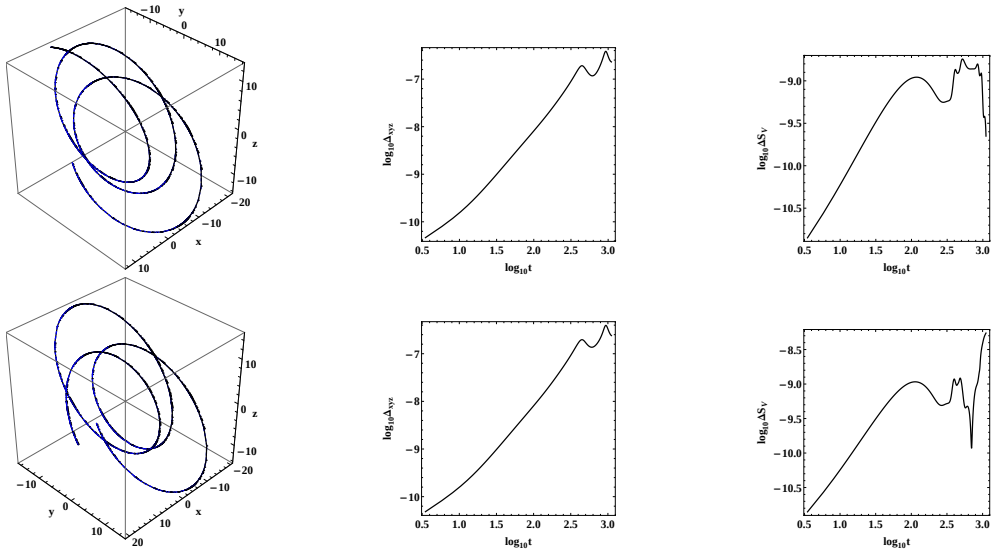

Figure D-2: see caption of fig. D-8.

- **Small Spin** $S = 10^{-8}$

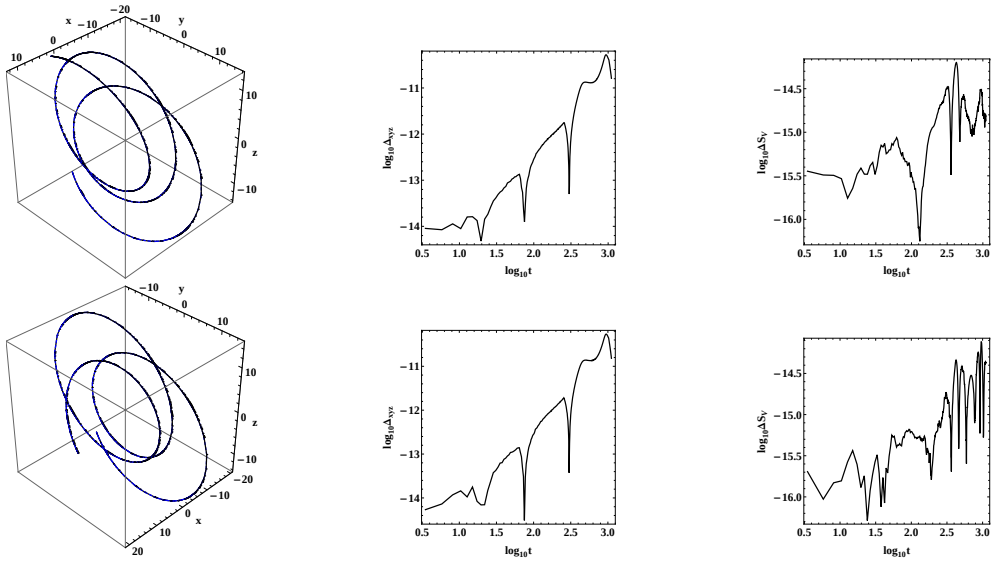

Figure D-3: see caption of fig. D-8.

D1-2: Constants of Motion

- **The evolution of the constants of motion for a black hole spin of $a = 0.9$:**

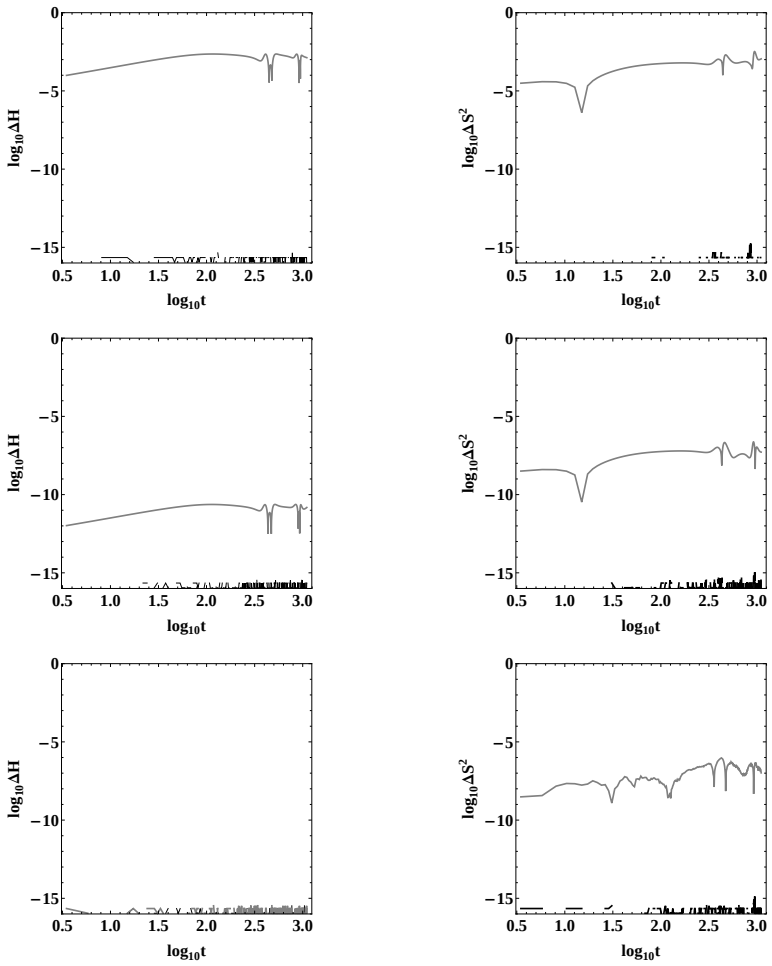

Figure D-4: Evolution of the MP equations (grey lines) and evolution of Hamilton's equations (black lines). Left column: relative error in the preservation of the Hamiltonian function; Right column: relative error in the preservation of the spin. Top Row: $S = 1$, Middle Row: $S = 10^{-4}$, Bottom Row: $S = 10^{-8}$.

The corresponding relative error of the Hamiltonian and the spin as a function of the spin measure:

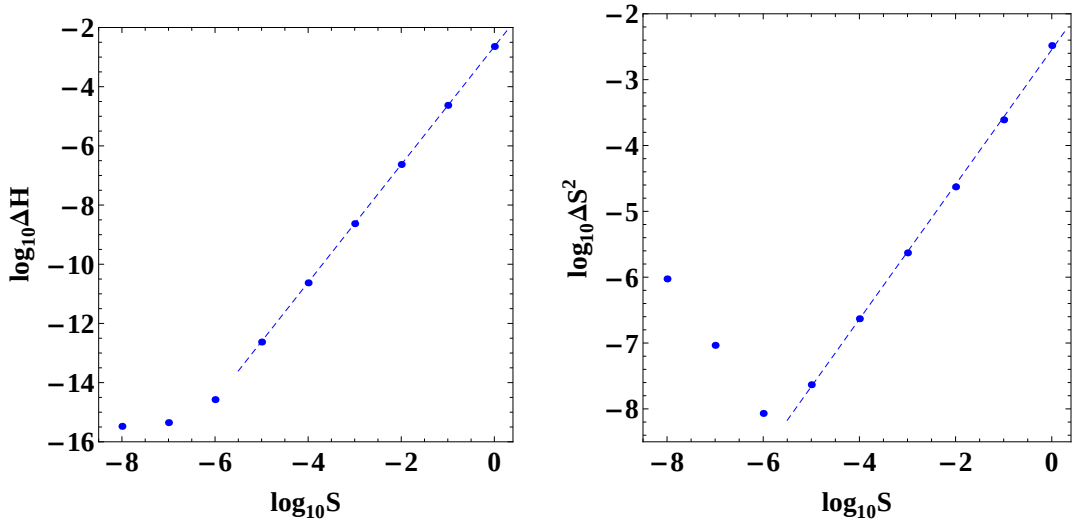

Figure D-5: The left panel shows the relative error of the Hamiltonian ΔH of orbits evolved through the MP equations for different spin measures S of the particle, while the right panel shows the corresponding preservation of the measure of the 3-vector ΔS^2. The black dots correspond to the maximum values of ΔH, ΔS^2 respectively for each S. The dashed lines are linear fits of the form $\log_{10}\Delta H = a\log_{10} S + b$, and
$\log_{10}\Delta S^2 = c\log_{10} S + d$ respectively for data with $S > 10^{-6}$, where $a = 1.993 \pm 0.003,\ b = -2.645 \pm 0.011$, and
$c = 1.023 \pm 0.011,\ d = -2.545 \pm 0.033$.

- **The evolution of the constants of motion for a black hole spin of $a = 0.1$:**

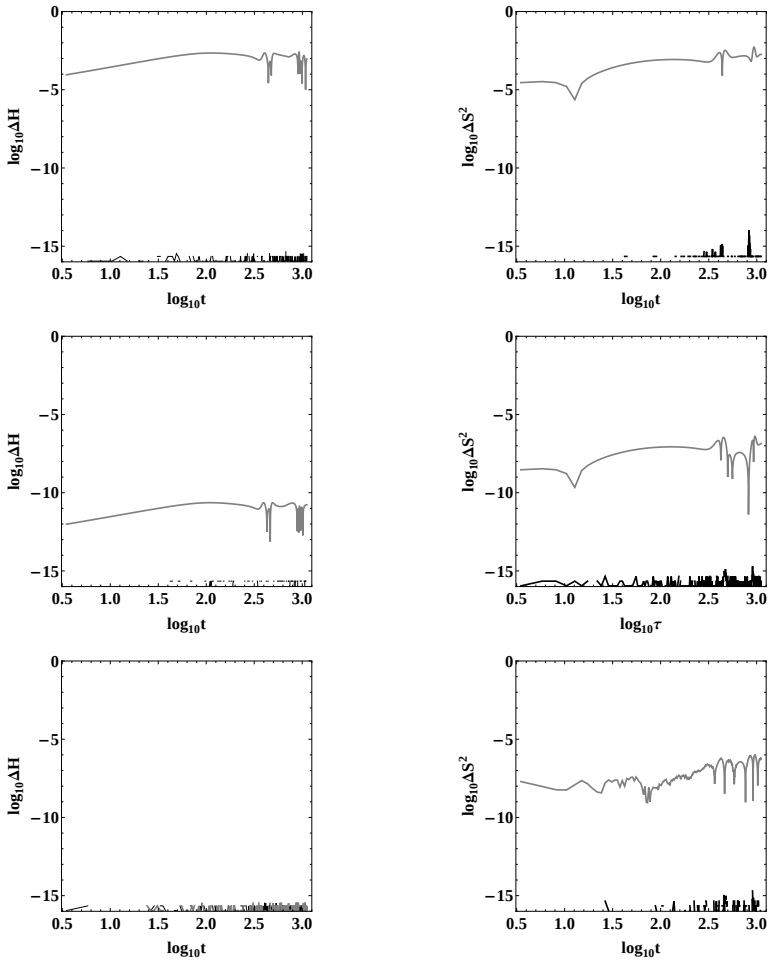

Figure D-6: Evolution of the MP equations (grey lines) and evolution of Hamilton's equations (black lines). Left column: relative error in the preservation of the Hamiltonian function; Right column: relative error in the preservation of the spin. Top Row: $S = 1$, Middle Row: $S = 10^{-4}$, Bottom Row: $S = 10^{-8}$.

The corresponding relative error of the Hamiltonian and the spin as a function of the spin measure:

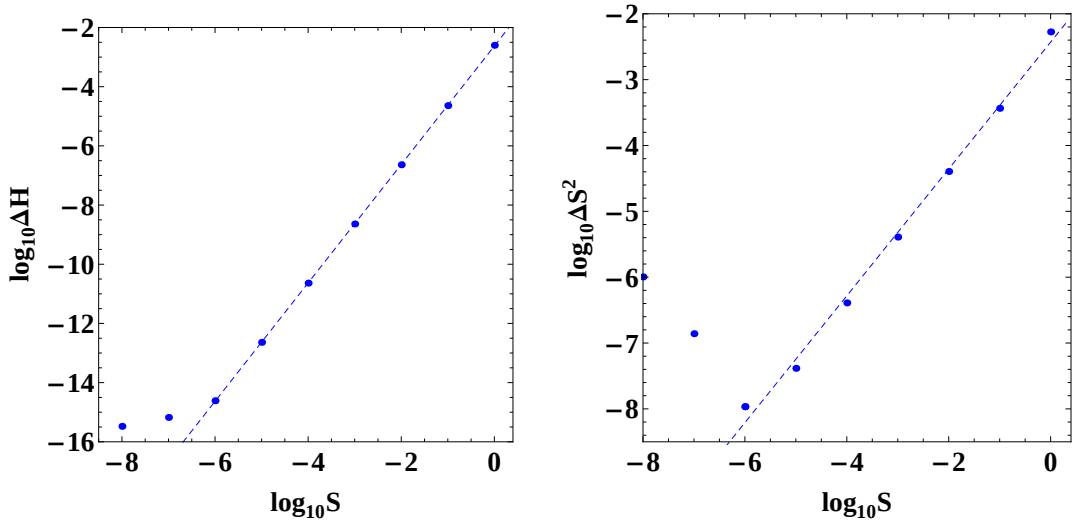

Figure D-7: The left panel shows the relative error of the Hamiltonian ΔH of orbits evolved through the MP equations for different spin measures S of the particle, while the right panel shows the corresponding preservation of the measure of the 3-vector ΔS^2. The black dots correspond to the maximum values of ΔH, ΔS^2 respectively for each S. The dashed lines are linear fits of the form $\log_{10}\Delta H = a\log_{10} S + b$, and
$\log_{10}\Delta S^2 = c\log_{10} S + d$ respectively for data with $S > 10^{-6}$, where $a = 2.001 \pm 0.003,\ b = -2.626 \pm 0.012$, and
$c = 1.012 \pm 0.013,\ d = -2.350 \pm 0.040$.

D2: Negative Spin

The initial conditions are given by $a = 0.5$, $r = 11.7$, $\theta = \pi/2$, $p^r = 0.1$, $S = 0.1\ S$, $S^\theta = 0.08\ S$, $E = 0.97$, $J_z = 3$, and $\mathcal{M} = 1$.

D1-1: Orbital Evolution

- **Large Spin (absolute value)** $S = -1$

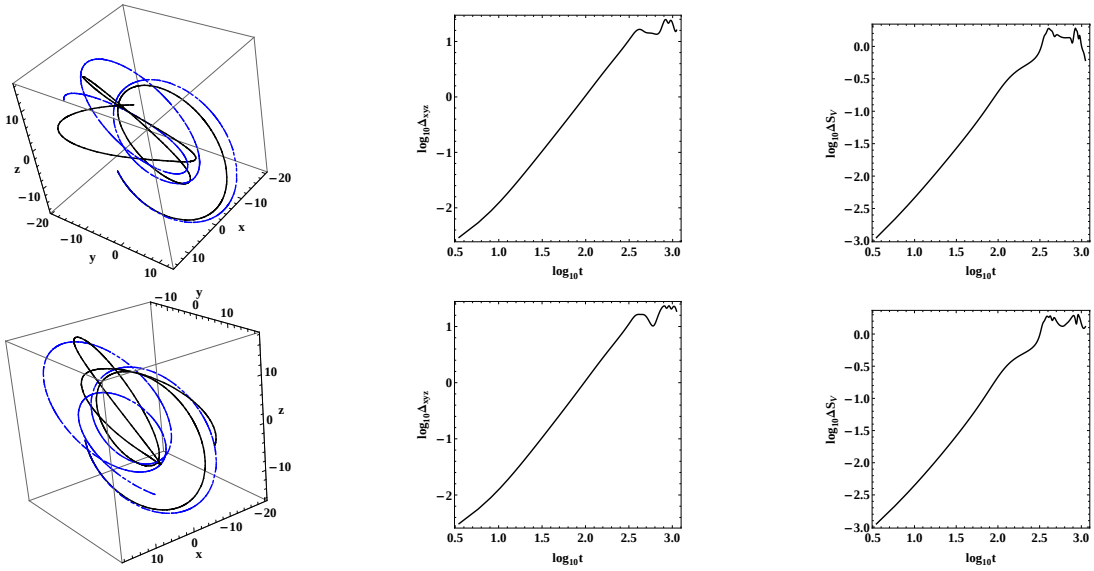

Figure D-8: Left panel: Orbit by MP equations (blue dots) and Hamilton's equations (black dots) in configuration space x, y, z (Cartesian coordinates). Central panel: Logarithm of the Euclidean distance in configuration space between these two orbits as a function of the proper time. Right panel: Logarithm of the difference ΔS_V between the spin vectors of these two orbits as a function of coordinate time. Top Row: $a = 0.9$. Bottom Row: $a = 0.1$.

- **Medium Spin** $S = -10^{-4}$

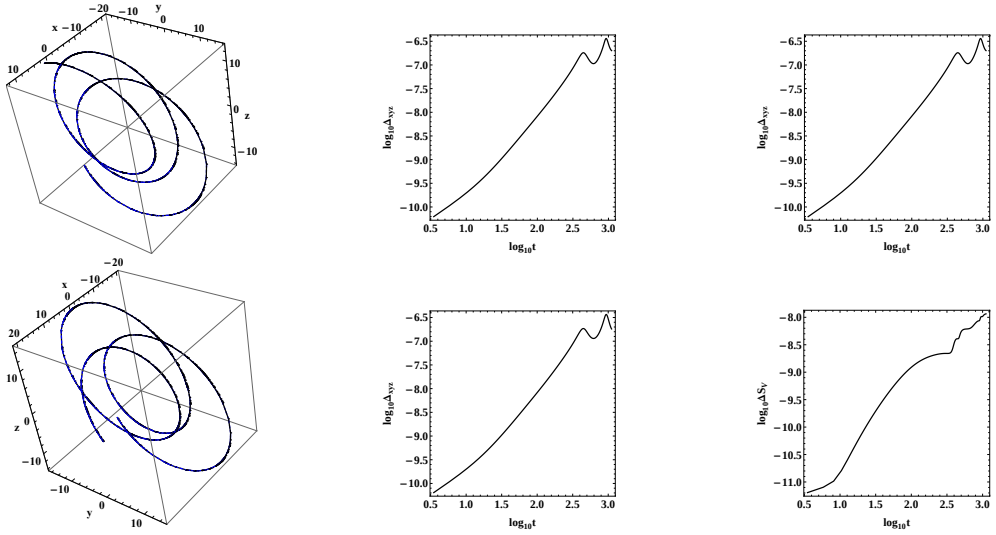

Figure D-9: see caption of fig. D-8.

- **Small Spin** $S = -10^{-8}$

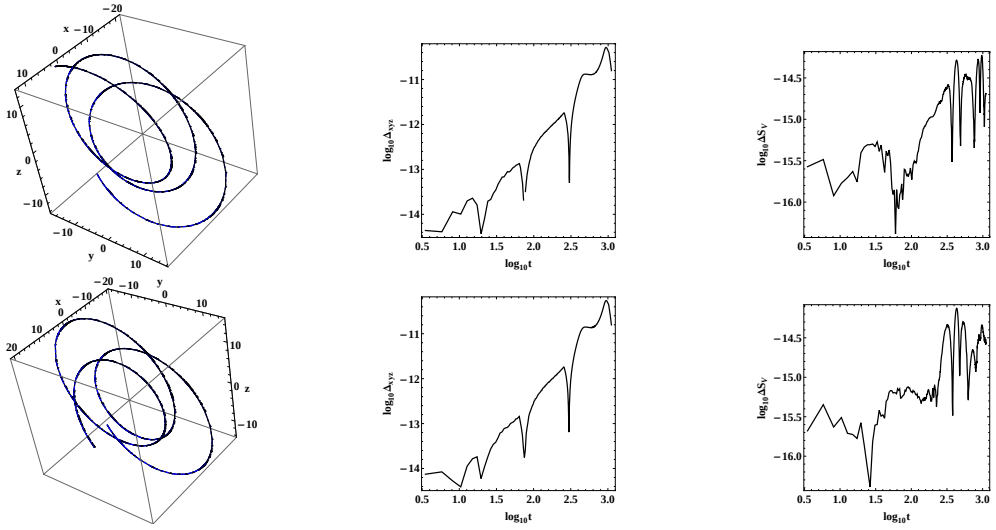

Figure D-10: see caption of fig. D-8.

D1-2: Constants of Motion

- **The evolution of the constants of motion for a black hole spin of $a = 0.9$:**

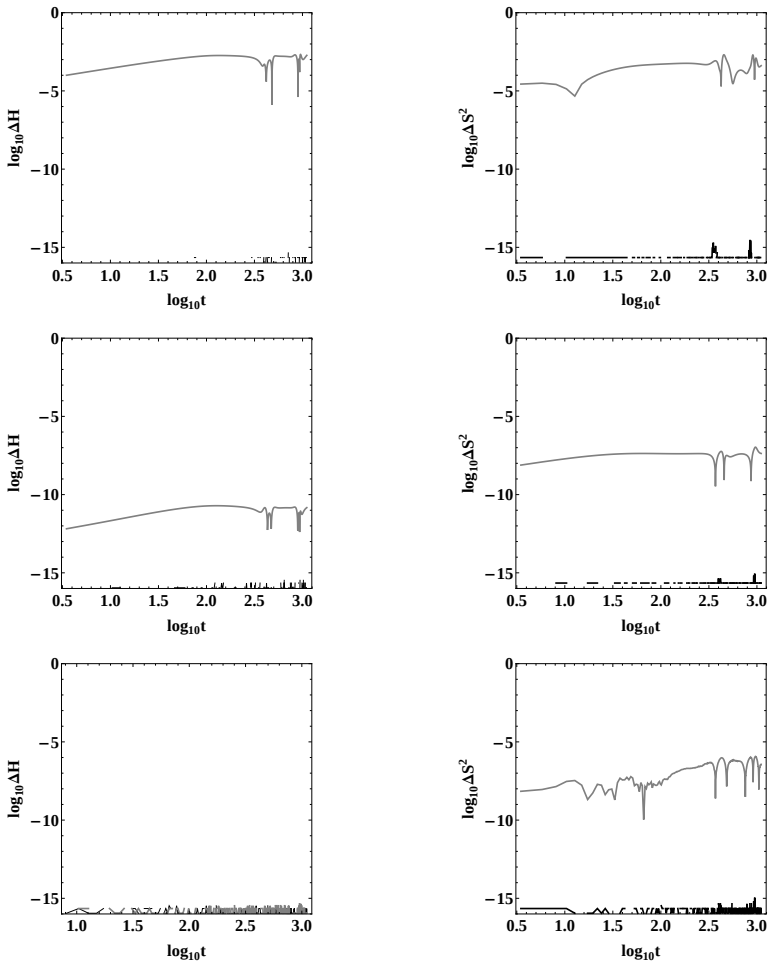

Figure D-11: Evolution of the MP equations (grey lines) and evolution of Hamilton's equations (black lines). Left column: relative error in the preservation of the Hamiltonian function; Right column: relative error in the preservation of the spin. Top Row: $S = -1$, Middle Row: $S = -10^{-4}$, Bottom Row: $S = -10^{-8}$.

The corresponding relative error of the Hamiltonian and the spin as a function of the spin measure:

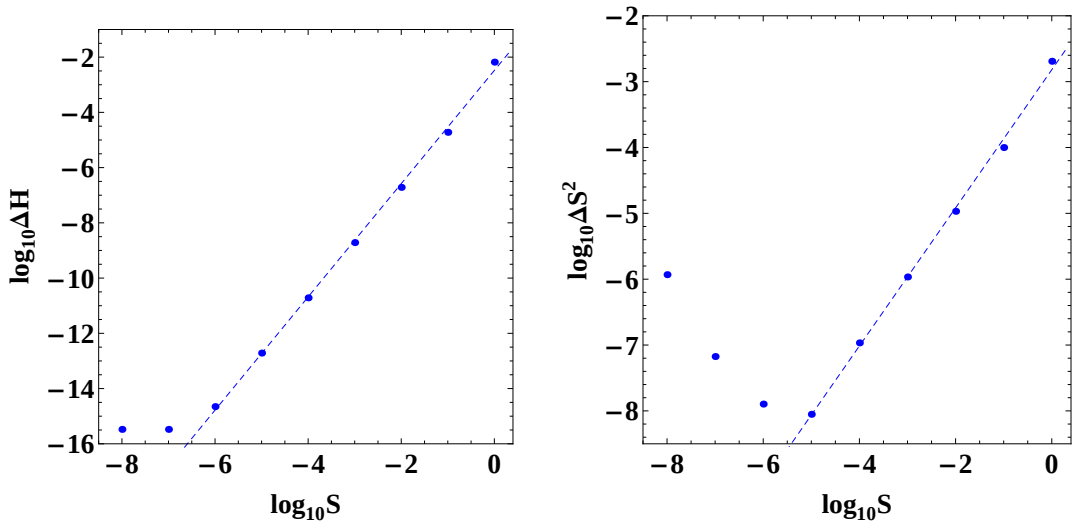

Figure D-12: The left panel shows the relative error of the Hamiltonian ΔH of orbits evolved through the MP equations for different spin measures S of the particle, while the right panel shows the corresponding preservation of the measure of the 3-vector ΔS^2. The black dots correspond to the maximum values of ΔH, ΔS^2 respectively for each S. The dashed lines are linear fits of the form $\log_{10}\Delta H = a\log_{10} S + b$, and
$\log_{10}\Delta S^2 = c\log_{10} S + d$ respectively for data with $S > 10^{-6}$, where $a = 2.020 \pm 0.035,\ b = -2.481 \pm 0.125$, and
$c = 1.049 \pm 0.024,\ d = -2.819 \pm 0.072$.

- **The evolution of the constants of motion for a black hole spin of $a = 0.1$:**

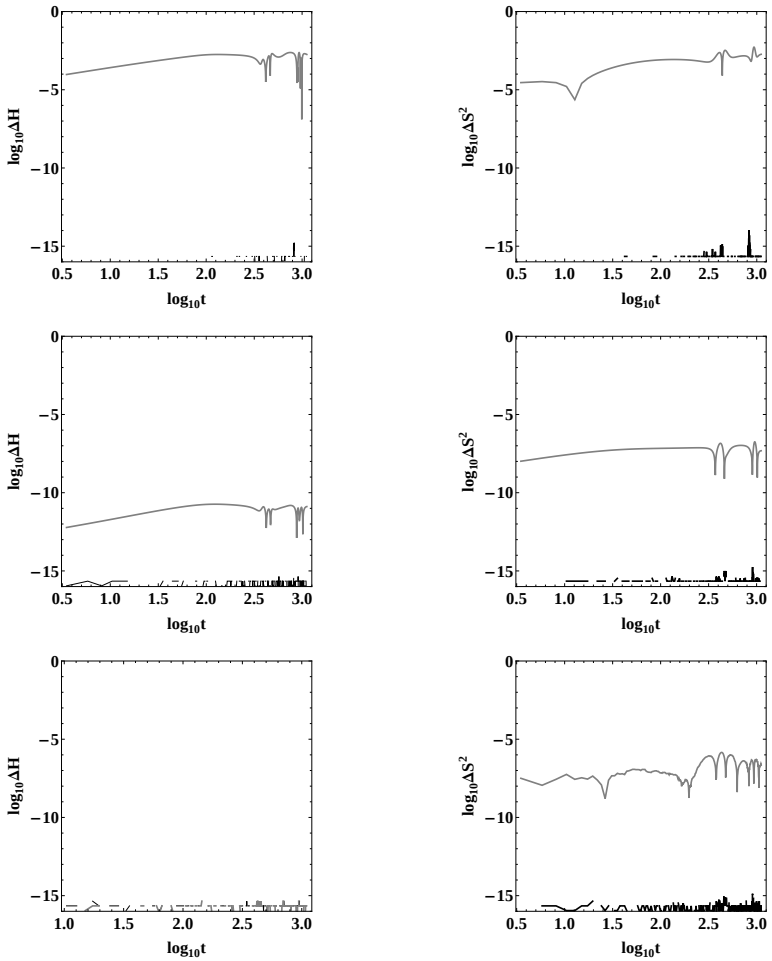

Figure D-13: Evolution of the MP equations (grey lines) and evolution of Hamilton's equations (black lines). Left column: relative error in the preservation of the Hamiltonian function; Right column: relative error in the preservation of the spin. Top Row: $S = -1$, Middle Row: $S = -10^{-4}$, Bottom Row: $S = -10^{-8}$.

The corresponding relative error of the Hamiltonian and the spin as a function of the spin measure:

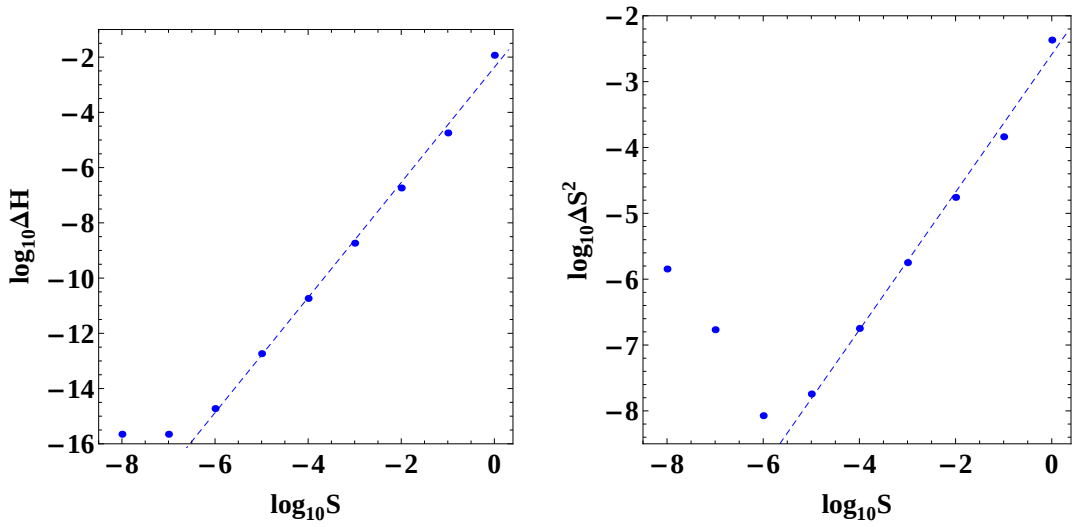

Figure D-14: The left panel shows the relative error of the Hamiltonian ΔH of orbits evolved through the MP equations for different spin measures S of the particle, while the right panel shows the corresponding preservation of the measure of the 3-vector ΔS^2. The black dots correspond to the maximum values of ΔH, ΔS^2 respectively for each S. The dashed lines are linear fits of the form $\log_{10}\Delta H = a\log_{10} S + b$, and $\log_{10}\Delta S^2 = c\log_{10} S + d$ respectively for data with $S > 10^{-6}$, where $a = 2.084 \pm 0.050,\ b = -2.369 \pm 0.181$, and $c = 1.046 \pm 0.038,\ d = -2.586 \pm 0.116$.

Bibliography

[1] G. Lukes-Gerakopoulos, J. Seyrich, D. Kunst, "Investigating spinning test particles: Spin supplementary conditions and the Hamiltonian formalism", *Phys. Rev. D* **90**, 104019 (2014).

[2] D. Kunst, V. Perlick and C. Lämmerzahl, "Isofrequency Pairing of spinning particles in Schwarzschild-de Sitter spacetime", *Phys. Rev. D* **92**, 024029 (2015)

[3] D. Kunst, T. Ledvinka, G. Lukes-Gerakopoulos and J. Seyrich, "Comparing Hamiltonians of a spinning test particle for different tetrad fields", *Phys. Rev. D* **9**3, 044004 (2016)

[4] J. Vines, D. Kunst, J. Steinhoff and T. Hinderer, "Canonical Hamiltonian for an extended test body in curved spacetime: To quadratic order in spin", in preparation; arXiv:1601.07529 (2016)

[5] Albert Einstein: "Die Feldgleichungen der Gravitation", *Sitzungsberichte der Preussischen Akademie der Wissenschaften zu Berlin*, 844, 25. November 1915.

[6] Charles W. Misner, Kip S. Thorne, John A. Wheeler, *Gravitation*, Macmillan Education 1973.

[7] Sean M. Carroll, *Spacetime and Geometry: An Introduction to General Relativity*, Cummings 2003.

[8] F. W. Dyson, A. S. Eddington and C. Davidson, "A Determination of the Deflection of Light by the Sun's Gravitational Field, from Observations Made at the Total Eclipse of May 29, 1919" *Philosophical Transactions of the Royal Society of London. Series A* **220**, 291 (1920).

[9] L. I. Schiff, "Motion of a gyroscope according to Einstein's theory of gravitation", *Proc. Natl. Acad. Sci.* **46**, 871 (1960).

[10] C. Cutler and K. D. Thorne, "An overview of gravitational-wave sources", *General Relativity and Gravitation. Proceedings of the 16th International Conference*, edited by N. T. Bishop and S. D. Maharaj, World Scientific, Singapore (2002)

[11] B. S. Sathyaprakas and B. Schutz, "Physics, Astrophysics and Cosmology with Gravitational Waves", *Living Re. Relativity* **12**, 2 (2009).

[12] K. Riles, "Gravitational Waves: Sources, Detectors and Searches", *Prog. in Particle & Nuclear Phys.* **68**, 1 (2013).

[13] J. M. Weisberg, J. H. Taylor and L. A. Fowler, "Gravitational waves from an orbiting pulsar", *Scientific American* **245**, 74 (1981).

[14] J. M. Weisberg, D. J. Nice and J. H. Taylor, "Timing Measurements of the Relativistic Binary Pulsar PSR B1913+16", *Astrophysical Journal* **722**, 1030 (2010).

[15] A. Le Tiec, "The Overlap of Numerical Relativity, Perturbation Theory and Post-Newtonian Theory in the Binary Black Hole Problem", *Int. J. Mod. Phys. D* **23**, 1430022 (2014).

[16] P. Amaro-Seoane, J. R. Gair, A. Pound, S. A. Hughes, and C. F.Sopuerta, "Research Update on Extreme-Mass-Ratio Inspirals", *J. Phys.: Conf. Ser.* **610**, 012002 (2015).

[17] R. O'Shaughnessy, "Transition from inspiral to plunge for eccentric equatorial Kerr orbits", *Phys. Rev. D* **67**, 044004 (2003).

[18] S. Drasco, É. É. Flanagan, S. A. Hughes, "Computing inspirals in Kerr in the adiabatic regime. I. The scalar case", *Class.Quant.Grav.* **22**, 801 (2005).

[19] R. N. Lang and S. A. Hughes, "Measuring coalescing massive binary black holes with gravitational waves: The impact of spin-induced precession", *Phys. Rev. D* **74**, 122001 (2006).

[20] J. Levin and G. Perez-Giz, "Homoclinic Orbits around Spinning Black Holes I: Exact Solution for the Kerr Separatrix", *Phys. Rev. D* **79**, 124013 (2009).

[21] E. Hackmann and C. Lämmerzahl, "Geodesic equation in Schwarzschild-(anti-)de Sitter space-times: Analytical solutions and applications", *Phys. Rev. D* **78**, 024035 (2008).

[22] E. Hackmann, C. Lämmerzahl, V. Kagramanova, and J. Kunz, "Analytical solution of the geodesic equation in Kerr-(anti-) de Sitter space-times", *Phys. Rev. D* **81**, 044020 (2010)

[23] E. Hackmann, "Geodesic equations in black hole space-times with cosmological constant", PhD thesis, Universit¨at Bremen, (2010).

[24] C. Cutler, D. Kennefick and E. Poisson, "Gravitational radiation reaction for bound motion around a Schwarzschild black hole", *Phys. Rev. D* **50**, 3816 (1994).

[25] J. Levin and G. Perez-Giz, "A periodic table for black hole orbits", *Phys. Rev. D* **77**, 103005 (2008).

[26] L. Barack and N. Sago, "Beyond the geodesic approximation: Conservative effects of the gravitational self-force in eccentric orbits around a Schwarzschild black hole", *Phys. Rev. D* **83**, 084023 (2011).

[27] L. Blanchet, "Gravitational Radiation from Post-Newtonian Sources and Inspiralling Compact Binaries", *Living Rev. Rel.* **9**, 4 (2006).

[28] J. Levin, R. O'Reilly and E. J. Copeland, "Gravity waves from homoclinic orbits of compact binaries", *Phys. Rev. D* **62**, 024023 (2000).

[29] K. Glampedakis, D. Kennefick, "Zoom and whirl: Eccentric equatorial orbits around spinning black holes and their evolution under gravitational radiation reaction", *Phys. Rev. D* **66**, 044002 (2002).

[30] S. N. Rasband, "Black Holes and Spinning Test Bodies", *Phys. Rev. Lett.* **30**, 111 (1973).

[31] T. Tanaka, Y. Mino, M. Sasaki and M. Shibata, "Gravitational waves from a spinning particle in circular orbits around a rotating black hole", *Phys. Rev. D* **54**, 3762 (1996).

[32] M. Saijo, K. Maeda, M. Shibata and Y. Mino, "Gravitational waves from a spinning particle plunging into a Kerr black hole", *Phys. Rev. D* **58**, 064005 (1998).

[33] A. Buonanno, Y. Chen and M.Vallisneri, "Detecting gravitational waves from precessing binaries of spinning compact objects: Adiabatic limit", *Phys. Rev. D*, **67**, 104025 (2003).

[34] M. Favata, "Conservative corrections to the innermost stable circular orbit (ISCO) of a Kerr black hole: a new gauge-invariant post-Newtonian ISCO condition, and the ISCO shift due to test-particle spin and the gravitational self-force", *Phys. Rev. D* **83**, 024028 (2011).

[35] S. Suzuki and K. Maeda, "Chaos in Schwarzschild spacetime: The motion of a spinning particle", *Phys. Rev. D* **55**, 4848 (1997).

[36] M. D. Hartl, "Dynamics of spinning test particles in Kerr spacetime", *Phys. Rev. D* **67**, 024005 (2003).

[37] M. D. Hartl, "A survey of spinning test particle orbits in Kerr spacetime", *Phys. Rev. D* **67**, 104023 (2003).

[38] C. Verhaaren, E. W. Hirschmann, "Chaotic orbits for spinning particles in Schwarzschild spacetime", *Phys. Rev. D* **81**, 124034 (2010).

[39] N. Warburton, L. Barack, N. Sago, "Isofrequency pairing of geodesic orbits in Kerr geometry", *Phys. Rev. D* **87**, 084012 (2013).

[40] S. Shaymatov, F. Atamurotov, B. Ahmedov, "Isofrequency pairing of circular obits in Schwarzschild spacetime in the presence of magnetic field", *Astrophys. Space Sci.* **350**, 413 (2014).

[41] H. P. Pfeiffer, "Numerical simulations of compact object binaries", *Class. Quantum Grav.* **29**, 124004 (2012).

[42] T. Damour, P. Jaranowski, and G. Sch¨afer, "Determination of the last stable orbit for circular general relativistic binaries at the third post-Newtonian approximation", *Phys. Rev. D* **62**, 084011 (2000).

[43] G. Schäfer, "Post-Newtonian methods: Analytic results on the binary problem", *Mass and Motion in General Relativity,* Fundamental Theories of Physics **162**, 167 edited by L. Blanchet, A. Spallicci and B. Whiting (2011).

[44] A. Buonanno and T. Damour, "Effective one-body approach to general relativistic two-body dynamics", *Phys. Rev. D* **59**, 084006 (1999).

[45] T. Damour, "Introductory lectures on the Effective One Body formalism", *Int. J. Mod. Phys. A* **23**, 1130 (2008).

[46] T. Damour, "The General Relativistic Two Body Problem and the Effective One Body Formalism", *General Relativity, Cosmology and Astrophysics*, Fundamental Theories of Physics **177** edited by J. Bičák and T. Ledvinka, 111 (2014).

[47] E. Barausse, and A. Buonanno, "An improved effective-one-body Hamiltonian for spinning black-hole binaries", *Phys. Rev. D* **81**, 084024 (2010).

[48] T. Hinderer, A. Buonanno, A. H. Mroué et. al, "Periastron advance in spinning black hole binaries: comparing effective-one-body and numerical relativity", *Phys. Rev. D* **88**, 084005 (2013).

[49] R. L. Arnowitt, S. Deser, and C. W. Misner, "Dynamical structure and definition of energy in general relativity", *Phys. Rev.* **116,** 1322 (1959).

[50] R. L. Arnowitt, S. Deser, and C. W. Misner, "Canonical variables for general relativity", *Phys. Rev.* **117**, 1595 (1960).

[51] R. L. Arnowitt, S. Deser, and C. W. Misner, "The dynamics of general relativity", in *Gravitation: An Introduction to Current Research*, L. Witten, ed., pp. 227–265. John Wiley, New York, (1962).

[52] R. L. Arnowitt, S. Deser, and C. W. Misner, "Republication of: The dynamics of general relativity", *Gen. Rel. Grav.* **40,** 1997 (2008).

[53] E. Barausse, E. Racine, and A. Buonanno, "Hamiltonian of a spinning test-particle in curved spacetime", *Phys. Rev. D* **80**, 104025 (2009).

[54] W. Tulczyjew, "Motion of multipole particles in general relativity theory", *Acta Phys. Polonica* **18**, 393 (1959).

[55] L. F. O. Costa, J. Natário, M. Zilhão, "Spacetime dynamics of spinning particles - exact gravito-electromagnetic analogies", preprint arXiv:1207.0470 (2012).

[56] T. D. Newton and E. P. Wigner, "Localized States for Elementary Systems", *Rev. Mod. Phys.* **21**, 400 (1949).

[57] M. H. L. Pryce, "The Mass-Centre in the Restricted Theory of Relativity and Its Connexion with Quantum Theory of Elementary Particles", *Proc. R. Soc. London, Ser A* **195**, 62 (1948).

[58] J. Steinhoff, "Canonical Formulation of Spin in General Relativity", PhD Thesis, *Ann. Phys. (Berlin)* **523**, 296 (2011).

[59] J. Steinhoff, "Spin gauge symmetry in the action principle for classical relativistic particles", arXiv:1501.04951 [gr-qc] (2015).

[60] J. C. Baez and E. F. Bunn, *The meaning of Einstein's equation*, http://math.ucr.edu/home/baez/, (2006).

[61] K. Schwarzschild, "Über das Gravitationsfeld eines Massenpunktes nach der Einsteinschen Theorie", *Sitzungsberichte der Königlich Preussischen Akademie der Wissenschaften* **7**, 189 (1916).

[62] L. Gualtierie and V. Ferrari, "Lecture notes for a graduate course on black holes in general relativity", (2011).

[63] W. Rindler, *Relativity* (Oxford University Press, Oxford, 2001).

[64] R. P. Kerr, "Gravitational field of a spinning mass as an example of algebraically special metrics", *Phys. Rev. Let.* **11**, 237 (1963).

[65] B. Carter, "Global structure of the Kerr family of gravitational fields", *Phys. Rev.* **174**, 1559 (1968).

[66] M. Mathisson, "Neue Mechanik materieller Systeme", *Acta Phys. Polonica* **6**, 163 (1937)
Republication: M. Mathisson, "Republication of: New mechanics of material systems", *Gen. Relativ. Gravit.* **42**, 1011 (2010).

[67] A. Papapetrou, "Spinning Test-Particles in General Relativity. I", *Proc. R. Soc. London Ser. A* **209**, 248 (1951).

[68] R. Micoulaut, "Über die Bewegungsgleichungen eines makroskopischen rotierenden Teilchens gemäßder allgemeinen Relativitätstheorie", *Zeitschrift für Physik* **206**, 394 (1967).

[69] K. Westpfahl, "Das freie Spinteilchen", *Annalen der Physik* **475**, 113 (1967).

[70] M. Carmeli, *Classical Fields - General Relativity and Gauge Theory*, J. Wiley, (1982) Chapter 6 and Appendix A.

[71] P. A. M. Dirac, *Lectures on quantum mechanics*, Belfer Graduate School of Science Monographs Series 2, Belfer Graduate School of Science, New York, MR 2220894 Reprinted by Dover in 2001. (1964).

[72] W. G. Dixon, "The definition of multipole moments for extended bodies", *Gen. Rel. and Grav.* **4**, 199 (1973).

[73] W. G. Dixon, "Dynamics of extended bodies in general relativity. III. Equations of motion", *Philos. Trans. R. Soc. London Ser. A* **277**, 59 (1974).

[74] L. F. Costa and J. Natário, "Center of mass, spin supplementary conditions, and the momentum of spinning particles", *Equations of Motion in Relativistic Gravity*, Fundamental Theories of Physics **179** edited by D. Pützfeld, C. Lämmerzahl and B. Schutz, 215 (2015).

[75] L. F. Costa, C. Herdeiro, J. Natário and M. Zilhão, "Mathisson's helical motions for a spinning particle: Are they unphysical?", *Phys. Rev. D* **85**, 024001 (2012).

[76] W. G. Dixon, "Dynamics of Extended Bodies in General Relativity. I. Momentum and Angular momentum", *Proc. R. Soc. London Ser. A* **314**, 499 (1970).

[77] W. G. Dixon, "Dynamics of Extended Bodies in General Relativity. II. Moments of the Charge-Current Vector", *Proc. R. Soc. London Ser. A* **319**, 509 (1970).

[78] R. Wald, "Gravitational Spin Interaction", *Phys. Rev. D* **6**, 406 (1972).

[79] C. Møller, "Sur la dynamique des systemes ayant un moment angulaire interne.", *Ann. Inst. Henri Poincar´e* **11**, 251 (1949).

[80] E. Corinaldesi and A. Papapetrou, "Spinning Test-Particles in General Relativity. II", *Proc. R. Soc. London Ser. A* **209**, 259 (1951).

[81] B. M. Barker and R. F. O'Connell, "Nongeodesic motion in General Relativity", *Gen. Rel. Grav.* **5**, 539 (1974).

[82] S. Ragusa and M. Bailyn, "The Center of Trace in Spinning Particles in General Relativity", *Gen. Rel. Grav.* **27**, 163 (1995).

[83] K. Kyrian, and O. Semerák, "Spinning test particles in a Kerr field – II", *Mon. Not. R. Astron. S.* **382**, 1922 (2007).

[84] O. Semerák, M. Šrámek, "Spinning particles in vacuum space-times of different curvature types – I", arXiv:1505.01069 [gr-qc] (2015).

[85] R. Rüdiger, "Conserved Quantities of Spinning Test Particles in General Relativity. I", *Proceedings of the Royal Society London A* **375**, 185 (1981).

[86] R. Rüdiger, "Conserved Quantities of Spinning Test Particles in General Relativity. II", *Proceedings of the Royal Society London A* **385**, 229 (1983).

[87] O. Semerák, "Spinning test particles in a Kerr field - I", *Mon. Not. R. Astron. S.* **308**, 863 (1999).

[88] Y. N. Obukhov, D. Pützfeld, "Dynamics of test bodies with spin in de Sitter spacetime", *Phys. Rev. D* **83**, 044024 (2011).

[89] R. Penrose, *The Road to Reality: A Complete Guide to the Laws of the Universe,* Vintage; Auflage: Reprint (9. Januar 2007).

[90] W. Beiglböck, "The Center-of-Mass in Einsteins Theory of Gravitation", *Commun. math. Phys.* **5**, 106 (1967).

[91] R. Schattner, "The Center of Mass in General Relativity", *Gen. Rel. Grav.* **10**, 377 (1979).

[92] R. Schattner, "The uniqueness of the center of mass in general relativity", *Gen. Rel. Grav.* **10**, 395 (1979).

[93] H. P. Künzle, "Dynamics of a Rigid Test Body in Curved Space-Time", *Commun. math. Physics* **27**, 23 (1972).

[94] H. P. Künzle, "Canonical Dynamics of Spinning Particles in Gravitational and Electromagnetic Fields", *J. Math. Phys.* **13**, 739 (1972).

[95] F. A. E. Pirani, *Acta Phys. Polonica* **15**, 389 (1956)
Republication: F. A. E. Pirani, "On the physical significance of the Riemann tensor", *Gen. Relativ. Gravit.* **41**, 1215 (2009).

[96] D. C. Wilkins, "General Equation for the Precession of a Gyroscope", *Annals of Physics* **61**, 277 (1970).

[97] G. Börner, J. Ehlers and E. Rudolph, "Relativistic Spin Precession in Two-body Systems", *Astron. & Astrophys.* **44**, 417 (1975).

[98] K. P. Tod and F. de Felice, "Spinning Test Particles in the Field of a Black Hole", *Nuovo Cimento* **34**, 365 (1976).

[99] B. M. Barker and R. F. O'Connell, "The Gravitational Interaction: Spin, Rotation and Quantum Effects - A Review", *Gen. Rel. Grav.* **11**, 149 (1979).

[100] M. A. Abramowicz and M. Calvani, "Spinning particles orbiting the Kerr black hole", *Mon. Not. R. astr. Soc.* **189**, 621 (1979).

[101] T. A. Apostolatos, "A spinning test body in the strong field of a Schwarzschild black hole", *Class. Quant. Grav.* **13**, 799 (1996).

[102] R. M. Plyatsko, A. L. Vynar and Ya. N. Pelekh, "Conditions for the appearance of gravitational ultrarelativistic spin-orbital interaction", *Soviet Physics Journal* **28**, 773 (1985).

[103] R. Plyatsko, O. Stefanyshyn and M. Fenyk, "Higly relativistic spinning particle starting near $r_{\rm ph}^{(-)}$ in a Kerr field", *Phys. Rev. D* **82**, 044015 (2010).

[104] D. Bini, A. Geralico, R. T. Jantzen, "Spin-geodesic deviations in the Schwarzschild spacetime", *Gen. Rel. Grav.* **43**, 959 (2011).

[105] B. Mashoon and D. Singh, "Dynamics of extended spinning masses in a gravitational field", *Phys. Rev. D* **74**, 124006 (2006).

[106] S. Suzuki and K. Maeda, "Innermost stable circular orbit of a spinning particle in Kerr spacetime", *Phys. Rev. D* ***58***, 023005 (1998).

[107] E. Hackmann, C. Lämmerzahl, Y. N. Obukhov, D. Pützfeld, I. Schaffer, "Motion of spinning test bodies in Kerr spacetime", *Phys. Rev. D* **90**, 064035 (2014).

[108] C. W. F. Everitt, D. B. DeBra, B. W. Parkinson, J. P. Turneaure, J. W. Conklin, M. I. Heifetz, G. M. Keiser, A. S. Silbergleit, T. Holmes, J. Kolodziejczak, M. Al-Meshari, J. C. Mester, B. Muhlfelder, V. G. Solomonik, K. Stahl, P. W. Worden, Jr., W. Bencze, S. Buchman, B. Clarke, A. Al-Jadaan, H. Al-Jibreen, J. Li, J. A. Lipa, J. M. Lockhart, B. Al-Suwaidan, M. Taber, and S. Wang, "Gravity Probe B: Final Results of Space Experiment to Test General Relativity", *Phys. Rev. Lett.* **106**, 221101 (2011).

[109] K. Glampedakis, "Extreme mass ratio inspirals: LISA's unique probe of black hole gravity", *Class. Quant. Grav.* **22**, 605 (2005).

[110] S. Drasco and S. A. Hughes, "Rotating black hole orbit functionals in the frequency domain", *Phys.Rev. D* **69**, 044015 (2004).

[111] G. N. Fleming, "Covariant Position Operators, Spin and Locality", *Phys. Rev. B* **137**, 188 (1965).

[112] O. B. Karpov, "The Papapetrou Equations and supplementary conditions", arXiv: 0406002 [gr-qc] (2004).

[113] B. M. Barker and R. F. O'Connell, "Lagrangian-Hamiltonian formalism for the gravitational two-body problem with spin and parametrized post-Newtonian parameters γ and β", *Phys. Rev. D* **14**, 861 (1976).

[114] J. Weyssenhoff and A. Raabe, "Relativistic dynamics of spin-fluids and spin particles", *Acta Phys. Pol.* **9**, 7 (1947).

[115] W. G. Dixon, "Classical theory of charged particles with spin and the classical limit of the Dirac equation", *Il Nuovo Cimento* **38**, 1616 (1965).

[116] J. Steinhoff, G. Schäfer, and S. Hergt, "The next-to-leading order gravitational spin(1)-spin(2) dynamics in Hamiltonian form", *Phys. Rev. D* **77**, 104018 (2008).

[117] H. Goldstein, *Classical Mechanics* (2nd edition ed.). Addison Wesley (1980).

[118] Sean M. Carroll, *Lecture Notes on General Relativity*, arXiv:9712019 [gr-qc] (1997).

[119] S. Drasco, "Verifying black hole orbits with gravitational spectroscopy", *Phys. Rev. D* **79**, 104016 (2009).

[120] W. de Sitter, "On the Relativity of Inertia. Remarks Concerning Einstein's Latest Hypothesis", *Proc. Royal Acad. Amsterdam* **19**, 1217 (1917); and "On the curvature of space", *Proc. Royal Acad. Amsterdam* **20**, 229 (1917).

[121] G. Lemaître, "Un univers homogène de masse constante et de rayon croissant rendant compte de la vitesse radiale des nébuleuses extra-galactiques", *Annales de la Société Scientifique de Bruxelles A* **47**, 49 (1927). Partially translated in G. Lemaître, "Expansion of the universe: A homogeneous universe of constant mass and increasing radius accounting for the radial velocity of extra-galactic nebulae", *Mon. Not. R. Astron. Soc.* **91**, 483 (1931).

[122] E. Hubble, "A relation between distance and radial velocity among extra-galactic nebulae", *Proc. Nat. Acad. Sci.* **15**, 168 (1929).

[123] A . Einstein, "Kosmologische Betrachtungen zur allgemeinen Relativitaetstheorie", *Sitzungsberichte der Königlich Preussischen Akademie der Wissenschaften Berlin*, 142 (1917).

[124] G. Gamow, *My World Line*, Viking Press 1970, p. 44.

[125] A. G. Riess, A. Filippenko, P. Challis, A. Clocchiattia, A. Diercks, P. Garnavich, R. Gilliland, C. Hogan, S. Jha, R. Kirshner, B. Leibundgut, M. Phillips, D. Reiss, B. Schmidt, R. Schommer, R. Smith, J. Spyromilio, C. Stubbs, N. Suntzeff, J. Tonry, "Observational Evidence from Supernovae for an Accelerating Universe and a Cosmological Constant" (High-Z Supernova Search), *Astron. J.* **116**, 1009 (1998).

[126] S. Perlmutter, G. Aldering, G. Goldhaber, R. Knop, P. Nugent, P. Castro, S. Deustua, S. Fabbro, A. Goobar, D. Groom, I. Hook, A. Kim, M. Kim, J. Lee, N. Nunes, R. Pain, C. Pennypacker, R. Quimby, C. Lidman, R. Ellis, M. Irwin, R. McMahon, P. Ruiz-Lapuente, N. Walton, B. Schaefer, B. Boyle, A. Filippenko, T. Matheson, A. Fruchter, N. Panagia, H. Newberg, W. Couch, "Measurements of Ω and Λ from 42 High-Redshift Supernovae" (Supernova Cosmology Project), *Astrophys. J.* **517**, 565 (1999).

[127] Z. Stuchlík and S. Hledík, "Some properties of the Schwarzschild–de Sitter and Schwarzschild–anti-de Sitter spacetimes", *Phys. Rev. D* **60**, 044006 (1999).

[128] Z. Stuchlík and J. Kovář, "Properties of pseudo-Newtonian gravitational potential in Schwarzschild–de Sitter spacetimes", in *Proceedings of RAGtime* 8/9*: Workshops on black holes and neutron stars*, edited by S. Hledík and Z. Stuchlík (Silesian University of Opava, 2007) 417.

[129] P.J.E. Peebles and B. Ratra, "The cosmological constant and dark energy", *Rev. Mod. Phys.* **75**, 559, (2003).

[130] Z. Stuchlík, "Equilibrium of spinning test particles in the Schwarzschild-de Sitter spacetimes", *Acta Physica Slovaca* **49**, 319 (1999).

[131] M. Mortazavimanesh and M. Mohseni, "Spinning particles in Schwarzschild-de Sitter space-time", *Gen. Rel. Grav.* **41**, 2697 (2009).

[132] J. Steinhoff and D. Puetzfeld, "Influence of internal structure on the motion of test bodies in extreme mass ratio situations", *Phys. Rev. D* **86**, 044033 (2012).

[133] A. Ya. Sochnev, "Approximation of ultra-elliptic and elliptic integrals without infinite series expansion of the integrands", *Uk. Math. Journal* **20**, 442 (1968).

[134] V. Perlick, "Betrand spacetimes", *Class. Quant. Grav.* **9**, 1009 (1992).

[135] W. Han, "Chaos and dynamics of spinning particles in Kerr spacetime", *General Relativity and Gravitation* **40**, 1831 (2008).

[136] X. Wu and Y. Xie, "Symplectic structure of post-Newtonian Hamiltonian for spinning compact binaries", *Phys. Rev. D* **81**, 084045 (2010).

[137] J. Steinhoff, "Spin and quadrupole contributions to the motion of astrophysical binaries", *Proceedings of the 524. WE-Heraeus-Seminar Equations of Motion in Relativistic Gravity*, arXiv:1412.3251 [gr-qc] (2014).

[138] R. Plyatsko, M. Fenyk, "Highly relativistic circular orbits of spinning particle in the Kerr field", *Phys. Rev. D* **87**, 044019 (2013).

[139] R. Plyatsko, M. Fenyk, "Highly relativistic spinning particle in the Schwarzschild field: Circular and other orbits", *Phys. Rev. D* **85**, 104023 (2012).

[140] J. Kánnár, "A Note on the Lagrangian Formalism of Spinning Particles in General Relativity", *Gen. Rel. and Grav.* **26**, 311 (1994).

[141] K. Westpfahl, "Das Spinteilchen in äußeren Maxwell-Feldern", *Annalen der Physik* **475**, 241 (1967).

[142] H. Römer and K. Westpfahl, "Rotator-Spinteilchen in schwachen Gravitationsfeldern", *Annalen der Physik* **477**, 264 (1969).

[143] K. Westpfahl, "Rotator-Spinteilchen und allgemeine Relativitätstheorie", *Annalen der Physik* **477**, 361 (1969).

[144] A. J. Hanson and T. Regge, "The Relativistic Sperical Top", *Annals of Physics* **87**, 498 (1974).

[145] P. A. M. Dirac, "Generalized Hamiltonian Dynamics", *Canadian Journal of Mathematics* **2**, 129 (1950).

[146] I. Bailey, and W. Israel, "Lagrangian Dynamics of Spinning Particles and Polarized Media in General Relativity", *Commun. Math. Phys.* **42**, 65 (1975).

[147] I. Bailey and W. Israel, "Relativistic Dynamics of Extended Bodies and Polarized Media: An Eccentric Approach", *Annals of Physics* **130**, 188 (1980).

[148] R. A. Porto, "Post-Newtonian corrections to the motion of spinning bodies in non-relativistic general relativity", *Phys. Rev. D* **73**, 104031 (2006).

[149] G. E. Tauber, "Canonical Formalism and Equations of Motion for a Spinning Particle in General Relativity", *International Journal of Theoretical Physics* **27**, 335 (1988).

[150] J. C. Baez, B. Smith and D. Wise, *Lectures on Classical Mechanics*, http://math.ucr.edu/home/baez/classical/, (2005).

[151] S. J. A. Malham, *An introduction to Lagrangian and Hamiltonian mechanics-Lecture notes*, http://www.macs.hw.ac.uk/˜simonm/, (2015).

[152] B. DeWitt, *Bryce DeWitt's Lectures on Gravitation*, Edited by Steven M. Christensen, Springer; 2011 edition (February 25, 2011).

[153] E. Gourgoulhon, "3+1 formalism and bases of numerical relativity", *Lecture Notes in Physics* **846** (2012).

[154] W. R. Hamilton, "On a general method in dynamics", *Phil. Trans. R. Soc.* **part II**, 247 (1834).

[155] Y. Tavakoli, *Hamiltonian formulation of general relativity*, http://www.cosmo-ufes.org/mini-courses.html, (2014).

[156] G. Darboux, "Sur le problème de Pfaff", *Bull. Sci. Math.* **6**, 14–36, 49–68 (1882).

[157] A. Knauf, *Mathematische Physik: Klassische Mechanik* (Springer-Lehrbuch Masterclass), Springer; Auflage: 2012 (28. September 2011).

[158] J. M. Pons, "On Dirac's incomplete analysis of gauge transformations", *Stud. Hist. Philos. Mod. Phys.* **36** , 491-518 (2005).

[159] E. Hairer, C. Lubich and G. Wanner, *Geometric numerical integration. Structure-preserving algorithms for ordinary differential equations* (Springer, 2006), 2nd ed.

[160] J. Seyrich, "Gauss collocation methods for efficient structure preserving integration of post-Newtonian equations of motion", *Phys. Rev. D* **87**, 084064 (2013).

[161] J. Seyrich and G. Lukes-Gerakopoulos, "Symmetric integrator for nonintegrable Hamiltonian relativistic systems", *Phys. Rev. D* **86**, 124013 (2012).

[162] L. Mei, M. Ju, X. Wu and S.-Q. Liu, "Dynamics of spin effects of compact binaries", *Mon. Not. R. Astron. S.,* **435**, 2246 (2013).

[163] S. Y. Zhong, X. Wu, S.-Q. Liu and X.-F. Deng, "Global symplectic structure-preserving integrators for spinning compact binaries", *Phys. Rev. D* **82**, 124040 (2010).

[164] G. Date, *Lectures on Constrained Systems*, arXiv:1010.2062v1 [gr-qc] (2010).

[165] J. Frenkel, "Die Elektrodynamik des Rotierenden Elektrons", *Z. Phys.* **37**, 243 (1926).

[166] C. Duval, H. H. Fliche, J. M. Souriau, "Un modèle de particule à spin dans le champ gravitationnel et électromagnétique. ", *C. R. Acad. Sci. Paris* **274**, 1082 (1972).

[167] K. Yee and M. Bander, "Equations of motion for spinning particles in external electromagnetic and gravitational fields", *Phys. Rev. D* **48**, 2797 (1993).

[168] R. M. Wald, *General Relativity*, The University of Chicago Press (15. Juni 1984).

[169] R. L. Znajek, "Black hole electrodynamics and the Carter tetrad", *Mon. Not. R. astr. Soc.* **179**, 457 (1977).

[170] O. Semerák, "Stationary Frames in the Kerr Field", *Gen. Rel. Grav.* **25**, 1041 (1993).

[171] E. Hairer, S. P. Nørsett and G. Wanner, *Solving Ordinary Differential Equations I* (Springer, 1993), 2nd ed.

[172] W. Press, S. Teukolsky, W. Vetterling and B. Flannery, *Numerical Recipes in C. The art of scientific computing* (Cambridge University Press, 1992), 2nd ed.

[173] J. Steinhoff and D. Puetzfeld, "Multipolar equations of motion for extended test bodies in General Relativity", *Phys. Rev. D* **81**, 044019 (2010).

[174] G. Lukes-Gerakopoulos, M. Katsanikas, P. Patsis and J. Seyrich, in preparation